THE JOURNAL OF

PHYSICAL

CHEMISTRY

THE JOURNAL OF
PHYSICAL CHEMISTRY

COMMUNICATIONS TO THE EDITOR

■ Supplementary material for this paper is available separately, in photocopy or micro-
fiche form. Ordering information is given in the paper.

* In papers with more than one author, the asterisk indicates the name of the author to
whom inquiries about the paper should be addressed.

AUTHOR INDEX

A Variational Solution of the Poisson–Boltzmann Equation for a Spherical Colloidal Particle

Stephen L. Brenner*

Department of Chemistry, University of Kentucky, Lexington, Kentucky 40506

and Robert E. Roberts

Department of Chemistry, Indiana University, Bloomington, Indiana 47401   (Received May 4, 1973)

A variational principle associated with the free energy is used to determine an accurate yet simple analytical form for the electrostatic potential surrounding a spherical colloid particle. Although the proposed function contains only one variational parameter, fixed by optimization of the free energy, it is of comparable accuracy to exact numerical solutions even in regions of relatively large particle size and high surface potentials. Furthermore, the potential approaches the Debye-Hückel limiting case for dilute electrolyte solutions or very small surface potentials. It is anticipated that this solution will be useful in investigations of colloid stability and micelle–micelle interactions.

Introduction

A knowledge of the electrostatic potential in the diffuse double layer surrounding charged colloid particles has been of great interest for many years.[1] Such knowledge is useful, for example, in studies of colloid stability,[1] and various electrokinetic phenomena.[2] For most of these cases the analog of the usual procedure used for dilute electrolytic solutions, namely, Debye-Hückel theory,[3] is not applicable. This is because there are usually prohibitively large surface potentials involved so that the linearized Poisson-Boltzmann equation is no longer valid.

A standard method of dealing with this problem is that of Gouy[4] and Chapman[5] who treat the colloid particle as being so large as to be well approximated by an infinite flat plane. For large colloid particles this is quite reasonable. However, for particles of micellar size, the approximation is clearly invalid. The combination of a diffuse Gouy-Chapman layer with Stern's method,[6] which takes into account finite ion size, does nothing to improve the situation.

The non-linearized Poisson-Boltzmann equation cannot be solved analytically for a spherical geometry but numerical solutions have been given.[2,7-9] Clearly, a simple closed form approximation to the potential in the double layer would be most useful, particularly in those regions where both the Debye-Hückel and Gouy-Chapman theories are not applicable.

We present a simple analytical approximation to the solution of the non-linearized Poisson-Boltzmann equation which yields the Debye-Hückel results in the limit of dilute solutions or small surface potentials and is of comparable accuracy to the numerical solutions even for large surface potentials and concentrated solutions, well into the region where the Gouy-Chapman theory becomes applicable. Included in the region where this approximation is essentially exact are those surface potentials and colloid sizes which are of particular interest in the study of micelles. The potential function contains a single parameter which is determined by a variational principle associated with the free energy.

It is well known that the non-linear Poisson-Boltzmann equation has no firm statistical-mechanical foundation and in fact is physically inconsistent. Any solution of this equation will therefore reflect this inconsistency. In the regime of high surface potentials an exact solution of the nonlinear equation will provide at best a good approximation to the true potential and it is in that spirit that this calculation is presented.

Theory

We consider a rigid spherical colloid particle of radius a immersed in a z–z electrolyte of dielectric constant ϵ. The extension to a z–z' electrolyte is straightforward. The charge on the particle is assumed to be uniformly distributed over the surface of the sphere and is arbitrarily taken as positive. The concentration of colloid particles is assumed small so that interactions between particles can be neglected. We wish to find the electrostatic potential, $\psi(r)$, at a distance $r - a$ from the surface of the spherical particle and calculate the free energy of the system.

The relationship between the electrical potential at a point r and the charge density, $\rho(r)$, is given by Poisson's equation

$$\nabla^2 \psi(\vec{r}) = -(4\pi/\epsilon)\rho(\vec{r}) \tag{1}$$

Making the usual assumptions of a Boltzmann distribution of ions[3] one obtains the non-linear Poisson–Boltzmann equation

$$\nabla^2 \psi(r) = (8\pi n e z/\epsilon)\sinh(ze\psi/kT) \tag{2}$$

where n is the concentration of electrolyte (negative ions/cm^3), T is the absolute temperature, and k is Boltzmann's constant. The solutions to this equation are required to satisfy the boundary conditions

$$\psi(a) = \psi_a$$

and

$$\lim_{r \to \infty} \psi(r) = 0 \tag{3}$$

Defining the reduced potential and distance by

$$\begin{aligned} y &= ze\psi/kT \\ q &= \kappa r \end{aligned} \tag{4}$$

where κ is the Debye–Hückel constant

$$\kappa = (8\pi n e^2 z^2/\epsilon kT)^{1/2} \tag{5}$$

and substituting (4) into (2) gives the reduced Poisson–Boltzmann equation

$$\nabla_q^2 y(q) = \sinh(y(q)) \tag{6}$$

where, for a spherically symmetric problem

$$\nabla_q^2 = \frac{1}{q^2}\frac{d}{dq}\left(q^2\frac{d}{dq}\right) \tag{7}$$

The solutions $y(q)$ clearly obey the boundary conditions

$$y(q_0) = y_0 = ze\psi_a/kT$$

where $q_0 = \kappa a$, and

$$\lim y(q) = 0 \tag{8}$$

To obtain the Debye–Hückel approximation from (6) one expands the exponentials and retains only linear terms. This is valid if $y \ll 1$ for important values of q and in fact under more general conditions as discussed below. One then obtains the linearized Poisson–Boltzmann equation

$$\nabla_q^2 y = y \tag{9}$$

which has the solution

$$y_{DH} = y_0 q_0 (e^{-(q-q_0)}/q) \tag{10}$$

The Gibbs free energy, ϕ, associated with the double-layer system is given by[1]

$$\phi = \int_0^\sigma \psi_a(\sigma')\,d\sigma' - \psi_a\sigma \tag{11}$$

The first term in (11) is the electrical work necessary to create the surface charge distribution σ while the second term represents the change in chemical potential of the ions (creating σ) on adsorption from solution. In the final charged state this change in chemical potential exactly equals the electric potential due to the double layer and therefore equals $-e\psi_a$ per ion or $-\sigma\psi_a$ per unit area of surface.

Equation 11 is valid for lyophobic systems in which σ is due to ion adsorption. When σ is due to the dissociation of ionizable groups, the second term in (11) is replaced by a more complicated expression (see, for example, ref 10). The electrical free energy term is still of great interest, however, even for lyophilic systems. This electrical term is just

$$\phi_{el} = \phi + \psi_a\sigma \tag{12}$$

The free energy (in reduced units) associated with the Debye–Hückel solution (10) is given by[2]

$$F_{DH} = -(4\pi e^2 z^2/\epsilon \kappa k^2 T^2)\phi$$

or

$$F_{DH} = \frac{1}{2}y_0^2\left(1 + \frac{1}{q_0}\right) \tag{13}$$

There are several equivalent ways to write the free energy associated with the Poisson–Boltzmann equation.[1,2,11] Levine[11] has derived the convenient reduced expression

$$F = \frac{1}{2q_0^2}\int_{q_0}^\infty \left\{\left(\frac{dy}{dq}\right)^2 + \left[2\sinh\left(\frac{y}{2}\right)\right]^2\right\}q^2\,dq \tag{14}$$

where

$$\phi = -(\kappa\epsilon k^2 T^2/4\pi e^2 z^2)F$$

The particular form given in (14) is only valid for spherical systems. See ref 11 for the general expression. Arthurs and Robinson[12] have derived generalized complimentary variational principles for non-linear second-order differential equations such as (6). In an application of their method one finds that the above expression for F provides a variational upper bound to the true free energy

$$F(\bar{y}) \geq F(y) \tag{15}$$

where $\bar{y}$ is a trial function. The purpose of this paper is to present an accurate $\bar{y}$ obtained from the optimization of (14). It should be noted that the fact that the Poisson–Boltzmann equation can be derived from a variational functional of the form of (14) was first pointed out by Levine[13] in a footnote and has recently been exploited by several authors.[14-16]

A natural way of writing the trial solution is with a "correction" function

$$\bar{y} = y_{DH}P(y_0, q_0, q) \tag{16}$$

where y_{DH} is given by (10). We propose and subsequently show the accuracy of the simple one parameter form for P

$$P = [a_0 - a_3 y_{DH}^3]^{-1} \tag{17}$$

The boundary conditions on y, (8), require

$$P(q = q_0) = 1$$

or

$$a_0 = 1 + a_3 y_0^3 \tag{18}$$

Let Y denote the variational parameter which can be thought of as that surface potential which, when substituted for y_0 in (10), yields a Debye–Hückel function with

the same asymptotic form as $\bar{y}$. Then

$$a_0 = y_0/Y$$

and

$$a_3 = \frac{1}{y_0{}^2}\left(\frac{1}{Y} - \frac{1}{y_0}\right) \tag{19}$$

The solution $\bar{y}$ is optimized by determining that Y which gives the minimal value of the reduced free-energy F of (14). The correction function P in (17) was by far the most successful of any of the functions that were examined.

In order to optimize the free energy it is necessary to perform several one-dimensional numerical integrations for different values of Y and for each set of initial conditions (q_0, y_0). In most instances it was found that a sixteen-point Gauss–Legendre quadrature was sufficient to provide seven-place precision. For all of the cases reported in this paper the number of points was increased to ensure convergence. The amount of computer time necessary to obtain an optimized solution was negligible.

Results

The results of the free energy optimization for a 1-1 electrolyte $(z = 1)$ are summarized in Tables I–III (abbreviated tables are presented here, see paragraph at end of paper regarding supplementary material) and Figure 1 for cases which can be directly compared with the numerical calculations of Loeb, Wiersema, and Overbeek.[2]

Table I presents a direct comparison of our optimized results with the exact results for (q_0, y_0) values pertinent to colloids. For most of the cases given the trial solution gives F correctly to four digits. The average relative deviation is 0.1%, and the worst error (corresponding to $q_0 = 20$ and $y_0 = 8$) is 1.5%. It should be noted that the fifth place in the "exact" results is not usually significant[2] and hence our agreement for more than 80% of the cases is essentially exact. In the few instances indicated by an asterisk in Table I we find $F/F_{\text{exact}} < 1$ in the fifth place, indicating a slightly improved result due to the bounded nature of the variational principle.

Table II gives values of F/F_{DH} which permits a direct calculation of the free energy function, ϕ, for a given surface potential, ion concentration, and colloid radius using (13). This table also gives an indication of the breakdown of the Debye–Hückel approximation for the cases considered. Note that even for $y_0 \gg 1$ the DH approximation is quite good if q_0 is small. It has recently been shown[17] that the DH solution asymptotically approaches the exact solution for all y_0 as $q_0 \rightarrow 0$.

The optimal values for the variational parameter $Y(q_0, y_0)$ are given in Table III. They are presented to three places since the free energy is insensitive to changes at the fourth place. Due to this insensitivity it is relatively simple to extract optimal values of Y_{opt} for (q_0, y_0) values not presented in Table III via a simple interpolation. This gives a convenient method for obtaining a simple and accurate analytic potential function using (16), (17), and (19).

For the case $q_0 = 2$ and $y_0 = 6$ Figure 1 presents a plot of $y(q)$ vs. $q - q_0$ for the Debye–Hückel approximation, for the optimized potential function of (16), and for the exact solution of ref 2. The actual agreement is generally to three places and so differences between our results and the exact results are indistinguishable on this figure.

There are several reasons why the grid of q_0 and y_0 values presented is particularly appropriate. First, Table
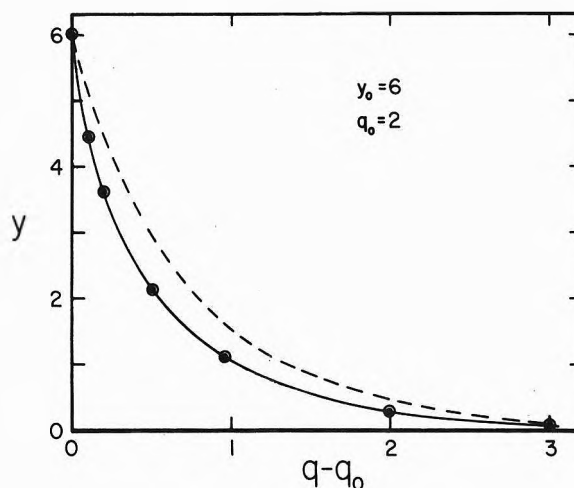
Figure 1. Comparison of exact y (solid curve) with the variational approximation (solid circles) and the Debye–Hückel approximation (dashed curve). The case presented corresponds to $q_0 = 2$ and $y_0 = 6$.

TABLE I: F/F_{exact} as a Function of q_0 and $y_0{}^a$

	q_0					
y_0	0.1	1.0	2.0	5.0	10.0	20.0
1	1.0000*	1.0000	1.0000*	1.0000	1.0000	1.0001
2	1.0000	1.0000	1.0001	1.0001	1.0000	1.0001
4	1.0000	1.0002	1.0002	1.0001	1.0001	1.0001
6	1.0000*	1.0003	1.0006	1.0010	1.0013	1.0014
8	1.0001	1.0056	1.0093	1.0126	1.0139	1.0146

^{a} Values marked with an asterisk are actually 0.999 and correspond to free energies which are slightly better than the numerical solution of ref 2.

TABLE II: F/F_{DH} as a Function of q_0 and y_0

	q_0					
y_0	0.1	1.0	2.0	5.0	1C.0	20.0
1	1.0004	1.0074	1.0114	1.0160	1.0182	1.0196
2	1.0019	1.0307	1.0475	1.0661	1.0750	1.0804
4	1.0090	1.1438	1.2178	1.2974	1.3350	1.3570
6	1.0282	1.4123	1.6069	1.8098	1.0939	1.9582
8	1.0816	2.0091	2.4440	2.8886	3.0927	3.2097

TABLE III: Y_{opt} as a Function of q_0 and y_0

	q_0					
y_0	0.1	1.0	2.0	5.0	10.0	20.0
1	1.00	0.99	0.99	0.99	0.99	0.99
2	2.00	1.95	1.93	1.90	1.89	1.89
4	3.96	3.59	3.44	3.29	3.23	3.19
6	5.83	4.60	4.22	3.89	3.76	3.68
8	7.41	4.79	4.19	3.73	3.55	3.45

II clearly indicates that these values are generally out of the range of validity of the Debye–Hückel approximation. Second, even an *empirical* free energy function derived from the exact solution together with the Gouy–Chapman theory[2] gives an average relative error of about 3% over this range of q_0 and y_0 compared to the 0.1% error of our function. Besides, the empirical solution for F when used to obtain y yields a complicated function and is not a particularly good approximation.[2] Finally, for micellar sys-

tems these values are particularly important. For an examination of several studies of detergent micelles[18,19] we find that for sodium dodecyl sulfate, and dodecyl ammonium chloride, for example, typical values of y_0 range from 4 to 7 while typical values of q_0 range from 0.5 to 5.0 (variations due to added salt). Figure 1 corresponds to a typical case of a sodium dodecyl sulfate micelle of radius ~ 20 Å, in a ~ 0.1 M NaCl solution. Beyond the limits of Tables I–III the Gouy–Chapman theory is quite adequate.

Conclusion

The trial function obtained in this work provides a simple accurate solution to the Poisson–Boltzmann for a wide range of surface potentials, ion concentration, and particle size. It should be particularly useful in studies of micelle–micelle interactions. Furthermore, this technique should be easy to extend to nonspherical systems.

The complementary (lower) bound to F is currently under study for spherical systems and calculations are also in progress for cylindrical systems. The availability of complementary bounds for nonspherical system is particularly useful because of the lack of tabulated numerical solutions for these cases.

Supplementary Material Available. Complete copies of Tables I–III will appear following these pages in the microfilm edition of this volume of the journal. Photocopies of the supplementary material from this paper only or microfiche (105 × 148 mm, 20× reduction, negatives) containing all of the supplementary material for the papers in this issue may be obtained from the Journals Department, American Chemical Society, 1155 16th St., N.W., Washington, D. C. 20036. Remit check or money order for $3.00 for photocopy or $2.00 for microfiche, referring to code number JPC-73-2367.

References and Notes

(1) See, for example, E. J. W. Verwey and J. Th. G. Overbeek, "Theory of the Stability of Lyophobic Colloids," Elsevier, New York, N. Y., 1948.
(2) A. L. Loeb, J. Th. G. Overbeek, and P. H. Wiersema, "The Electrical Double Layer Around a Spherical Colloid Particle," M. I. T. Press, Cambridge, Mass., 1961.
(3) T. L. Hill, "An Introduction to Statistical Thermodynamics," Addison-Wesley, Reading, Mass., 1960.
(4) G. Gouy, *J. Phys.*, **9**, 457 (1910).
(5) D. L. Chapman, *Phil. Mag.*, **25**, 475 (1913).
(6) O. Stern, *Z. Elektrochem.*, **30**, 508 (1924).
(7) H. Muller, *Kolloidchem. Beih.*, **26**, 257 (1928).
(8) N. E. Hoskin, *Trans. Faraday Soc.*, **49**, 1471 (1953).
(9) N. E. Hoskin and S. Levine, *Trans. Roy. Soc. Sec. A*, **248**, 433, 449 (1956).
(10) S. L. Brenner and D. A. McQuarrie, *J. Theor. Biol.*, **39**, 343 (1973).
(11) S. Levine, *Proc. Phys. Soc., Sec. A*, **44**, 781 (1951).
(12) A. M. Arthurs and P. D. Robinson, *Proc. Camb. Phil. Soc.*, **65**, 535 (1969).
(13) S. Levine, *J. Chem. Phys.*, **7**, 836 (1939).
(14) A. D. MacGillivray and A. I. McMullen, *J. Theor. Biol.*, **19**, 159 (1968).
(15) L. Dresner, *J. Phys. Chem.*, **67**, 2333 (1963).
(16) A. D. MacGillivray and J. D. Swift, *J. Phys. Chem.*, **72**, 3575 (1968).
(17) A. D. MacGillivray, *J. Theor. Biol.*, **23**, 205 (1969).
(18) M. F. Emerson and A. Holtzer, *J. Phys. Chem.*, **69**, 3718 (1965).
(19) D. Stigter, *J. Phys. Chem.*, **68**, 3603 (1964).

Isothermal Diffusion Measurements on the System Water–Choline Chloride–Potassium Chloride at 25°[1]

Robert Fleming[2]* and Louis J. Gosting

The Institute for Enzyme Research, University of Wisconsin, Madison, Wisconsin 53706 (Received July 26, 1972; Revised Manuscript Received July 20, 1973)

Publication costs assisted by the School of Pharmacy, University of London

The Gouy diffusiometer has been used to study the isothermal diffusion process at 25° in the binary system H₂O–choline chloride and in the ternary system H₂O–choline chloride–KCl. Values for the mutual diffusion coefficient for choline chloride in water are reported over the concentration range 0.0073–0.2232 g cc⁻¹. The diffusion in a ternary system can be described by four volume-fixed diffusion coefficients, and these were obtained at each of four compositions of the system. For a ternary system a measure of the deviation of the flow of each solute from Fick's first law is given by a cross-term diffusion coefficient. One of these coefficients was found to be large, and the other small, and this is in accordance with the predictions of the first-order equations of O'Donnell and Gosting. Density data and refractive index derivatives for both the binary and ternary systems are reported, together with the partial specific volumes for the ternary system.

Introduction

The purpose of this investigation was to study the deviations of solute flows from Fick's first law for the ternary system H₂O–choline chloride–KCl by measuring the main and cross-term diffusion coefficients.[3-5] It was thought that these diffusion coefficients should be of help in the understanding of diffusion processes that occur during nerve conduction.

Isothermal diffusion in one dimension in a ternary solution can be described along the x coordinate by the two flow equations

$$(J_1)_V = -(D_{11})_V \frac{\partial \rho_1}{\partial x} - (D_{12})_V \frac{\partial \rho_2}{\partial x} \qquad (1)$$

$$(J_2)_V = -(D_{21})_V \frac{\partial \rho_1}{\partial x} - (D_{22})_V \frac{\partial \rho_2}{\partial x} \qquad (2)$$

where the solute concentrations ρ_1 and ρ_2 are expressed in g cc⁻¹. Throughout this article subscript 1 will denote choline chloride and subscript 2 will denote potassium chloride. The solute flows $(J_i)_V$ are referred to the volume-fixed frame of reference and have units of g cm⁻² sec⁻¹. The four volume-fixed diffusion coefficients $(D_{ij})_V$ have units of cm² sec⁻¹. For the small concentration differences used in these experiments the volume-fixed frame of reference may be considered identical with the cell-fixed (or apparatus-fixed) reference frame.[6,7]

The size of the cross-term diffusion coefficients $(D_{12})_V$ and $(D_{21})_V$ can be predicted qualitatively from the limiting equivalent conductances of the ions present in the system.[8] The choline ion has a much lower limiting equivalent conductance[9] than either the K⁺ or Cl⁻ ions, which have almost equal values. Consequently the flow of choline chloride, $(J_1)_V$, produced by a concentration gradient of KCl will be small, hence $(D_{12})_V$ is small. Because of the large difference between the limiting equivalent conductances of the Cl⁻ and choline ions, the flow of KCl, $(J_2)_V$, produced by a concentration gradient of choline chloride will be relatively large, and accordingly $(D_{21})_V$ will be much larger than $(D_{12})_V$ and quite different from zero.

The ternary system was studied at four compositions with the following concentrations of the solutes: $\bar{\rho}_1 = 0.05$, $\bar{\rho}_2 = 0.05$; $\bar{\rho}_1 = 0.05$, $\bar{\rho}_2 = 0.025$; $\bar{\rho}_1 = 0.025$, $\bar{\rho}_2 = 0.05$; $\bar{\rho}_1 = 0.025$, $\bar{\rho}_2 = 0.025$. Here and throughout this paper $\bar{\rho}_i$ (with $i = 1$ or 2) denotes a particular solute concentration chosen for experimental investigation.

Experimental Section

Only a brief outline of the experimental procedure and information specific to this study is given here. For a full description of the standard experimental details and procedures the reader is referred to a paper by Woolf, Miller, and Gosting.[10]

Materials. Choline chloride for the binary experiments was purchased from Eastman Organic Chemicals Department of Distillation Products Industries, and was recrystallized five times from a solvent consisting of a mixture (volume basis) of 70% absolute ethanol and 30% dry acetone. The crystals were dried *in vacuo* over magnesium perchlorate. Volumetric assay of the material for chloride content, and calculated as choline chloride, showed it to be 100% pure within the limits of experimental error (±0.25%). Choline chloride for the ternary experiments was purchased from the British Drug Houses, Ltd., England (99% pure with reference to the dried material). It was recrystallized twice using a solvent mixture of the same composition as described above and then dried *in vacuo* over magnesium perchlorate.

In all ternary experiments the KCl was part of a batch recrystallized by Woolf, *et al.*,[10] and was used without further purification.

For preparation of the ternary solutions distilled water from a Barnstead steam-heated still was further purified by passing through a Barnstead purification system. The latter consisted of an organic removal column, a mixed-bed ion-exchange column, a submicron filter, and a 5-gallon reservoir tank. It was designed so that water could continuously circulate through the columns, filter, and tank. The water was allowed to circulate for 12 hr and was

then drawn off (specific resistance 12–14 megohm cm) and put in a glass carboy. It was then saturated with air.

Molecular Weights. The molecular weights (M_i) of H_2O, choline chloride, and KCl were taken to be 18.016, 139.627, and 74.557, respectively.

Solutions. Water used in the preparation of the binary solutions had been previously purified by Woolf, *et al.*[10] For the ternary experiments the solutions were made up with water purified according to the procedure described above.

The density of each solution at 25 ± 0.003° was measured in triplicate in 30-ml single-necked pycnometers, which were always weighed against a sealed tare of similar volume. The measurements for each solution were averaged and are recorded as experimental densities in Tables I and II.

All solutions were prepared by weight, and the weights of choline chloride, KCl, and the final solutions were each converted to weights in vacuum using the density values 1.155,[11] 1.984, and the solution density, respectively. The concentrations in g cc^{-1} were calculated using the experimental densities.

Diffusion Experiments. All diffusion experiments were performed with a Gouy diffusiometer which has been described previously.[4,12,13] The optical lever arm,[14,15] b, from the center of the cell to the emulsion of the photographic plate, was 307.05$_5$ cm. The thickness, a, of the 11-ml quartz Beckman/Spinco electrophoresis–diffusion cell was measured with a special internal caliper and was found to be 2.505$_9$ cm.

The positions of the fringe intensity minima and maxima on the photographs were measured with a photoelectric null indicator, mounted on a Gaertner M2001RS toolmakers' microscope. This has been described in detail by Wendt[16] and Albright.[17] Approximately 18–20 fringe minima throughout each Gouy photograph, including the lower 7 ($j = 0$ through 6), were measured in accordance with the procedure described previously. Each value of C_t (the maximum displacement of light on a photograph according to ray optics) was obtained by the usual extrapolation procedure.[15,18,19] Values of $\mathfrak{D}_A'$, at time t', which are preliminary values for the reduced height–area ratio, $\mathfrak{D}_A$, for each experiment, were calculated using the following expression.

$$\mathfrak{D}_A' = (J\lambda b)^2 / 4\pi C_t^2 t' \qquad (3)$$

The plot of $\mathfrak{D}_A'$ *vs.* $1/t'$ was extrapolated to $1/t' = 0$ to obtain $\mathfrak{D}_A$, which is the reduced height–area ratio corrected for initial imperfections in the boundary.[20,21] The starting time correction Δt, which was found from the slope of the graph, ranged from 7 to 29 sec. A fringe deviation graph for each experiment was made by calculating the average values of Ω, the reduced fringe deviation of each f(ζ), and plotting them against f(ζ), the reduced fringe number.[22] The area of this graph

$$Q = \int_0^1 \Omega \, df(\zeta) \qquad (4)$$

was obtained by applying Simpson's ⅓ rule for numerical integration; values of Ω were read at intervals of 0.025 along the f(ζ) axis from a smoothed curve drawn through all the average values of ζ on the graph.

Calculation of the Four Diffusion Coefficients $(D_{ij})_V$. These coefficients were calculated according to the method developed by Fujita and Gosting[19] which utilizes the areas, Q, of the fringe deviation graphs.

Results

Experimental results for the binary system H_2O–choline chloride are shown in Table I. The mean solute concentrations, $\bar{\rho}_1$ (line 2), were obtained (eq 5) from the initial concentrations of the upper solutions, $(\rho_1)_A$, and the lower solutions, $(\rho_1)_B$, which are given on lines 3 and 5. The experimental densities of the initial solutions, d_A and d_B (lines 4 and 6, experiments 4–8), show reasonable agreement (average deviation 0.0013%) with the corresponding values calculated from the polynomial equation

$$d = 0.997048 + 0.11725\rho_1 - 0.03133\rho_1^2 + 0.09597\rho_1^3 \qquad (5)$$

which was fitted by the method of least squares[23] to the experimental densities using the Atlas computer. The concentration differences, $\Delta\rho_1$ (line 7), between the initial solutions in the first two experiments were sufficiently large to give approximately 100 fringes (J, line 8) so that accurate values of $\mathfrak{D}_A$ and Q could be determined. However, the areas of the fringe deviation graphs (line 10) for each of these experiments were significantly different from zero. This could be due to (a) optical imperfections in the apparatus, (b) solute impurity, or (c) the dependence of certain properties of the solution on solute concentration.[18,24] The first possibility was considered to be remote, as previous experiments in the same cell and apparatus with pure solutes having negligibly concentration dependent properties gave values of $Q = 0 \mp 2 \times 10^{-4}$, which indicated an absence of optical imperfections. Also a preliminary test experiment with 1.5% sucrose in water at the start of the present study yielded a value of Q which was approximately 2×10^{-4}. Possibilities b and c can be distinguished because if $\bar{\rho}_1$ is held constant, and $\Delta\rho_1$ is decreased, Q should remain constant for b, and Q should approach zero for c. Therefore experiment 3 was performed with a smaller value of $\Delta\rho_1$, using solute from the same batch as in the first two experiments. In this experiment Q became nearly zero (within experimental error) thus ruling out possibility b and indicating that values of $\Delta\rho_1$ between 0.008 and 0.0110 should be the best compromise for the remainder of the experiments. With these concentration differences the effects of concentration-dependent properties of the solution are minimized, yet J is large enough for reasonable accuracy. Furthermore, in accordance with expectation[25] Q decreased approximately in proportion to $(\Delta\rho_1)^2$. If $\mathfrak{D}_A$ (line 9) from experiment 1 is adjusted slightly to correspond to $\bar{\rho}_1 = 0.00816$ (by using data from other experiments in Table I to estimate the slope of $\mathfrak{D}_A$ *vs.* $\sqrt{\rho_1}$) a value of $\mathfrak{D}_A = 1.224_5 \times 10^{-5}$ is obtained. When this value of $\mathfrak{D}_A$ together with those from experiments 2 and 3 are plotted against the corresponding $(\Delta\rho_1)^2$, the graph is found to be approximately linear in agreement with theory,[18,24] and it has a very small slope. Thus $\mathfrak{D}_A$ for experiments 3–8 may be identified with the mutual diffusion coefficient, D, within the limits of experimental error.

In the study of the ternary system, four sets of experiments were performed corresponding to the four compositions specified by the values of $\bar{\rho}_1$ and $\bar{\rho}_2$ in line 1 of Table II.[26] For each experiment the mean concentrations of the solutes, $\bar{\rho}_1$ and $\bar{\rho}_2$ are listed on lines 3 and 4; they are seen to be very close to the corresponding values of ρ_1 and $\bar{\rho}_2$. The experimental densities (lines 7 and 10) were determined as previously described, and the method of least squares was used to evaluate the constants H_1 and H_2 in eq 6; the results of these calculations are shown in Table III.[26] In all experiments the values of

TABLE I: Data for the Binary System H₂O-Choline Chloride at 25° [a]

1 Expt no.[b]	1	2	3	5	8	7	4	6
2 $\bar{\rho}_1$	0.00730_9	0.00813_4	0.00817_8	0.02716_4	0.04997_2	0.06512_2	0.12384_9	0.22316_7
3 $(\rho_1)_A$	0	0	0.00411_1	0.02316_4	0.0044632	0.06029_2	0.11887_6	0.21918_8
4 d_A			0.99749^c	0.0075_3	1.00224_5	1.00401_1	1.01073_5	1.02225_5
5 $(\rho_1)_B$	0.01461_9	0.01626_8	0.01224_5	0.03116_5	0.05531_3	0.06995_1	0.12882_2	0.22714_5
6 d_B	0.99875^c	0.99894^c	0.99846^c	1.00067_6	1.00346_8	1.00512_1	1.01182_0	1.02319_2
7 $\Delta\rho_1$	0.01461_9	0.01626_8	0.00813_3	0.00800_1	0.01068_2	0.00965_9	0.00994_6	0.00795_7
8 J	100.53	111.89	55.92	54.77	73.30	66.16	68.45	55.12
9 $D_A \times 10^5$	1.227_4	1.224_0	1.225_2	1.173_8	1.136_7	1.121_4	1.090_4	1.070_2
10 $Q \times 10^4$	$9._{14}$	$10._{94}$	$3._{67}$	$5._{21}$	$2._{75}$	$2._{81}$	$3._{96}$	$7._{16}$
11 $\Delta n/\Delta\rho_1$	0.1498_6	0.1498_8	0.1498_3	0.1491_7	0.1495_4	0.1492_3	0.1499_8	0.1509_5

[a] Units: concentrations and densities, g cc⁻¹; D_A, cm² sec⁻¹; $\Delta n/\Delta\rho_1$, cc g⁻¹. For all experiments except 1 and 2, $\Delta\rho_1$ was sufficiently small that D_A should be numerically equal to the mutual diffusion coefficient, D, with experimental error; this D is defined by Fick's first law in the form $(J_1)_v = -D(\partial\rho_1/\partial x)$ and corresponds to the concentration $\rho_1 = \bar{\rho}_1$. Similarly $\Delta_n/\Delta\rho_1$ may be identified with R_1 for the composition $\rho_1 = \bar{\rho}_1$ and $\rho_2 = 0$. [b] Experiments numbered chronologically. [c] Interpolated from a large graph of experimental densities measured at other concentrations.

TABLE II: Data for the Ternary System H₂O-Choline Chloride-KCl at 25° [a,b]

1 Composition	Set I: $\bar{\rho}_1 = 0.05$, $\bar{\rho}_2 = 0.05$				Set II: $\bar{\rho}_1 = 0.05$, $\bar{\rho}_2 = 0.025$			
2 Expt no.[c]	9	12	11	10	13	17	18	14
3 $(\rho_1)_A$	0.049987_0	0.048965_0	0.045682_5	0.044500_7	0.049998_1	0.049013_0	0.045723_0	0.044498_9
4 $(\rho_2)_A$	0.044490_8	0.045523_3	0.048819_0	0.050000_7	0.019999_9	0.020489_9	0.023776_0	0.025001_1
5 d_A	1.03011_5	1.03060_9	1.03223_3	1.032816	1.01491_9	1.01540_4	1.017043	1.01766_7
6 $(\rho_1)_B$	0.049997_5	0.051029_2	0.054318_1	0.055500_1	0.049997_6	0.050985_6	0.054277_0	0.055494_4
7 $(\rho_2)_B$	0.055497_9	0.054469_5	0.051184_4	0.049977_7	0.030498_3	0.029516_8	0.026225_0	0.024997_5
8 d_B	1.03671_5	1.036217	1.034587	1.033992	1.02162_4	1.021142	1.019497	1.01889_5
9 J	63.73	65.72	72.04	74.47	65.46	66.86	73.03	74.90
10 $D_A \times 10^5$	1.867_0	1.662_2	1.220_0	1.124_5	1.818_5	1.629_6	1.210_7	1.106_6
11 $Q \times 10^4$	$-15._{18}$	$25._{53}$	$57._{07}$	$43._{18}$	$-7._{13}$	$24._{36}$	$48._{10}$	$29._{40}$
12 $(D_{11})_v \times 10^5$	0.989_0				1.010_2			
13 $(D_{12})_v \times 10^5$	0.051_9				0.029_5			
14 $(D_{21})_v \times 10^5$	0.232_5				0.162_8			
15 $(D_{22})_v \times 10^5$	1.781_2				0.769_9			

1 Composition	Set III: $\bar{\rho}_1 = 0.025$, $\bar{\rho}_2 = 0.05$				Set V: $\bar{\rho}_1 = 0.025$, $\bar{\rho}_2 = 0.025$			
2 Expt no.	21	22	23	24	15	19	20	16
3 $(\rho_1)_A$	0.024998_5	0.024020_1	0.020731_7	0.019500_3	0.025002_5	0.024005_5	0.020716_1	0.019496_5
4 $(\rho_2)_A$	0.044498_5	0.045477_1	0.048770_2	0.050000_{15}	0.019503_2	0.020495_0	0.023785_7	0.024995_6
5 d_A	1.027333	1.027801	1.029801	1.030110	1.012106	1.012599	1.014249	1.014862
6 $(\rho_1)_B$	0.025000_3	0.025978_5	0.029269_3	0.030501_2	0.025004_8	0.025995_0	0.029284_3	0.030494_6
7 $(\rho_2)_B$	0.055502_4	0.054518_2	0.051234_9	0.050000_{18}	0.030508_4	0.029505_4	0.026220_4	0.024996_1
8 d_B	1.034023	1.033535	1.031917	1.031307	1.018860	1.018356	1.016710	1.016085
9 J	64.18	65.89	72.04	74.17	65.89	67.41	72.55	74.76
10 $D_A \times 10^5$	1.858_8	1.662_1	1.230_3	1.122_7	1.819_4	1.629_1	1.213_8	1.111_7
11 $Q \times 10^4$	$-6._{17}$	$30._{09}$	$60._{04}$	$45._{99}$	$-0._{41}$	$32._{21}$	$46._{37}$	$35._{65}$
12 $(D_{11})_v \times 10^5$	0.979_0				1.002_9			
13 $(D_{12})_v \times 10^5$	0.025_4				0.006_3			
14 $(D_{21})_v \times 10^5$	0.246_3				0.179_1			
15 $(D_{22})_v \times 10^5$	1.816_1				1.807_6			

[a] Units: concentrations and densities, c cc⁻¹; D_A, cm² sec⁻¹; R_i, cc g⁻¹; D_{ij}, cm² sec⁻¹ (see eq 1 and 2 for their complete definition). [b] 0 = H₂O, 1 = choline chloride, 2 = KCl. [c] Experiments numbered chronologically.

$$d(\rho_1, \rho_2) = d(\tilde{\rho}_1, \tilde{\rho}_2) + H_1(\rho_1 - \tilde{\rho}_1) + H_2(\rho_2 - \tilde{\rho}_2) \quad (6)$$

$\Delta\rho_1 + \Delta\rho_2$ were close to 0.0110 g cc⁻¹. Since choline chloride is a hygroscopic substance and difficult to weigh accurately the agreement between the experimental and the calculated number of fringes, J, was considered to be satisfactory. The partial specific volumes, $\bar{v}_k$, of the solutes and solvent (lines 8, 9, and 10 of Table III) for the ternary solutions were calculated using the equation[27]

$$\bar{v}_k = \frac{1 - H_k}{d - H_1\rho_1 - H_2\rho_2} \quad (k = 1, 2) \quad (7)$$

Here H_k are the coefficients given in Table III, d is the experimental density given as $d(\tilde{\rho}_1, \tilde{\rho}_2)$, and $\rho_j = \tilde{\rho}_j$ ($j = 1,2$) is the concentration of each solute expressed in g cc⁻¹.

Discussion

The three-dimensional graphs of the $(D_{ij})_v$ in Figure 1 illustrate the relationships between (a) previous data for diffusion in the binary system H₂O-KCl,[28,29] (b) the new binary diffusion data in Table I for H₂O-choline chloride, and (c) the new data in Table II for diffusion at four com-
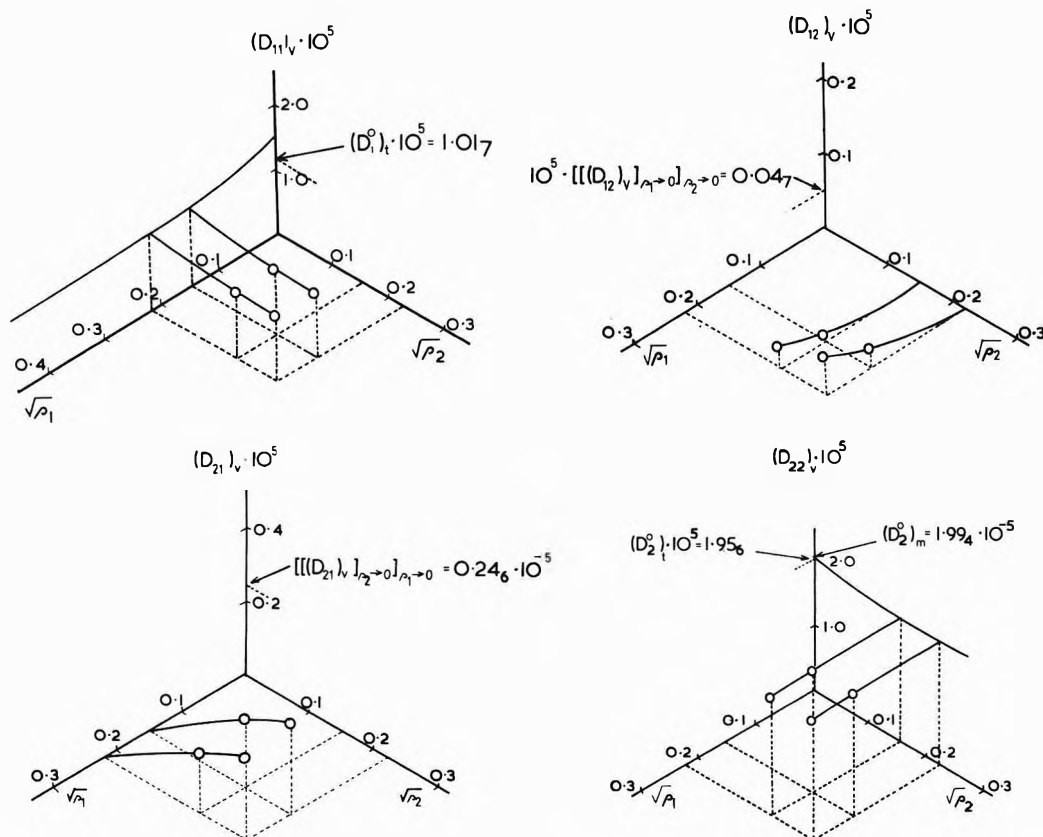
Figure 1. Variation with solute concentrations of the volume fixed diffusion coefficients, $(D_{ij})_V$, defined by eq 1 and 2 for the system H_2O-choline chloride-KCl at 25°. Circles represent the ternary data. These ternary data for the main diffusion coefficients are connected to data for the appropriate binary system by solid curves. Solid curves also represent the data for binary systems in their respective planes. The scales of the vertical axes in the graphs of the cross-term diffusion coefficients, $(D_{12})_V$ and $(D_{21})_V$, have been expanded. All the $(D_{ij})_V$ have units of $cm^2 \ sec^{-1}$ and correspond to solute concentrations expressed in $g \ cc^{-1}$.

TABLE III: Constants of Eq 6 for the Densities, and Values of the Partial Specific Volumes, for the System H_2O-Choline Chloride-KCl at 25° [a]

1 Set	I	II	III	IV
2 $\bar{\rho}_1$	0.050	0.050	0.025	0.025
3 $\bar{\rho}_2$	0.050	0.025	0.050	0.025
4 $d(\bar{\rho}_1,\bar{\rho}_2)$	1.03341_4	1.01827_4	1.03069_1	1.01547_7
5 H_1	0.1082_9	0.1120_7	0.1087_3	0.1117_9
6 H_2	0.6004_3	0.6102_6	0.6089_9	0.6140_1
7 % error[b]	0.0005	0.0005	0.0015	0.0003
8 $\bar{v}_0$	1.0020_3	1.0025_9	1.0024_9	1.0026_7
9 $\bar{v}_1$	0.893_5	0.890_2	0.893_5	0.890_6
10 $\bar{v}_2$	0.400_4	0.390_8	0.392_0	0.387_0

[a] Units: concentrations and densities, $g \ cc^{-1}$; partial specific volumes, $cc \ g^{-1}$. [b] Per cent error = [average deviation/$d(\bar{\rho}_1,\bar{\rho}_2)$] × 100.

positions of the ternary system H_2O-choline chloride-KCl. In addition, certain limiting values of these $(D_{ij})_V$ in regions where no experimental data are yet available were computed from values of the limiting equivalent ionic conductances, λ_i^0, and are also shown. Because choline chloride and KCl are both electrolytes, the diffusion coefficients were plotted against $\rho_i^{1/2}$ rather than ρ_i to avoid infinite slopes as ρ_1 and ρ_2 approach zero.

Data for the curve in the $(D_{11})_V - \rho_1^{1/2}$ plane were taken from Table I, because as $\rho_2 \to 0$ in the ternary system, with ρ_1 constant, $(D_{11})_V$ becomes identical with the mutual diffusion coefficient,[30] $(D_1)_m$, for choline chloride in water at that value of ρ_1

$$[(D_{11})_V]_{\rho_2 \to 0} \longrightarrow (D_1)_m \quad (\rho_1 \ \text{constant} \neq 0) \quad (8)$$

As $\rho_1 \to 0$ in this plane the Nernst limiting value

$$[(D_1)_m]_{\rho_1 \to 0} \longrightarrow (D_1^0)_m \quad (9)$$

may be calculated from the equation[32]

$$(D_1^0)_m = \frac{2RT}{F^2}\left[\frac{\lambda_1^0\lambda_3^0}{\lambda_1^0 + \lambda_3^0}\right] \times 10^{-7} \quad (10)$$

A value of $(D_1^0)_m = 1.35_5 \times 10^{-5} \ cm^2 \ sec^{-1}$ was obtained with $F = 96493 \ C \ equiv^{-1}$, $R = 8.314_6 \times 10^7 \ erg \ deg^{-1} \ mol^{-1}$, $T = 298.16°$, λ_1^0 (choline ion)[9] 38.2 and λ_3^0 (chloride ion)[33] $= 76.35 \ cm^2 \ ohm^{-1} \ equiv^{-1}$. It is seen that the decrease of $(D_1)_m$ as ρ_1 increases from 0.000 to 0.007 g cc^{-1} is greater than its decrease over the entire concentration range studied in this investigation. The dependence of this mutual diffusion coefficient on ρ_1 is seen more clearly in Figure 2, where the data may be compared with the limiting slope predicted by the Onsager-Fuoss theory.[34,35]

The adjustable parameter b in the equation

$$\log y_\pm = -\frac{A[Z_1Z_2]\sqrt{c}}{1 + Ba\sqrt{c}} + bc \quad (11)$$

was found by fitting the above equation to the experimental activity coefficient data of Lindenbaum and Boyd.[36] Equation 5 was used to convert their molal concentrations to molar, and the values of A, B, and a were taken to be 0.5115, 0.3291 × 10^8, and 4 × 10^{-8} cm, respectively.

Theoretical diffusion coefficients over the concentration range 0.001–0.01 M were calculated using the equation of Onsager and Fuoss.[37]

$$D = 16.629 \times 10^{10}T \frac{M}{c}(1 + c \ d \ln y_\pm/dc) \quad (12)$$

where $\bar{M}/c$ is the mobility term and $(1 + c \, d \ln y_\pm/dc)$ is the thermodynamic term and is represented by the dashed line in Figure 2.

Diffusion coefficients were also calculated according to the equation

$$D = D^0(1 + c \, d \ln y_\pm/dc) \qquad (13)$$

D^0 (1.3558×10^{-5} cm² sec⁻¹) was calculated from the limiting equation of Onsager and Fuoss[38] and the thermodynamic term was estimated using the value b of 11 together with eq 6-10-2 and 6-10-3 of ref 29. Since the solutions are very dilute, the density term $c\psi(d)$ was omitted. The results of these calculations are represented by a dotted line in Figure 2. Diffusion coefficients calculated according to eq 13 deviate only slightly from the straight line joining D^0 and the lowest experimentally determined diffusion coefficient.

As $\rho_1 \to 0$ in the ternary system, with ρ_2 constant, $(D_{11})_V$ approaches the tracer diffusion coefficient, $(D_1)_t$, of choline ion for concentration ρ_2 of KCl in water

$$[(D_{11})_V]_{\rho_1 \to 0} \longrightarrow (D_1)_t \qquad (\rho_2 \text{ constant} \neq 0) \quad (14)$$

These data in the $(D_{11})_V - \rho_2^{1/2}$ plane were not available, but the limiting tracer diffusion coefficient

$$[(D_1)]_{\rho_2 \to 0} \longrightarrow (D_1^0)_t \qquad (15)$$

was calculated from the relation[39]

$$(D_1^0)_t = (RT/F^2)\lambda_1^0 \times 10^{-7} \qquad (16)$$

The resulting value, $1.01_7 \times 10^{-5}$ cm² sec⁻¹, is shown in Figure 1.

A description of the graph of $(D_{22})_V$ in Figure 1, showing how it includes the mutual diffusion coefficient, $(D_2)_m$, of H₂O–KCl and the tracer diffusion coefficient, $(D_2)_t$, of potassium ion (or KCl) as limiting cases, is readily obtained from the preceding discussion of $(D_{11})_V$ by changing the word choline to potassium and replacing subscripts 1 by 2 and 2 by 1 (except where numerical values are given). With the additional value λ_2^0 (potassium ion)[33] = 73.50 cm² ohm⁻¹ equiv⁻¹ one may calculate the limiting mutual and tracer diffusion coefficients $(D_2^0)_m = 1.99_4 \times 10^{-5}$ and $(D_2^0)_t = 1.95_6 \times 10^{-5}$, respectively, which are shown on the graph.

In the limits $\rho_1 \to 0$ or $\rho_2 \to 0$ the cross-term diffusion coefficients $(D_{12})_V$ and $(D_{21})_V$, shown in Figure 1, do not reduce to diffusion coefficients which have been commonly measured before. As pointed out previously[8] $(D_{12})_V \to 0$ as $\rho_1 \to 0$ with ρ_2 constant and nonzero, and $(D_{21})_V \to 0$ as $\rho \to 0$ with ρ_1 constant and nonzero. However, in the opposite limiting case for $(D_{12})_V$ or $(D_{21})_V$ each cross-term diffusion coefficient approaches a nonzero value (when both solutes are electrolytes). For example, if first $\rho_2 \to 0$ and then $\rho_1 \to 0$ in approaching infinite dilution, $(D_{12})_V$ for this system approaches the relatively small value[40]

$$\{[(D_{12})_V]_{\rho_1 \to 0}\}_{\rho_2 \to 0} \longrightarrow \frac{RTM_1\lambda_1^0}{F^2M_2}\left[\frac{\lambda_3^0 - \lambda_2^0}{\lambda_3^0 + \lambda_1^0}\right] \times 10^{-7}$$

$$= 0.04_7 \times 10^{-5} \text{ cm}^2 \text{ sec}^{-1} \quad (17)$$

However, if first $\rho_1 \to 0$ and then $\rho \to 0$, $(D_{21})_V$ approaches the much larger value[40]

$$\{[(D_{21})_V]_{\rho_2 \to 0}\}_{\rho_1 \to 0} \longrightarrow \frac{RTM_2\lambda_2^0}{F^2M_1}\left[\frac{\lambda_3^0 - \lambda_1^0}{\lambda_3^0 + \lambda_2^0}\right] \times 10^{-7}$$

$$= 0.24_6 \times 10^{-5} \text{ cm}^2 \text{ sec}^{-1} \quad (18)$$

These limiting values are included in Figure 1.
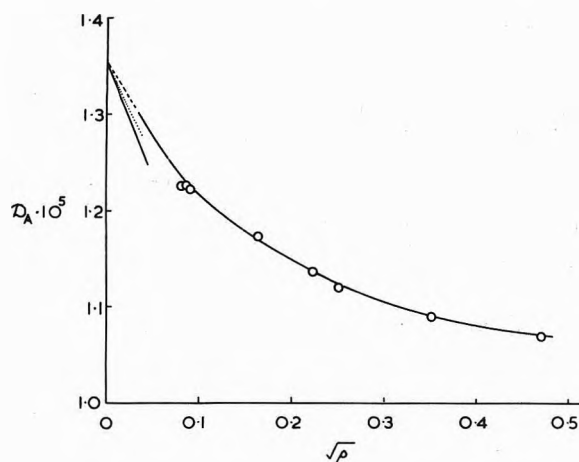
Figure 2. Variation of the mutual diffusion coefficient (as represented by $\mathfrak{D}_A$) of choline chloride at various concentrations in water at 25°. Circles represent experimental data. The solid line in the very dilute region represents values of the mutual diffusion coefficient predicted by the Onsager–Fuoss theory (eq 6-10-6 of ref 29). Units D_A, cm² sec⁻¹; ρ_1, g cc⁻¹. The dotted line represents the mutual diffusion coefficient predicted by 6-10-15 of ref 29, and the dashed line by eq 6-10-3.

The present study was undertaken as part of a series of physical-chemical measurements on solutions containing choline chloride.[42,43] This compound can be prepared in high purity, and it forms stable solutions suitable for accurate measurements. The results in this paper show that the H₂O–choline chloride–KCl system exhibits marked deviations from Fick's first law. For the compositions studied, the relatively large values of $(D_{21})_V$ indicate that a concentration gradient of choline chloride is 15–25% as effective as a gradient of KCl in producing a flow of KCl. Therefore a suitable concentration gradient of choline chloride can cause KCl to flow from a region of lower KCl concentration to a region of higher KCl concentration against an appreciable concentration gradient of KCl. It should be noted that the values of the cross-term diffusion coefficients reported in Table II are for solute flows and concentration gradients expressed in grams in eq 1 and 2. If these quantities were expressed in moles the values of $(D_{21})_V$ would be nearly twice as large, because then they must be multiplied by the molecular weight ratio M_1/M_2 = 1.872₈; the values of $(D_{12})_V$ would be about half as large because then they must be divided by 1.872₈.[40] The addition of other solute components, such as those commonly found in nerve cells, to the present system would cause some change in the values of the diffusion coefficients reported in Table II; also, additional diffusion coefficients[3,5] would be required to describe completely diffusion in the more complicated systems. The present data represented by the three-dimensional graphs in Figure 1 would then represent parts of the graphs for these four diffusion coefficients in more complicated systems.

Supplementary Material Available. Listings of the calculated values of J, $\mathfrak{D}_A$, Q, the refractive index increments, and Table III will appear following these pages in the microfilm edition of this volume of the journal. Photocopies of the supplementary material from this paper only or microfiche (105 × 148 mm, 20× reduction, negatives) containing all of the supplementary material for the papers in this issue may be obtained from the Journals Department, American Chemical Society, 1155 16th St., N.W., Washington, D. C. 20036. Remit check or money order for $3.00

for photocopy of \$2.00 for microfiche, referring to code number JPC-73-2371.

References and Notes

(1) One of us (R. F.) is indebted to the Wellcome Trust (London) for the award of a Travel Grant. This investigation was supported in part by the National Science Foundation (U. S.) Research Grant No. G-179 and by the National Institute of Arthritis and Metabolic Diseases (USPHS) Research Grant No. AM-05177 and career award AM-K6-16,715 (to L. J. G.)
(2) Present address, School of Pharmacy, University of London, London, England.
(3) R. L. Baldwin, P. J. Dunlop, and L. J. Gosting, *J. Amer. Chem. Soc.*, **77**, 5235 (1955).
(4) P. J. Dunlop and L. J. Gosting, *J. Amer. Chem. Soc.*, **77**, 5238 ica, **19**, 1095 (1953).
(5) G. J. Hooyman, *Physica*, **22**, 751 (1956).
(6) G. J. Hooyman, H. Holtan, Jr., P. Mazur, and S. R. de Groot, *Physica*, **19**, 1095 (1953).
(7) J. G. Kirkwood, R. L. Baldwin, P. J. Dunlop, L. J. Gosting, and G. Kegeles, *J. Chem. Phys.*, **33**, 1505 (1960).
(8) I. J. O'Donnell and L. J. Gosting in "The Structure of Electrolytic Solutions," W. J. Hamer, Ed., Wiley, New York, N. Y., 1959, Chapter 11.
(9) H. O. Spivey and F. M. Snell, *J. Phys. Chem.*, **68**, 2126 (1964).
(10) L. A. Woolf, D. G. Miller, and L. J. Gosting, *J. Amer. Chem. Soc.*, **84**, 317 (1962).
(11) Estimated from data given in the "Handbook of Chemistry and Physics," 41st ed, Chemical Rubber Publishing Co., Cleveland, Ohio, 1959, and Heilbron's Dictionary of Organic Compounds, Oxford University Press, New York, N. Y., 1943.
(12) L. J. Gosting, E. M. Hanson, G. Kegeles, and M. S. Morris, *Rev. Sci. Instr.*, **20**, 209 (1949).
(13) P. J. Dunlop and L. J. Gosting, *J. Amer. Chem. Soc.*, **75**, 5073 (1953).
(14) Footnote 27 of ref 15.
(15) D. F. Akeley and L. J. Gosting, *J. Amer. Chem. Soc.*, **75**, 5685 (1953).
(16) R. P. Wendt, Ph.D. Thesis, University of Wisconsin, Madison, Wisconsin, 1961 (Microfilm No. 61-680).
(17) J. Albright, Ph.D. Thesis, University of Wisconsin, Madison, Wisconsin, 1963 (Microfilm No. 63-2878).
(18) L. J. Gosting and H. Fujita, *J. Amer. Chem. Soc.*, **79**, 1359 (1957).
(19) H. Fujita and L. J. Gosting, *J. Phys. Chem.*, **64**, 1256 (1960).
(20) L. G. Longsworth, *J. Amer. Chem. Soc.*, **69**, 2510 (1947).
(21) H. Fujita, *J. Phys. Soc. Jap.*, **11**, 1018 (1956).
(22) Equations 8 and 9 of ref 17 or eq A-5 and A-8 of ref 21.
(23) Method of least squares—Mercury Autocode program P 1000, used on Atlas Computer, University of London.
(24) H. Fujita, *J. Amer. Chem. Soc.*, **83**, 2862 (1961).
(25) See p 173 of ref 8.
(26) See paragraph at end of paper regarding supplementary material.
(27) P. J. Dunlop and L. J. Gosting, *J. Phys. Chem.*, **63**, 86 (1959).
(28) L. J. Gosting, *J. Amer. Chem. Soc.*, **72**, 4418 (1950).
(29) H. S. Harned and B. B. Owen, "The Physical Chemistry of Electrolytic Solutions," 3rd ed, Reinhold, New York, N. Y., 1958.
(30) The mutual diffusion coefficient for a binary liquid system is defined to correspond to a volume-fixed frame of reference so, for any given composition of the system, it will have the same value in Fick's first law written for either the solute or solvent (see ref 31). Because this choice of reference frame is not arbitrary the subscript v is omitted in the symbol $(D_1)_m$; the subscript number after D is included to designate the system considered (1 for H_2O–choline chloride or 2 for H_2O–KCl).
(31) R. P. Wendt and L. G. Gosting, *J. Phys. Chem.*, **63**, 1287 (1959).
(32) For this limiting case where first $(\rho_2/\rho_1) \to 0$ and then $\rho_1 \to 0$ see, for example, eq 11.4 of ref 33.
(33) R. A. Robinson and R. H. Stokes, "Electrolyte Solutions," 2nd ed, Butterworths, London, 1968.
(34) L. Onsager and R. M. Fuoss, *J. Phys. Chem.*, **36**, 2689 (1932).
(35) This limiting slope was computed from eq 6-10-6 of ref 29 with the values 0.008903 P and 78.30 for the viscosity and dielectric constant, respectively, of water at 25°.
(36) G. E. Boyd, A. Schwartz, and S. Lindenbaum, *J. Phys. Chem.*, **70**, 821 (1966).
(37) Equation 4-4-24 of ref 29.
(38) Equation 6-10-5 of ref 29.
(39) For this case where first $(\rho_1/\rho_2) \to 0$ and then $\rho_2 \to 0$ see, for example, 18 and 23 of ref 8 or the first term on the right of eq 6-10-13 of ref 29.
(40) Relations 17 and 18 were obtained by taking the appropriate limits of eq 19 and 20 of ref 8, after first multiplying the latter equations by ratios of the solute molecular weights so they will give diffusion coefficients corresponding to grams instead of moles (see ref 41). When the equations of ref 8 were derived, only the requirements of electroneutrality and zero net electric current were considered; hence the electrophoretic effect, the time of relaxation effect, and the effects of changes of activity coefficients with concentrations were neglected. These effects should not influence relations 17 and 18 for infinite dilution, but they may contribute substantially to values of the $(D_{ij})_v$ as the solute concentrations are increased. Because the electrolyte concentrations used in this investigation are relatively high, no comparison is included of the $(D_{ij})_v$ reported in Table II with values predicted from the equations of ref 8.
(41) See the footnote to Table 3 of ref 8.
(42) R. Fleming, *J. Chem. Soc.*, 946 (1966).
(43) R. Fleming, *J. Chem. Soc.*, 3100 (1961).

Viscosity Behavior of Solutions of Sodium Tetraphenylboron and Its Glyme Complexes in Ethereal Solvents

J. Smid*

Chemistry Department, The State University of New York, College of Environmental Science and Forestry, Syracuse, New York 13210

and A. M. Grotens

Department of Physical Chemistry, University of Nymegen, Nymegen, The Netherlands (Received March 22, 1973)

Densities and viscosities of solutions of $NaBPh_4$ in tetrahydrofuran and 2-methyltetrahydrofuran were measured as a function of salt concentration and temperature. The concentration dependence of the viscosity can best be described by the Vand equation for the viscosity of concentrated dispersions, the moving entity being a solvent-separated ion pair the shape of which can be approximated by a prolate elipsoid of axial ratio 2. Between 0.05 and 0.5 m $NaBPh_4$ in THF at 20° the ratio $c_m/\log \eta_r$ is nearly constant. The effective volume $V_e°$ of the flowing unit was found to be 0.72 M^{-1} at 20°, and increases at lower temperature according to the relationship $\log V_e° = -0.613 + 138/T$. A $V_e°$ value of 0.72 M^{-1} is consistent with conductance data on $NaBPh_4$ solutions which show that $NaBPh_4$ is a solvent-separated ion pair in THF. Approximately six THF molecules may be bound to the Na^+ ion. On addition of glymes (*e.g.*, hexaethylene glycol dimethyl ether or glyme 7) the THF solvation shell is replaced by the glyme, and a plot of η *vs.* the glyme to salt ratio shows a distinct break at a ratio of unity. Crystalline 1:1 complexes of $NaBPh_4$ with glyme 5, glyme 6, and glyme 7 were obtained, as well as a 2:1 complex with glyme 4.

In the course of a study dealing with the broadening of [23]Na nuclear magnetic resonance lines of solvation complexes of sodium salts in ethereal solvents[1] it became necessary to measure the viscosity of the salt solutions over a wide range of temperature and concentration. Data pertaining to the viscosity of electrolyte solutions in media where ion pairs are the predominant species, *e.g.*, tetrahydrofuran, are scarce. Such data are important in order to test previously made assumptions regarding the concentration and temperature dependence of the viscosity of these salt solutions and their ultimate effects on the widths of alkali nmr absorption lines.[2,3]

In this paper the results are reported of a series of viscosity measurements on 0.05–0.7 M solutions of sodium tetraphenylboron in tetrahydrofuran (THF) over a temperature range from +20 to −70°. A few experiments were carried out in 2-methyltetrahydrofuran (MTHF). Also included are data showing the viscosity change of a salt solution on addition of small quantities of the cation coordinating polyglycol dimethyl ether glyme 7. A plot of viscosity *vs.* the molar ratio of glyme to salt provides information about the stoichiometry of the salt–glyme complex. In the course of this work, several stoichiometric glyme complexes of sodium tetraphenylboron were isolated in the solid state, including a crystalline complex of $NaBPh_4$ with two molecules of $CH_3O(CH_2CH_2O)_3CH_3$ (glyme 4).

Experimental Section

Sodium tetraphenylboron (Fisher, 99.9% purity) was used without further purification. Tetrahydrofuran, 2-methyltetrahydrofuran, and the polyglycol dimethyl ethers (glyme 4, 5, 6, and 7, the number referring to the number of *oxygen* atoms in the glyme) were dried over sodium potassium alloy and distilled off under vacuum.[4]

Densities. The densities of the salt solutions were determined with a pycnometer of approximately 5 ml to which a calibrated true bore stem was attached. The pycnometer was calibrated with mercury.

Viscosities. Salt solutions were prepared at 20° by weighing the appropriate amount of salt in a 25-ml volumetric flask, then adding the purified solvent up to the 25 ml mark and weighing the solution. From this the molar and molal concentrations were calculated. The salt solution each time was carefully filtered through a glass filter into an Ubbelohde viscometer and placed in a constant temperature bath in which the temperature variation was kept within 0.1°. Measurements of flow times were repeated until the average deviation in three consecutive readings amounted to less than 0.2 sec, the accuracy of the readings being 0.1 sec. Flow times varied from 100 to 600 sec, and were taken at approximately 10° intervals. When dealing with mixtures of sodium tetraphenylboron and glyme the flow time of a 0.2 M salt solution was first measured in the absence of glyme. Then small aliquots of pure glyme were added from a microburet to a known quantity of the salt solution in the viscometer, and after each addition and thorough mixing the flow time was measured. The respective densities of the glyme–salt solutions were also measured.

Solid Glyme–Salt Complexes. In a typical experiment, 250 mg of $NaBPh_4$ and about 0.4 ml of glyme 7 were dissolved in a few ml of tetrahydropyran at about 50°. Upon standing in the refrigerator crystals formed in the solution which were filtered off and dried under vacuum at 50°. The composition of the solids was determined by ^{1}H nmr in $CDCl_3$. When using glyme 5, 6, or 7 the molar glyme to salt ratio in the starting mixture was about 2:1. For glyme 4, which was found to form a 2:1 complex with $NaBPh_4$,

the molar ratio in solution was about 4:1. The crystalline complexes can also be obtained by dissolving the salt–glyme mixture in THF, diluting the solution close to the precipitation point with hexane, followed by cooling.

Results and Discussion

The densities of the salt solutions in THF as a function of temperature were found to fit the relationship $d_t{}^S = d_{20}{}^S + a(20 - t)$, where $d_{20}{}^S$ denotes the density of the salt solution at 20°, t is the temperature in °C, and a is a constant. The relationship is graphically depicted for a few systems in Figure 1, and values of $d_{20}{}^S$ and of a are given in Table I. The a values calculated from the respective slopes of the density $vs.$ temperature plots reproduce the experimentally observed densities to within 0.1%. The temperature coefficient of the density appears to decrease at higher salt concentrations, possibly due to a closer packing of solvent molecules as more THF molecules become bound to Na^+ ions.

The dependence of the density on the salt concentration, also shown in Figure 1, can be described by the relationship $d_s = d_0 + bc$, where d_0 is the density of the pure solvent and c denotes the molar concentration. At 20° the constant b is equal to 0.118 g ml^{-1} M^{-1}. From the densities the apparent molal volume can be calculated by means of the equation $\phi_v = 1000(d_0 - d_s)/cd_0 + M_2/d_0$, where M_2 is the molecular weight of the salt.[5] The observed linear relationship between the density and the molar salt concentration implies that the apparent molal volume ϕ_v is independent of c and equal to $\phi_v = (M_2 - 1000b)/d_0$, the constant b representing the slope of the density $vs.$ concentration plot.[6] At 20° the apparent molal volume is calculated to be 252 ml. Although ϕ_v is often found to depend on the square root of the concentration,[7] the constancy of ϕ_v for $NaBPh_4$ in THF is not unique and has also been found in other systems, $e.g.$, for sodium salts in formamide.[6]

The ϕ_v value of 252 ml is about 10% lower than that found for $NaBPh_4$ in H_2O, where $\phi_v = 277$ ml.[8] The lower volume in THF can probably be attributed to the ion pair state of the ionic species. Such a decrease has been found for other salts on changing to solvents where ion pairs are predominant.[8]

$Viscosities.$ The temperature dependence of the viscosities of the salt solutions in THF is shown in Figure 2 as plots of log η $vs.$ $1/T$. Linear relationships are obtained over the indicated temperature ranges (the measurements at higher concentrations were limited to the higher temperatures due to precipitation). The respective values of the slopes and intercepts are reported in Table II, together with the activation energies of viscous flow, $E\eta$. The viscosities can be reproduced from the respective equations to about 0.1%.

The concentration dependence of the reduced viscosity of electrolyte solutions has been successfully described in both aqueous and nonaqueous media by the Jones–Dole equation $\eta_r = 1 + A(c)^{1/2} + Bc$, where the coefficient A can be calculated from the Debye–Hückel theory and B is an empirical constant which qualitatively may be interpreted in terms of ion–solvent interactions.[9] In most of the systems where this relationship is obeyed, the dielectric constant of the medium, or the nature or concentration of the salt, is such that mainly free ions are the moving ionic entities.[10-14] The situation is less clear when ion pair formation becomes an important factor. For sodium iodide in monohydric alcohols up to hexanol the Jones–
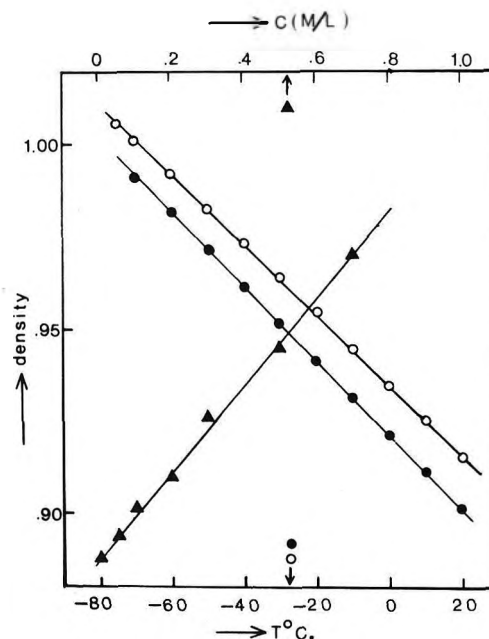
Figure 1. Temperature ($\bullet$,$\circ$) and concentration ($\blacktriangle$) dependence of the densities (in g/ml) of $NaBPh_4$ solutions in THF: ($\blacktriangle$), $T = 20°$; ($\bullet$), 0.1 M $NaBPh_4$ at 20°; ($\circ$). mixture of 0.2 M $NaBPh_4$ and 0.2 M glyme 7 at 20°.

TABLE I: Temperature Dependence of the Densities of Solutions of $NaBPh_4$ in Tetrahydrofuran^a

[NaBPh$_4$],^{b} M	$d_{20}{}^S$, g/ml	$a \times 10^3$, g ml^{-1} deg^{-1}	Temp range
0^c	0.888	1.01	−70 to 20
0.05	0.894	1.02	−70 to 20
0.1	0.901	1.01	−70 to 20
0.2	0.9095	0.97	−40 to 20
0.3	0.9255	0.99	−20 to 20
0.5	0.944	0.93	0 to 20
0.7	0.970	0.86	20 to 40
0.2^d	0.916	0.95	−75 to 20

^{a} Experimental points were fitted to the equation $d_t{}^S = d_{20}{}^S + a(20 - t)$. ^{b} Molar concentrations at 20°, accurate to 0.1%. ^{c} Data taken from ref 18. ^{d} A mixture of 0.2 M $NaBPh_4$ and 0.2 M glyme 7 in THF.

Dole equation was found to be applicable up to 0.2 M salt.[15] In these systems, at least in hexanol ($\epsilon = 13$), ion pairs are likely to exist although no attempts were made to identify the species. In other cases such as potassium iodide in methanol a plot of $\eta_{sp}c^{-1/2}$ $vs.$ $c^{1/2}$ reveals two linear regions.[15,16]

It has been argued[17] that ion pair formation considerably lowers the B coefficient, especially in systems with a high positive B value. For $NaBPh_4$ the respective dissociation constants in THF and MTHF at 20° are 8.8×10^{-5}[18] and 1.7×10^{-5} M.[19] Hence, in the concentration region of our measurements (0.05–0.7 M) ion pairs are the main ionic species. Plots of $\eta_{sp}/c^{1/2}$ $vs.$ $c^{1/2}$, and of η_r $vs.$ c strongly curve upward above 0.1 M $NaBPh_4$ and it is clear that additional concentration terms of higher power must be used to fit the data over the entire concentration range. For an equation of the form $\eta_r = 1 + A'c + A''c^2 + A'''c^3$ one finds for $NaBPh_4$ in THF at 20° the relationship $\eta_r = 1 + 3.21c - 6.65c^2 + 20.0c^3$, c being the molar concentration. Agreement between calculated and experimental viscosities between 0.05 and 0.7 M is better than

TABLE II: Temperature Dependence of the Viscosity of Sodium Tetraphenylboron Solutions in THF and MTHF at Different Salt Concentrations.^{a,b}

[Na$^+$ BPh$_4^-$],^{c} M	Temp range, °C	K (η in P)	S	E_η, kcal
(THF)	−70 to 20	−3.655	393	1.8
0.05	−70 to 20	−3.673	412	1.88
0.1	−70 to 20	−3.741	445	2.04
0.2	−40 to 20	−3.790	487	2.23
0.3	−20 to 20	−3.888	546	2.5
0.5	0 to 20	−4.028	657	3.0
0.7	20 to 40	−4.352	842	3.86
0.2 (GL-7)	−75 to 20	−3.805	497	2.28
(MeTHF)	−75 to 25	−3.635	386	1.78
0.2	−40 to 60	−4.049	513	2.36
0.2 (GL-7)	−40 to 60	−3.715	481	2.22
0.05 (GL-5)	−50 to 40	−3.700	417	1.92
0.2 (GL-5)	−40 to 40	−3.712	468	2.15
0.4 (GL-5)	−40 to 40	−4.023	636	2.92

^{a} K and S denote the respective intercepts and slopes of the equation log η = K + S/T (see Figures 2 and 4). ^{b} The data for THF and MeTHF were taken from T. E. Hogen Esch and J. Smid, *J. Amer. Chem. Soc.*, **88**, 318 (1966), and from ref 19, respectively. Salt concentrations are given at 20°, and the notation GL-5 or GL-7 refers to mixtures in which equal molar quantities of salt and glyme 5 or glyme 7 are present. ^{c} Molar concentrations at 20°, accurate to 0.1%.

1%. Other equations such as η_r = 1 + 2.2c + 1.9c^2 + 14.1c^4 also reproduce the data to better than 1%. Hence, the values of the respective A coefficients strongly depend on the chosen expression.

Recently, Eagland and Pilling suggested another approach to treat the viscosity of concentrated electrolyte solutions, *viz.*, by applying the Vand equation for the viscosity of concentrated dispersions.[20] For spherical particles Vand obtained the relationship ln η_r = 2.5ϕ/(1 − $k\phi$) where ϕ is the volume fraction occupied by the particles and k is a particle interaction constant.[21] The moving entity in the NaBPh$_4$–THF system is a solvent-separated ion pair, and conductance data show that the two free ions are of nearly identical size.[18] The shape of the moving ion pair is of course not spherical, but it may in first approximation be represented by a prolate ellipsoid of axial ratio 2.0. For ellipsoids of revolution the constant 2.5 in the Vand equation is replaced by a constant a_1^9 which was found to depend only on the axial ratio.[22,23] The value of a_1 is calculated to be 2.90 for a prolate ellipsoid of axial ratio 2.0. By substituting ϕ = cV_e and rearranging the Vand equation as suggested by Eagland and Pilling[20] one obtains the expression

$$\frac{c}{\log \eta_r} = \frac{2.3}{2.9 V_e} - \frac{2.3kc}{2.9} \qquad (1)$$

In this equation c denotes the molar concentration of the salt in THF and V_e the molar volume of the solvated ion pair. The latter quantity has been referred to as the "effective volume of the flowing unit"[20,24] and has been found to depend on c,[24] but its limiting value $V_e°$ at $c \rightarrow 0$ can be obtained from a plot of $c/\log \eta_r$ *vs.* c.[20]

We calculated the ratio $c/\log \eta$ as a function of c at the respective temperatures. The quantity decreases approximately linearly with c, at least above −40°. If molal (c_m) instead of molar concentrations are used in the calculation[20] the ratios are nearly constant over the entire concentration range. Values for $c_m/\log \eta_r$ are collected in Table III. At the very low temperatures only a few data
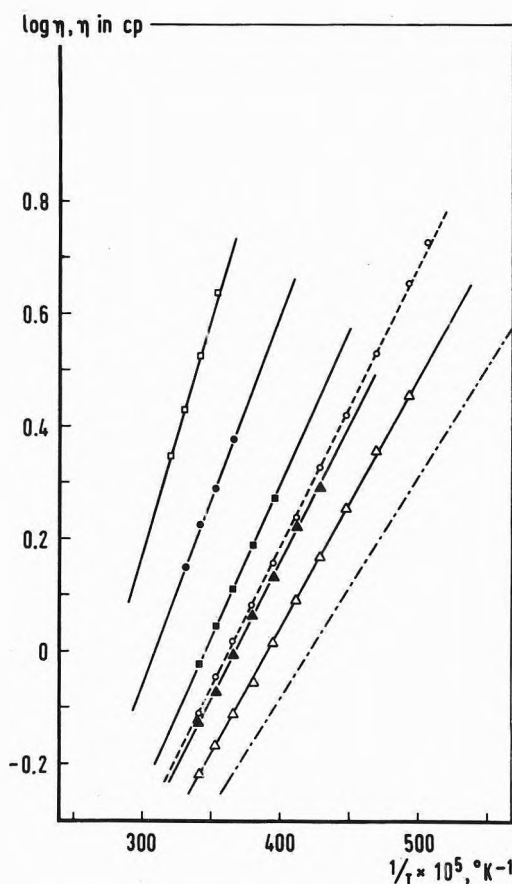
Figure 2. Plots of log η *vs.* 1/T for NaBPh$_4$ solutions in THF: (−·−) pure THF, from ref 18; (△) = 0.1 M; (▲) 0.2 M; (○) 0.2 M NaBPh$_4$ + 0.2 M glyme 7; (■) 0.3 M; (○) 0.5 M; (□) = 0.7 M.

are available and the corresponding $c_m/\log \eta_r$ ratios are therefore less reliable.

The limiting values of the effective flowing unit, $V_e°$, were calculated by means of eq 1, using the average value of $c_m/\log \eta_r$ and converting this ratio to molar concentration units (for $c \rightarrow 0$, c = c_m × density of THF). The results are given in the last column of Table III and show that $V_e°$ gradually increases as the temperature is lowered. Also, the values are nearly identical with those obtain from the intercepts of $c/\log \eta_r$ *vs.* c plots (see bracketed values in last column of Table III).

The value of 720 ml/mol for $V_e°$ of NaBPh$_4$ in THF appears to be very reasonable. For a prolate ellipsoid of axial ratio 2.0 a molar volume of 720 ml is obtained when the minor semiaxis is 5.2 Å. If we consider the ion pair as consisting of two spherical ions of radii 5.2 Å, then 1 mol of ion pairs occupies a volume of 705 ml, very close to what is found experimentally. The Stokes radii for the solvated Na$^+$ ion and for the BPh$_4^-$ ion, calculated from conductance data, were found to be 3.95 and 4.35 Å, respectively.[18] However, the Stokes radii are usually underestimated for ions less than 5 Å. Actually, the value of 5.2 Å is in between the estimated radii derived from molecular models[25] for N$^+$Bu$_4$ (4.94 Å) and for N$^+$Am$_4$ (5.29 Å). And the mobilities of these two ions are close to that of BPh$_4^-$ (Λ_0^- for BPh$_4^-$ is equal to Λ_0^+ for (i-Am)$_3$BuN$^+$, see ref 26).

Since $V_e°$ is the molar volume of the solvated ion pair, the number of solvent molecules bound to the Na$^+$ ion can be estimated[9] by dividing the difference between $V_e°$

TABLE III: Values of the Ratio $c_m/\log \eta_r$ and of $V_e°$ for NaBPh$_4$ in THF

	[NaBPh$_4$] in THF,[a] m							
T, °C	0.0572	0.116	0.238	0.365	0.648	0.960	$V_e°$, M^{-1}[b]	
			Values of $c_m/\log \eta_r$					
20	1.23	1.20	1.27	1.26	1.22	1.15	0.72 ± 0.02	(0.715)
10	1.14	1.16	1.21	1.19	1.17		0.755 ± 0.02	(0.74)
0	1.14	1.11	1.13	1.12	1.10		0.78 ± 0.01	(0.775)
−10	1.08	1.08	1.05	1.06			0.81 ± 0.01	(0.80)
−20	1.04	1.00	1.02	0.98			0.85 ± 0.02	(0.835)
−30	0.94	0.93	0.92				0.915 ± 0.01	(0.910)
−40	0.92	0.86	0.91				0.935 ± 0.02	(≈ 0.980)
−50	0.83	0.805					1.02 ± 0.02	(1.01)
−60	0.82	0.70					1.09 ± 0.08	
−70	0.76	0.66					1.15 ± 0.08	

[a] The corresponding molar concentrations at 20° are 0.05, 0.1, 0.2, 0.3, 0.5, and 0.7 M. [b] Calculated from eq 1 using the average value of the ratio $c_m/\log \eta_r$, ($c = c_m \times$ density of THF for $c \to 0$). The $c_m/\log \eta_r$ value at 20° for 0.7 M salt concentration was not used in calculating the average at 20°. The values given in parentheses were obtained from the intercepts of $c/\log \eta_r$ vs. c plots.
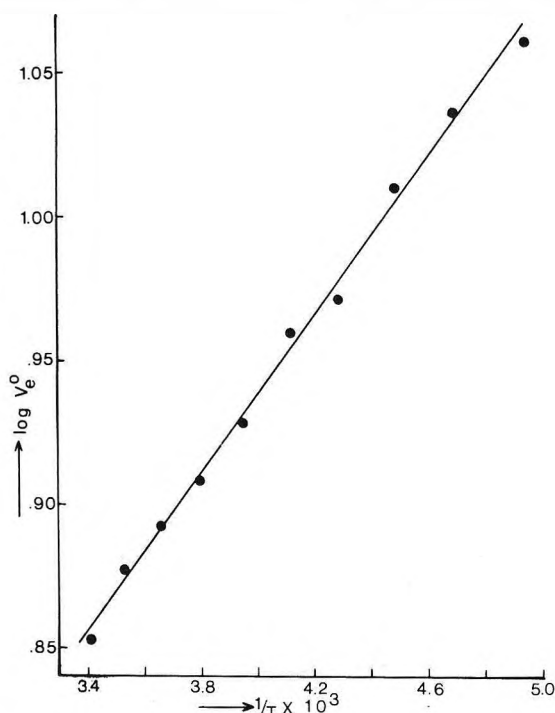
Figure 3. Plot of log $V_e°$ vs. $1/T$ for NaBPh$_4$ in THF, $V_e°$ being the limiting value of the flowing unit.

and the apparent molal volume of the unsolvated NaBPh$_4$ (252 ml) by the molar volume of THF (81 ml at 20°). This comes close to six molecules of THF per Na$^+$, BPh$_4$$^-$ ion pair. It has been reported that four THF molecules bind to sodium tetraalkylaluminum on addition of small quantities of THF to this salt in hydrocarbon solvents.[27] In pure THF this number is likely to increase, as the interaction is essentially an ion–dipole interaction and not restricted to a tetrahedral configuration. With six THF molecules a more or less octahedral arrangement may sterically be the most favorable. The strong binding of two glyme 4 molecules to NaBPh$_4$ (see below) indicates that certainly more than four oxygen atoms may coordinate with a Na$^+$ ion if a proper arrangement of the solvent molecules around the Na$^+$ ion permits it.

A plot of log $V_e°$ vs. $1/T$ yields a good straight line (see Figure 3) described by the relationship log $V_e° = -0.613 + 138/T$. The increase in $V_e°$ on lowering the temperature

was also observed for tetraalkylammonium salts in water,[20] and suggests an enlargement of the solvated ion pair, most likely due to enhanced ion–solvent interactions. This agrees with the trend found for the Stokes radii of the free ions, which for Na$^+$ in THF changes from 3.95 Å at 25° to 4.4 Å at −50°,[18] an increase similar to that found when the ionic radius is calculated from $V_e°$ (i.e., a change from 5.2 Å at 20° to 5.9 Å at −50°).

The activation energy for viscous flow is concentration dependent (see Table III), changing from 1.8 kcal for pure THF to 3.86 kcal for 0.7 M NaBPh$_4$ in THF. A plot of E_η vs. the molal concentration c_m yields a straight line, dE/dc_m being 2 kcal/m. An increase of E_η with salt concentration is not unexpected and has been found in other systems.[14]

Care should be used in applying the linear log η − $1/T$ relationship beyond the indicated temperature ranges. The ion pair structure may change at higher temperatures from a loose to a tight ion pair,[4a,19,28] and this in turn is likely to affect $V_e°$. For example, conductance measurements reveal a substantial increase in the exothermicity of the dissociation of NaBPh$_4$ in MTHF above −20°, suggesting formation of a considerable fraction of tight NaBPh$_4$ ion pairs.[19] We therefore checked the temperature dependence of the viscosity of a 0.2 M NaBPh$_4$ solution in MTHF, but, as shown in Figure 4 and Table II, the log η vs. $1/T$ plot is linear down to −40°. Apparently, the volume of the flowing unit is not significantly altered by the change in ion pair structure, possibly because the anion is large and the cation is still externally solvated. A salt such as NaBH$_4$ may show a more pronounced change in its volume $V_e°$. It is unlikely that the observed deviation from linearity below −40° is caused by a change in the solvation state of the ion pair, as it is also found in MTHF solutions of glyme 5–NaBPh$_4$ complexes (Figure 4). These complexes are loose ion pairs over the entire temperature range. The stronger than normal increase in viscosity at low temperature appears to be more pronounced at higher salt concentrations, and aggregation of ion pairs may be a likely cause. Formation of these aggregates is of course facilitated by the lower polarity of MTHF. It is also worth pointing out that activation energy plots of some of the pure ether solvents reveal a considerable curvature, e.g., the higher glymes.[3] Even for MTHF a rather abrupt increase in E_η is observed,[29] its value changing from 1.8 kcal above −100° to 3.6 kcal below this temperature.

Figure 4. Plots of log η vs. $1/T$ for $NaBPh_4$ solutions in MTHF: (----) pure MTHF, from ref 19; ($\triangle$) 0.05 M $NaBPh_4$/glyme 5; (●) 0.2 M $NaBPh_4$, log η values on graph lowered by 0.1; (○) 0.2 M $NaBPh_4$/glyme 5; (▲) 0.4 M $NaBPh_4$/glyme 5.

Figure 5. Plot of viscosity in cP vs. the molar ratio of glyme 7 to $NaBPh_4$ in THF at 20°. Init al salt concentration 0.2 M.

The parameter a_1 in the Vand equation for spherical or nonspherical particles has been correlated with the B coefficient in the Jones-Dole equation by the expression $B = a_1 V_e°$.[9,20,24] This makes the B coefficient in our system at 20° equal to 2.9 × 0.72 = 2.1 To obtain an experimental B value viscosity measurements are needed at lower salt concentrations. A few experiments were carried out in THF below 0.1 M $NaBPh_4$ and a η_r vs. c plot yielded a straight line with slope 2.0 ± 0.3. However, more accurate measurements are required to arrive at reliable B values.

The results described above demonstrate that above 0.1 M salt concentration the assumption of a proportionality between η_r and c[2,3] is not a valid one in these systems. The same must be said for the assumed temperature independence of the B coefficient.[2,3] Concentration terms higher than c become very significant, and the increase of $V_e°$ on lowering the temperature implies that the constant B has a negative temperature coefficient. The picture is further complicated by the possibility of ion pair aggregation at low temperature in less polar solvents. This is likely to be a more serious problem when dealing with salts of aromatic radical anions[3] or of carbanions,[30] due to the planar structure of the anion.

Glyme Complexes of Sodium Tetraphenylboron. Linear polyglycol dimethyl ethers are known to form stoichiometric complexes with either free alkali ions or alkali ion pair salts in ethereal solvents.[4b,31,32] Mixing glymes with tight ion pairs produces a mixture of externally glymated tight ion pairs and glyme separated ion pairs.[4,31] As stated earlier, sodium tetraphenylboron in THF is a loose ion pair. On addition of glyme 7, the boron salt remains a loose ion pair (e.g., essentially no change in conductance is observed). However, the presence of glyme 7 leads to a considerable broadening of the ^{23}Na nmr line, demonstrating

that THF molecules in the solvation shell of the Na^+ ion have been replaced by glyme 7.[1]

The addition of the viscous glyme 7 to THF should result in a measurable increase in the viscosity of the solution. On the other hand, if glyme 7 replaces the solvation shell of the Na^+ ion, the actual size of the moving ion pair is not substantially altered. Assuming a high complexation constant, little change in the viscosity is expected until the glyme to salt ratio exceeds the stoichiometry of the complex. Beyond this point the free glyme which now accumulates in the solution should enhance the viscosity. A plot of viscosity vs. the ratio glyme/$NaBPh_4$ may therefore provide information about the stoichiometry of the complex.

To check this hypothesis we measured the viscosity of a 0.2 M $NaBPh_4$ solution in THF in the presence of increasing quantities of glyme 7. The results, shown in Figure 5, reveal a slight increase in the viscosity of the mixture below a ratio of glyme 7 to $NaBPh_4$ equal to unity, followed by a much more rapid increase beyond this ratio. In the latter region the increase in viscosity is not much different from that found on addition of comparable quantities of glyme 7 to THF in the absence of salt (actually, both slopes in Figure 5 should be slightly higher because the successive additions of pure glyme to the 0.2 M salt solution gradually decreases the salt concentration; the total decrease is less than 10% and does not affect our argument). These results again demonstrate that glyme 7 replaces THF molecules around the alkali ion, that the flowing unit is not significantly changed in size, and that a 1:1 glyme 7-$NaBPh_4$ complex is formed.

We succeeded in isolating a number of pure crystalline glyme-$NaBPh_4$ compounds by a procedure outlined in the Experimental Section. The complexes, analyzed in $CDCl_3$ by proton nmr, contain no residual solvent molecules, and have exact 1:1 stoichiometries for the following combinations: $NaBPh_4$-glyme 7 (mp 118-120°), $NaBPh_4$-glyme 6 (mp 125-127°), and $NaBPh_4$-glyme 5, the latter one giving a diffuse melt at 155-160° that appears to contain solid $NaBPh_4$. With glyme 4 a sharp melting compound (mp 131-132°) containing two glyme 4 molecules is formed. The latter result is not unexpected, since kinetic studies on the glyme 4-polystyrylsodium system in tetrahydropyran[33] have provided evidence that the free sodium ion is solvated with two glyme 4 molecules. For potassium salts 2:1 glyme-ion pair complexes were detect-

ed with both glyme 4 and glyme 5.[4b] It would be interesting to check whether in the $NaBPh_4$–$(glyme 4)_2$ complex all eight oxygen atoms or only six are coordinated to the Na^+ ion.

Preparation of single crystals of radical anion salts such as sodium biphenyl with glyme 4 and glyme 5 have recently been reported.[34] For glyme 4 with Na^+, biphenyl$^-$ a composition $Na_2Bp_2(G4)_5$ was found. Since these complexes were formed by cooling 0.5–1.0 M solutions in the *pure* glyme solvents, some free glyme may have been present in the solids.[35] Complexes of glymes with $HgCl_2$ have also been reported, such as a 2:1 $HgCl_2$–glyme 7 complex (with ethyl instead of CH_3 groups at the end of the chain) and a 1:1 complex with glyme 5.[36] X-Ray studies of the crystal structure of the latter complex shows the glyme 5 molecule to be nearly circular, the oxygen atoms being coplanar with the Hg.

At 0.2 M concentration the glyme 5 and glyme 7 complexes of $NaBPh_4$ in THF and MTHF are stable, but this is not certain for the 2:1 glyme 4 complex. Viscosity measurements at different glyme 4 to $NaBPh_4$ ratios in THF show a similar pattern as found for glyme 7 (see Figure 5), the break in the viscosity plot occurring at a glyme to salt ratio of about unity. Conductance measurements on $NaBPh_4$[37] and kinetic measurements on sodium carbanion salts,[33,38] both carried out in mixtures of THF or THP and glyme 4, suggest that at glyme 4 concentrations below 0.1 M the ion pair is complexed to only one glyme 4 molecule.

In conclusion, we have found that viscosity measurements can provide valuable information on the solvation state of ion pairs in media where ion pairs are the predominant species. The use of the Vand equation for the viscosity of concentrated dispersions appears to provide a reasonable approach to describe the viscosity behavior of these ion pair solutions.

References and Notes

(1) A. M. Grotens, J. Smid, and E. de Boer, *Chem. Commun.*, **759** (1971).
(2) B. M. P. Hendriks, G. W. Canters, C. Corvaja, J. W. M. de Boer, and E. de Boer, *Mol. Phys.*, **20**, 193 (1971).
(3) G. W. Canters, *J. Amer. Chem. Soc.*, **94**, 5230 (1972).
(4) (a) T. E. Hogen Esch and J. Smid, *J. Amer. Chem. Soc.*, **88**, 307 (1966); (b) L. L. Chan, K. H. Wong, and J. Smid, *ibid.*, **92**, 1955 (1970).
(5) H. S. Harned and B. B. Owen, "The Physical Chemistry of Electrolyte Solutions," 3rd ed, Reinhold, New York, N. Y., 1958, p 358.
(6) P. Bruno and M. D. Monica, *J. Phys. Chem.*, **76**, 3034 (1972).
(7) D. O. Masson, *Phil. Mag.*, **8** (7), 218 (1929).
(8) W. G. Gilkerson and J. L. Stewart, *J. Phys. Chem.*, **65**, 1465 (1961).
(9) R. H. Stokes and R. Mills, "Viscosities of Electrolytes and Related Properties," Pergamon Press, New York, N. Y., 1965.
(10) D. Fu Tai-Tuan and R. M. Fuoss, *J. Phys. Chem.*, **67**, 1343 (1963).
(11) R. L. Kay, T. Vituccio, C. Zawoyski, and D. F. Evans, *J. Phys. Chem.*, **70**, 2336 (1966).
(12) D. Feakins and K. G. Lawrence, *J. Chem. Soc. A*, 212 (1966).
(13) K. Crickard and J. F. Skinner, *J. Phys. Chem.*, **73**, 2060 (1969).
(14) F. J. Millero, *J. Phys. Chem.*, **72**, 3209 (1968).
(15) J. P. Bare and J. F. Skinner, *J. Phys. Chem.*, **76**, 434 (1972).
(16) G. Jones and H. J. Fornwalt, *J. Amer. Chem. Soc.*, **57**, 2041 (1935).
(17) C. W. Davis and V. E. Malpass, *Trans. Faraday Soc.*, **60**, 2075 (1964).
(18) C. Carvajal, K. J. Töile, J. Smid, and M. Szwarc, *J. Amer. Chem. Soc.*, **87**, 5548 (1965).
(19) D. Nicholls, C. Sutphen, and M. Szwarc, *J. Phys. Chem.*, **72**, 1021 (1968).
(20) D. Eagland and G. Pilling, *J. Phys. Chem.*, **76**, 1902 (1972).
(21) V. Vand, *J. Phys. Chem.*, **52**, 277 (1948).
(22) R. Simka, *J. Phys. Chem.*, **44**, 25 (1940).
(23) R. Eisenschitz, *Z. Phys. Chem. A*, **103**, 133 (1933).
(24) B. R. Breslau and I. F. Miller, *J. Phys. Chem.*, **74**, 1056 (1970).
(25) R. A. Robinson and R. H. Stokes, "Electrolyte Solutions," Butterworths, London, 1959, p 125.
(26) M. A. Coplan and R. M. Fuoss, *J. Phys. Chem.*, **68**, 1177 (1964).
(27) E. Schaschel and M. C. Day, *J. Amer. Chem. Soc.*, **90**, 503 (1968).
(28) J. Smid, *Angew Chem., Int. Ed. Engl.*, **11**, 112 (1972).
(29) L. J. Giling, Ph.D. Thesis, University of Amsterdam, The Netherlands, 1972, p 21.
(30) U. Takaki, T. E. Hogen Esch, and J. Smid, *J. Phys. Chem.*, **76**, 2152 (1972).
(31) R. V. Slates and M. Szwarc, *J. Amer. Chem. Soc.*, **89**, 6043 (1967).
(32) E. M. Arnett, H. C. Ko, and C. C. Chao, *J. Amer. Chem. Soc.*, **94**, 4776 (1972).
(33) M. Shinohara, J. Smid, and M. Szwarc, *J. Amer. Chem. Soc.*, **90**, 2175 (1968).
(34) G. W. Canters, A. A. K. Klaassen, and E. de Boer, *J. Phys. Chem.*, **74**, 3299 (1970).
(35) A recent X-ray analysis has shown that the composition of the sodium biphenyl–glyme 4 complex is $NaBp(G4)_2$ (two molecules per unit cell). B. M. P. Hendriks, private communication.
(36) R. Iwamoto, private communication.
(37) M. Shinohara, Ph.D. Thesis, State University of New York, College of Forestry, Syracuse, N. Y., 1969.
(38) J. M. Ginn and K. J. Ivin, *Makromol. Chem.*, **139**, 47 (1970).

Dielectric Characterization of Lecithins in Media of Differing Dielectric Constants

Bernard E. Pennock,* David E. Goldman, George K. Chacko, and Stephen Chock

Department of Physiology and Biophysics, The Medical College of Pennsylvania, Philadelphia, Pennsylvania 19129 (Received March 8, 1973)

The dielectric constant and conductivity of lecithin and diacetyllecithin solutions were determined at several concentrations in solvents of differing dielectric constant and at frequencies from 0.5 to 250 MHz. These data were shown to fit the general formula $\epsilon^* = \epsilon_\infty + (\epsilon_0 - \epsilon_\infty)/\{1 + [j(f/f_c)]^{1-\alpha}\}$, where ϵ^* is the complex dielectric constant, ϵ_0 and ϵ_∞ are the low- and high-frequency dielectric constants, f is the frequency, f_c is a generalized characteristic frequency, and α is a constant, $0 < \alpha < 1$. A linear dependence of the low-frequency dielectric constant on concentration was also found. These two results permitted a complete description of the data in terms of characteristic frequency and dielectric increment which are indices of molecular size and dipole length. The values for these parameters were consistent with the known structure of lecithin in high dielectric constant media ($\epsilon > 30$). However, the dielectric increment was found to decrease with decreasing solvent dielectric constant. This is interpreted as an increase in dipole–dipole interaction to produce small molecular aggregates.

Introduction

Previously reported dielectric measurements of phospholipid solutions[1,2] preceded recent advances in phospholipid purification or were restricted to very low-frequency measurements of lecithin in chloroform.[3] We have attempted to characterize the polar properties of phospholipids containing the phosphoryl choline group more completely by making dielectric measurements over a range of frequencies sufficiently high (0.5–250 MHz) to include portions of the dielectric dispersion region. We have made these dielectric measurements with lecithin in chloroform, chloroform:methanol (1:1), and methanol and with diacetyllecithin in chloroform, chloroform:methanol (1:1), methanol, methanol:water (1:1), and water. The several solvents were chosen to permit examination of the polar properties of the phosphoryl choline group in media of widely varying dielectric constant.[4] The characterization of the dielectric behavior of these phospholipid solutions permits interpretation in terms of molecular size and molecular aggregation in varying dielectric environments.

Theory

Measurements of the dielectric constant of small dipolar molecules in solution have been reported,[5-14] primarily using amino acids in water. The dielectric behavior can be characterized by two descriptive formulations.

First, the dielectric constant of a solution of dipolar molecules can generally be characterized by a dielectric dispersion and described by the equation

$$\epsilon^* = \epsilon - j\epsilon'' = \epsilon_\infty + \frac{\epsilon_0 - \epsilon_\infty}{1 + [j(f/f_c)]^{1-\alpha}} \qquad (1)$$

where ϵ^* is the complex dielectric constant, ϵ is the dielectric constant, ϵ'' is the dissipation factor, $j = (-1)^{1/2}$, f is the frequency, f_c is the characteristic frequency, ϵ_0 is the dielectric constant at low frequencies, ϵ_∞ is the dielectric constant at high frequencies, and α is a parameter which varies from 0 to 1.[15] When the dispersion is characterized by a single characteristic frequency, $\alpha = 0$ and eq

1 can be written as the two equations

$$\epsilon = \epsilon_\infty + \frac{\epsilon_0 - \epsilon_\infty}{1 + (f/f_c)^2} \qquad (2)$$

$$K = K_c + \frac{(K_\infty - K_0)(f/f_c)^2}{1 + (f/f_c)^2} \qquad (3)$$

where K is the conductivity and is equal to $2\pi f \epsilon_f \epsilon''$, ϵ_f is the dielectric constant of free space, K_0 is the conductivity at low frequencies, and K_∞ is the conductivity at high frequencies. Equation 1 predicts that a plot of ϵ'' vs. ϵ will be a circular arc with intercepts at ϵ_0 and ϵ_∞ on the ϵ axis (Cole–Cole plot[15]). When $\alpha = 0$, the center of the circle will be on the ϵ axis. We will use the Cole–Cole plot to confirm the applicability of eq 1 to our dielectric data and to aid in the extrapolation of the high-frequency value of the dielectric constant which will be an important parameter for purposes of interpretation of the results.

The characteristic frequency in eq 1 is given approximately by the equation[10]

$$f_c = RT/6\pi V \eta \qquad (4)$$

where R is the gas constant, T the absolute temperature, V is the molecular volume, and η is the viscosity. Although this equation was developed for spherical particles only, it has proved to be a very satisfactory approximation for molecules whose shape does not depart radically from the spherical. Thus the characteristic frequency determined from dielectric measurements permits the determination of V, the molecular volume.

Secondly, the low-frequency dielectric constant (ϵ_0) of a solution of dipolar molecules is linearly related to the concentration of molecules in solution. This property permits the formulation of the descriptive term dielectric increment, which is the slope of the dielectric constant vs. concentration curve or the measured increase in the dielectric constant above that of the solvent per mole of dipolar solute per liter. The dielectric increment at low frequencies is a measure of molecular polarization. Although the applicability of existing theoretical methods for the calcula-

tion of the molecular dipole moment from the dielectric increment are of limited value in this problem, the proportionality of the dipole moment to the square root of the increment is sufficiently general to permit the use of the increment as an index of dipole moment. (The Onsager theory predicts this behavior in media of high dielectric constant. In media of low dielectric constant this is not as evident. However insertion of the values of dielectric constant and refractive index for water, methanol, and chloroform in the Onsager relation shows that the proportionality constant relating the dielectric increment to the square of the dipole moment varies less than 4% among these solvents.)

Both characteristic frequency and dielectric increment will be used to characterize the molecular properties of the phospholipids in solution.

Experimental Section

Materials. Solvents were all reagent grade and unless otherwise specified were used as received. The solvents were mixed in volume proportions. Phosphorus was determined according to the method of Ames.[16]

Lecithin was prepared from egg yolk by extraction with chloroform–methanol and purification by silicic acid (silic AR, CC-7) column chromatography using standard procedures. The lecithin produced only one spot when analyzed by thin-layer chromatography. The thin-layer chromatograms were performed on silica gel G (Merck, Darmstadt) in the following solvent systems: chloroform–methanol–water (95:35:4) and chloroform–methanol–acetic acid–water (50:30:8:4).

Diacetyllecithin was prepared by acylation of the cadmium chloride derivative of glycerol-3-phosphorylcholine, $(GPC)_2-(CdCl)_3$, with acetyl chloride in carbon tetrachloride in the presence of pyridine according to the procedure of Brandt and Lands.[17] The $(GPC)_2-(CdCl)_3$ was prepared according to the method of Hanahan.[18] Purification of the diacetyllecithin was accomplished by silicic acid (Mallinkrodt, AR, 100 mesh) column chromatography.

A mechanically stirred mixture of 9.4 g of $(GPC)_2-(CdCl_3)_3$ (530 mg total P), 40 ml of carbon tetrachloride, and about 100 ml of 4-mm diameter glass beads was put into a three-necked round-bottom flask which was placed in an ice bath. To this were added 6.2 ml of acetyl chloride (Allied Chemicals) in 50 ml of carbon tetrachloride followed by 9.4 ml of pyridine in 30 ml of carbon tetrachloride. The reaction mixture was stirred for 0.5 hr at the ice-bath temperature and another 0.5 hr at room temperature. The brown reaction mixture was filtered. The residue was treated with 50 ml of methanol and filtered. The combined filtrates were evaporated to a brown viscous residue, dissolved in 200 ml of 90% methanol, and passed through a mixed bed resin column made of 150 ml of Amberlite IRC 50 (H^+) and IR 45 (OH^-). The column was washed with 500 ml of 90% methanol. The combined eluate was evaporated to an oily residue containing 333 mg of total phosphorus. Paper chromatography[19] of the preparation using the solvent system 1-butanol–ethanol–water (5:5:2 by volume) on Whatman No. 1 paper followed by visualization of components by phosphate spray[20] showed the presence of three phosphorus positive components other than the desired diacetyllecithin, which was the major component. For purification of the diacetyllecithin, 100 mg of the phosphorous-containing sample in 30 ml of methanol was placed on a column made of 200 g of silicic acid (Mallinkrodt, AR, 100 mesh) and the column was

eluted successively with methanol containing 0% water (500 ml), 4% water (500 ml), 7% water (1000 ml), 10% water (1000 ml), and 25% water (1000 ml). Most of the diacetyllecithin in chromatographically pure form was eluted with 10% water in methanol and the remaining with 25% water in methanol. The fractions containing diacetylecithin were combined and evaporated to dryness, yielding a light yellow viscous oil. This was decolorized by treatment with activated charcoal (Darco) in methanol and contained 79 mg of phosphorus. This diacetyllecithin preparation gave a single spot on thin-layer chromatography using Brinkman precoated sil G-25 plates and the following solvent systems: methanol–water (80:20), butanol–ethanol–acetic acid–ammonium hydroxide–water (6:10:2:4:6), and chloroform–methanol–ammonium hydroxide (5:5:0.4). The chromatographic plate was exposed to iodine vapor for visualization of the component. *Anal.* Calcd for $C_{12}H_{24}O_8PN \cdot 2H_2O$: N, 3.71%; P, 8.23%; C, 38.2%; H, 7.43%. Found: N, 2.89%; P, 8.68%; C; 38.66%, 38.91%, H, 7.37%, 7.43%.

Measurement Technique. The dielectric measurements were made with a Boonton RX meter using a cell similar to that described by Schwan.[21] The sample liquid (5 ml) was put into the Teflon cylindrical cavity of the cell. Two silver needle electrodes connected to the terminals of the RX meter extend into the sample from the bottom of the cell. The temperature of the sample was maintained at 25° by circulating water through a jacket surrounding the cell. The dielectric constant at each frequency was determined by making measurements of capacitance and resistance of the empty cell, the cell filled with solvent, and the cell filled with the sample. Each measurement was corrected for a series inductance[21] and the sample dielectric constant was determined from the set of three equations

$$C_{air} = \epsilon_f G + S$$

$$C_{solvent} = \epsilon_{solvent} \epsilon_f G + S$$

$$C_{sample} = \epsilon_{sample} \epsilon_f G + S$$

where G is an unknown cell constant, S a stray capacitance, ϵ_f is the dielectric constant of free space, and the C's are inductance corrected, measured capacitances.

The conductivity of the solvent was adjusted in each case by adding $CaCl_2 \cdot 2H_2O$ to match that of the sample solution in order to make the inductance correction as precise as possible and to help eliminate electrode polarization errors. The amount of water of hydration added to the solvents in this process was negligible. In all cases the conductivity of the sample solution was low (less than 10^{-4} mho cm). The conductivity of sample solution was calculated from the equation

$$K = G/R \qquad (5)$$

where K is the conductivity, G the same cell constant, and R is the inductance corrected, measured resistance.

Results

1. Dielectric Dispersion of a Solution of Lecithin in Methanol. The dielectric constant and conductivity of a 0.258 M solution of lecithin in methanol were measured at frequencies from 0.5 to 250 MHz. Figure 1 shows the dielectric constant as a function of frequency. It is apparent from this figure that lecithin causes an increase of the low-frequency dielectric constant above that of the solvent alone ($\epsilon_{MeOH} = 32.6$) and that the characteristic frequency

Figure 1. Dielectric constant vs. frequency for a 0.258 M solution of lecithin in methanol at 25°. The dielectric constant for methanol is 32.6.

for the dielectric dispersion of lecithin is near the upper limit of our measurement, 250 MHz. The low value of dielectric constant at 0.5 MHz appears to be an experimental error. It is not characteristic of all measurements. In order to characterize the dispersion more completely, the dielectric and conductance data were plotted in Figure 2 as the dissipation factor, ϵ'', against the dielectric constant, ϵ. The dissipation factor is calculated from the relation

$$\epsilon'' = (K - K_0{}^*)/2\pi f \epsilon_f$$

where $K_0{}^*$ is the sum of the low-frequency value of the conductivity and the conductivity due to the dispersion of the solvent. The low-frequency conductivity is the low-frequency limiting value of the sample conductivity. The solvent dispersion conductivity at each frequency is obtained from conductivity measurements of the solvent alone. (This measured solvent conductivity when plotted against frequency on log–log paper gave a straight line with a slope of 2 in the frequency range 0.5–250 MHz for all of the solvents, in agreement with the behavior predicted by eq 3.) The Cole–Cole plot for the lecithin solution is fitted with a circular arc, by trial and error,[22] having a center slightly depressed below the ϵ axis and thus the data correspond to a dielectric dispersion with a narrow band of characteristic frequencies. The average characteristic frequency for this dispersion can be calculated from eq 2, after ϵ_∞ is found from the Cole–Cole plot, and is about 300 MHz.

2. Dielectric Dispersion of Solutions with Varying Concentrations of Lecithin in Methanol. Characteristic Frequency. The characteristic frequencies of the dispersions at each concentration were calculated from the Cole–Cole plots of the data as previously described. All of the plots except that at the highest concentration were fitted to semicircles with the center on the ϵ axis. Figure 3 shows that this characteristic frequency varies with solute concentration.

Dielectric Increment. The dielectric increment is the slope of the dielectric constant vs. concentration plot for measurements at a fixed frequency. The results for measurements at 20 MHz are shown in Figure 4. The dielectric constant increases linearly with concentration. The dielectric increment, from this plot, for lecithin in methanol is 24 dielectric units per mole per liter. The dielectric constant vs. concentration curves for measurements at frequencies lower than 100 MHz were all linear and had the same slope. At frequencies greater than 100 MHz the dielectric constant vs. concentration curves were not lin-

Figure 2. Dissipation factor (ϵ'') vs. dielectric constant (ϵ) for a 0.258 M solution of lecithin in methanol at 25°. The circles are experimental points. A semicircle with center slightly below the ϵ axis is fitted to the experimental points (Cole–Cole plot[15]). A high-frequency dielectric constant of 23.8 predicted from this curve corresponds to the value 23.2 (shown as an enclosed cross) calculated from the Maxwell–Wagner formula (see text).

Figure 3. Characteristic frequency calculated from dielectric dispersion vs. concentration of lecithin dissolved in methanol: measurements at 25°.

Figure 4. Increase in the dielectric constant of solutions of lecithin in methanol above the dielectric constant of methanol vs. concentration of the lecithin solutions: measurements at 20 MHz, 25°.

ear. Curve A of Figure 5 illustrates this for measurements at 200 MHz. This can be explained on the basis of dielectric dispersion behavior in which the characteristic frequency varies with solute concentration as already described (Figure 3). When a correction is made for this characteristic frequency variation, the dielectric constant vs. concentration curves become linear with a slope in agreement with the slope at lower frequencies. This corrected value of ϵ_0 is calculated from

$$\epsilon_0 = \epsilon + \left[1 - \frac{1}{1 + (f/f_c)^2}\right](\epsilon_0 - \epsilon_\infty) \qquad (6)$$

where f is the measurement frequency of 200 MHz, f_c is taken from Figure 3 for each concentration, and ϵ is the measured dielectric constant. This corrected value, ϵ_0, is shown as curve B of Figure 5, a straight line with a slope matching that of the low-frequency data (Figure 4). Thus the increment is concentration independent.

3. Dielectric Dispersion of Lecithin in Other Solvents. Dielectric measurements were also made of lecithin in chloroform and chloroform-methanol (1:1). The dielectric constant *vs.* concentration curves were again (except at

Figure 5. Increase in the dielectric constant of a solution of lecithin in methanol above the dielectric constant of methanol vs. concentration of solution: (A) measured dielectric constant at 200 MHz; (B) dielectric constant corrected to allow for characteristic frequency variation shown in Figure 3 (see text).

Figure 6. Dissipation factor vs. dielectric constant of solutions of lecithin in chloroform–methanol (1:1) at 25°. The circles are experimental points. The highest measurement frequency in each set is 250 MHz. Each arc represents measurements at one concentration. From outside to inside the concentrations are 0.28, 0.236, 0.173, 0.11, and 0.072.

TABLE I

	Solvent	Low-frequency dielectric increment[a]	Characteristic frequency,[b] MHz
Diacetyllecithin	Water	32.5	660
	Water–methanol (1:1)	34.0	479
	Methanol	37.0	550
	Methanol–chloroform (1:1)	33.0	255
	Chloroform	6.5	200[c]
Lecithin	Methanol	24.0	490
	Methanol–chloroform (1:1)	25.7	320
	Chloroform	5.0	300[c]

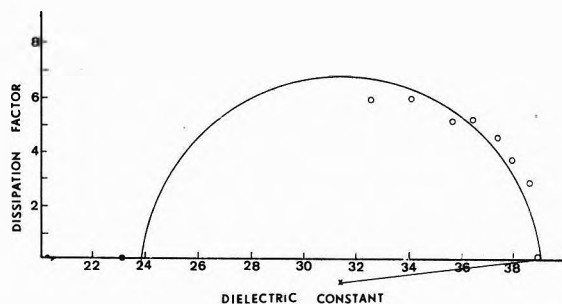[a] Dielectric units per mole per liter. [b] Calculated from dielectric data. [c] Distribution of frequencies.

Figure 7. Dissipation factor vs. dielectric constant of a 0.284 M solution of lecithin in chloroform at 25°. The circles are experimental points. The depressed center for the circular arc is shown with a connecting radius.

high frequencies) linear. The dielectric increments were 4.95 and 25.7 dielectric units per mole per liter in chloroform and chloroform-methanol (1:1), respectively. Figure 6 shows Cole-Cole plots for several concentrations of lecithin in chloroform-methanol (1:1). The dispersions are characterized by a single characteristic frequency of 320 MHz (extrapolated to zero concentration). A Cole-Cole plot for a 0.28 M concentration of lecithin in chloroform is shown in Figure 7. The dispersion is characterized by a distribution of frequencies, as indicated by a depressed center of the semicircle, near 300 MHz.

4. Dielectric Dispersion of Diacetyllecithin in Several Solvents. We made dielectric measurements of diacetyllecithin in water, water-methanol (1:1), methanol, methanol-chloroform (1:1), and chloroform. The dielectric dispersion was again apparent and the dielectric constant varied linearly with diacetyllecithin concentration at all frequencies. The scatter of points of Figure 1 is typical of these data also and represent a precision of about ±0.1 dielectric units. The dielectric increments and characteristic frequencies calculated from these data are given in Table I along with the values for lecithin.

Discussion

Dielectric Increment. The dielectric increment for dipolar molecules in solution is normally used as an index of dipole moment of these molecules. The dipole moment of lecithin and diacetyllecithin in solution can, however, be more appropriately described by a quantity which differs from the dielectric increment in that it measures the differences between the low- and high-frequency values of the dielectric constant of the solution rather than the difference between the low-frequency value and the solvent value. In the case of these molecules the high-frequency dielectri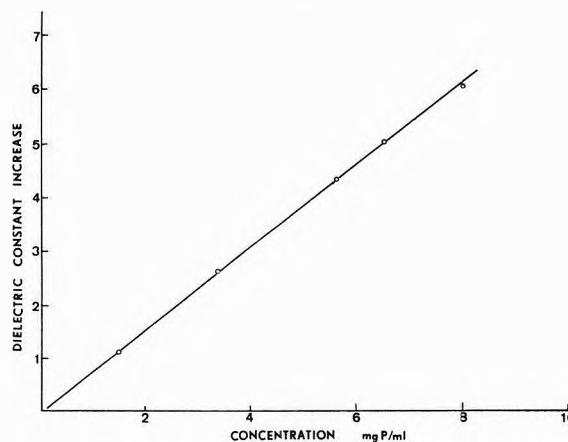c constant is significantly less than the dielectric constant of the solvent. This difference is much more pronounced with phospholipids than with amino acids because the specific volume is larger, and the proportion of the molecule making up the dipole is smaller in the phospholipid.

We could not measure the high-frequency value of the dielectric constant directly because of instrumental limitations. The value can, however, be calculated by two independent methods. The first method uses the Maxwell-Wagner mixture formula for ellipsoidal particles of one dielectric constant suspended in a medium of another dielectric constant[23,24]

$$\epsilon = \epsilon_s\left[\epsilon_p\frac{1 + xp}{1 - p} + x\epsilon_s\right] \Big/ \left[\epsilon_p + \epsilon_s\frac{x + p}{1 - p}\right] \qquad (7)$$

TABLE II

| | Solvent | ϵ_s, solvent dielectric ccnstant | Decrement | |
			Maxwell–Wagner formula	Cole–Cole plot
Diacetyl-lecithin	Water	78.5	32.9	29.4
	Water–methanol (1:1)	55.6	23.6	22.8
	Methanol	32.6	13.3	12.6
	Methanol–chloroform (1:1)	18.7	7.1	5.8
	Chloroform	4.81	1.24	0.78
Lecithin	Methanol	32.6	36.0	33.1
	Methanol–chloroform (1:1)	18.7	19.9	16.1
	Chloroform	4.81	3.6	3.31

where x is a parameter which varies as a function of the axis ratio of the ellipsoidal particle (for particles with a lower dielectric constant than the surrounding medium, x varies from 1 for a rod to 2 for a sphere), ϵ is the desired dielectric constant of mixture, ϵ_s is the dielectric constant of solvent, ϵ_p is the dielectric constant of the solute, and p the volume concentration. The following assumptions are required for the use of eq 7.

(1) The lecithin molecule has the form of a prolate spheroid with an axis ratio of 2:1. (This ratio was derived from approximate length measurements on a molecular model of lecithin made from CPK atomic models.) The parameter x of eq 7 then takes the value 1.8.[24] An axis ratio anywhere from 1:1 to 4:1 would not cause a significant variation in x.

(2) The lecithin molecule has a specific volume of 1[25] and a molecular weight of 824.

(3) The diacetyl lecithin is spherical. (Derived from visual inspection of a molecular model.) The parameter x then equals 2. A distortion from the spherical shape of up to 2:1 would not significantly effect the results.

(4) The diacetyllecithin has a specific volume of 0.9 and a molecular weight of 377.[26]

(5) The high-frequency value of the dielectric constant for pure phospholipid is 2.0.[27]

The second method is to use the value for ϵ_∞ given by the intercept of the circular arc with the ϵ axis in the Cole–Cole plots of the dielectric data.

A dielectric decrement at high frequencies, defined as the decrease in the dielectric constant below the solvent value per mole per liter, is calculated from the values of ϵ_∞ determined by the two methods and is given in Table II. Addition of the measured dielectric increment and the derived dielectric decrement (average of the two values given) yields a total dielectric increment which characterizes the polar properties of the molecule. Figure 8 is a plot of this total increment vs. dielectric constant of the solvent.

The total dielectric increments for diacetyllecithin in water and for lecithin in methanol are similar and about the same as those found for amino acids with dipoles of a length similar to the lecithin dipole (i.e., δ-aminovaleric acid has an increment of 63[9] and diglycine 70[9]). In the above two cases the molecules probably exist as free dipoles. As the dielectric constant of the solvent decreases, so does the total dielectric increment (Figure 8). If the dipole moment were unaffected by a change in dielectric constant of the surrounding environment this curve would

Figure 8. Total dielectric increment vs. dielectric constant of the solvent for (A) lecithin and (B) diacetyllecithin.

TABLE III

| | Solvent | Viscosity,[a] cP | Characteristic frequency, MHz | |
			Calcd from dielectric data	Calcd from eq 4 (Stokes law)
Diacetyl-lecithin	Water	0.89	660	506
	Water–methanol	1.57	479	288
	Methanol	0.547	550	822
	Methanol–chloroform	0.624	255	722
	Chloroform	0.542	200	832
Lecithin	Methanol	0.89	490	337
	Methanol–chloroform	0.624	320	296
	Chloroform	0.542	300	340

[a] Reference 29.

be a straight line with a slope of zero. Any variation from this behavior signifies that some alteration of the moment is occurring. The decreased increment is probably the result of aggregation of the dipoles such that the dipole moments of individual molecules tend to cancel each other. A decrease in the distance between the oppositely charged ends of the dipole could also reduce the increment. However, the phosphoryl choline group does not have sufficient flexibility to account for the large changes observed. The sharp change in the slope of the increment vs. dielectric constant curve for diacetyllecithin at a solvent dielectric constant of about 25 indicates that there is a change in the amount of dipole moment alteration as a function of dielectric surround. There is a more pronounced effect in the lower dielectric media.

Characteristic Frequency. Information about the size of the molecule or molecular aggregate can be obtained from the measured characteristic frequency. Table III compares the measured characteristic frequency with the characteristic frequency calculated from eq 4 for an equivalent sphere[28] of the size of the particular molecule in the several solvents

The measured characteristic frequencies for diacetyllecithin are higher than those calculated assuming a rigid particle in water and in water–methanol (1:1). This would suggest that the molecule exists as a monomer in these solvents, agreeing with the conclusion reached from the

dielectric increment behavior. The discrepancy between the measured and the calculated characteristic frequencies can be attributed to experimental error as well as inadequacy of the theoretical eq 4. (The formulation, for example, is not strictly applicable for particles as small as diacetyllecithin.) As the dielectric constant of the solvent decreases, the measured characteristic frequency falls significantly below the theoretical value. This suggests that in methanol the diacetyllecithin may exist as a dimer and that in methanol–chloroform and chloroform it may exist as a small molecular aggregate.

Reexamination of the total dielectric increment data (Figure 8) suggests that the dimer of diacetyllecithin in methanol probably exists in a form with the nonpolar portions entangled and the dipole portions of the molecules extending freely from the pair since the increment is only slightly decreased suggesting minimal cancellation of dipole moments. As the dielectric constant of the solvent is lowered further (in methanol–chloroform (1:1) and in chloroform) the sharp reduction in increment suggests that aggregates are formed with the dipolar portions coupled and antiparallel thus cancelling the molecular dipole moments.

The measured characteristic frequency of the lecithin in methanol is considerably higher than the theoretical value. This suggests that the dipolar portion of the molecule may be free to rotate without necessarily carrying the long fatty acid chains with it, i.e., the molecule is flexible and its characteristic frequency is determined primarily by the size of the polar portion of the molecule. The relatively small lowering of the characteristic frequency with decreasing solvent dielectric constant for measurements with lecithin suggests aggregation of only small numbers of lecithin molecules.

An increasing aggregation of lecithin (polar end coupling) with decreasing solvent dielectric constant agrees with the conclusions of Kuhn,[2] Price and Lewis,[30] Faure and Legault-Demare,[31] and of Elworthy and McIntosh[32] derived from other techniques although we obtained a smaller aggregate size than some of the others.[32] An increase in dipole binding energy in going from methanol (ϵ = 32.6) to chloroform (ϵ = 4.8) agrees with the prediction from electric field theory. Specifically, if we modify the treatment of Fuoss and Kraus[33] of ionic dissociation in media of varying dielectric constant to dipolar association as a function of dielectric constant of the solvent, we can predict from our experimental data the distance of closest approach of the lecithin molecules is about 10 Å in agreement with the value expected (see Appendix).

Biological membranes generally appear to have a relatively high proportion of phospholipids. The phenomena reported here could well be present in such membranes and may play some role in the configurational changes which take place during excitability processes. The interaction energies of adjacent dipoles and of dipoles with ionic components of their immediate environments seem quite sensitive to the local dielectric constant and to distances of closest approach. Both of these may well be influenced by alterations in water content and by local changes in molecular configuration.

Conclusions

The dielectric properties of solutions of lecithin in methanol and diacetyllecithin in water are consistent with the behavior expected from the phosphoryl choline dipole. The measured characteristic frequency agrees with that

expected from molecular size and the dielectric increment agrees (when a correction is made to account for a large dielectric decrement at high frequencies) with that expected from the dipole length.

When these molecules are placed in media of dielectric constant lower than about 25 the molecules aggregate via dipole–dipole interaction. This binding increases with decreasing dielectric constant of the solvent. A theoretical analysis (see Appendix) explains this relation and also implicates the "distance of closest approach" of the dipoles as an important factor in determining association energy.

Appendix

Dipole Pair Formation as a Function of the Dielectric Constant of the Medium. The basic procedure for relating interaction energy to the dielectric constant of the environment is that of Bjerrum[34] as extended by Fuoss and Kraus[33] but applied to dipole–dipole interaction rather than to ion–ion interaction. A complete analysis of the problem is very complex; only a crude approach will be followed here. Given a solution of dipolar molecules, some of these will form pairs. Of all possible pair configurations only an antiparallel alignment (with equal positive–positive and negative–negative separation) will be a stable pair. The concentration of associated pairs of this type with a dipole separation, r, is related to the total concentration of such pairs by the Boltzmann relation

$$n_A = n_{ref} \exp(-W/kT) \qquad (A1)$$

where

$$W = -\frac{2e^2}{4\pi\epsilon\epsilon_f}\left[\frac{1}{r} - \frac{1}{\sqrt{r^2 + l^2}}\right]$$

is the dipole–dipole attraction energy between an antiparallel pair separated by a distance r; n_A is the concentration of pairs with separation, r, or the concentration of associated dipoles at this separation; n_{ref} is the total concentration of pairs or the concentration of reference dipoles from each pair; e is the electronic charge; l is the dipole length; ϵ is the dielectric constant; ϵ_f is the dielectric constant of free space; k is the Boltzmann constant, and T is the absolute temperature. The number of dipoles within a cylindrical shell of thickness, dr, at a distance r from the reference dipole is then

$$dn = 2\pi n_{ref}lr \exp\left\{\alpha\left[\frac{1}{r} - \frac{1}{\sqrt{r^2 + l^2}}\right]\right\}dr \qquad (A2)$$

where $\alpha = 2e^2/4\pi\epsilon\epsilon_f kT$. A plot of dn/dr vs. r will have a minimum at some r_m. The dipoles within this distance r_m from the reference dipole are considered as bound to the reference dipole.[33] The value of r_m is given by the equation

$$\frac{d}{dr}\left(\frac{dn}{dr}\right) = 0 \qquad (A3)$$

which is

$$1 + \frac{\alpha r_m^2}{(r_m^2 + l^2)^{3/2}} - \frac{\alpha}{r_m} = 0 \qquad (A4)$$

When the calculated value of r_m is equal to or less than a distance of closest approach between two dipoles they

cannot be bound. An interpretation of Figure 8 (dielectric increment vs. dielectric constant of the solvent for diacetyllecithin) identifies a dielectric constant of about 25 as the value above which no dipolar binding occurs. It is then possible to calculate the distance of closest approach, a, from eq A4 by using $\epsilon = 25$, $a = r_m$, and an approximate value of the dipole length, l, of 5.1 Å. This latter value is calculated from the empirical equation[10b] $l = (10\delta)^{1/2}/e$ where δ is the total dielectric increment and is 60 as taken from Figure 8. (Measurements on a CPK molecular model of lecithin indicate that l could be 3-6 Å.) The calculated value of a from eq A4 is then 11.1 Å. This agrees fairly well with the value that would be expected from lecithin monolayer studies[35] (11 Å) and with the distance of closest approach as measured on a CPK molecular model of lecithin containing a hydrated phosphoryl choline group (~ 7 Å).

References and Notes

(1) I. Hausser, *Sitzungber. Heidelberg. Akad. Wiss., Math. Naturwiss. Kl.*, 6, 3 (1935).

(2) R. Kuhn, I. Hausser, and W. Brydowna, *Ber. Deut. Chem. Ges.*, 68, 2386 (1935).

(3) D. L. Jernigan, G. M. Adams, and T. L. Sallee, *Chem. Phys. Lipids*, 6, 135 (1971).

(4) See Table II, column 1.

(5) W. P. Conner, R. P. Clarke, and C. P. Smyth, *J. Amer. Chem. Soc.*, 64, 1379 (1942).

(6) W. P. Conner and C. P. Smyth, *J. Amer. Chem. Soc.*, 64, 1870 (1942).

(7) H. Fricke and A. Parts, *J. Phys. Chem.*, 42, 1171 (1938).

(8) W. L. G. Gent, *Trans. Faraday Soc.*, 50, 1229 (1954).

(9) J. Wyman, Jr., *Chem. Rev.*, 19, 213 (1936).

(10) J. T. Edsall in "Proteins, Amino Acids, and Peptides," E. J. Cohn and J. T. Edsall, Ed., Reinhold, New York, N. Y., 1943, (a) Chapter 6; (b) p 252.

(11) J. P. Greenstein, J. Wyman, Jr., and E. J. Cohn, *J. Amer. Chem. Soc.*, 57, 637 (1935).

(12) J. P. Greenstein and J. Wyman, Jr., *J. Amer. Chem. Soc.*, 58, 463 (1936).

(13) H. O. Marcy, 3rd, and J. Wyman, Jr., *J. Amer. Chem. Soc.*, 63, 3388 (1941).

(14) M. W. Aaron and E. H. Grant, *Brit. J. Appl. Phys.*, 18, 957 (1967).

(15) K. S. Cole and R. H. Cole, *J. Chem. Phys.*, 9, 341 (1941).

(16) B. N. Ames, *Methods Enzymol.*, 8, 115 (1966).

(17) A. E. Brandt and W. E. M. Lands, *Biochim. Biophys. Acta*, 144, 605 (1967).

(18) D. J. Hanahan, *Biochem. Prep.*, 9, 55 (1962).

(19) F. Kogl, G. H. deHaas, and L. L. M. van Deenen, *Recl. Trav. Chim. Pays-Bas*, 79, 661 (1960).

(20) R. S. Bandurski and B. Axelrod, *J. Biol. Chem.*, 193, 405 (1951).

(21) H. P. Schwan in "Physical Techniques in Biological Research," Vol. 6, W. L. Nastuk, Ed., Academic Press, New York, N.Y., 1963, p 378.

(22) The range of semicircles which can be fitted to the data points can be reasonably limited to those giving values of ϵ_∞ which are within ± 1.5 dielectric units from the value shown. This represents a possible error in f_c of about 35%. This error does not significantly affect our interpretation of the results.

(23) B. E. Pennock and H. P. Schwan, *J. Phys. Chem.*, 73, 2600 (1969). The Maxwell-Wagner (M-W) interfacial polarization does not contribute significantly to the observed variation of the dielectric constant with frequency. (A 0.25 M solution of lecithin in water would be expected to have only a 0.05 dielectric unit high to low frequency change with a characteristic frequency of about 2 MHz.) The measured variation is accounted for by a dipolar mechanism. However, at frequencies much higher than the measured dielectric relaxation frequency the M-W equation is applicable as a mixture equation for particles of one dielectric constant (high-frequency value for the particle in this case) in a medium of another dielectric constant (solvent). A lowering of the solution dielectric constant below the value for the solvent results because the effective dielectric constant of the particle (at these high frequencies) is lower than that of the solvent.

(24) H. Fricke, *Phys. Rev.*, 24, 575 (1924).

(25) Merck Index, Merck and Co., Rahway, N. J., 1968.

(26) If the average density for the fatty acids of egg lecithin is taken as 0.92 (Handbook of Chemistry and Physics) then $\bar{v}$ for the diacetyllecithin can be calculated and is 0.88. The value 0.9 is used for convenience in view of the approximations already made and the noncritical nature of the value for the purposes of this paper.

(27) T. J. Buchanan, *J. Chem. Phys.*, 22, 578 (1954).

(28) The use of a speroidal shape (assumed previously) of the lecithin would make the calculated characteristic frequency for this molecule up to about 20% too high. (Appendix, ref 10). This error would not significantly alter the conclusions.

(29) Viscosities used for this calculation were measured with an Oswald viscometer at 25°.

(30) H. I. Price and W. C. M. Lewis, *Biochem. J.*, 23, 1030 (1929).

(31) M. Faure and J. Legault-Demare, *Bull. Soc. Chim. Biol.*, 32, 509 (1950).

(32) P. H. Elworthy and D. S. McIntosh, *J. Pharm. Pharmacol.*, 13, 633 (1961).

(33) R. M. Fuoss and C. A. Kraus, *J. Amer. Chem. Soc.*, 55, 1019 (1933).

(34) N. Bjerrum, *Kgl. Dan. Vidensk.*, 7, 2 (1926).

(35) R. T. Holman, *Progr. Chem. Fats Other Lipids, Part 1*, 8, 13 (1965).

Enthalpies of Dilution of Tetra-n-alkylammonium
Bromides in Water and Heavy Water[1]

A. S. Levine and R. H. Wood*

Department of Chemistry, University of Delaware, Newark, Delaware 19711   *(Received December 29, 1972)*

The enthalpies of dilution of R_4NBr (where R = methyl, ethyl, n-propyl, and n-butyl) have been measured at 25° from 3 m' (aquamolality) to about 0.08 m' in D_2O and from 3 m' to about 0.008 m' in H_2O. The results for H_2O were extrapolated to infinite dilution using an extended Debye–Hückel equation. The difference between H_2O and D_2O was fit to a polynomial in m'. The results for low concentrations in H_2O indicate that cation–cation interactions have a large positive effect on the excess enthalpy while cation–anion interactions have a large negative effect on the excess enthalpy. An equation is derived which shows that at low enough concentrations these effects can be separated by the concentration dependance of the ion atmospheres of the single ions and the pairs. The difference between the excess enthalpy in H_2O and D_2O shows that structural effects present in H_2O are magnified in D_2O. The difference between H_2O and D_2O solutions for the alkali halides and tetraalkylammonium bromides have the same shape as that predicted by Ramanathan and Friedman's model calculation for a change in cation–anion cosphere overlap. This is surprising for the tetrabutylammonium and tetrapropylammonium bromides where cation–cation overlap is expected to be important. A saturation effect can explain the results.

Introduction

The tetraalkylammonium halides in aqueous solution have received a great deal of attention in recent years because of their very unusual properties. These results will not be summarized here because they have been presented in two recent reviews.[2,3] In addition, the properties of D_2O solutions have recently been reviewed.[4] The present experiments were undertaken because the isotope effect shows how a change in the cosphere overlap term affects the thermodynamics of tetraalkylammonium halides. This is possible because both the electrostatic attraction and the short-range ion–ion repulsive forces are essentially unchanged by substitution of D_2O for H_2O. In addition, the more accurate low-concentration data for H_2O solutions reported here allows a qualitative understanding of how like-charged and unliked-charged interactions affect the thermodynamics of these solutions.

Experimental Section

A detailed description of the experimental procedures and tests of the calorimeter has been described previously.[5] The calorimeter employed was the LKB 10700-2 batch microcalorimeter which was described in detail by Wadso.[6] The calorimeter uses the twin principle with the thermopiles of the two 18-k gold cells connected in opposition so that all external disturbances are cancelled. The electrical voltage, which is proportional to the heat flow, is amplified and fed to a recorder equipped with a disk integrator.

From the voltage *vs.* time plot for a dilution experiment

$$Q = \Sigma \int E \ dt \qquad (1)$$

where Q is the heat liberated, E is the recorder deflection which represents the voltage, and t is the time. The proportionality constant, Σ, was determined from a cali-

bration experiment which was performed immediately after a dilution run.

The heat of friction was measured for each experiment and was 0 ± 30 μcal where 1 cal = 4.184 J. The difficulties in achieving this are described in ref 5.

The heat of dilution of urea was chosen as a standard reaction to test the accuracy and precision of the calorimeter since urea is a good primary standard and its solutions can be prepared to concentrations as high as 12 m. This is high enough to absorb large heats upon dilution. The experimental results for the heat of dilution of urea agree within 0.4% of values calculated using the equation of Gucker and Pickard[7] and the observed heats are reproducible to within 0.1%.

The tetramethylammonium, tetraethylammonium, tetra-n-propylammonium, and tetra-n-butylammonium bromides (Me_4NBr, Et_4NBr, Pr_4NBr, and Bu_4NBr, respectively) were obtained from Eastman Organic Chemicals and they were purified and dried according to the procedures of Unni, Elias, and Schiff.[8] The purity of the salts was determined by measuring the bromide content with a potentiometric precipitation titration using a silver|silver bromide electrode. Duplicate determinations agreed to within 0.1%. The results of the analyses are as follows: Me_4NBr, 99.72% pure; Et_4NBr, 99.98% pure; Pr_4NBr, 99.99% pure; Bu_4NBr, 99.83% pure. Earl Fischer titrations showed that the dried salts contained 0.1% or less water impurity. The salts were kept in tightly capped polyethylene bottles and stored in a drybox where the dew point was always kept below −50°.

The concentration scale used is the aquamolality scale,[9] m', defined as the moles of solute per 55.51 moles of solvent. The D_2O was obtained commercially with a purity of 99.77%. The water content was 0.2% before the solutions were made and it did not change when checked after

all of the dilution experiments were completed. All the analyses of the D_2O for water content were performed by proton nmr spectroscopy.

A fresh solution which was 3 m' in salt was prepared by weight in the drybox for each run. The 3 m' R_4NBr solutions were diluted to about 0.8 m' in the first step. This solution was then diluted in a second experiment to about 0.25 m'. A third experiment reduced the concentration to about 0.08 m'. Water analyses of the final solution from each dilution showed less than 0.05 mol % change in the amount of H_2O during the course of the three consecutive dilutions and the difference in water content between each solution and the solvent D_2O was less than 0.1%. The errors produced by the H_2O impurity[10] are less than 1 cal/mol in H^{ex}.

The relative pH of the D_2O solvent (measured with a glass electrode) was 6.4. The pH of the R_4NBr solutions in D_2O was 6.5 ± 0.2 pH units.

Experiments in Water. The experimental procedure for the water experiments was the same as that used for the D_2O experiments without the use of the drybox. Deionized water with a pH of 5.7 was used. The solutions of R_4NBr salts had pH values of 6.3 ± 0.2. Each 3 m' R_4NBr solution was diluted to about 0.008 m' in a series of steps.

Results and Discussion

The changes in excess enthalpy (for a group of experiments at similar concentrations), ΔH^{ex} or $\Delta\phi_L$,[11] measured in the calorimeter were corrected to the same initial and final concentrations. This was accomplished by first correcting the water experiments to the same initial and final molality. The small correction was obtained by multiplying the difference in molalities by the slope of a plot of ΔH^{ex} vs. m' for the water experiments. The ΔH^{ex} values for the water experiments were then averaged. The same procedure was used for the D_2O experiments except that the slopes of ΔH^{ex} vs. m' in D_2O were used. The data appear in Table I. The heat of dilution of Et_4NBr from 3.0 to 0.7334 m' and Pr_4NBr from 3.0 to 0.6983 m' were omitted because these points are clearly outside the normal experimental error which is ± 2 cal/mol or $\pm 0.3\%$ (whichever is larger). The Et_4NBr results have a larger experimental error than expected ($\pm 1\%$). The explanation for this is unknown.

A least-squares fit of the low-concentration water data employing the Debye–Hückel limiting law[12,13] yielded accurate relative apparent molal heat content values. It was shown[13] that this procedure gives excess enthalpy values good to about 1 cal/mol using accurately known heat of dilution data. The extrapolations, combined with the data in Table I, give $H^{ex}(\phi_L)$ at all concentrations.

In order to calculate $H^{ex}{}_{D_2O}(m_i')$, the difference in the apparent molal heat content between the water and D_2O solutions was represented by the equation

$$H^{ex}{}_{H_2O} - H^{ex}{}_{D_2O} = \phi_L(H_2O) - \phi_L(D_2O) =$$
$$k_1 m' + k_2 m'^2 \quad (2)$$

Kerwin[9] has shown that the first term of an equation of this form works well for free energy differences and Wood, Rooney, and Braddock[10] have shown that this relationship gives good results for heat of dilution differences. This equation can be combined with the following relationship

$$\Delta\phi_L(H_2O) = \Delta H^{ex}{}_{H_2O} = H^{ex}{}_{H_2O}(m_f') - H^{ex}{}_{H_2O}(m_i') \quad (3)$$

to give

$$\frac{\Delta\phi_L(D_2O) - \Delta\phi_L(H_2O)}{m_i' - m_f'} = \frac{\Delta H^{ex}{}_{D_2O} - \Delta H^{ex}{}_{H_2O}}{m_i' - m_f'} =$$
$$k_1 + k_2(m_i' + m_f') \quad (4)$$

In these equations, m_i' and m_f' are the initial and final aquamolalities. In order to compare the heats of dilution in water and D_2O, it was necessary to calculate the heats of dilution for identical initial and final concentrations. A plot of eq 4 using the corrected data appears in Figure 1. The values of k_1 and k_2, which were determined from this plot, are listed in Table II. The $H^{ex}{}_{D_2O}(m_f')$ values at the lowest final concentration for each salt were calculated using eq 2. These $H^{ex}{}_{D_2O}(m_f')$ values were then according to eq 3 to calculate $H^{ex}{}_{D_2O}(m_i')$. The H^{ex} values for the water and D_2O experiments are shown in Table I along with some values reported for H_2O by Lindenbaum.[14] The precision of the H^{ex} values for the R_4NBr salts in D_2O is the same as those in water ($\pm 0.3\%$).

Most of the values reported by Lindenbaum agree with the present results within the reported experimental error ($\pm 2\%$ and ± 10 cal/mol for Lindenbaum's results and $\pm 0.3\%$ and ± 2 cal/mol for the present results). The values at 3 m' for Pr_4NBr and Bu_4NBr differ by more than the expected experimental error. A recent remeasurement by Lindenbaum[15] confirms the present results (see Table I). Higher accuracy was necessary in the present investigation because the differences between H_2O and D_2O solutions are not very large. Recently Cassel and Wen[16] have reported values for the excess enthalpy, H^{ex}, for the tetramethyl-, -ethyl, and -butylammonium bromides at low concentrations in H_2O and for the butyl bromide in D_2O. These results are in reasonable agreement with the present experiments considering the expected experimental errors in both measurements. The present results are preferred because they do not involve small differences between two relatively large heats of solution.

Results in H_2O. A plot of the results of this work for aqueous solutions at low concentrations is given in Figure 2. The lack of a regular trend in this figure is striking. The same kinds of reversals in trends are found in the activity coefficient data.[18-20] In order to explain the reversals in Figure 2, we will use a method similar to the one used by Robinson, Wood, and Reilly[21] to derive the limiting behavior of the excess free energy and the excess enthalpy of mixing two electrolytes with a common ion. The method takes into account the Debye–Hückel limiting law and pair-wise interactions. For the pair-wise interactions of a cation, M, with an anion, X, we use the equation

$$M^+ + X^- \rightarrow MX \quad (5)$$

with the equilibrium constant

$$K(MX) = \{MX\}\gamma_{MX}/(\{M\}\{X\}\gamma_M\gamma_X) \quad (6)$$

Similar equations are used for the interactions of any two ions. When the effect of these interactions on the excess free energy per mole of salt, G^{ex}, is calculated using the same procedure as Robinson, Wood, and Reilly,[21] the result is

$$G^{ex}m/RT = DHLL - m^2(K(MX)\gamma_M\gamma_X/\gamma_{MX} +$$
$$K(MM)\gamma_M^2/\gamma_{MM} + K(XX)\gamma_X^2/\gamma_{XX}) \quad (7)$$

where DHLL is the appropriate Debye–Hückel limiting

TABLE I: Enthalpy of Dilution of R$_4$NBr Salts in H$_2$O and D$_2$O

Solvent	m_i'	m_f'	ΔH^{ex}(expt), cal mol^{-1}	ΔH^{ex}(corr),[b] cal mol^{-1}	$H^{ex}(m_i)$, cal mol^{-1}
			(A) Me$_4$NBr		
	(3.000)[b]	(0.8150)[b]			
H$_2$O	3.000	0.8194	630.9	632.9	−1110 (−1080)[a]
H$_2$O	3.000	0.8150	631.6	631.6	
D$_2$O	3.000	0.8087	703.6	700.5	−1227
D$_2$O	3.000	0.8230	698.4	700.4	
	(0.8150)	(0.2469)			
H$_2$O	0.8194	0.2551	311.7	315.4	−478.1 (−481)[a]
H$_2$O	0.8150	0.2469	315.6	315.6	
D$_2$O	0.8087	0.2564	339.7	350.2	−526.7
D$_2$O	0.8230	0.2575	344.0	348.2	
	(0.2469)	(0.8083)			
H$_2$O	0.2551	0.08379	138.1	134.9	−162.6 (−166)[a]
H$_2$O	0.2469	0.08083	133.3	133.3	
D$_2$O	0.2564	0.08241	150.7	144.8	−177.5[c]
D$_2$O	0.2575	0.08337	148.1	142.3	
	(0.08083)	(0.02636)			
H$_2$O	0.08029	0.02636	42.12	42.54	−28.5
H$_2$O	0.08030	0.02724	42.83	43.83	
	(0.02636)	(0.008598)			
H$_2$O	0.02618	0.008598	6.9	7.0	+14.7
H$_2$O	0.02705	0.008951	7.7	7.3	
H$_2$O	0.008598	0.00000			+21.9[d]
			(B) Et$_4$NBr		
	(3.000)	(0.7503)			
H$_2$O	3.000	0.7451	414.7	412.4	−913 (−902)[a]
H$_2$O	3.000	0.7503	418.6	418.6	
H$_2$O	3.000	0.7334	433.6	426.0[e]	
D$_2$O	3.000	0.7467	420.2	418.6	−923
D$_2$O	3.000	0.7291	428.9	419.4	
	(0.7503)	(0.2256)			
H$_2$O	0.7451	0.2294	302.0	307.4	−497 (−480)[a]
H$_2$O	0.7503	0.2256	305.2	305.2	
H$_2$O	0.7334	0.2266	302.2	310.6	
D$_2$O	0.7467	0.2221	312.1	310.8	−504
D$_2$O	0.7291	0.2256	302.3	311.8	
	(0.2256)	(0.07304)			
H$_2$O	0.2294	0.06993	150.0	143.4	−190 (−168)[a]
H$_2$O	0.2256	0.07304	144.8	144.8	
H$_2$O	0.2266	0.07308	145.9	145.1	
D$_2$O	0.2221	0.07210	144.9	146.8	
D$_2$O	0.2256	0.07306	147.0	147.0	−193[c]
	(0.07304)	(0.02447)			
H$_2$O	0.07256	0.02447	51.3	51.8	−45.1
H$_2$O	0.07253	0.02405	49.4	49.6	
	(0.02447)	(0.008009)			
H$_2$O	0.02431	0.008009	11.3	11.5	5.6
H$_2$O	0.02390	0.008033	12.6	13.1	
H$_2$O	0.008009	0.00000			17.9[d]
			(C) Pr$_4$NBr		
	(3.000)	(0.7086)			
H$_2$O	3.000	0.7086	−1579	−1579	1632 (1480)[a]
H$_2$O	3.000	0.6983	−1596	−1592[e]	(1595)[f]
H$_2$O	3.000	0.7041	−1583	−1581	
D$_2$O	3.000	0.6719	−1758	−1740	1873
D$_2$O	3.000	0.7090	−1738	−1738	
	(0.7086)	(0.2106)			
H$_2$O	0.7086	0.2106	−108.7	−108.7	
H$_2$O	0.6983	0.2050	−103.4	−108.0	52.0
H$_2$O	0.7041	0.2155	−106.2	−107.1	
D$_2$O	0.6719	0.2066	−148.4	−166.8	134.0
D$_2$O	0.7090	0.2250	−167.0	−165.9	

TABLE I (Continued)

Solvent	m_i'	m_f'	ΔH^{ex}(expt), cal mol⁻¹	ΔH^{ex}(cor)[b], cal mol⁻¹	$H^{ex}(m_i)$, cal mol⁻¹
	(0.2106)	(0.06910)			
H_2O	0.2091	0.06910	41.91	42.14	−55.9 (−26)[a]
H_2O	0.2091	0.06697	42.63	41.69	
D_2O	0.2066	0.07000	25.65	26.33	−32.4[c]
D_2O	0.2250	0.07182	27.58	27.33	
	(0.06910)	(0.02274)			
H_2O	0.06744	0.02274	28.2	29.1	−14.0
H_2O	0.06865	0.02319	27.7	28.1	
	(0.02274)	(0.007646)			
H_2O	0.02259	0.007646	5.2	5.3	14.6
H_2O	0.02304	0.007761	5.9	5.7	
H_2O	0.007646	0.00000			20.1[d]

(D) Bu$_4$NBr

Solvent	m_i'	m_f'	ΔH^{ex}(expt), cal mol⁻¹	ΔH^{ex}(cor)[b], cal mol⁻¹	$H^{ex}(m_i)$, cal mol⁻¹
	(3.000)	(0.6357)			
H_2O	3.000	0.6357	−4440	−4440	5709 (5500)[a]
H_2O	3.000	0.6361	−4418	−4419	
D_2O	3.000	0.6160	−4781	−4724	6194
D_2O	3.000	0.5921	−4869	−4743	
	(0.6357)	(0.1912)			
H_2O	0.6357	0.1912	−1000	−1000	1279 (1295)[a]
H_2O	0.6361	0.1884	−1008	−1002	
D_2O	0.6160	0.1783	−1093	−1126	1460
D_2O	0.5921	0.1782	−1026	−1128	
	(0.1912)	(0.06194)			
H_2O	0.1912	0.06194	−195.5	−195.5	278 (270)[a]
H_2O	0.1884	0.06032	−196.9	−199.5	
D_2O	0.1783	0.05669	−218.6	−234.0	333[c]
D_2O	0.1782	0.05568	−219.1	−233.1	
	(0.06194)	(0.02006)			
H_2O	0.06151	0.02006	−41.1	−41.7	79.9
H_2O	0.06153	0.02078	−41.3	−42.4	
	(0.02006)	(0.006828)			
H_2O	0.02030	0.006828	−12.9	−12.7	37.8
H_2O	0.02065	0.006918	−11.5	−11.0	
	(0.03973)	(0.01329)			
H_2O	0.03973	0.01329	−22.9	−22.9	
H_2O	0.03973	0.01332	−22.7	−22.7	54.5
H_2O	0.03973	0.01345	−21.6	−21.7	
	(0.01329)	(0.004432)			
H_2O	0.01336	0.004432	−10.0	−9.9	32.1
H_2O	0.01323	0.004511	−9.1	−9.4	
H_2O	0.004432	0.00000			22.4[d]
H_2O	0.006828	0.00000			25.9[d]

[a] Reference 14. [b] The ΔH^{ex}(corr) values for all experiments within a given concentration range are corrected to the m_i' and m_f' in parentheses. [c] $\phi_L(D_2O)$ was calculated using eq 2; $\phi_L(H_2O) - \phi_L(D_2O) = k_1 m' + k_2 m'^2$. [d] From the computer extrapolation of the data. [e] This point was omitted because it was clearly outside the normal experimental error. [f] This value is a recent unpublished measurement by S. Lindenbaum.

law, and W is the weight of solvent. Similarly, the effect of these interactions on the heat content per mole of salt, H^{ex}, is

$$H^{ex}m = \text{DHLL} + m^2(\{MX\}_h \gamma_M \gamma_X / \gamma_{MX} + \{MM\}_h \gamma_M^2 / \gamma_{MM} + \{XX\}_h \gamma_X^2 / \gamma_{XX}) \quad (8)$$

where the symbol $\{MX\}_h$ includes terms for both $\partial K/\partial(1/T)$ and $\partial \gamma/\partial(1/T)$. When the activity coefficients are calculated using the Debye–Hückel limiting law

$$\gamma = \exp(-AZ^2\sqrt{m}) \simeq 1 - AZ^2\sqrt{m} + \ldots \quad (9)$$

the result is

$$H^{ex} = \phi_L = \text{DHLL} + \{MX + MM + XX\}_h m + \{MM + XX - MX\}_h m^{3/2} 2A + \ldots \quad (10)$$

where $\{MX + MM + XX\}_h$ equals $\{MX\}_h + \{MM\}_h + \{XX\}_h$ and DHLL is the Debye–Hückel limiting law for excess enthalpy. This equation gives the effects of all pairs and the ion atmospheres of those pairs on the excess enthalpy of the solution. The symbol $\{MX\}_h$ denotes the heat effect of the MX interaction (the major term is just $(K_{MX}\Delta H_{MX})$, the product of equilibrium constant for pair formation times the change in enthalpy for ion pair formation). The derivation of this equation neglects the hy-
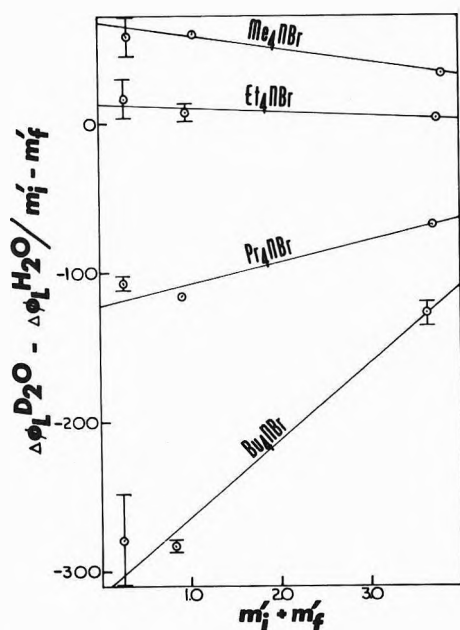
Figure 1. A plot of $[\Delta\phi_L(D_2O) - \Delta\phi_L(H_2O)]/(m_i' - m_f')$ vs. $(m_i' + m_f')$, eq 3.

TABLE II: Values of Constants in Eq 2^a

Salt	$k_1,^b$ cal mol	$k_2,$ cal mol
Me$_4$NBr	67 (5)^c	−9 (1)
Et$_4$NBr	12 (5)	−3 (2)
Pr$_4$NBr	−122 (10)	14 (1)
Bu$_4$NBr	−315 (10)	50 (5)

^{a} The constants were obtained from the plot of eq 4 given in Figure 1.
^{b} The units of k_1 and k_2 are based on the definition of aquamolality (moles per 55.51 moles) which makes this a dimensionless concentration. ^{c} The number in parentheses is the estimated standard deviation of the least significant digit.

dration effects discussed by Stokes and Robinson.[22] This neglect does not alter the conclusions discussed below.[23] The result then is that at low concentrations (where the m term predominates) the deviation from the Debye–Hückel limiting law is the sum of the like and oppositely charged interactions. However, as the concentration increases and the $m^{3/2}$ term becomes more important, the effect of oppositely charged interactions is reduced and the effect of like-charged interactions is increased. This is just what is qualitatively expected since as the ionic strength increases, the divalent ion (produced by two singly charged ions coming together) is stabilized more than the separate ions. This is the same effect found previously to occur in mixtures of electrolytes.[21] Similarly the cation–anion pair (with zero charge) is not stabilized by the increase in ionic strength but the separated ions are stabilized. This result shows that if we go to low enough concentrations so that higher order terms are negligible, we can separate the like-charged from the oppositely charged interactions by the difference in concentrations dependence of their ion atmospheres. The above discussion gives a qualitative reason for the fact that Ramanathan and Friedman,[24] using hypernetted chain calculations for model systems, are able to separate the effects of oppositely charged ions from like-charged ions by the difference in their concentration dependence. In fact, the limiting behavior predicted by eq 10 is also shown in Figures 7 and 9 of their paper.

Figure 2. A plot of excess enthalpy, H^{ex} or ϕ_L (cal/mol) in water for the tetraalkylammonium bromides at low concentrations vs. the square root of aquamolality. The dashed line labeled DHLL is the Debye–Hückel limiting law.

The present results do not go to low enough concentrations to use eq 10 and the experimental data for a quantitative separation of the like-charged from the oppositely charged interactions. This is because eq 10 assumes $m^{1/2}$ dependence of activity coefficients and this limiting law behavior is correct only at extremely low concentrations. The hypernetted chain calculations do not have this limitation. Recent calculations by Ramanathan, Krishnan, and Friedman[25] show that even with the hypernetted chain equation, accurate data below 0.1 m is necessary for an unambiguous separation of like-charged from unlike-charged interactions for the tetraalkylammonium halides.

The behavior of the tetrapropyl- and tetrabutylammonium bromides at low concentrations (Figure 2) is very striking. There is an initial negative deviation from the Debye–Hückel limiting law followed by an inflection point. Interpreted with the aid of eq 10, this means that the effect of cation–anion pairs is to reduce the excess enthalpy and the effect of cation–cation and anion–anion pairs is to increase the excess enthalpy. In order to get the large effects observed in Figure 2, both interactions must be large. For Bu$_4$NBr, where accurate free energy data are available below 0.1 m, the hypernetted chain calculations[25] yield large overlap parameters which are consistent with the above interpretations.

Recent measurements in this laboratory[26] of heats of mixing tetrabutylammonium chloride with potassium chloride down to 0.02 m confirm the large cation–cation interactions deduced from measurements at higher concentrations.[27]

It is interesting to note that the unusual behavior of the larger R$_4$N$^+$ salts observed in water is not present when

Figure 3. A plot of the excess enthalpy, H^{ex} or ϕ_L (cal/mol), vs. m' (aquamolality) for tetra-n-alkylammonium bromides: solid lines in D_2O, dashed lines in H_2O.

Figure 4. A plot of the excess enthalpy, H^{ex} or ϕ_L (cal/mol), vs. the aquamolality.

N-methylacetamide is the solvent. This is true for both the excess free energy[28] and excess heat.[29]

The reasons for the high concentration behavior of the excess enthalpy of aqueous solutions of tetraalkylammonium halides have been discussed previously[14,25,30] and the re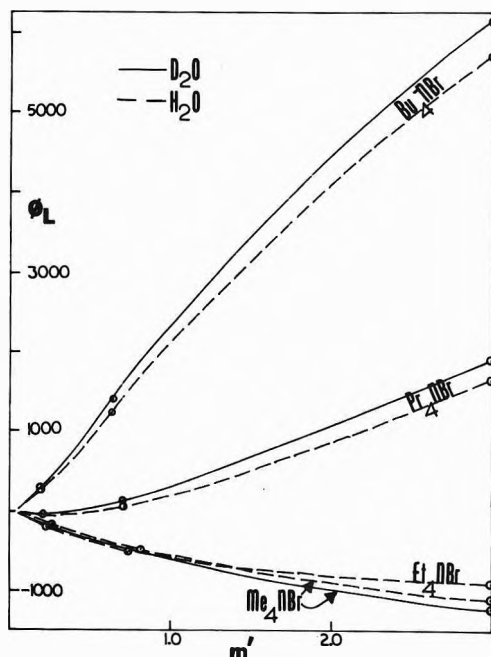sults of a wide variety of measurements on tetraalkylammonium halides have been reviewed recently by Wen[2] and by Franks.[3] Briefly, the hydrophobic hydration around the larger tetraalkylammonium ions is responsible for the extremely high heats of dilution of these compounds (see Figure 3).[31] As the solution is diluted, there is more room for the cospheres around the tetraalkylammonium ions and so part of the water that dilutes the solution is used to form cospheres. Since the cospheres are more hydrogen bonded there is an increase in the number of hydrogen bonds in this process and a large amount of heat is given off.

Results in D_2O. In D_2O, the excess enthalpy is even more positive for the larger tetraalkylammonium ions (Figure 3). This same effect is seen in the heats of dilution of the alkylamine hydrobromides measured by Desnoyers, et al.,[32] and in the results of Snell and Greyson on the sodium salts of aliphatic acids.[23] The tetramethylammonium ion does not have appreciable hydrophobic hydration. In fact, it is thought to have an opposite effect on the structure of water (structure breaking)[2,3,31,33-37] and the present results show that the effect of changing to D_2O from H_2O decreases the excess enthalpy of this salt. Tetraethylammonium bromide is an intermediate case and there is practically no difference in the heats of dilution in the two solvents (see Figures 3 and 4). This fits in with other data[2,3,31,35-38] which indicate that the tetraethylammonium ion is an intermediate case in which the effects of structure breaking and structure making are balanced. The present results as well as previous measurements[2-4,9,36-41] indicate that the effects that are present in water are magnified in D_2O solutions. Ions which are felt to be structure breaking in H_2O are more struc-

Figure 5. Plot of $\phi_L(D_2O) - \phi_L(H_2O)$ vs. molality for the tetra-n-alkylammonium bromides and some alkali halides. Note that the scale in the top half of the figure is compressed relative to the bottom half. A straight line was drawn through the points for NaCl, NaBr, and KCl to show the curvature necessary for the results to approach zero as $m \rightarrow 0$.

ture breaking in D_2O and ions which are thought to be structure making in H_2O are more structure making in D_2O. This is an important result that will have to be explained by theories of the effect of solutes on water.

It is possible to treat the difference in the heat contents of H_2O and D_2O solutions in a somewhat quantitative manner. Because the dielectric constants are so similar, the long-range forces in the two solvents will be almost identical. Similarily, the short-range repulsions due to the overlap of the electronic clouds of the two ions will be

identical. The only substantial change will be to the forces due to the ionic solvation, i.e., the cosphere overlap term in Ramanathan and Friedman's model.[24-25] In fact, as discussed above, Ramanathan and Friedman have calculated the effect of a small change in the cosphere term for cation–cation interactions and for cation–anion interactions. The results for the alkali halide models shows that a change in the cation–anion interactions gives a proportionately larger effect at low concentrations (that is the curve is less steep at high concentrations) and the effect of the cation–cation interactions is proportionately larger at high concentrations (that is the curve is steeper at higher concentrations). This is just the kind of effect predicted by eq 10. Figure 5 shows a plot of $\phi_L(D_2O)$ − $\phi_L(H_2O)$ (or $H^{ex}_{D_2O}$ − $H^{ex}_{H_2O}$) vs. molality for the tetraalkylammonium bromides and some alkali halides.[10,32] The curves for sodium chloride, potassium chloride, and sodium bromide are similar in shape to the curves calculated by Ramanathan and Friedman (Figures 7 and 9 of ref 22) for a change in cation–anion interaction in alkali halide solutions. Lithium chloride shows a barely detectable curvature. The curves for the tetraalkylammonium bromides are very similar to those for the alkali halides. This is a little surprising for the larger tetraalkylammonium ions. For these salts it would be expected that the cation–cation interactions were very important and that the curves should bend away from the axis at low concentrations as predicted by eq 12. There is a curvature away from the axis at low concentrations for Bu_4NBr and Pr_4NBr but it could be experimental error. The high concentration behavior may be a saturation effect due to the large size of the ions. This is reasonable since even at fairly low concentrations, there is not enough solvent to form the cospheres of all of the ions and cation–cation interactions cannot increase as rapidly as in dilute solutions. All of the curves in Figure 3 become less steep at high concentrations and this effect is responsible for the surprising regularity found in the values of k_1/k_2 of eq 2. For all of the results so far measured k_2 has an opposite sign to k_1 and is an order of magnitude smaller. The present discussion also shows why eq 2 does not represent the data accurately, particularly at high concentrations. Both the present results and the calculations of Ramanathan and Friedman indicate that the equation $H^{ex}_{H_2O}$ − $H^{ex}_{D_2O}$ = $A + Bm'$ would fit the data better at high concentrations but, of course, it would be wrong at low concentrations.[42]

References and Notes

(1) Taken in part from the Ph.D. Thesis of A. S. Levine, University of Delaware, June, 1971.
(2) W. Y. Wen, "Water and Aqueous Solutions, Structure, Thermodynamics and Transport Processes," R. A. Horne, Ed., Wiley-Interscience, New York, N. Y., 1971.
(3) F. Franks in "Hydrogen Bonded Solvent Systems," A. K. Covington and P. Jones, Ed., Taylor and Francis, London, 1968, pp 31–48.
(4) E. M. Arnett and D. R. McKelvey, "Solute-Solvent Interactions," J.
F. Coetzee and C. D. Ritchie, Ed., Marcel Dekker, New York, N. Y., 1969, Chapter 6.
(5) A. S. Levine, Ph.D. Thesis, University of Delaware, 1971.
(6) I. Wadso, Acta Chem. Scand., 22, 927 (1968).
(7) F. T. Gucker, Jr., and H. B. Pickard, J. Amer. Chem. Soc., 62, 1464 (1940).
(8) A. K. R. Unni, L. Elias, and H. I. Schiff, J. Phys. Chem., 67, 1216 (1963).
(9) R. E. Kerwin, Ph.D. Thesis, University of Pittsburgh, 1964.
(10) R. H. Wood, R. A. Rooney, and J. N. Braddock, J. Phys. Chem., 73, 1673 (1969).
(11) Excess enthalpy (H^{ex}) per mole of electrolyte is preferred (see H. L. Friedman, J. Chem. Phys., 32, 1351 (1960)) to the older nomenclature "relative apparent molal heat content, (ϕ_L)" (see ref 9). For clarity, both will be given in the major equations of this paper.
(12) H. S. Harned and B. B. Owen, "The Physical Chemistry of Electrolytic Solutions," 3rd ed, Reinhold, New York, N. Y., 1958, p 173.
(13) R. H. Wood, unpublished data. For a brief description, see H. S. Jongenburger and R. H. Wood, J. Phys. Chem., 69, 4231 (1965).
(14) S. Lindenbaum, J. Phys. Chem., 70, 814 (1966).
(15) S. Lindenbaum, private communication.
(16) R. B. Cassel and W-Y. Wen, J. Phys. Chem., 76, 1369 (1972). See also ref 17.
(17) B. Cassel, Ph.D. Thesis, Clark University, 1971.
(18) S. Lindenbaum and G. E. Boyd, J. Phys. Chem., 68, 911 (1964).
(19) (a) J. P. Rupert, Ph.D. Thesis, University of Pittsburgh, 1969. (b) J. C. Ku, Ph.D. Thesis, University of Pittsburgh, 1971.
(20) W. Y. Wen, S. Saito, and C. Lee, J. Phys. Chem., 70, 1244 (1966).
(21) R. A. Robinson, R. H. Wood, and P. J. Reilly, J. Chem. Thermodyn., 3, 461 (1971).
(22) R. H. Stokes and R. A. Robinson, J. Amer. Chem. Soc., 70, 1870 (1948).
(23) The equation would be exact in the McMillan-Mayer standard state (W. G. McMillan and J. E. Mayer, J. Chem. Phys., 13, 276 (1945)) if the equilibrium constants were replaced by the appropriate cluster integrals (H. L. Friedman, "Ionic Solution Theory," Interscience, New York, N. Y., 1962). These cluster integrals include the contributions of hydration effects to the excluded volume. The correction term includes the effects of changes in hydration due to changes in water activity.
A rough calculation of the correction to the McMillan–Mayer standard state (H. L. Friedman, J. Solution Chem., 1, 387 (1972)) shows that these terms are not negligible ($\Delta\phi_L \simeq$ 20 cal/mol at m = 0.1 mol/kg) but they are smooth functions of molality and do not affect the conclusions of this paper.
(24) P. S. Ramanathan and H. L. Friedman, J. Chem. Phys., 54, 1086 (1971).
(25) P. S. Ramanathan, K. V. Krishnan, and H. L. Friedman, J. Solution Chem., 1, 237 (1972).
(26) J. S. Falcone, A. S. Levine, and R. H. Wood, J. Phys. Chem., in press.
(27) R. H. Wood and H. L. Anderson, J. Phys. Chem., 71, 1871 (1967). Note in Table I of this paper the values of ΔH_m in the last column are four times the correct values. The values of RTh_0 (column 4) are correct. The authors are indebted to Professor W. Y. Wen for pointing out this error.
(28) R. W. Kreis and R. H. Wood, J. Phys. Chem., 75, 2319 (1971).
(29) J. S. Falcone, Ph.D. Thesis, University of Delaware, June, 1973.
(30) R. H. Wood, H. L. Anderson, J. D. Beck, J. R. France, W. E. DeVry, and L. J. Soltzberg, J. Phys. Chem., 71, 2149 (1967).
(31) For a different point of view see J. E. Prue, A. J. Read, and G. Romeo in "Hydrogen Bonded Solvent Systems," A. K. Covington and P. Jones, Ed., Taylor and Francis, London, 1968, pp 155–160; J. E. Prue, A. J. Read, and G. Romeo, Trans. Faraday Soc., 67, 420 (1971).
(32) J. E. Desnoyers, R. Francescon, P. Picker, and C. Jolicoeur, Can. J. Chem., 49, 3460 (1971).
(33) H. Snell and J. Greyson, J. Phys. Chem., 74, 2148 (1970).
(34) W. Y. Wen and S. Saito, J. Phys. Chem., 68, 2639 (1964).
(35) R. L. Kay and D. F. Evans, J. Phys. Chem., 70, 2325 (1966).
(36) P. R. Philip and J. E. Desnoyers, J. Solution Chem., 1, 353 (1972).
(37) P. R. Philip, J. E. Desnoyers, and A. Hade, Can. J. Chem., 51, 187 (1973).
(38) R. L. Day, T. Vituccio, C. Zawoyski, and D. F. Evans, J. Phys. Chem., 70, 2336 (1966).
(39) D. B. Dahlberg, J. Phys. Chem., 76, 2045 (1972).
(40) The heat capacities of G. C. Kresheck, J. Chem. Phys., 52, 5966 (1970), are in apparent disagreement with this conclusion.
(41) O. Ya. Samoilov and V. G. Tsvetkov, Zh. Strukt. Khim., 9, 193 (1968).
(42) A simple calculation shows that the poor fit of eq 2 to the difference between H_2O and D_2O causes only a very small (less than 3 cal/mol) error in the extrapolation of the results in D_2O.

Thermodynamic Investigation of Complex Formation by Hydrogen Bonding in Binary Liquid Systems. Chloroform with Triethylamine, Dimethyl Sulfoxide, and Acetone

Takeki Matsui,[1a] Loren G. Hepler,[1b] * and David V. Fenby[1c]

Departments of Chemistry, University of Lethbridge, Lethbridge, Alberta, Canada, and University of Otago, Dunedin, New Zealand
(*Received May 21, 1973*)

Calorimetric measurements have led to partial molar enthalpies of solution at infinite dilution and at stoichiometric mole fraction 0.5 in binary mixtures of chloroform with triethylamine, dimethyl sulfoxide, and acetone. We have derived and used thermodynamic equations that relate these partial molar enthalpies of solution to equilibrium constants and enthalpies of formation of AB and AB_2 complexes. Several procedures for obtaining molar enthalpies of complex formation are compared.

Introduction

Complex formation equilibria in dilute nonelectrolyte solutions have been investigated by various spectroscopic methods and also by such classical thermodynamic methods as distribution between immiscible solvents and measurements of colligative properties. There are many equilibrium constants that have been determined by way of one or more of these methods. But very few such equilibrium constants, particularly for weak complexes, have been determined with sufficient accuracy to permit useful evaluation of the molar enthalpy of complex formation by means of $\Delta H° = RT^2(\ln K/\partial T)_p$. Partly because of the difficulty of obtaining accurate $\Delta H°$ and $\Delta S°$ values from equilibrium constants at different temperatures, there have been several calorimetric investigations of complex formation. Most of these investigations have been concerned with reactions of type A + B = AB in some more or less "inert" solvent. Similar investigations of this kind of reaction in binary mixtures of A and B over the entire range of composition from pure A to pure B are much less common. In this paper we describe some calorimetric methods for investigation of complex formation (AB and AB_2) in such binary mixtures and apply these methods to mixtures of chloroform with triethylamine, dimethyl sulfoxide, and acetone.

Many years ago Dolezalek[2] and his followers tried to account for all deviations from ideal solution behavior in terms of chemical equilibria. This approach was soon shown to be chemically unrealistic and numerically inadequate for many systems. But many subsequent investigations of nonelectrolyte liquid mixtures have provided compelling evidence for various complexes. For those systems in which complex formation takes place, it is often convenient to divide the deviation from ideal solution behavior into "physical" and "chemical" contributions, with the latter being due to the complex formation. The "physical" contribution can be considered to be negligible compared to the "chemical" contribution in certain systems so that it is appropriate to attribute all deviations from ideality to the chemical reactions. The chemical species present (noncomplexed molecules and complexes) are thus assumed to mix ideally and we have what has been called the "ideal associated solution" model.

In a previous paper[3a] we have shown how it is possible to analyze integral molar enthalpies of mixing (ΔH_m) for binary mixtures in terms of the equilibrium constant (K_1) and the molar enthalpy of reaction ($\Delta H_1°$) for the complex formation represented by

$$A + B = AB \tag{1}$$

This method of analysis was applied to triethylamine (A) plus chloroform (B). We have also applied[3b] the related McGlashan–Rastogi[4] method of analysis (requires vapor pressures for evaluation of equilibrium constants and enthalpies of mixing for evaluation of molar enthalpies of complex formation) to dimethyl sulfoxide (A) plus chloroform (B) in which there are AB and AB_2 complexes so that values of K_2 and $\Delta H_2°$ for the reaction represented by

$$A + 2B = AB_2 \tag{2}$$

are obtained along with K_1 and $\Delta H_1°$. Here we report on our use of differential or partial molar enthalpies of solution ($\bar{L}$) in connection with investigation of reactions represented by eq 1 and 2 in mixtures of chloroform with triethylamine, dimethyl sulfoxide, and acetone. Our analysis is directly related to earlier attempts[5,6] to relate calorimetric results to enthalpies of hydrogen bond formation in these and similar systems.

Experimental Section

Enthalpies of solution have been measured by the ampoule method with an LKB precision reaction calorimetry system. Ampoules containing about 10^{-3} mol of a pure liquid were broken in calorimetric vessels containing 100 ml of another pure liquid or 100 ml of a solution with stoichiometric mole fraction $x = 0.500 \pm 0.002$. Thus the observed enthalpies of solution (with corrections for vapor space in the ampoules) are very close to the desired differential or partial molar enthalpies of solution ($\bar{L}$). All results refer to 298.15 $\pm$ 0.05°K.

Chloroform (Spectroanalyzed, Fisher Scientific Co.) was washed several times with distilled water, dried over fused $CaCl_2$, and then fractionally distilled. The middle fraction was dried over P_2O_5 and then fractionally distilled in an atmosphere of dried N_2. The resulting middle fraction was stored in an atmosphere of N_2 in the dark. Even with these precautions, it was found that calorimetric measurements made with chloroform that had been stored more than 2 days sometimes yielded erratic results.

Triethylamine (BDH Laboratory Reagent) was refluxed over KOH pellets, distilled from KOH, and then dried over CaH_2. The middle fraction was again fractionally distilled at about 100 mm pressure in an atmosphere of N_2.

Dimethyl sulfoxide (Baker Analyzed Reagent) was dried with Type 4A molecular sieve for at least 1 week and then distilled at reduced pressure ($t < 50°$) in an atmosphere of N_2. The middle fraction was again treated with the molecular sieve and then distilled as above before being stored in a desiccator in the dark.

Acetone (Analar grade) was dried by prolonged contact with molecular sieve and then twice fractionally distilled.

Results

Our experimental results are summarized in Table I. All reported partial molar enthalpies of solution ($\bar{L}$) are based on at least four separate calorimetric measurements. In the next section of this paper we are concerned with interpretation of these results in terms of the reactions represented by eq 1 and 2. In this section we compare our experimental results with those we calculate from ΔH_m values reported by other investigators.

Molar enthalpies of mixing (ΔH_m) may be calculated from partial molar enthalpies of solution ($\bar{L}$) by means of

$$\Delta H_m = x_A \bar{L}_A + x_B \bar{L}_B \qquad (3)$$

in which x_A and x_B represent stoichiometric mole fractions in the final solution formed from the pure components. Using this equation with our $\bar{L}$ values for triethylamine plus chloroform at $x = 0.5$, we calculate $\Delta H_m = -4.08$ kJ mol^{-1}, in excellent agreement with $\Delta H_m = -4.07$ kJ mol^{-1} reported previously[2b] on the basis of integral molar enthalpies of mixing measured with an entirely different calorimeter. A similar calculation with our present results for acetone plus chloroform at $x = 0.5$ gives $\Delta H_m = -1.84_5$ kJ mol^{-1}, in satisfactory agreement with $\Delta H_m = -1.85$ kJ mol^{-1} and $\Delta H_m = -1.9_2$ kJ mol^{-1} interpolated from the integral molar enthalpies of mixing reported by Campbell and Kartzmark[7] and by Morcom and Travers.[8]

Calculation of partial molar enthalpies of solution at infinite dilution ($\bar{L}°$) from integral molar enthalpies of mixing necessarily involves some sort of differentiation and/or extrapolation. Even using the "best" method[9,10] of data treatment, partial molar enthalpies of solution at infinite

dilution derived from ΔH_m results that typically cover the composition range $x \simeq 0.1$ to $x \simeq 0.9$ have considerably larger uncertainties than do the presently reported $\bar{L}°$ values that are based on measurements on solutions with $x \simeq 10^{-3}$.

Following Van Ness and Mrazek,[9,10] we have constructed graphs of $\Delta H_m / x_A x_B$ vs. x_A and x_B to obtain $\bar{L}°$ values from the extrapolated intercepts. These graphs were based on ΔH_m values from our previous investigation[2b] of triethylamine plus chloroform, on ΔH_m values from Fenby, Billing, and Smythe[11] for dimethyl sulfoxide plus chloroform, and on ΔH_m values from Campbell and Kartzmark[7] for acetone plus chloroform. (The ΔH_m results for acetone plus chloroform from Morcom and Travers[8] do not extend close enough to $x = 0$ to permit evaluation of $\bar{L}°$.) The results of these graphical evaluations of $\bar{L}°$, given in parentheses in Table I, are in satisfactory agreement with the considerably more accurate $\bar{L}°$ values based on our enthalpies of solution in very dilute solution.

Evaluation of the Molar Enthalpy of Complex Formation (AB Complexes)

Several earlier workers (see, for example, ref 5 and 6) have implicitly assumed or explicitly stated that partial molar enthalpies of solution at infinite dilution ($\bar{L}°$) can be related directly to formation of 1 mol of hydrogen bonds. We now consider this matter in relation to our analysis of $\bar{L}°$ values in terms of chemical reactions such as those represented by eq 1 and 2.

At first we restrict our attention to systems in which only AB complexes are formed, as represented by eq 1. The (mole fraction) equilibrium constant for this reaction may be written (all activity coefficients are unity in the "ideal associated solution" model)

$$K_1 = n_{AB}(\Sigma n_i)/n_A n_B \qquad (4)$$

in which n_A, n_B, and n_{AB} represent the numbers of moles of each species at equilibrium and (Σn_i) represents the total number of moles of all species in the solution at equilibrium. In the limit of infinitely dilute solution of B in A, $n_B/n_A \rightarrow 0$ and $(\Sigma n_i) \rightarrow n_A$ so that $K_1 \rightarrow n_{AB}/n_B$. The fraction of B that is complexed is therefore

$$n_{AB}/(n_B + n_{AB}) = K_1/(1 + K_1) \qquad (5)$$

Taking A + B to be an "ideal associated solution" in which all enthalpy changes are due to the reaction represented by eq 1, we have $\bar{L}_B° = K_1 \Delta H_1°(1 + K_1)$ and hence

$$\Delta H_1° = \bar{L}_B°(1 + K_1)/K_1 \qquad (6)$$

in which $\bar{L}_B°$ represents the partial molar enthalpy of solution of B (at infinite dilution) in A. Because the system A + B is symmetrical when AB is the only complex, we also have

$$\Delta H_1° = \bar{L}_A°(1 + K_1)/K_1 \qquad (7)$$

in which $\bar{L}_A°$ represents the partial molar enthalpy of solution of A (at infinite dilution) in B. Our eq 6 and 7 show that it is proper to take $\bar{L}° \simeq \Delta H_1°$ only when $K_1 \gg 1$. Since reported K_1 values (cited below) for the three systems under consideration in this paper range from 0.97 to 4.7 at 298°K, the factor $(1 + K_1)/K_1$ ranges from 2.0 to 1.2 and cannot properly be approximated by unity.

To make use of our $\bar{L}_A°$ and $\bar{L}_B°$ values (Table I) in eq 6 and 7 we must have an independently determined value of K_1. The nmr measurements of Huggins, Pimentel, and Shoolery[12] on triethylamine plus chloroform led them to

TABLE I: Partial Molar Enthalpies of Solution at 298°K

"Solute" in "solvent"	$\bar{L}$, kJ mol^{-1}	
HCCl$_3$ in Et$_3$N	−12.68	(−12.$_7$)[a]
Et$_3$N in HCCl$_3$	−11.55	(−11.$_1$)[a]
HCCl$_3$ in (CH$_3$)$_2$CO	−5.06	(−5.$_0$)[a]
(CH$_3$)$_2$CO in HCCl$_3$	−8.24	(−8.$_7$)[a]
HCCl$_3$ in DMSO	−5.68	(−5.$_9$)[a]
DMSO in HCCl$_3$	−13.1	(−14)[a]

	$\bar{L}_{0.5}$, kJ mol^{-1}
HCCl$_3$ in HCCl$_3$−Et$_3$N ($x = 0.5$)	−3.950
Et$_3$N in HCCl$_3$−Et$_3$N ($x = 0.5$)	−4.217
(CH$_3$)$_2$CO in HCCl$_3$−(CH$_3$)$_2$CO ($x = 0.5$)	−1.18
HCCl$_3$ in HCCl$_3$−(CH$_3$)$_2$CO ($x = 0.5$)	−2.51

[a] All values in parentheses have been derived graphically from previously reported ΔH_m values and have considerably greater uncertainties than do the values based on measurements with very dilute solutions.

report $K_1 = 3.0 \pm 1.0$. Subsequent nmr measurements on triethylamine plus chloroform in cyclohexane as solvent led Creswell and Allred[13] to report $K_1 = 4.20$. The nmr investigation of the same system by Howard, Jumper, and Emerson[14] led to a reported $K_1 = 4.70 \pm 0.12$. They[14] also quote $K_1 = 4 \pm 1$ from Martin's nmr investigation of triethylamine plus chloroform. On the basis of these results (all for 298°K), we take $3 < K_1 < 4.7$. Thus we calculate (using an average of $\bar{L}_A{}^\circ$ and $\bar{L}_B{}^\circ$) a range of $\Delta H_1{}^\circ$ from -16.2 to -14.7 kJ mol^{-1}. We adopt $\Delta H_1{}^\circ = -15.4$ kJ mol^{-1} as the best value to be obtained by this method.

It is also possible to use our partial molar enthalpies of solution in solutions with stoichiometric mole fraction $x = 0.5$ $(\bar{L}_{0.5})$ to obtain $\Delta H_1{}^\circ$ as follows. In our earlier investigation[3a] of complexing in triethylamine plus chloroform we derived and used the equation

$$x_A x_B / \Delta H_m = -[(K_1 + 1)/K_1(\Delta H_1{}^\circ)^2]\Delta H_m + (K_1 + 1)/K_1 \Delta H_1{}^\circ \quad (8)$$

We also have

$$\Delta H_m = \Delta H/(N_A + N_B) \quad (9)$$

and

$$x_A x_B = N_A N_B/(N_A + N_B)^2 \quad (10)$$

in which ΔH_m represents the molar enthalpy of mixing, ΔH represents the enthalpy of mixing of N_A moles of A with N_B moles of B, and x_A and x_B are stoichiometric mole fractions. Combination of eq 8–10 gives

$$[(K_1 + 1)\Delta H^2/K_1(\Delta H_1{}^\circ)^2] - [(K_1 + 1)\Delta H(N_A + N_B)/K_1 \Delta H_1{}^\circ] + N_A N_B = 0 \quad (11)$$

Solving this quadratic equation for ΔH and then differentiating as indicated by $(\partial \Delta H/\partial N_A)_{N_B, T, p}$ gives a complicated general expression for $\bar{L}_A$, which concerns us only in two special cases. In the limit of small N_A that corresponds to infinitely dilute A in B, we obtain eq 7 as previously derived in a simpler way. At $x_A = 0.5 = x_B$ we obtain

$$\Delta H_1{}^\circ = 2\bar{L}_{0.5}/[1 - (1 + K_1)^{-1/2}] \quad (12)$$

in which $\bar{L}_{0.5}$ represents the partial molar enthalpy of solution of a pure component into solution with stoichiometric mole fraction $x = 0.5$. Because of the symmetry of the system under consideration, eq 12 applies to $\bar{L}_{0.5}$ values for both A and B.

On the basis of an average of our $\bar{L}_{0.5}$ values for triethylamine plus chloroform and $3 < K_1 < 4.7$ as above, we find from eq 12 $\Delta H_1{}^\circ$ between -16.3 and -14.2 kJ mol^{-1}. We chose $\Delta H_1{}^\circ = -15.2$ kJ mol^{-1} as the best value to be obtained by this method.

We may also solve (analytically or graphically) the simultaneous equations 6 or 7 and 12 for both K_1 and $\Delta H_1{}^\circ$ in terms of $\bar{L}^\circ$ and $\bar{L}_{0.5}$. Using our partial molar enthalpies for the triethylamine plus chloroform system in this way, we calculate $K_1 = 3.3$ and $\Delta H_1{}^\circ = -15.8$ kJ mol^{-1}.

All of our results for triethylamine plus chloroform as described above are summarized in Table II, along with results of some earlier investigations of this system. It may be that the overall "best" $\Delta H_1{}^\circ$ value will be obtained by combination of calorimetric results with a K_1 derived spectroscopically. But it should be noted that our treatment of $\bar{L}^\circ$ and $\bar{L}_{0.5}$ values in the combination of eq 6, 7, and 12 leads to $\Delta H_1{}^\circ$ and K_1 values that are within the ranges of values obtained in other ways.

TABLE II: Comparison of $\Delta H_1{}^\circ$ Values for Triethylamine Plus Chloroform

Source	$\Delta H_1{}^\circ$, kJ mol^{-1}
Present work, eq 6, 7	-15.4
Present work, eq 12	-15.2
Present work, eq 6, 7, 12	-15.8 (and $K_1 = 3.3$)
Previous calorimetry[d] (ΔH_m)	-14.2 (and $K_1 = 4.7$)
Reference 12	-17^{ab}
Reference 13	-17^{ac}

[a] Based on $\Delta H_1{}^\circ = RT^2 (\partial \ln K_1/\partial T)_p$. [b] K_1 values at only two temperatures. [c] Based on triethylamine plus chloroform in cyclohexane as solvent. [d] Reference 3a.

Evaluation of Molar Enthalpies of Complex Formation (AB and AB$_2$ Complexes)

Consider partial molar enthalpies of solution at infinite dilution for binary systems in which both AB and AB$_2$ complexes may form as represented by eq 1 and 2. In this case we have

$$K_2/K_1 = n_{AB_2}(\Sigma n_i)/n_{AB}n_B \quad (13)$$

In the limit of infinitely dilute B in A, $n_B/n_A \to 0$ and $(\Sigma n_i) \to n_A$ so that eq 13 becomes

$$n_{AB_2}/n_{AB} = K_2 n_B/K_1 n_A = 0 \quad (14)$$

Because eq 14 shows that only A, B, and AB need be considered in the limit of infinitely dilute B in A, we have eq 6 applicable to solutions of the type now under consideration as well as to the solutions considered in the preceding section.

It is not correct to interpret the infinite dilution partial molar enthalpy of solution of A in B in terms of complete conversion of A to AB$_2$. Rather, it is necessary to consider fractional conversion of A to both AB and AB$_2$ as in

$$L_A{}^\circ = f_{AB}\Delta H_1{}^\circ + f_{AB_2}\Delta H_2{}^\circ \quad (15)$$

in which

$$f_{AB} = n_{AB}/(n_A + n_{AB} + n_{AB_2}) \quad (16)$$

and

$$f_{AB_2} = n_{AB_2}/(n_A + n_{AB} + n_{AB_2}) \quad (17)$$

In the limit of infinitely dilute A in B, $n_A/n_B \to 0$ and $(\Sigma n_i) \to n_B$. We therefore have

$$f_{AB} = K_1/(1 + K_1 + K_2) \quad (18)$$

and

$$f_{AB_2} = K_2/(1 + K_1 + K_2) \quad (19)$$

Substitution of eq 18 and 19 in 15 gives

$$\Delta H_2{}^\circ = [\bar{L}_A{}^\circ(1 + K_1 + K_2)/K_2] - [K_1\Delta H_1{}^\circ/K_2] \quad (20)$$

Further substitution of eq 6 in 20 gives

$$\Delta H_2{}^\circ = [\bar{L}_A{}^\circ(1 + K_1 + K_2)/K_2] - [\bar{L}_B{}^\circ(K_1 + 1)/K_2] \quad (21)$$

For the system dimethyl sulfoxide (A) plus chloroform (B) we take $K_1 = 1.2$ and $K_2 = 4.5$ from our analysis[3b] of the vapor pressures reported by Philippe, Jose, and Clechet.[15] Use of this K_1 with our $\bar{L}_B{}^\circ = -5.68$ kJ mol^{-1} from Table I in eq 6 gives $\Delta H_1{}^\circ = -10.4$ kJ mol^{-1} as compared to $\Delta H_1{}^\circ = -11$ kJ mol^{-1} found previously[3b] by way of a McGlashan–Rastogi[4] analysis. Use of the above

K_1, K_2, and $\bar{L}_B{}^\circ$ with $\bar{L}_A{}^\circ = -13.1$ kJ mol^{-1} from Table I in eq 21 leads to $\Delta H_2{}^\circ = -16.7$ kJ mol^{-1} as compared to the previously found[3b] $\Delta H_2{}^\circ = -16$ kJ mol^{-1}.

For the system acetone plus chloroform we take $K_1 = 0.967$ and $K_2 = 1.117$ from analysis of vapor pressures by Kearns.[16] Use of these values with our $\bar{L}_A{}^\circ$ and $\bar{L}_B{}^\circ$ values for this system from Table I in eq 6 and 21 leads to $\Delta H_1{}^\circ = -10.3$ kJ mol^{-1} and $\Delta H_2{}^\circ = -13.0$ kJ mol^{-1}. Morcom and Travers[8] have reported $\Delta H_1{}^\circ = -10.3$ kJ mol^{-1} and $\Delta H_2{}^\circ = -13.0$ kJ mol^{-1} on the basis of their McGlashan–Rastogi[4] analysis.

Discussion

In the "ideal associated solution" approach used in this paper it is assumed that the chemical species (A, B, AB, AB$_2$) mix ideally; i.e., deviations from ideal solution behavior are attributed entirely to the chemical reactions represented by eq 1 and 2. The activity coefficients of all chemical species are therefore taken to be unity, and all enthalpies of solution and mixing are attributed to chemical reactions represented by eq 1 and 2. This approximation is expected to be reasonable only for those systems in which the "physical" interaction is negligible compared with the "chemical" interaction. This requirement suggests that $-\Delta H_m$ should be greater than about 1.5 kJ mol^{-1} at $x = 0.5$ and that $-\bar{L}^\circ$ should be greater than about 3 kJ mol^{-1}.

It is to be emphasized that this "ideal associated solution" assumption is not peculiar to calorimetric methods. In application of other methods (spectroscopy, vapor pressures, etc.) it has been necessary (and reasonable) to attribute all of some observed property to specific chemical species (AB, AB$_2$, etc.) in solution and to take all activity coefficients to be unity. When this kind of treatment with activity coefficients taken equal to unity is carried out at more than one temperature, it follows that all enthalpies of mixing and solution are attributed to the chemical reactions represented by eq 1 and 2.

Because the methods we have described in this paper and also the other methods mentioned that lead to equilibrium constants at different temperatures are based on the same "ideal associated solution" model, we cannot say that any one method is fundamentally better than any of the others. We can, however, offer some generalizations about advantages, disadvantages, and limitations of the various approaches.

For systems in which there are only AB complexes, we have shown here and earlier[3a] that calorimetric measurements can lead to reasonable values of both K_1 and $\Delta H_1{}^\circ$. Other methods, such as spectroscopy, can lead to K_1

values at several temperatures and thence to $\Delta H_1{}^\circ$ from $RT^2(\partial \ln K_1/\partial T)_p$. It is reasonable to expect, however, that the best approach is one in which K_1 from some noncalorimetric method is combined with calorimetric results to yield $\Delta H_1{}^\circ$.

For systems in which there are AB and AB$_2$ complexes, noncalorimetric methods can lead to values of K_1 and K_2 at several temperatures and thence to values of $\Delta H_1{}^\circ$ and $\Delta H_2{}^\circ$. But the difficulties associated with simultaneous evaluation of both K_1 and K_2 are such that it is reasonable to expect that there will be substantial uncertainties associated with the derived $\Delta H_1{}^\circ$ and $\Delta H_2{}^\circ$ values. Although it is possible in principle to evaluate all four reaction parameters (K_1, K_2, $\Delta H_1{}^\circ$, and $\Delta H_2{}^\circ$) from ΔH_m values that cover a substantial range of composition or from $\bar{L}$ values at a suitable number of mole fractions, it is unreasonably optimistic to expect one set of enthalpy values to lead to accurate and unequivocal determination of all of these parameters. It is again reasonable to expect the best approach to be one in which K_1 and K_2 from some noncalorimetric measurements are combined with calorimetric results for evaluation of $\Delta H_1{}^\circ$ and $\Delta H_2{}^\circ$.

References and Notes

(1) (a) University of Lethbridge. (b) Mellor Visiting Professor, University of Otago, on leave from the University of Lethbridge. (c) University of Otago.
(2) F. Dolezalek, Z. Phys. Chem., **64**, 727 (1908).
(3) (a) L. G. Hepler and D. V. Fenby, J. Chem. Thermodyn., in press; (b) D. V. Fenby and L. G. Hepler, to be submitted for publication.
(4) M. L. McGlashan and R. P. Rastogi, Trans. Faraday Soc., **54**, 496 (1958).
(5) S. Murakami, M. Koyama, and R. Fujishiro, Bull. Chem. Soc. Jap., **41**, 1540 (1968).
(6) T. J. V. Findlay, J. S. Keniry, A. D. Kidman, and V. A. Pickles, Trans. Faraday Soc., **63**, 846 (1967).
(7) A. N. Campbell and E. M. Kartzmark, Can. J. Chem., **38**, 652 (1960).
(8) K. W. Morcom and D. N. Travers, Trans. Faraday Soc., **61**, 230 (1965).
(9) H. C. Van Ness, "Classical Thermodynamics of Non-Electrolyte Solutions," Pergamon Press, New York, N. Y., 1964.
(10) H. C. Van Ness and R. V. Mrazek, AIChE J., **5**, 209 (1959).
(11) D. V. Fenby, G. J. Billing, and D. B. Smythe, J. Chem. Thermodyn., **5**, 49 (1973).
(12) C. M. Huggins, G. C. Pimentel, and J. N. Shoolery, J. Chem. Phys., **23**, 1244 (1955).
(13) C. J. Creswell and A. L. Allred, J. Phys. Chem., **66**, 1469 (1962).
(14) B. B. Howard, C. F. Jumper, and M. T. Emerson, J. Mol. Spectrosc., **10**, 117 (1963).
(15) R. Philippe, J. Jose, and P. Clechet, Bull. Chim. Soc. Fr., 2866 (1971).
(16) E. R. Kearns, J. Phys. Chem., **65**, 314 (1961).

Infrared Spectroscopic Studies of *N,N*-Disubstituted Amides as Models for the Peptide Bond in Hydrogen Bonded Interactions with Water Molecules

David B. Henson and Charles A. Swenson*

Department of Biochemistry, University of Iowa, Iowa City, Iowa 52240   (Received November 2, 1972; Revised Manuscript Received April 30, 1973)
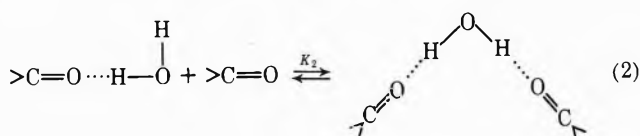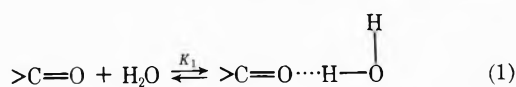
The hydrogen bonded interactions between water and a series of *N,N*-disubstituted amides, which are models for the peptide bond, have been measured in carbon tetrachloride with infrared spectroscopic techniques in the fundamental region. Thermodynamic parameters for the interaction between water molecules and the carbonyl oxygen were determined by the usual van't Hoff methods. The measured enthalpies ranged from -3.2 to -7.6 kcal/mol and were affected by substitution on both the carbonyl carbon and the amide nitrogen. These substituents appear to influence the interaction by steric, inductive, and field effects. In a comparison of proton donor strengths, water ranks below phenols and is similar to alcohols for this hydrogen bonded interaction in carbon tetrachloride.

Introduction

Protein molecules in biological systems are surrounded by a predominantly aqueous solvent which has its peculiar characteristics for interacting with solutes. Thus one postulates that the various protein–solvent interactions must be a determinant of the macromolecular conformation which the protein assumes. One interaction between the protein and the aqueous solvent which undoubtedly contributes to the overall conformational stability is the hydrogen-bonded interaction between the carbonyl of the peptide groups and the protons of water molecules in the immediate environment. A knowledge of the strengths of such solvent interactions is important for any complete conformational calculation as some macromolecules drastically change their conformations as the solvent is varied.

Although there are numerous reports of studies involving alcohols and phenols as donors in hydrogen bonding studies with amides,[1-4] water has seldom been used as a proton donor.[5-11] We have noted only one attempt to measure the thermodynamic parameters for the processes defined by eq 1 and 2 and that was a pmr determination

$$>C=O + H_2O \underset{}{\overset{K_1}{\rightleftharpoons}} >C=O\cdots H-\overset{\displaystyle H}{\underset{\displaystyle |}{O}} \qquad (1)$$

$$>C=O\cdots H-\overset{\displaystyle H}{\underset{\displaystyle |}{O}} + >C=O \overset{K_2}{\rightleftharpoons} \qquad (2)$$

of K_2 for dimethylacetamide (C=O).[7] The high concentrations of amide and water required for the pmr studies precluded any determination of K_1. In highly aqueous solutions the equilibrium represented by eq 1 is the one of importance as an interaction of this type occurs for each peptide linkage in the polypeptide or protein. In the present study the thermodynamic parameters for the hydrogen bonded interaction of water molecules with *N,N*-disubstituted amides as models for the peptide bond with various side chain substituents have been measured in carbon tetrachloride solution. We fully realize that there is yet a considerable extrapolation to a peptide chain in aqueous solution which will change these numbers; however, their

relative values may still be useful. Thus in addition to finding the specific hydrogen-bonded energies for water interacting with the amide bases another measure of their relative base strengths will be obtained. For example, they ought to be useful in making a choice between two or more peptide groups of equal spatial probability for a hydrogen bonded interaction with a proton donor in the interior of a protein.

Experimental Section

Materials. Fisher Certified carbon tetrachloride was used without further purification. *N,N*-Dimethylformamide, *N,N*-dimethylacetamide, *N,N*-dimethylpropionamide, *N,N*-dimethylbutyramide, and *N,N*-dimethylbenzamide from Eastman Organic Chemicals were purified by vacuum distillation.[12] *N*-Methylacetanilide, which was purchased from Eastman Organic Chemicals, was used without further purification.

N,N-dimethylisovalerylamide, *N,N*-dimethylisobutyramide, *N*-benzyl-*N*-methylacetamide, *N*-butyl-*N*-methylacetamide, and *N*-butyl-*N*-methylphenylacetamide were synthesized in this laboratory by acylating the appropriate secondary amines with acyl chlorides.[12,13] All of the amines and acyl chlorides used in the syntheses were from Eastman Organic Chemicals. Molecular sieve, Type 4A (Fisher Scientific Co.), was used for drying the carbon tetrachloride and the liquid amides. Calcium chloride dihydrate from Fisher Scientific Co. was used for the preparation of aqueous solutions of known water activity.

Methods. Solutions of water in carbon tetrachloride were prepared by the methods described by Christian, *et al.*,[14] and used by these authors in numerous studies (see, for example, ref 15–17). The isopiestic apparatus consisted of a wide-mouth ointment jar in which the lid was fitted with a long stainless steel needle which could be stoppered with a Teflon plug. Approximately 50 ml of the appropriate concentration of aqueous salt solution was placed in the bottom and a small beaker containing the carbon tetrachloride set upright in the jar. The screw lid was then tightened with the end of the needle positioned below the level of the carbon tetrachloride in the beaker. After equilibration, which was complete in 10 hr in agreement with the experiments of Christian, *et al.*,[14] the solu-

tion was withdrawn with a syringe and used for preparation of the ternary solutions. Water concentrations in the range 4×10^{-3}–7×10^{-3} M could be obtained using aqueous $CaCl_2$ solutions ranging from 8.0 to 1.0 m, respectively, at 25°.

Constant total water concentration in the carbon tetrachloride solutions during preparation of the ternary amide–water–carbon tetrachloride solutions and subsequent transfer to the infrasil cells for spectrophotometric measurements was assured by fitting the Teflon caps on the volumetrics and the Infrasil cells with Luer-Lok connectors and performing the transfer with syringes. The preparations and transfers were made in humidity- and temperature-controlled glove boxes.

Most of the amides used were hygroscopic and were stored over molecular sieves in a drybox. Transfers for weighing and preparations of solutions were made in a glove box which was constantly flushed with dry air from a Gilbarco air dryer and which had open dishes of phosphorus pentoxide. The ternary solutions were prepared by adding water–carbon tetrachloride of known water activity to volumetrics which contained weighed amounts of amide which had been dried with molecular sieves. Even with the rigorous drying and handling techniques used, small amounts of water remained in some of the amide solutions. Where the absorbance of these amide solutions at 3706 cm^{-1} was greater than 0.005 in a 1-cm cell, which corresponds to an added water concentration of 1×10^{-4} M, the data were discarded. At the average water concentration for these experiments (5.0×10^{-3} M) the error in the total water concentration from this cause was 3% or less.

Spectra were measured on a Perkin-Elmer Model 521 infrared spectrometer in 1- or 2.5-cm Infrasil cells and in some cases (the pure amides) in 0.1-mm CaF_2 cells. The spectral slit for all measurements was 2.0–2.5 cm^{-1}. Temperature was controlled to ±0.5° in the sample and reference compartments with Barnes Engineering Co. Model 104 variable-temperature chambers, which were fitted with CaF_2 windows. The temperatures inside the chambers were monitored by copper–constantan thermocouples which were connected to a direct reading potentiometer from Biddle-Gray, Inc. The monochromator, source optics, and the variable-temperature chambers were constantly flushed with a small stream of dry air to eliminate imbalance due to atmospheric water absorption. In a typical run, equilibrium spectra of the ternary solutions were measured at 25, 15, 35, 45, and 25°. Most runs included a repeat at one temperature to check for loss of contents. Density corrections were made on the absorbance, A, to give A_{cor} using the equations[16]

$$V_t = V_0(1 + 1.18384 \times 10^{-3}t + 0.89881 \times 10^{-6}t^2 + 1.35135 \times 10^{-8}t^3)$$

$$X_t = V_t/V_0$$

$$A_{cor} = AX_t/X_{20} = AX_t/1.02414$$

In these equations, t is the temperature in °C, V_t is the volume at temperature t, V_0 is the volume at 0°, and X_t is the density correction factor for carbon tetrachloride. The reference temperature is 20°.

Number average molecular weights of the amides in carbon tetrachloride at 37° were measured with a Mechrolab vapor pressure osmometer.
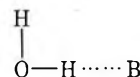
Resolution of overlapping absorptions was accomplished using approximately Gaussian functions on a Du Pont Model 310 curve resolver. The pmr spectra were measured on a Varian A-60 nuclear magnetic resonance spectrometer at ambient temperature (40°).

Results and Discussion

Determination of K. A set of spectra typical of those required to provide data for the calculation of a single equilibrium constant is shown in Figure 1. Curve A is a spectrum of dry carbon tetrachloride *vs.* air which is used to verify that the solvent is dry. Curve B is a spectrum of dry amide in carbon tetrachloride *vs.* carbon tetrachloride and serves as a check for amide dryness and possible interfering amide absorptions which need to be subtracted. Curve C is a spectrum of water at the concentration initially in the ternary solution, C_{iw}, *vs.* carbon tetrachloride. Curve D is a spectrum of the ternary solution *vs.* carbon tetrachloride from which equilibrium concentrations of water, C_{fw}, and complex C_{com}, were measured. The baseline position for each spectrum, as determined by a measurement of the absorbance of carbon tetrachloride *vs.* carbon tetrachloride, was constant at each temperature and coincided with the sample spectrum in regions of no absorption.

The spectrum presented in 1D is typical of all the water–amide complexes in carbon tetrachloride solution and is characteristic of a 1:1 complex of base and water. These absorptions can be assigned as first suggested by Mohr, *et al.*[18] Water in carbon tetrachloride shows two absorptions at 3706 and 3615 cm^{-1} which are respectively the antisymmetric and symmetric stretching vibrations of the monomer. Addition of base, B, at the concentrations used in this study gives rise to two new absorptions, a sharp band at slightly lower frequencies (~3680 cm^{-1}) than the antisymmetric stretching vibration of water characteristic of a free O–H vibration and a very broad absorption at much lower frequency (~3470 cm^{-1}) characteristic of a hydrogen bonded vibration. A plot of the resolved water and complex absorption after subtracting amide absorption is shown in Figure 2. This suggests a complex of the type

$$\begin{array}{l} H \\ | \\ O\!-\!H \cdots\!\cdots B \end{array}$$

At higher base concentrations, a 2:1 complex would be expected. This complex is characterized by two broad O–H stretching vibrations, antisymmetric and symmetric, as the symmetry is restored. Mohr, *et al.*,[18] typically observed these absorptions at frequencies intermediate to those of the two absorptions of the 1:1 complex. We did not observe these characteristic absorptions for any of our ternary solutions and estimate them to contribute less than 5% to the total hydrogen-bonded species assuming an extinction coefficient similar to that for the hydrogen bonded absorption of the 1:1 complex. Thus we have neglected any contribution of a 2:1 complex in our calculation of the equilibrium constant for the 1:1 complex.

Determination of the equilibrium constant for the process is then seemingly straightforward using the concentrations of free water, complex, and free base in the ternary solution, as determined by absorbances and extinction coefficients. The extinction coefficients for the absorptions of the complex are not known, however, and thus we used the stoichiometry and the known extinction for water and determined the complex concentration as a difference between the total water and free water. This is analogous to the procedure used, for example, to study the dimeriza-
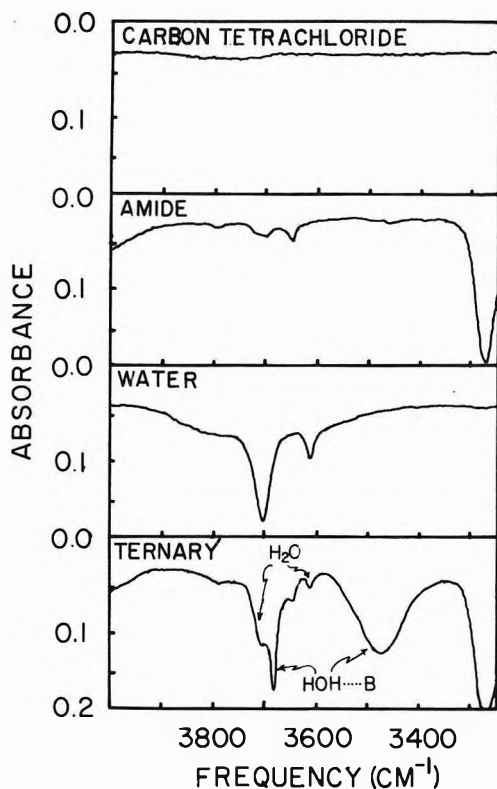
Figure 1. Typical infrared spectra used for determination of K: (A) dry carbon tetrachloride vs. empty cell; (B) dry amide in carbon tetrachloride vs. carbon tetrachloride; (C) water in carbon tetrachloride vs. carbon tetrachloride; (D) amide plus water in carbon tetrachloride vs. carbon tetrachloride. The path length is 1 cm.

Figure 2. Resolution of ternary solution spectra after subtracting amide absorptions.

tion of alcohols and lactams.[19-21] This method can give rise to large errors, particularly when the fraction of the complex formed is low, and thus other methods were investigated.

A standard procedure for analyzing the data on weak complexes is to employ either a Scott or Benesi–Hildebrand plot and determine both the equilibrium constant and the extinction coefficient for an absorption characteristic of the complex from the slope and intercept.[22,23] In order to obtain reliable constants one works over a range of fractional saturation values, preferably between 0.20 and 0.80 and further, the stoichiometry should be known. The limitations and assumptions of the method were discussed earlier by Person[24] with respect to slope and intercept errors and more recently with respect to errors on K and ϵ by Deranleau.[25] For our system the stoichiometry is established by the spectra. The difficulty with the application of these approaches arises with the limitations on the concentration range accessible to the components. The water concentration is necessarily in the range 4–6 × 10^{-4} M; the lower limit is determined by observability and the upper by solubility. The amide concentration is limited by solubility for some of the amides and for others at higher concentrations the ternary amide–water–carbon tetrachloride system is unstable and phase separation occurs. Another limitation is the possibility of formation of 2:1 complexes at high amide concentrations. A Scott plot of our data thus has points over only a very narrow range of saturation for which the slope and intercept, and thus K and ϵ, are poorly defined. In the limit of only a single saturation value, the slope and intercept are not defined at all. Some of our data were plotted in this manner and,
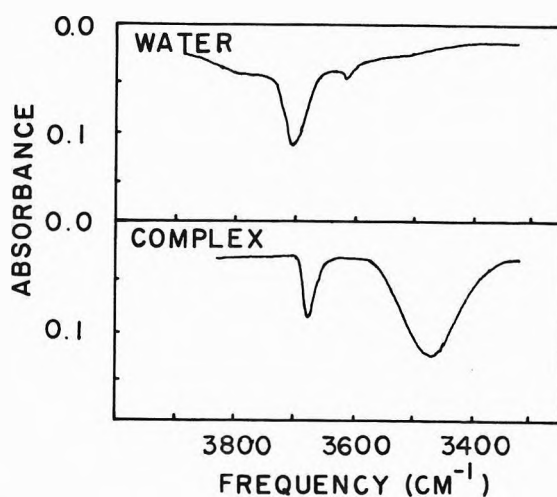
when a slope was established, showed errors on K similar to those of the procedure used, wherein with a known extinction coefficient for the absorption of the antisymmetric stretching vibration of water, and with the given stoichiometry and the concentration of amide as determined by weight, a value for K can be determined from a single experiment as is often done in hydrogen bonding studies.[19-21]

For these reasons the procedure described in detail below was adopted in spite of known limitations as there seemingly is no other direct way to obtain thermodynamic parameters for this important process (water hydrogen bonding to model peptide groups).

The equilibrium constant, K_1, was calculated from eq 3 and 4 using the 1:1 stoichiometry as verified by the

$$K_1 = C_{com}/C_{fw}C_B \qquad (3)$$

$$K_1 = (C_{iw} - C_{fw})/C_{fw}C_B \qquad (4)$$

spectrum.[18] In eq 3 and 4 C_{com} is the concentration of complex, C_{iw} is the concentration of initial water which was obtained from absorption at 3706 cm^{-1} in spectrum 1C, and C_{fw} is the final water concentration in the ternary solution which was obtained from the 3706-cm^{-1} absorption in spectrum 1D. The water concentrations were calculated from the measured absorbances and the known molar extinction coefficient at 3706 cm^{-1}, 37 M^{-1} cm^{-1},[26] and the base concentration, C_B, was calculated by weight. Density corrections were made on all solutions. The equilibrium base concentrations were set equal to the total base concentrations for these measurements. In all cases the initial base concentration was at least ten times greater than the initial water concentration and with 20% of the water complexed, the resulting error is 2% or less.

In order to verify that the absorbance at 3706 cm^{-1} was a valid measure of free water concentration in the ternary solution, the overlapping absorptions were resolved with a Du Pont curve resolver on a large number of spectra for each amide. This showed that the absorption at 3706 cm^{-1} was not significantly overlapped at the maximum by the absorption of the complex (see Figure 2). The water absorption at 3706 cm^{-1} is broader than the complex absorption at 3680 cm^{-1}, $\Delta\nu_{1/2}{}^a$ being 50 cm^{-1} vs. 25 cm^{-1} for the complex. For the fractional saturations used

TABLE I: K Values Calculated from Spectra of Ternary (CCl$_4$–H$_2$O–Amide) Solutions for 1:1 Hydrogen Bond Formation between Water and Carbonyl of N,N-Disubstituted Amides

Amide	15°	25°	35°	45°
N,N-Dimethylformamide	5.81 ± 2.26	4.39 ± 1.74	3.70 ± 1.65	2.75 ± 1.61
N,N-Dimethylacetamide	10.29 ± 3.18	8.66 ± 2.45	6.94 ± 2.02	6.22 ± 2.15
N,N-Dimethylpropionamide	6.66 ± 2.54	5.08 ± 2.31	4.34 ± 1.63	3.72 ± 1.64
N,N-Dimethylbutyramide	7.84 ± 1.59	5.72 ± 1.03	4.81 ± 1.38	4.63 ± 1.27
N,N-Dimethylisobutyramide	8.42 ± 2.61	5.91 ± 2.31	5.10 ± 2.04	4.87 ± 3.04
N,N-Dimethylisovalerylamide	8.45 ± 2.18	5.45 ± 1.61	4.92 ± 2.36	3.68 ± 2.00
N,N-Dimethylbenzamide	3.50 ± 1.02	3.03 ± 0.97	2.00 ± 0.57	1.27 ± 0.41
N-Butyl-N-methylphenylacetamide	6.18 ± 1.86	4.89 ± 1.26	3.81 ± 1.59	2.60 ± 1.42
N-Butyl-N-methylacetamide	8.12 ± 2.37	6.49 ± 1.48	4.86 ± 1.52	3.94 ± 2.84
N-Methylacetanilide	7.37 ± 1.19	5.21 ± 0.79	4.77 ± 1.35	3.94 ± 1.44

in these studies, the complex typically contributes less than 1% to the absorption of water at 3706 cm^{-1}.

Table I presents values of the measured equilibrium constants as a function of temperature with their standard errors. At each of the four temperatures 20 to 35 values of the equilibrium constants were measured for each amide. The large standard errors arise from the numerator of eq 4. These errors are in agreement with 30–50% error calculated by Deranleau[25] for our range of saturation, 0.10–0.25, using the Scott or Benesi-Hildebrand equations for the analysis. The values of the equilibrium constants presented in Table I are likely to bracket the true values in spite of the large standard errors.

An estimate of the contribution of the numerator term to the standard error can be made by using the data to back calculate an extinction coefficient for the hydrogen bonded absorption of the complex at 3470 cm^{-1}. Using this extinction coefficient and the measured absorbances at 3470 cm^{-1} to determine the complex concentration, equilibrium constants of the same magnitude were obtained with standard errors of less than 5%. (This calculation assumes, as is usual, that all the temperature dependence of the absorption at 3470 cm^{-1} is due to the making or breaking of hydrogen bonds.) The equilibrium constants obtained in this manner are, of course, not subject to the large error arising from the difference term in eq 4 (although their magnitude is) and the results suggest that the large standard errors did arise from the large random scatter in the values for the complex concentration.

Several competing equilibria and the inherent temperature dependences of extinction coefficients of the absorption bands were considered and were shown to make negligible contributions to the error of the measured equilibrium constants. A brief discussion of these points follows.

The extinction coefficients of infrared absorptions can show significant temperature dependences even after correcting for density. Such temperature effects can be reduced to a few per cent over our temperature range if integrated absorption coefficients are used. We used molar extinction coefficients for reasons of convenience (for a large number of measurements) and because integrated absorption coefficients are not without subjective aspects (e.g., wing corrections) and in our case, curve resolution was necessary prior to integration. Thus we determined concentrations for calculation of the equilibrium constant using extinction coefficients as discussed earlier.

The error arising from the temperature dependence of extinction coefficients is removed in our procedure as C_{com}/C_{fw} is determined as a ratio of water absorbances from which the extinction coefficient cancels.

$$K = \frac{C_{com}}{C_{fw}C_B} = \frac{C_{iw} - C_{fw}}{C_{fw}C_B} = \left(\frac{A_{3706(i)} - A_{3706(f)}}{\epsilon_m t}\right) \Big/ \left(\frac{A_{3706(f)}}{\epsilon_m t C_B}\right)$$

The amide concentration was determined by weight with a correction for density and is not subject to the same error.

Dimerization of water in carbon tetrachloride has been studied by several workers.[17,27,28] Using the dimerization constant measured by Magnusson, $K_d = 2.2\ M^{-1}$ at 25°, less than 1.5% of the total water exists as dimer in our solutions and therefore dimer formation was neglected in our determination of the equilibrium constant. Hydrogen bonding of water to solvent was also ignored.[29,30]

Water was assumed to be hydrogen bonded to the amide carbonyl as the amide nitrogen has been shown by experimental studies to be a much weaker proton acceptor.[31,32]

N,N-Disubstituted amides can associate by dipolar interactions in carbon tetrachloride solution. From the studies of Neuman, Snider, and Jonas[33] on N,N-dimethylacetamide and N,N-dimethylformamide, we calculate that less than 6% of these amides would be dimerized at the highest concentrations used. The extent of dimerization for our other amides was checked by number average molecular weight measurements in the range of concentration used, 0.01–0.08 M. The values obtained agreed with the theoretical molecular weight to within 3%, which is the expected experimental error, and thus the amides were assumed to be present as monomers.

Thermodynamic Parameters. The values of the equilibrium constants determined as a function of temperature were plotted as ln K vs. $1/T$ (van't Hoff) and $\Delta H°$ was calculated from the slope of a least-squares line fitted to the 80 or more data points. These values of $\Delta H°$ as well as $\Delta G°$ and $\Delta S°$ at 25° are presented in Table II with their standard errors. The standard enthalpies were also obtained from equilibrium constants determined by using the absorptions at 3470 cm^{-1} to calculate complex concentrations. These values were 5% or less lower in magnitude with a 5–10% standard error. The values of $\Delta H°$ so determined do not depend on the absolute magnitude of K, only the change in ln K with $1/T$. Thus the good agreement of these values with those presented in Table I suggests that the $\Delta H°$ for the process are probably better than the standard errors indicate whereas the free energies and entropies have the given standard errors.

When considering the amides as models for the peptide bond, results such as these provide a crude but important preliminary step in our understanding of polypeptide and protein solvent interactions and how they might contrib-

TABLE II: Thermodynamic Parameters for 1:1 Hydrogen Bond Formation between a Water Proton and the Carbonyl Oxygen of N,N-Disubstituted Amides

Amide	K, M^{-1} (25°)	$-\Delta H°$, kcal/mol	$-\Delta G°$ (25°), kcal/mol	$-\Delta S°$ (25°), eu
N,N-Dimethylformamide	4.39 ± 1.74^a	3.20 ± 0.68^b	0.88 ± 0.24^c	7.78 ± 3.08^d
N,N-Dimethylactamide	8.66 ± 2.45	3.17 ± 0.41	1.28 ± 0.17	6.33 ± 1.94
N,N-Dimethylpropionamide	5.08 ± 2.31	3.69 ± 0.56	0.96 ± 0.27	9.14 ± 2.78
N,N-Dimethylbutyramide	5.72 ± 1.03	4.03 ± 0.63	1.03 ± 0.11	10.07 ± 2.48
N,N-Dimethylisobutyramide	5.91 ± 2.31	4.30 ± 0.80	1.05 ± 0.23	10.88 ± 3.45
N,N-Dimethylisovalerylamide	5.45 ± 1.61	4.74 ± 0.83	1.00 ± 0.17	12.55 ± 3.35
N,N-Dimethylbenzamide	3.03 ± 0.97	7.57 ± 0.51	0.66 ± 0.19	23.18 ± 2.35
N-Butyl-N-methylphenylacetamide	4.89 ± 1.26	5.71 ± 1.24	0.94 ± 0.15	16.02 ± 4.66
N-Butyl-N-methylacetamide	6.49 ± 1.48	4.45 ± 1.04	0.81 ± 0.13	12.22 ± 3.92
N-Methylacetanilide	5.21 ± 0.79	3.78 ± 0.51	0.98 ± 0.09	9.42 ± 2.00

^{a} Standard errors. The standard error of the mean is one-fifth of this error. ^{b} Standard errors of slope multiplied by $2.3R$. The standard error of the mean is one-fifth of this error. ^{c} Error is $(RT/K)\delta K$ where δK is the standard error on K. ^{d} Error is $(\delta H + \delta G)/T$ where δH and δG are the standard errors on $\Delta H°$ and $\Delta G°$, respectively.

ute to the overall conformational stability of these molecules in aqueous solution. The hydrogen bonded interactions of water to various N,N-disubstituted amides show a wide variation in intrinsic strengths as measured by $\Delta H°$ and a small variation in tendency to form as measured by $\Delta G°$. We are aware that there is yet an extrapolation to the aqueous solvent which will alter these thermodynamic parameters. The results of this study then lead to an interesting conclusion. The nature of the substituents on either side of the peptide group influences the intrinsic strength of the hydrogen bonds as measured by $\Delta H°$ and, to a lesser extent, their tendency to form as measured by $\Delta G°$. This suggests that the amino acid side chains which occur on either side of the peptide group must be noted when considering hydrogen bonds to solvent and that each hydrogen bond must be evaluated on the basis of its unique environment.

The trends of the equilibrium constants in this series of amides allow several other points to be made which are particularly pertinent due to the few studies using water as a proton donor. To a large extent the chemical properties of amides are determined by resonance effects. The substituent groups R_1, R_2, and R_3 in the structure

$$R_1-\overset{\overset{\displaystyle O}{\|}}{C}-N\overset{\displaystyle R_2}{\underset{\displaystyle R_3}{<}}$$
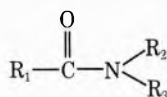
influence the resonance and affect the basicity of the oxygen and thus its ability to form a hydrogen bond.[34-36] Of the numerous studies that have investigated amide basicity, one of the most comprehensive is that of Adelman[34] which showed that the basicity of N,N-disubstituted amides is related to $\Sigma\sigma^*$, the sum of the polar contributions of the substituents on the amide group as quantitated by Taft's polar factor σ^*.[37] Correlations between the polar factors and carbonyl frequency or other parameters indicative of base strength such as K were linear for most studies of homologous series of amides. Adelman suggests that correlation in the series depends on inductive effects, resonance effects, and bond angle strain and deviations likely indicate steric effects. Plots of carbonyl frequency and log K vs. $\Sigma\sigma^*$ for the amide studied are presented in Figure 3. The amides containing aromatic substituents on the peptide group, N,N-dimethylbenzamide, N-butyl-N-methylphenylacetamide, and N-methylacetanilide, showed large deviations which likely arise from steric and other electronic effects peculiar to the aromatic system. N,N-

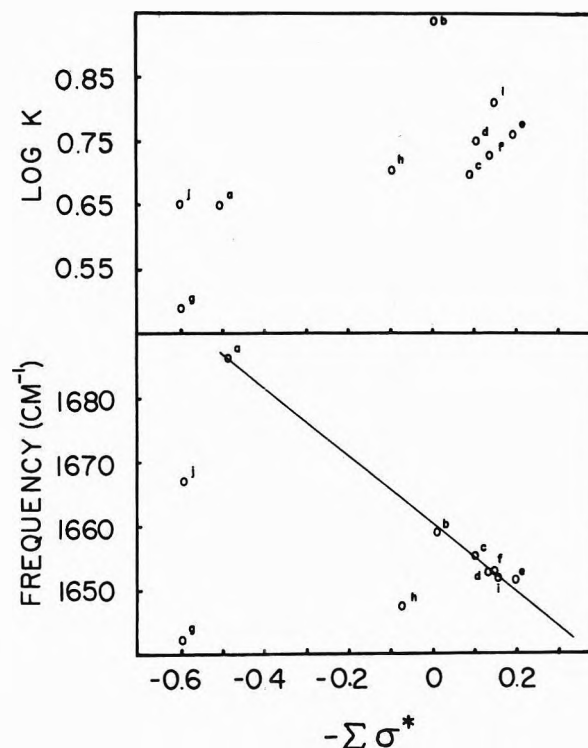**Figure 3.** Equilibrium constant and carbonyl frequency of the disubstituted amides as a function of Taft's polar factor, σ^*. (a) N,N-dimethylformamide; (b) N,N-dimethylacetamide; (c) N,N-dimethylpropionamide; (d) N,N-dimethylbutyramide; (e) N,N-dimethylisobutyramide; (fi) N,N-dimethylisovalerylamide; (g) N,N-dimethylbenzamide; (h) N-butyl-N-methylphenylacetamide; (i) N-butyl-N-methylacetamide; (j) N-methylacetanilide.

Dimethylbenzamide, for example, shows strong conjugative effects of the ring and peptide carbonyl as is evidenced by the low carbonyl frequency.
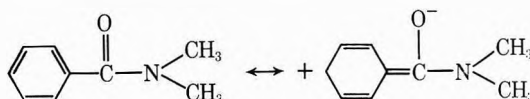
Further support for this idea comes from its pmr spectrum in carbon tetrachloride which shows one N-methyl resonance indicating that the two methyls are magnetically equivalent; that is, free rotation exists about the C–N bond at 40° in contrast to most of the other N,N-disubstituted amides which show cis and trans methyl resonances.

TABLE III: A Comparison of Water as a Proton Donor with Other Donors at 25° in Carbon Tetrachloride

Amide	Donor	K, M^{-1}	$-\Delta H$, kcal/mol	$-\Delta S$, eu	Ref
N,N-Dimethylformamide	Water	4.4	3.2	7.8	a
N,N-Dimethylformamide	2-Propanol		3.9		4
N,N-Dimethylformamide	Phenol	64.0	6.1	12.1	1
N,N-Dimethylformamide	PFP[b]	116.0	7.0	12.7	c
N,N-Dimethylacetamide	Water	8.7	3.2	6.3	a
N,N-Dimethylacetamide	Methanol	5.5	3.7	9.1	4
N,N-Dimethylacetamide	Ethanol	3.5	3.9	10.5	4
N,N-Dimethylacetamide	2-Propanol	2.7	2.4		d
N,N-Dimethylacetamide	2-Methyl-2-propanol	2.9	3.9	11.0	4
N,N-Dimethylacetamide	Phenol	134.0	6.4	11.7	1
N,N-Dimethylacetamide	PFP[c]	260.0	7.4	13.9	c

[a] Our results. [b] p-Fluorophenol. [c] E. M. Arnett, L. Joris, E. Mitchell, T. S. S. R. Murty, T. M. Gorrie, and P. v. R. Schleyer, *J. Amer. Chem. Soc.*, **92**, 2365 (1970). [d] F. Takahashi and N. C. Li, *J. Phys. Chem.*, **68**, 2136 (1964).

An investigation of the barrier heights to free rotations as a function of substituent group by pmr would be an interesting extension of these studies.

An interesting comparison can be made of the proton-donating strength of water and other better studied proton donors. This comparison is made in Table III. Here water is seen to have a donor strength similar to alcohols but significantly poorer than phenol or p-fluorophenol.

Upon comparing these data there is an interesting unexplained regularity. In at least three examples of complex formation of N,N-dimethylformamide and N,N-dimethylacetamide with electron acceptors, the association constant for the formation of the latter is twice that of the former while the ΔH values are similar.

In summary, we have measured the thermodynamic parameters for the hydrogen bonded interaction of the carbonyl groups of some N,N-disubstituted amides with water in carbon tetrachloride. The enthalpy of the interaction is noted to be more dependent upon the nature of the substituents on both sides of the mode peptide bond than is the free energy.

Our data place water below phenols and similar to aliphatic alcohols as a proton donor in a comparison of strengths of hydrogen bonds formed with these model peptides.

References and Notes

(1) M. D. Joesten and R. S. Drago, *J. Amer. Chem. Soc.*, **84**, 2696 (1962).
(2) F. Takahashi and N. C. Li, *J. Phys. Chem.*, **69**, 1622 (1965).
(3) R. L. Middaugh, R. S. Drago, and R. J. Niedzielski, *J. Amer. Chem. Soc.*, **86**, 388 (1964).
(4) E. D. Becker, *Spectrochim. Acta*, **17**, 436 (1961).
(5) (a) F. Takahashi and N. C. Li, *J. Phys. Chem.*, **68**, 2136 (1964); (b) R. D. Grigsby, S. D. Christian, and H. E. Affsprung, *ibid.*, **72**, 2465 (1968).
(6) N. Muller and P. Simon, *J. Phys. Chem.*, **71**, 568 (1967).
(7) F. Takahashi and N. C. Li, *J. Amer. Chem. Soc.*, **88**, 1117 (1966).
(8) J. R. Holmes, D. Kivelson, and W. C. Drinkard, *J. Amer. Chem. Soc.*, **84**, 4677 (1962).
(9) W. McCabe, S. Subramanian, and H. F. Fisher, *J. Phys. Chem.*, **74**, 4360 (1970).
(10) A. Burneau and J. Corset, *J. Phys. Chem.*, **76**, 449 (1972).
(11) M. Tsuboi, *Chem. Soc. Jap.*, **25**, 160 (1952).
(12) D. B. Henson, Ph.D. Thesis, University of Iowa, Iowa City, Iowa, 1972.
(13) N. D. V. Sonntag, *Chem. Rev.*, **52**, 237 (1953).
(14) S. D. Christian, H. Affsprung, J. R. Johnson, and J. D. Worley, *J. Chem. Educ.*, **40**, 419 (1960).
(15) R. D. Grigsby, S. D. Christian, and H. E. Affsprung, *J. Phys. Chem.*, **72**, 2465 (1968).
(16) J. R. Johnson, S. D. Christian, and H. E. Affsprung, *J. Chem. Soc.*, 1 (1965).
(17) J. R. Johnson, S. D. Christian, and H. E. Affsprung, *J. Chem. Soc.*, 77 (1966).
(18) S. C. Mohr, W. D. Wilk, and G. M. Barrow, *J. Amer. Chem. Soc.*, **87**, 3048 (1965).
(19) C. Y. S. Chen and C. A. Swenson, *J. Phys. Chem.*, **73**, 1363 (1969).
(20) R. C. Lord and T. J. Porro, *Z. Elektrochem.*, **64**, 672 (1960).
(21) U. Liddel and E. D. Becker, *Spectrochim. Acta*, **10**, 70 (1957).
(22) R. L. Scott, *Recl. Trav. Chim. Pays-Bas*, **75**, 787 (1956).
(23) H. A. Benesi and J. H. Hildebrand, *J. Amer. Chem. Soc.*, **71**, 2703 (1949).
(24) W. B. Person, *J. Amer. Chem. Soc.*, **87**, 167 (1965).
(25) D. A. Deranleau, *J. Amer. Chem. Soc.*, **91**, 4044 (1969).
(26) J. W. Forbes, *Anal. Chem.*, **34**, 1125 (1962).
(27) S. D. Christian, A. A. Taha, and B. W. Gash, *Quart. Rev., Chem. Soc.*, **24**, 20 (1970).
(28) L. B. Magnusson, *J. Phys. Chem.*, **74**, 4221 (1970).
(29) A. N. Fletcher, *J. Phys. Chem.*, **73**, 2217 (1969).
(30) S. D. Christian and E. E. Tucker, *J. Phys. Chem.*, **74**, 214 (1970).
(31) R. B. Homer and C. D. Johnson in "The Chemistry of Amides," J. Zabicky, Ed., Interscience, New York, N.Y., 1970, p 189.
(32) A. Berger, A. Lowenstein, and S. Meiboom, *J. Amer. Chem. Soc.*, **81**, 62 (1959).
(33) R. C. Neuman, Jr., W. Snider, and V. Jonas, *J. Phys. Chem.*, **72**, 2469 (1968).
(34) R. L. Adelman, *J. Org. Chem.*, **29**, 1837 (1964).
(35) T. Gramstad, *Spectrochim. Acta*, **19**, 497 (1963).
(36) T. Gramstad and W. J. Fuglevik, *Acta Chem. Scand.*, **16**, 1369 (1962).
(37) R. W. Taft, Jr., in "Steric Effects in Organic Chemistry," M. S. Newman, Ed., Wiley, New York, N.Y., 1956, p 586.

Spectroscopic Studies of Ionic Solvation in Propylene Carbonate

Howard L. Yeager,* John D. Fedyk, and Richard J. Parker[1]

Department of Chemistry, The University of Calgary, Calgary, Alberta, Canada (Received May 17, 1973)

The solvation of lithium, sodium, potassium, silver, and tetra-*n*-butylammonium salts in propylene carbonate (PC) was studied by infrared and proton magnetic resonance techniques. Solvent band shifts were observed as a function of salt concentration using both methods. In addition, new infrared bands appeared and are attributed to solvated PC. Mole ratio studies were performed to obtain metal ion solvation numbers. Bromide and iodide ions were found to affect the PC pmr spectrum. No other anion effects were observed. A semiempirical molecular orbital calculation was performed, showing considerable electron density on all PC oxygen atoms and a diffuse positive end of the molecule's dipole.

Introduction

Propylene carbonate (PC) has generated much interest as a solvent for electrolytes. It has a wide liquid range (mp $-49.2°$; bp $241.7°$) and relatively high dielectric constant (64.92 at $25°$).[2] Although the PC molecule has a large dipole moment (4.94 D),[3] dielectric studies have suggested little if any intermolecular association.[2,4] Previous studies of PC electrolyte solutions, utilizing a variety of techniques,[5-10] generally have indicated strong cation solvation, weak anion solvation, and reasonable degrees of dissociation for electrolytes. Mukherjee and coworkers[7,8] have determined by conductance measurements that lithium perchlorate and several tetraalkylammonium halides and perchlorates are unassociated in dilute solution.

In addition to more traditional techniques, infrared and nuclear magnetic resonance methods have been applied in recent years to study ionic solvation in several dipolar aprotic solvents.[11-16] Perelygin observed the effect of alkali metal halides and perchlorates on the infrared spectra of acetonitrile[11a] and acetone.[11b] Coetzee and Sharpe[12] measured the influence of salts on the proton chemical shifts of dimethyl sulfoxide, sulfolane, and acetonitrile. Changes in the infrared spectrum of acetonitrile were also studied. Popov and coworkers[13] investigated ionic solvation in several solvents using a combination of infrared, Raman, and pmr techniques. In the far-infrared region cation–solvent vibrational bands have been studied.[13-15] These bands have been observed in PC solutions.[16]

Here we apply infrared and pmr techniques to the study of ionic solvation in PC. Our objective is to evaluate the nature of solvation processes for ions in this solvent, beginning with univalent ions. Changes in the infrared and pmr spectra of PC are studied as a function of salt and concentration.

Experimental Section

Reagents. Propylene carbonate (Jefferson Chemical Co.) was stirred over molecular sieves (J. T. Baker Type 5A) for 48 hr and then distilled using a 1.5-m vacuum-jacketed column packed with nichrome helices (Podbielniak, Inc.). The column was operated at a reflux ratio of 10:1, with a stillhead temperature of $80°$ at 1 mm pressure. Water content of the purified product by Karl Fischer titration was $<5 \times 10^{-4}$ M. Gas chromatographic analysis for organic impurities was performed using a Porapak Q column with N_2 carrier gas and flame ionization detector.

The largest impurity was 10 ppm of 1,2-propylene glycol. Other impurities were less than 4 ppm.

Nitromethane (Fisher Certified) was dried over molecular sieves for 24 hr and then distilled at 100 mm pressure; the stillhead temperature was $52°$.

Lithium perchlorate (MCB Polaroquality) and tetra-*n*-butylammonium bromide, iodide, and perchlorate (G. F. Smith Chemical Co., Polaroquality) were used as received. Lithium tetraphenylboride was prepared and purified by the method of Kunze and Fuoss.[17] Sodium perchlorate (Fisher Purified) was recrystallized from a 6:1 dioxane–water mixture and dried *in vacuo* at $200°$ for 3 days. Sodium tetraphenylboride (Fisher Certified) was dried *in vacuo* at $105°$ for 24 hr. Potassium thiocyanate (Fisher Certified) was dried *in vacuo* at $60°$ for 2 days. Silver perchlorate was prepared and purified as previously described.[18] All solutions were prepared in a glove box under strictly anhydrous conditions. Silver perchlorate solutions in PC showed slight discoloration almost immediately after preparation.

Infrared spectra in the 4000–600-cm^{-1} region were recorded on a Perkin-Elmer Model 337 spectrophotometer. Demountable cells with NaCl windows were used.

Nuclear magnetic resonance measurements were performed on a Varian A-60 spectrometer at a temperature of $37.5°$, as determined by a copper–constantan thermocouple. Tetramethylsilane (1%) was used as internal reference for all solutions. All spectra were scanned at least twice to ensure repeatability of ± 0.2 cps.

Results and Discussion

Infrared Spectra. Partial band assignments have been made for the infrared spectrum of PC.[19,20] We found that the spectra of lithium, sodium, potassium, and silver salt solutions showed several changes from that of pure PC. Generally the carbonyl stretching band at 1798 cm^{-1} exhibited a shoulder at lower frequency and the O–C–O skeletal stretch at 1182 cm^{-1} shifted to higher frequency. For lithium and silver salts, however, the 1182-cm^{-1} band showed a shoulder as well. In addition, bands at 1355, 1390, and 1450 cm^{-1} exhibited slight splitting. Solutions of tetra-*n*-butylammonium bromide, iodide, and perchlorate produced no observable changes in the PC spectrum. Presumably this is due to large size and consequent weak interaction of the cation with the solvent. For lithium as well as sodium ions, the perchlorate and tetraphenylboride
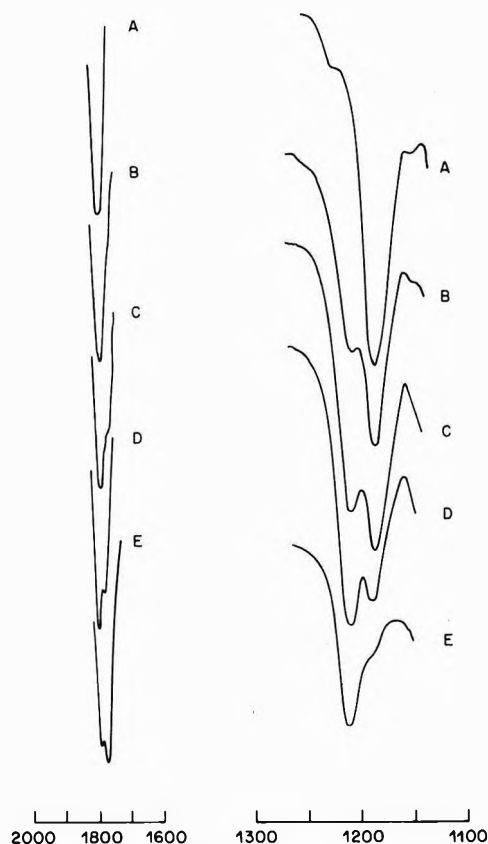
Figure 1. Splitting of the C=O (1798 cm^{-1}) and O-C-O (1182 cm^{-1}) PC bands at various mole ratios (R) of PC:LiClO$_4$: (A) 3 M PC in nitromethane; (B) R = 10.4; (C) R = 7.3; (D) R = 5.0; (E) R = 3.2.

TABLE I: Splitting of the 1182- and 1798-cm^{-1} Bands

Salt	$\Delta\nu$(O-C-O),[a] cm^{-1}	$\Delta\nu$(C=O),[b] cm^{-1}
LiClO$_4$	23	25
LiBPh$_4$	23	25
NaBPh$_4$	12	15
AgClO$_4$	18	40
(n-Bu)$_4$NClO$_4$	c	c

[a] Split to higher frequency from 1182 cm^{-1}. [b] Split to lower frequency from 1798 cm^{-1}. [c] No new bands.

salts showed similar changes. Therefore we assume that these effects are due to the metal ion interacting with the carbonate grouping in the PC molecule.

Attempts to study the alkali metal halide and thiocyanate solutions were unsuccessful except for potassium thiocyanate. These salts were generally too insoluble in PC; lithium bromide and iodide and lithium and sodium thiocyanate solutions decomposed at the concentrations required.

In order to obtain information about the stoichiometry of the solvated metal ions, an inert solvent should be used to prepare solutions containing varying ratios of PC to salt. We chose nitromethane in this work, with the assumption that it would not compete with PC in solvating metal ions.[13h] Varying amounts of lithium perchlorate were dissolved in nitromethane solutions containing 3 M PC. The 1182- and 1798-cm^{-1} bands split, with new bands appearing at 1205 and 1773 cm^{-1}, respectively. The positions of the new bands were independent of concen-

tration and their relative intensity increased with increasing concentration, as shown in Figure 1. Lithium and sodium tetraphenylboride and silver perchlorate gave similar splittings under the same experimental conditions. The magnitudes of these splits are presented in Table I.

The relative magnitudes of the O-C-O splittings suggest that the extent of interaction proceeds in the order Li$^+$ > Ag$^+$ > Na$^+$. This agrees with the calculated single-ion free energies of solvation for lithium, silver, and sodium ions in PC, -95.0, -85.4, and -71.9 kcal/mol, respectively.[9] The $\Delta\nu$ value for the silver perchlorate C=O band is much larger than would be expected on this basis, however.

These results are similar to those obtained for lithium perchlorate in dioxane solutions of 1-methyl-2-pyrrolidone, where a new carbonyl stretching band appeared at lower frequency.[13d] In another study,[12h] lithium perchlorate in nitromethane solutions of acetone showed a shifting of the carbonyl stretching band to lower frequencies and a split to higher frequency of the C-C asymmetric stretch. These phenomena are attributable to solvation of the lithium ion.

As an aid in understanding how PC interacts with ions, a semiempirical molecular orbital calculation was performed to obtain the electron density distribution of the PC molecule. The CNDO/2 method[21] was employed, and it was assumed that the ring system was planar with the double bond in the plane of the ring. The results (in 10^{-3} electron unit) are presented in Figure 2. The calculated dipole moment of 4.74 D agrees well with the true value of 4.94 D.[3] The distribution shows considerable electron density on the ring oxygens as well as on the carbonyl oxygen. It is reasonable to assume that the interaction of cations with PC is not restricted to the carbonyl oxygen alone, and also may involve extensive ring interaction. The positive centers in the PC molecule are much less accessible to ions, however, and it is difficult to see how specific anion solvation could occur. This agrees with observations that PC is a poor anion solvator.[10,22]

Infrared Mole Ratio Studies. In order to study the concentration dependence of infrared band shifts in pure PC, concentrated solutions of varying PC:salt ratio were prepared for salts with sufficient solubility. The position of the O-C-O band was measured as a function of mole ratio. Somewhat surprisingly, the resulting plots consisted of two straight line portions with a sharp break. The graphical results for lithium perchlorate and tetraphenylboride are presented in Figure 3. For all salts which were studied, the mole ratio values at the breaks, as determined by linear least-squares analysis, are listed in Table II.[23]

Again, no shift or break was observed for either the bromide or perchlorate salt of tetra-n-butylammonium ion, suggesting that the other shifts are caused by metal ion interactions. Because the mole ratio studies were performed without an inert diluent, it is difficult to interpret the break values unambiguously. However, the constancy of the 6:1 ratio appears to demonstrate a favored arrangement of PC in relation to the metal ions, at least in concentrated solution. It must be remembered that at these high concentrations (a PC:salt ratio of six corresponds to a 1.6 m solution) the salts are probably highly ion paired. If this is true, the lack of anion effect on the breaks suggests solvent-separated rather than contact ion pairs.

Proton Magnetic Resonance Mole Ratio Studies. Mole ratio studies were also performed by measuring the chem-
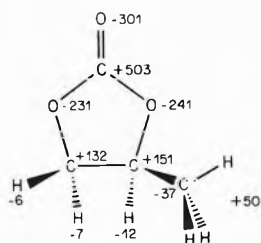
Figure 2. Electron density distribution of the propylene carbonate molecule.

TABLE II: Infrared Mole Ratio Plots

Salt	PC:salt ratio at break[a]	Salt	PC:salt ratio at break[a]
LiClO$_4$	6.2	KSCN	6.0
LiBPh$_4$	6.4	AgClO$_4$	6.4
NaClO$_4$	6.1	(n-Bu)$_4$NClO$_4$	b
NaBPh$_4$	6.3	(n-Bu)$_4$NBr	b

[a] Shift of 1182-cm^{-1} band was measured. [b] No shift or break was observed.

TABLE III: Pmr Mole Ratio Plots

Salt	PC:salt ratio at break[a]	Salt	PC:salt ratio at break[a]
LiClO$_4$	4.2	(n-Bu)$_4$NI	3.6
AgClO$_4$	4.0	(n-Bu)$_4$NClO$_4$	b
(n-Bu)$_4$NBr	4.0		

[a] Shift of CH$_2$ resonance at 275 cps was measured. [b] No break observed.

ical shift of PC protons in nitromethane solutions. The concentration of PC was fixed at 1 M and varying amounts of salts were used. Lithium and silver perchlorates as well as three tetra-n-butylammonium salts were studied; other alkali metal halides and perchlorates were too insoluble in this solvent mixture. All PC proton peaks shifted downfield from TMS with increasing salt concentration. The change in the chemical shift of the methyl doublet[24] was always about half that of the other resonances. The methylene proton peak[24] which occurs at 275 cps in 1 M PC–nitromethane solution produced slightly greater changes than the other resonances. This peak was monitored in all mole ratio studies. The results are presented in Figures 4 and 5.

With the exception of tetra-n-butylammonium perchlorate the plots show definite breaks. The PC:salt ratios at the breaks, as obtained by graphical analysis, are listed in Table III. The break at a ratio of 4.2 for lithium perchlorate is close to the value of 4.3 obtained by Popov and coworkers for similar mole ratio studies of lithium perchlorate in acetone[13h] and 1-methyl-2-pyrrolidone.[13d] Silver perchlorate shows a similar break at 4.0 here, suggesting that the dilute solution "solvation number" for both lithium and silver ions is 4. However, the magnitude of shift is much less for silver ion than for lithium ion, in agreement with the infrared results. The nitromethane resonance was also measured for each solution; its position did not shift more than 1 cps in any instance.

A mole ratio study was performed in 1 M PC–nitromethane solutions for sodium tetraphenylboride as well. However, large upfield shifts which increased with in-
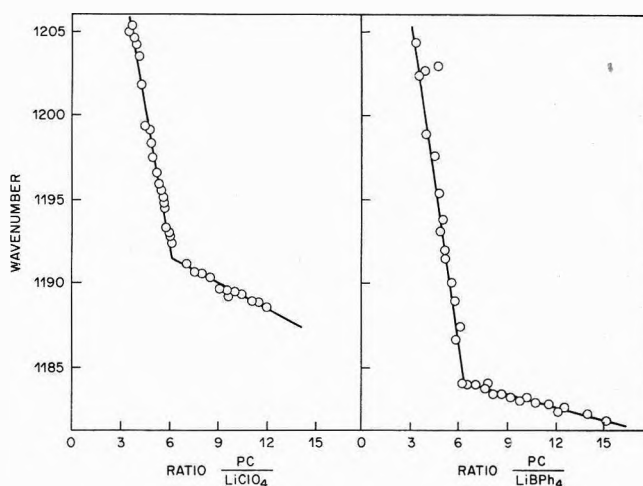

Figure 3. Position of the 1182-cm^{-1} band of PC vs. PC:Li$^+$ ratio.

Figure 4. Chemical shift of the PC CH$_2$ resonance at 275 cps vs. PC:salt ratio; 1 M PC in nitromethane solutions, concentration of salt varied.
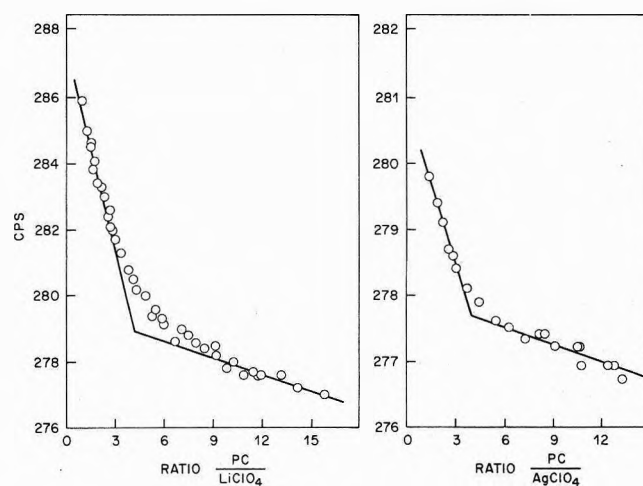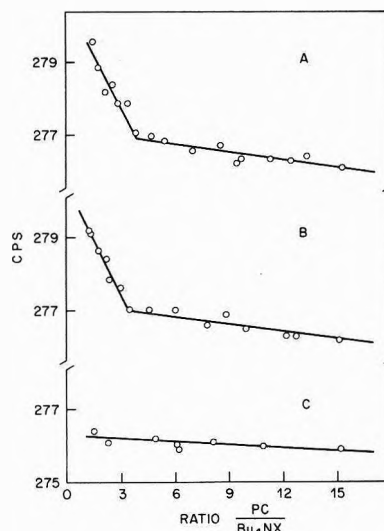

Figure 5. Chemical shift of the PC CH$_2$ resonance at 275 cps vs. PC:salt ratio; 1 M PC in nitromethane solutions, concentration of salt varied: (A) Br$^-$; (B) I$^-$; (C) ClO$_4^-$ salt.

creasing salt concentration were observed. These shifts, caused by magnetic anisotropy effects of the phenyl rings, have been seen in other solvents as well.[25] This effect pre-

vents study of cation solvation of tetraphenylboride salts by this mole ratio method.

To test the assumption that these breaks are due solely to metal ion solvation, tetra-n-butylammonium bromide, iodide, and perchlorate salts were studied. Although the perchlorate salt showed little shift and no break as expected, the bromide and iodide salts produced distinct breaks at a PC to salt ratio of about 4. In contrast to the findings of Wuepper and Popov,[13e] who observed no solvent proton shift for tetra-n-hexylammonium bromide in dioxane solutions of 1-methyl-2-pyrrolidone, it appears that halide ions can cause breaks in PC similar to those induced by metal ions. The deshielding effect of anions on acetonitrile protons has been measured as well.[12]

Buckson and Smith[26] have studied the changes in the chemical shifts of the α-methylene protons on the tetra-n-butylammonium ion in nitrobenzene, using the halide, perchlorate, and picrate salts. The results were interpreted in terms of ion pair association. The positions of the tetra-n-butylammonium ion resonances were measured here. No changes were observed.

The break values in Table III lead to the conclusion that the solvation number of lithium, silver, bromide, and iodide ions is four while tetrabutylammonium and perchlorate ions have a solvation number of zero. However, it is difficult to provide an exact description of the meaning of these numbers.

In summary, we find that infrared and pmr techniques yield similar qualitative information about ionic solvation in PC. However, the pmr method appears to be a more sensitive probe of anion interactions with the solvent. This aspect is under further investigation. Finally, solvation numbers determined by spectroscopic techniques are dependent on the experimental conditions used, and should be interpreted in this context.

Supplementary Material Available. The mole ratio plots for other salts listed in Table II will appear following these pages in the microfilm edition of this volume of the journal. Photocopies of the supplementary material from this paper only or microfiche (105 × 148 mm, 20× reduction, negatives) containing all of the supplementary material for the papers in this issue may be obtained from the Journals Department, American Chemical Society, 1155 16th St., N.W., Washington, D. C. 20036. Remit check or money order for $3.00 for photocopy or $2.00 for microfiche, referring to code number JPC-73-2407.

References and Notes

(1) Present address, Department of Chemistry University of New Brunswick, Fredericton, N. B., Canada.
(2) R. Payne and I. E. Theodorou, *J. Phys. Chem.*, **76**, 2892 (1972).
(3) R. F. Kempa and W. H. Lee, *J. Chem. Soc.*, 1936 (1958).
(4) L. Simeral and R. L. Amey, *J. Phys. Chem.*, **74**, 1443 (1970).
(5) W. H. Harris, Ph.D. Thesis, University of California, Berkeley, Calif., 1958, URCL Report No. 8381.
(6) C. V. Krishnan and H. L. Friedman, *J. Phys. Chem.*, **73**, 3934 (1969).
(7) L. M. Mukherjee and D. P. Boden, *J. Phys. Chem.*, **73**, 3965 (1969).
(8) L. M. Mukherjee, D. P. Boden, and R. Lindauer, *J. Phys. Chem.*, **74**, 1942 (1970).
(9) M. Salomon, *J. Phys. Chem.*, **74**, 2519 (1970).
(10) R. Jasinski, *Advan. Electrochem. Eng.*, **8**, 253 (1971).
(11) (a) I. S. Perelygin, *Opt. Spektrosk.*, **13**, 358 (1962); (b) *ibid.*, **16**, 40 (1964).
(12) J. F. Coetzee and W. R. Sharpe, *J. Solution Chem.*, **1**, 77 (1972).
(13) (a) B. W. Maxey and A. I. Popov, *J. Amer. Chem. Soc.*, **89**, 2230 (1967); (b) *ibid.*, **90**, 4470 (1968); (c) *ibid.*, **91**, 20 (1969); (d) J. L. Wuepper and A. I. Popov, *ibid.*, **91**, 4532 (1969); (e) *ibid.*, **92**, 1493 (1970); (f) M. K. Wong and A. I. Popov, *J. Inorg. Nucl. Chem.*, **33**, 1203 (1971); (g) W. J. McKinney and A. I. Popov, *J. Phys. Chem.*, **74**, 535 (1970); (h) M. K. Wong, W. J. McKinney, and A. I. Popov, *J. Phys. Chem.*, **75**, 56 (1971).
(14) M. J. French and J. L. Wood, *J. Chem. Phys.*, **49**, 2358 (1968).
(15) (a) W. F. Edgell, A. T. Watts, J. Lyford, and W. Risen, *J. Amer. Chem. Soc.*, **88**, 1815 (1966); (b) W. F. Edgell, J. Lyford, R. Wright, W. Risen, and A. Watts, *ibid.*, **92**, 2240 (1970).
(16) D. Wied, M. S. Thesis, Michigan State University, 1972.
(17) R. W. Kunze and R. M. Fuoss, *J. Phys. Chem.*, **67**, 385 (1963).
(18) H. L. Yeager and B. Kratochvil, *J. Phys. Chem.*, **73**, 1963 (1969).
(19) N. B. Colthup, L. H. Daly, and S. E. Wiberly "Introduction to Infrared and Raman Spectroscopy," Academic Press, New York, N. Y., 1964, p 379.
(20) J. L. Hales, J. I. Jones, and W. Kynaston, *J. Chem. Soc.*, 618 (1957).
(21) J. A. Pople and D. L. Beveridge, "Approximate Molecular Orbital Theory," McGraw-Hill, New York, N. Y., 1970.
(22) J. N. Butler, D. R. Cogley, and W. Zurosky, *J. Electrochem. Soc.*, **115**, 445 (1968).
(23) See paragraph at end of paper regarding supplementary material.
(24) H. Finegold, *J. Phys. Chem.*, **72**, 3244 (1968).
(25) J. F. Coetzee and W. R. Sharpe, *J. Phys. Chem.*, **75**, 3141 (1971).
(26) R. L. Buckson and S. G. Smith, *J. Phys. Chem.*, **68**, 1875 (1964).

On Infrared Stimulated Duryl Radical Fluorescence in Rigid Solutions of Durene in 3-Methylpentane at 77°K[1]

F. P. Schwarz and A. C. Albrecht*

Department of Chemistry, Cornell University, Ithaca, New York 14850 (Received March 22, 1973)

After a dilute solution of durene in 3-methylpentane at 77°K is photosensitized in the ultraviolet, not only is the normal infrared stimulated charge recombination (ISCR) durene luminescence seen, but a weaker ISCR duryl radical fluorescence is found as well. Unlike the durene ISCR luminescence, the intensity of the duryl radical ISCR fluorescence component increases linearly with photosensitization from a nonzero initial level. This initial level, however, behaves identically with the durene ISCR luminescence with regard to changes in various parameters such as intensity of ultraviolet light and sample preparation. When perdeuterated durene is examined in a similar fashion there is no change in the durene ISCR luminescence signal but the initial duryl radical ISCR luminescence is reduced by about one-third. This isotope effect is identical with that found for two-photon β-bond cleavage and the initial ISCR duryl radical fluorescence is attributed to a charge recombination β-bond cleavage yielding excited duryl radicals. The efficiency appears to be about 1 in 10^4 ISCR produced excited durene molecules. The growth of radical ISCR fluorescence with repeated cycling is attributable to the steady buildup of a new one-photon ionizable species which, when ionized, gives an ISCR luminescence in which the duryl radical fluorescence is a significant component.

I. Introduction

Infrared stimulated emission is now a well-known property of rigid organic solutions at 77°K which have been photosensitized with ultraviolet light. Such photosensitized solutions normally exhibit a weak visible emission or afterglow which is dramatically enhanced by exposing the solution to near-infrared light (red to $\sim 2\ \mu$). At the same time infrared stimulation is known to induce a transient increase in the electrical conductivity of the solution.[2] Without prior ultraviolet photosensitization however, the sample is unresponsive to such long wave illumination. The ultraviolet photosensitization brings about the ejection of an electron from the absorbing solute molecule (usually a biphotonic event), and the electron is trapped in the solvent matrix in the vicinity of the partner cation. This trapped electron can be ionized with low-energy light in the near-infrared region to cause either complete charge separation (photocurrent) or charge recombination to give luminescing excited states of the original solute molecule. Ionization of the solute molecule is not always the only conspicuous biphotonic chemistry occurring in such solid solutions. When the solute is a suitable benzene derivative, a biphotonic β-bond cleavage is often observed. Such biphotonic events appear to take place via excited solute states lying near the ionization continuum. Since infrared stimulated charge recombination (ISCR) leads to highly excited states of the solute molecule, the question is raised whether ISCR can bring about β-bond scission. Such charge recombination chemistry has been observed in solutions of 1,2,4,5-tetramethylbenzene (durene) in 3-methylpentane (3-MP) at 77°K and this forms the subject of the present report.

The durene–3-MP system exhibits both biphotonic ionization and biphotonic β-bond cleavage leading to a 1,2,4-trimethylbenzyl radical (duryl radical) and a hydrogen atom. A quantitative photochemical study of this system has just been completed[3] and it is found that both photochemical channels occur with similar quantum yields when exciting durene from its lowest triplet state into triplet states near its ionization continuum.[4] Incidentally, a one-photon route for β-bond cleavage via vibrationally excited S_1 was also discovered.[5] The ISCR in this system not only yields the usual durene recombination luminescence (fluorescence and phosphorescence) but in addition gives a recombination fluorescence in the green which appears to be that from an excited duryl radical. The charge recombination seems to bring about β-bond cleavage while leaving the benzyl radical product in its first excited doublet state.

When such rigid solutions are photosensitized, and then subjected to ISCR, the ionization channel is reversed. The biphotonic β-bond cleavage, however, is not reversed but instead is seen to increase upon repeated recycling of the uv-photosensitization–ISCR steps. As long as the uv-photosensitization step is not severe (or the irreversible steps are not efficient), the sample can endure many such cycles without significant depletion of the parent molecule. In fact, the ISCR induced durene luminescence is found to be reproducibly constant from cycle to cycle. But this is not true of the new green recombination fluorescence attributed to ISCR induced β-bond scission. This charge recombination induced duryl radical luminescence increases linearly with repeated cycling and extrapolates to a nonzero initial value. The presentation of this study is, thus, divided into two main parts. At first the behavior of the nonzero initial ISCR duryl radical fluorescence is compared with that of the more familiar ISCR durene fluorescence under a variety of conditions. It is shown how the initial level of ISCR duryl radical fluorescence is a consequence of ISCR β-bond cleavage leaving excited duryl radicals. The efficiency for this ISCR β-bond cleavage is compared with the efficiencies[3] for β-bond cleavage

by the one- and two-photon excitation of durene itself, and it is seen how still a third mechanism is indicated for this ISCR induced β-bond cleavage.

In the second part, the behavior of the growth portion of the ISCR duryl radical fluorescence seen upon repeated cycles is studied as a function of the photosensitization conditions of the sample. It is argued how the increase is due to ISCR between the electron and some unknown cationic species which is produced irreversibly during the photosensitization. The species is one photon, near-uv ionizable, and is, itself, stable with respect to infrared stimulation. Its characteristics closely resemble a new species which has been found in photoconductivity studies[2] of a variety of aromatic derivatives (including durene) in 3-MP at 77°K where, following an initial biphotonic sensitization, a one-photon induced photocurrent is found in the near-ultraviolet region (a region which had been inactive prior to photosensitization in the further uv).

II. Experimental Section

A. *Materials.* Durene, perdeuterated durene, and the 3-MP were obtained and purified as described earlier.[3]

B. *Apparatus.* The apparatus has been described previously and was used with one modification.[3] The green duryl radical fluorescence overlaps the spectral region of the durene phosphorescence. To separate one emission from the other, lock-in techniques were used. The ISCR radical fluorescence follows the modulation of the infrared light (100 Hz) (since recombination and fluorescence proceed on a nanosecond time scale). This modulation is achieved by a mechanical chopper placed between the sample and the infrared light source. A Par lock-in amplifier is used. ISCR radical fluorescence is thus studied by first uv photosensitizing the sample and then stimulating it with modulated near-ir light while observing the modulated emission using filters which isolate the green region of the spectrum.

All samples were 1.3×10^{-3} M of durene in 3-MP at room temperature and, unless otherwise specified, were purged with dry helium before cooling to 77°K. Except where otherwise noted, the uv photosensitizations were carried out at 275 nm with a bandwidth of ~15 nm. Under these conditions,[3] the photon flux was typically 7×10^{14} photons/cm^2 sec.

III. Results and Discussion

A. *Introduction.* A typical modulated ISCR green fluorescence signal, $F_R^*(t)$, as detected by the lock-in amplifier with a 0.3 sec time constant is presented in Figure 1a. In Figure 1b the modulated ISCR durene fluorescence $F^*(t)$, as detected by the same instrument (but with different detection filters) is displayed. The similarity of the time behavior of these fluorescences is apparent. (The asterisk signifies a recombination process in keeping with the notation previously used[3]).

In this investigation the time-integrated form of the ISCR fluorescence signals is used. These are symbolized by F_R^* and F^* and correspond to the areas under the curves in Figure 1a and 1b, respectively. Each of these parameters must be proportional to the total number of recombinations which lead to the given fluorescence and, as areas, are insensitive to the intensity of the infrared light used.

The spectrum of the duryl radical fluorescence in 3-MP at 77°K has been observed[6] and resembles closely the
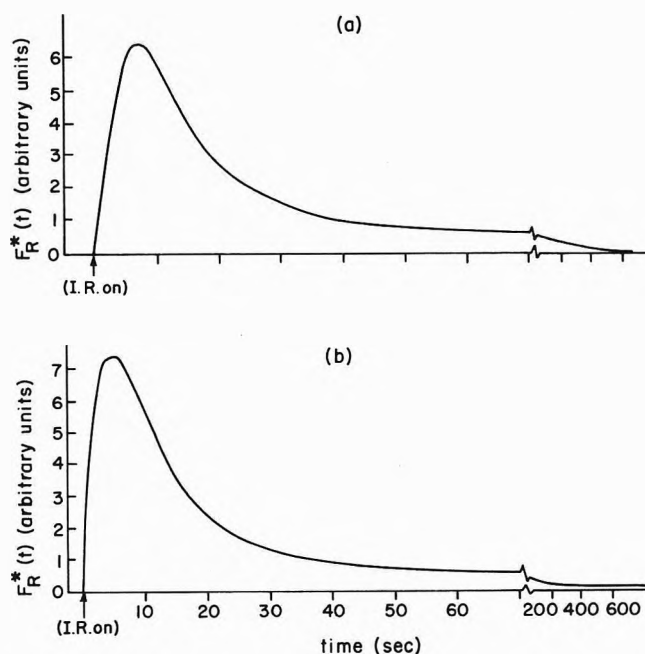
Figure 1. The time course of (a) the ISCR induced green fluorescence, $F_R^*(t)$, and (b) the ISCR induced durene fluorescence $F^*(t)$.

spectrum seen by others under different conditions. The green ISCR fluorescence, $F_R^*(t)$, seen in this present work, and regarded as duryl radical fluorescence, is quite weak and was not fully spectrally resolved. However, great pains were taken to identify its spectral characteristics using various filter combinations. Appropriate Varian monoband-pass and Corning filters are used to provide band passes $< \sim 20$ nm. The filter combinations were calibrated using the ISCR durene phosphorescence spectrum. This phosphorescence was measured with dc electronics. It has a maximum at 390 nm with a tail into the 500-nm region. The modulated ISCR fluorescence in the visible region, however, peaks at about 500 nm where the duryl fluorescence is known to occur. The only known fluorescence in the visible region from such a photosensitized system is that of the duryl radical. Finally, the efficiency for producing F_R^* exhibits essentially the same isotope effect (when changing to perdeuterated durene) as does the efficiency for the biphotonic mechanism for producing the known duryl radical. We, therefore, attribute the $F_R^*(t)$ (or F_R^*) luminescence to duryl radical fluorescence. A more direct demonstration would require a more resolved spectral identification and, possibly more practicably, a lifetime determination.

Since ISCR restores the sample approximately to its initial state, studies of F_R^* were carried out repeatedly on one sample. In Figure 2 it is seen how F_R^* increases linearly with each successive identical uv-photosensitization–ISCR cycle and extrapolates to a nonzero initial value. In contrast, the F^* signal exhibits the expected constancy following each photosensitization. To facilitate the investigation of F_R^* the signal is separated into its initial intrinsic nonzero value, $F_R^*(0)$, and the increasing portion represented by n ($dF_R^*(n)/dn$) where n refers to the number of uv-photosensitization–ISCR cycles which have taken place. The total ISCR radical fluorescence signal after n cycles is then given by

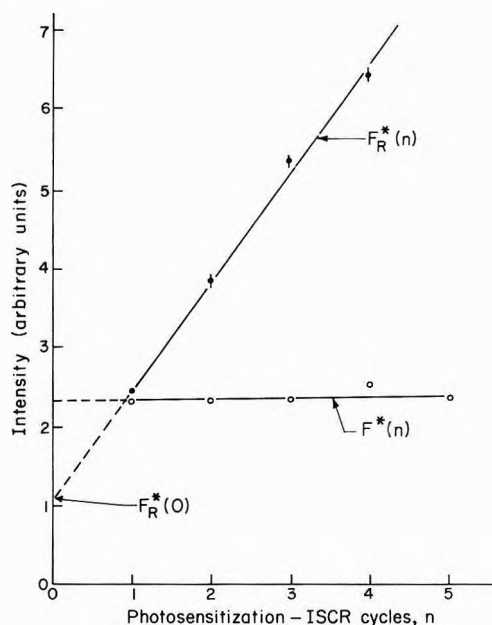$$F_R^*(n) = F_R^*(0) + n \, dF_R^*(n)/dn \qquad (1)$$

Figure 2. A plot of $F_R^*(n)$ (-●-) and $F^*(n)$ (-O-) vs. the number of uv-photosensitization-ISCR cycles, n. Extrapolations to n = 0 are indicated (- -) and the parameter $F_R^*(0)$ is indicated.

Figure 3. A plot of $F_R^*(0)$ vs. F^* for different experiments in which the sample and the intensity of the uv photosensitizing light is changed. In each experiment several cycles were carried out such as displayed in Figure 2. The scatter, here, is an indication of sample to sample reproducibility.

$F_R^*(0)$ then becomes the intercept at n = 0 of the observed $F_R^*(n)$ vs. n plot (n = 1,2,...). Since the $F_R^*(0)$ signal, like the ISCR durene fluorescence, F^*, is a basic constant of the sample, it is readily analyzed and will be examined first.

B. Properties of the $F_R^*(0)$ Signal in Relation to F^*. F^* is dependent on the photosensitization conditions in the sample. The actual photon flux within the sample during uv photosensitization determines the rate of photoionization and, thus, subsequently the magnitude of F^*. The ionization tends to saturate if any given ultraviolet exposure is sufficiently intense or enduring, because its reverse is radiatively stimulated even with uv light. Since the properties of F^* are relatively well understood it is convenient to employ F^* as an internal control. It represents a statement concerning the extent of the ionization under various conditions. The study of $F_R^*(0)$ then becomes a comparative study with respect to F^* as conditions are varied.

First, the intensity of the uv photosensitization light was varied from sample to sample. Equation 1 was then used to determine $F_R^*(0)$ in each case and $F_R^*(0)$ was compared to F^* obtained from the same sample. The results of these experiments are presented in Figure 3 where $F_R^*(0)$ is plotted as a function of F^*. It can be seen that $F_R^*(0)$ correlates fairly well with F^* as the uv photosensitization intensity is changed. Next, the photosensitization time was varied for several samples and the ratio $F^*/F_R^*(0)$ was determined for each sample. For two samples 3-min uv-photosensitization-ISCR cycles were used and the ratio $F^*/F_R^*(0)$ = 27 ± 2 was found. This compares with a similar ratio $F^*/F_R^*(0)$ = 23 ± 1 in a sample having 5-min uv-photosensitization-ISCR cycles. In general, experiment to experiment reproducibility is quite demanding when it is realized that one $F_R^*(0)$ measurement depends on an extrapolation of several photosensitization-ISCR cycles carried out on one sample under conditions as constant as possible.

Finally the $F^*/F_R^*(0)$ ratio from an air-saturated sample is compared with that from a helium purged sample
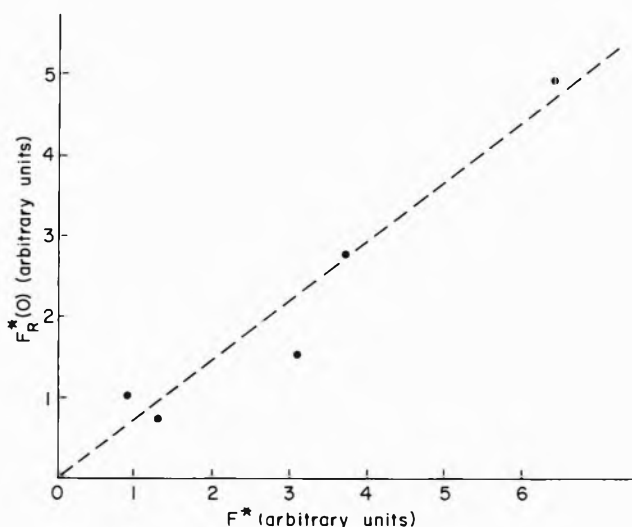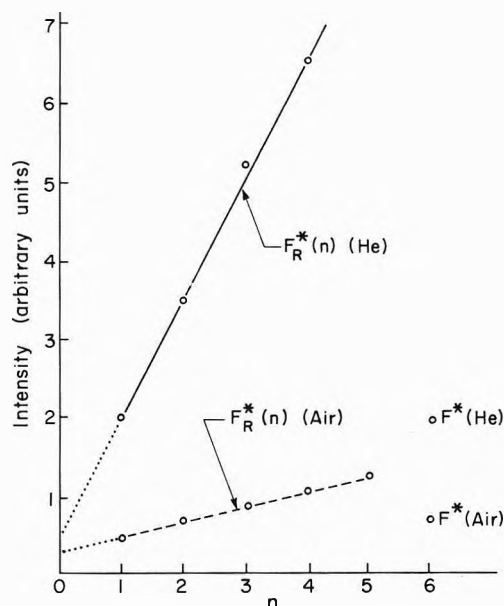

Figure 4. A plot of $F_R^*(n)$ vs. n for a nonpurged sample (- -O- -) and a He-purged sample (-O-). At the sixth cycle a measure of F^* was taken in each case. The extrapolations to n = 0 to determine the $F_R^*(0)$ are indicated.

(O_2 is known to quench ISCR). In Figure 4 $F_R^*(n)$ and F^* measurements appear (in separate, arbitrary units) for two such samples subjected to otherwise identical photosensitization conditions. It is seen how $F^*(n)$, (dF_R^*/dn), and F^* for any given n (F^* does not change with n) are greater in the helium-purged sample than in the air sample. On the other hand, the $F^*/F_R^*(0)$ ratios are invariant to helium purging. The observed ratios are 3 ± 1 in the air sample and 4 ± 2 in the helium-purged sample (values which contrast with the above mentioned only because of different detection conditions). These results show that $F_R^*(0)$ behaves identically with F^* under a variety of conditions. It appears that $F_R^*(0)$ is intimately related to F^* which is known to arise from direct charge recombination of the electron with the durene cation. It is then natural
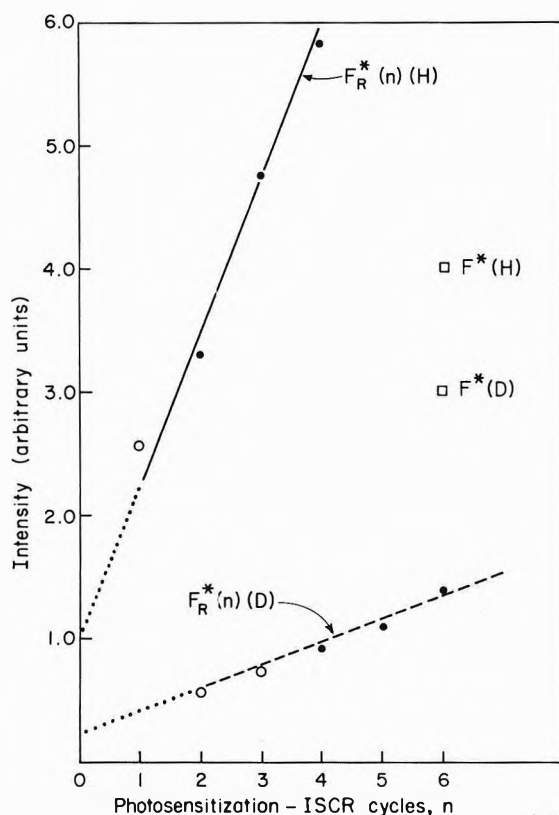
Figure 5. A plot of $F_R^*(n)$ vs. n for ordinary durene (-●-) and for perdeuterated durene (- -●- -). At the sixth cycle a measure of F^* was made in each case. The open circles are uncertain data. The extrapolations to $n = 0$ to determine the $F_R^*(0)$ are indicated.

to propose that this same recombination act leads to excited duryl radicals giving $F_R^*(0)$.

The step leading from the recombination act to the creation of excited duryl radicals should show an isotope effect. It has been shown that β-bond cleavage in perdeuterated durene is less efficient than in durene, whereas the photoionization rate is unchanged.[3] In Figure 5 the $F_R^*(n)$ and F^* data for a sample of perdeuterated durene in 3-MP and for protonated durene in 3-MP are compared. Both samples are equal in concentration and are uv photosensitized under almost identical conditions. To correct for the slight variation in the photoionization conditions, the observed $F^*(D)/F^*(H)$ (see the sixth cycle in Figure 5) is used as a correction factor to give $F_R^*(0)_H/F_R^*(0)_D = 3.2$ which compares favorably with an isotope effect of 3.3 ± 1 found for the biphotonic mechanism of β-bond scission.[3] This may be the single most convincing observation indicating that $F_R^*(0)$ comes from excited duryl radicals generated directly from ISCR β-bond scission in durene.

An effort is made next to calculate the efficiency of duryl radical production by the ISCR route. There are two obvious ways to excite the duryl radical luminescence. One is by ISCR, as being discussed, and the other is by direct excitation from the ground state of the duryl radical which has been photochemically produced. Since the optical density is usually known, and the photon flux can be determined, one can at least count the number of direct excitations (per sec) when irradiating the ground state of a given molecule. While considerable additional calibration would be needed to determine absolute quan-

tum yields for the fluorescence, one can make relevant comparison of ordinary radical fluorescence, F_R, to ordinary durene fluorescence, F (produced by direct excitation), under a set of detection conditions identical with those used for the measurement of $F^*/F_R^*(0)$ in these ISCR studies. Thus one can obtain the durene fluorescence to duryl radical fluorescence intensity expected when both species suffer the same frequency of excitation in the ultraviolet. This may be compared with the $F^*/F_R^*(0)$ ratio seen under identical detection conditions to obtain the number of excited duryl radicals made relative to the number of excited durene singlet states produced during the ISCR. Let this ratio of the number of ISCR made excited duryl radicals to ISCR made excited singlet states of durene be given by

$$\psi_{D_1 \cdot S_1} = \langle R_{ID_1 \cdot} \rangle / \langle R_{IS_1} \rangle \qquad (2)$$

where $R_{ID_1 \cdot}$ represents the rate of passage (under ir illumination) from the ionized condition, I, to the first excited doublet state, $D_1 \cdot$, of the duryl radical. Similarly R_{IS_1} refers to the rate of passage (M sec^{-1}) from the ionized condition to the first excited singlet state of durene. As before, when these symbols are in boldface an integral over time is indicated in this case the duration of the recombination pulse. The brackets indicate integrals over the depth, l, of the sample.[3] Thus $\langle R_{ID_1 \cdot} \rangle$ is the total millimoles of excited duryl radical made throughout the sample in 1-cm^2 cross section during one full ISCR pulse and similarly for $\langle R_{IS_1} \rangle$. The corresponding recombination fluorescence ratio is simply

$$F^*/F_R(0) = \frac{s k_F}{s_R k_{F_R}} \frac{\langle R_{IS_1} \rangle}{\langle R_{ID_1 \cdot} \rangle} \qquad (3)$$

where s and s_R are the instrumental factors for measuring, respectively, the durene fluorescence and the duryl radical fluorescence. The corresponding radiative rate constants are k_F and k_{F_R}. Thus the relative yield, $\psi_{D_1 \cdot S_1}$ of excited states in ISCR is simply

$$\psi_{D_1 \cdot S_1} = [s k_F / s_R k_{F_R}](F^*/F_R^*(0))^{-1} \qquad (4)$$

The expression in brackets is obtainable from direct uv excitation studies. Here the durene fluorescence, F, is excited at 270 nm and the duryl radical fluorescence, F_R, at 329 nm and the detection conditions are chosen to be identical with those used in the ISCR studies. Thus

$$\frac{F}{F_R} = \frac{s k_F I^0 (270 \text{ nm})(1 - \exp\{-A_{S_0}\})}{s k_{F_R} I^0 (329 \text{ nm})(1 - \exp\{-A_{D_0}\})} \qquad (5)$$

in which A_{S_0} and $A_{D_0 \cdot}$ are the measured Naperian optical densities of durene (at 270 nm) and the duryl radical (at 329 nm). The latter optical density was obtained by measuring the light transmitted before and after the photosensitization step. The relative intensities of the incident light at the two wavelengths were determined using a sodium salicylate integrating screen. In the calibration experiment $A_{S_0} = 0.90$, $A_{D_0} = 0.14$, and (F/F_R) $(I^0(329$ nm$))/I^0(270$ nm$)) = 4.98 \pm 0.05 \times 10^{-12}$ or $(s k_F)/(s_R k(F_R)) = 1.09 \pm 0.02 \times 10^{-2}$. (To a good approximation, the fact that the depth distribution of both the excited durene and the excited duryl radical is different in the ISCR work than in the uv excitation study will not invalidate the use of the same instrumental factor ratio s/s_R, for the two experiments.) The average value for $(F^*/F_R^*(0))$ was 17 ± 3 for a set of experiments in which the detection conditions matched those of the uv calibra-

tion experiment. Thus with eq 4 $\psi_{D_1 \cdot S_1} = 6.4 \pm 1.2 \times 10^{-4}$.

This says that for every excited durene singlet state made during one entire ISCR pulse 6.4×10^{-4} excited duryl radicals are made.

Presumably some of the ISCR events may lead directly to the ground-state duryl radical unaccompanied by emission. Experiments were undertaken to observe any increase of ground-state duryl radical during an ISCR pulse by monitoring the 329-nm excited green radical fluorescence before and after ISCR. An increase of duryl radical concentration of 0.5% should be detectable. Under the extreme photosensitization used, the effective concentration of radical produced was about 10^{-4} M and one ISCR produced a total of about 2×10^{-5} M recombinations essentially all of which generated luminescing excited durene states.[3] Now a 0.5% increase of R would amount to a growth of $\sim 5 \times 10^{-7}$ M radical during the ISCR as the lower detectable limit. Our failure to see any increase in radical fluorescence sets an upper limit of about 0.02 for the yield of ground-state radical production by ISCR and says that altogether less than $\sim 5 \times 10^{-7}$ radicals are produced as a result of ISCR. There must, of course, be some increase in radical concentration if only from the ISCR-produced luminescing radicals being studied in this work. For $\sim 2 \times 10^{-5}$ M recombinations $\sim 1/4$ of these produced durene in its first excited singlet state ($\sim 3/4$ go directly to the triplet) and, as this work has shown, for every one fluorescing durene singlet state 6.4×10^{-4} fluorescing radicals are formed. This route is responsible, then, for an increment of only $\sim 3.2 \times 10^{-9}$ M in radical concentration. We can only conclude that if any ground-state duryl radical is produced directly by ISCR the fraction of radical made *via* its luminescing state to that made directly in the ground state must be least one in about 160.

The observed yield of excited duryl radicals of 6.4×10^{-4} per excited durene singlet made during ISCR is remarkably close to the quantum yield of 10^{-4} found for the one-photon production of duryl radical when durene is excited to an upper vibration level of its first excited state.[3] However, this one-photon β-bond cleavage occurs at ≥ 4.66 eV. It is difficult to see how this energy could accomplish β-bond cleavage (~ 3.13 eV) while leaving the product in its luminescing state (~ 2.5 eV). It seems that the entry into the channel producing the excited duryl radical must occur at no less than 5.6 eV above the durene ground state. This is not much below the energy needed to achieve ionization (biphotonic) of durene in 3-MP at 77°K. It is approaching energies of pseudoionization continua (partial ionization) which must play a role in the ionization step as well as the recombination process. These states have been previously symbolized as $\{\chi\}$ and $\{\chi^*\}$, respectively,[3] recognizing that charge recombination must proceed *via* different nuclear geometries than the ionization process (if only because the equilibrium structure of the durene cation must differ from that of the durene triplet state, the last stable configuration of durene in the ionization process). The energies of $\{\chi\}$ and $\{\chi^*\}$ may differ as well. Now the quantum yield for β-bond scission *via* the $\{\chi\}$ state is very high (of the order of unity).[3] In contrast we have seen here that recombination *via* the $\{\chi^*\}$ states does not lead to such a high yield (it leads to very little β-bond scission). Why the $\{\chi\}$ states are so successful for β-bond cleavage but the $\{\chi^*\}$ so unsuccessful is an unresolved question.

C. Investigation of the Increase of F_R^* *with Each Uv Photosensitization Cycle.* The linear increase of the ISCR duryl radical fluorescence, $F_R^*(n)$, with successive uv-photosensitization-ISCR cycles contrasts with the repeatedly constant value observed for the ISCR durene luminescence. Presumably some new photoactive species is accumulating which can undergo ISCR leading to duryl radical fluorescence. The one species in this system which clearly builds up upon successive sensitization is the duryl radical itself. Its buildup is linear in time. Each ISCR more or less fully bleaches the available durene cation in any given cycle (therefore F^* is constant) but the neutral duryl radical is not susceptible to such a radiatively controlled reversibility. It is conceivable that the duryl radical itself undergoes ionization and subsequent ISCR produces duryl radical fluorescence at a heightened level with each new cycle. To test this possibility two photosensitizations were carried out, one at 268 nm where the duryl radical absorbs and one at 281 nm where it absorbs negligibly.[6] Conditions were adjusted to be otherwise equal. For example, the intensities were adjusted in a manner giving the same level of F^* in the two sensitizations. The $F_R^*(n)$ signal proved to be about the same in both instances. In particular, F_R^* readings after ~ 10 cycles give $F_R^*(n) \cong ndF_R^*/dn$ (for n large) (eq 1) and therefore equal values of $F_R^*(n)$ indicate equal values of dF_R^*/dn. It seems that the duryl radical is not photoactive in this sense. Incidentally, it may well be that the duryl radical is particularly immune to photoionization. It is probably biphotonic in this energy region and there are no metastable excited states available for capturing a second photon (the lowest quartet state lies above the first excited doublet and therefore ought not be metastable).

In fact it appears that the new photoactive species responsible for the ISCR (dF_R^*/dn) is one-photon ionizable. This was checked by taking the system through $n - 1$ cycles at one uv light level and then in the nth cycle the light intensity is changed by a factor, m. At large n the $F_R^*(0)$ term (which is biphotonic) can be neglected and as just stated above, the main contribution to the F_R^* in the nth cycle is from the ionization of the new photoactive species built up over the previous $n - 1$ cycles. Although the error is rather large such a study indicates that the ionization of the new photoactive species is monophotonic.

Previous photoconductivity work on these and similar systems[2] provides additional evidence for a new accumulating photoactive species. Solutions such as durene in 3-MP at 77°K initially exhibit photoelectric signals only when excited in the region of durene absorption. After uv sensitization, however, new photoelectric activity is seen throughout the visible and near-infrared in the form of a photocurrent spike. This signal represents photomobilized electrons which go into recombination (ISCR) giving the observed transient photocurrent. In the near-uv a second new induced photoelectric signal is seen which almost appears as a steady photocurrent but, in fact, is a transient on the time scale of tens of minutes. In a separate study[7] of the charge recombination bleaching of a solute cation, the normal ISCR bleaching was seen but, in addition, a very slow bleaching activity was found in the near-uv fully comparable to the very slow near-uv photocurrent transient. It was also observed in both studies that after exciting this new near-uv ionizable species new ISCR activity is generated. The new species, photoactive in the near-uv and apparently responsible for these various observations
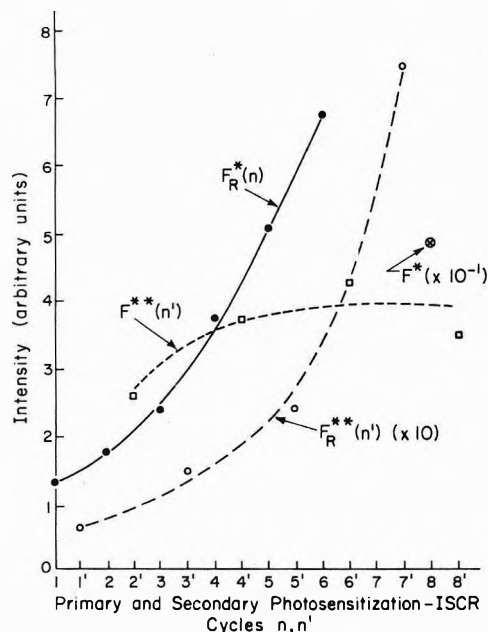
Figure 6. The results of a study in which the photosensitization–ISCR cycles are carried out at the primary wavelength (275 nm) followed by a cycle at a secondary wavelength (315 nm) where durene does not absorb. The cycles are enumerated n and n', respectively. The normal $F_R^*(n)$ seen in the primary cycle, is given by the solid curve. At $n = 8$ an F^* (scaled down by a factor of 10) is entered as well. The signals seen from the secondary photosensitization are $F_R^{**}(n')$ (--O--) at $n' = 1'$, $3'$, $5'$, and $7'$ and scaled up by a factor of 10; and $F^{**}(n')$ ($\cdots\square\cdots$) at $n' = 2'$, $4'$, $6'$, and $8'$. Extrapolations to n, $n' = 0$ have not been made.

appears to be one-photon produced (from the parent solute molecule) and one-photon ionized. It has never been identified but for want of a better description it was called a compact charge pair. Now, most recently, electrophotoluminescence (EPL) studies[8] of a typical rigid solution have revealed an exceptionally strong coupling with an applied electric field of what appears to be this very same intermediate species. The coupling is seen by the field-induced charge recombination to give luminescing parent molecules. If nothing else, these observations indicate that a long-lived *charge pair* type intermediate is present in such a system.

Given this history of these photosensitized solutions an effort was made in this work to see whether this long-lived intermediate might not be responsible for the buildup of F_R^* with each additional cycle. A clear symptom of such activity would be demonstration of near-uv activity for providing a new source of F_R^*.

Several samples were subjected to uv, near-uv, and infrared stimulation in the following cycle: (1) 275-nm photosensitization of the sample for 3 min; (2) infrared stimulation of the sample to determine F_R^* or F^*; (3) irradiation of the sample by intense uv at 290, 313, or 325 nm, well outside the durene absorption band, for 5 min; (4) infrared stimulation of the sample and measurement of any new F_R^* or F^* due to step 3. These are symbolized, respectively, by F_R^{**} and F^{**}.

Figure 6 displays the values of $F_R^*(n)$ (step 2), $F^{**}(n)$, and $F_R^{**}(n)$ (step 4) for eight cycles of steps 1-4. One measure of F^* (step 2) is entered at the eighth cycle. These results were obtained using 325-nm light but they differ insignificantly from what is found when either 290 or 313

nm are chosen for the step 3 illumination. First it is evident that following normal uv photosensitization *both* ISCR durene fluorescence, F^*, and duryl radical fluorescence F_R^*, can be generated using wavelengths longer than those needed to excite durene itself. The level of F_R^{**} is only about 5% of the F_R^* value seen at step 2 and therefore the buildup of the near-uv sensitive species cannot account for the entire dF_R^*/dn contribution unless this species experiences an abrupt gain in photoionization efficiency upon going to shorter wavelengths (~ 275 nm). What is most interesting is that F_R^{**} grows strongly with increasing n while F^{**} appears to level off after an initial rise. The accumulation of the near-uv sensitive species does appear to cease after a number of cycles from photoconductivity work, and the leveling off of F^{**} would agree with this. The continued growth of F_R^{**}, then, is all the more dramatic and suggests that with time the ionized near-uv species increasingly favors the formation of the excited duryl radical upon ISCR. This point may be crucial in explaining the unexpected superlinear dependence on n of the F_R^* signal excited at 275 nm when, as here, episodes at $\lambda > 275$ nm have been inserted. We recall how the normal pattern has been a good linear dependence of F_R^* on n. Perhaps the inserted $\lambda > 275$ nm-ISCR step which focuses on the long-lived intermediate is gradually providing an increasingly more "active" form of the intermediate for the next 275 nm-ISCR cycle. We have found no alternate explanation for the superlinear behavior of F_R^*. The photoconductivity work indicates that the ionization and ISCR cycles based on this intermediate are relatively stable. That is the intermediate state is not destroyed nor is it even easily returned to the ground state of the parent molecule. It may be that such extra radiative "working" of the intermediate occurring at each $\lambda > 275$ nm-ISCR cycle causes it to gradually shift toward the higher yield F_R^{**} form that appears to emerge. Clearly a much more detailed examination of these various events is needed before it becomes possible even to associate them all with a single intermediate state.

IV. Summary

Experiments reveal that charge recombination between electrons and durene cations in rigid 3-methylpentane at 77°K can lead to excited duryl radicals (β-bond scission) which are detected through their characteristic green emission. For every $\sim 6 \times 10^3$ recombination events which show the statistical 3 to 1 partitioning between the durene triplet and singlet manifolds and yield the accompanying durene phosphorescence and fluorescence only about one leads to the excited duryl radical. As many as ~ 160 of these recombinations could lead directly to the ground-state duryl radical and this would escape detection. The lock-in techniques used afford a very sensitive means for detecting fluorescing products of the charge recombination. When perdeuterated durene is examined a reduction by a factor of about 3 of the charge recombinational production of excited duryl radical is observed. This compares favorably with a similar reduction found for the yield of duryl radical produced biphotonically by direct excitation of durene in 3-MP.[3] In contrast, perdeuteration of durene does not detectably change the number of charge recombinations nor the number of these which lead to durene recombination fluorescence. It seems, not surprisingly, that the isotope effect appears at the point of β-bond scission whether this is occurring during charge re-

combination as in this work, or during the direct excitation of durene studied previously.[3]

The efficiency of the ISCR route for making excited duryl radicals is very close to the observed quantum yield for making duryl radical by direct one-photon excitation of durene into upper vibrational levels of its first excited singlet state.[3,5] However, on energetic grounds it does not appear possible to offer these vibrational levels as channels for generating duryl radical in its first *excited* state. The passage to *excited* duryl radicals upon charge recombination, involving β-bond scission, must occur from still more energetic levels of the durene–3-MP system, levels comparable in energy to the subionization continua of states just below the ionization energy of durene in 3-MP (probably about 6.5 eV[4]). In fact in the direct excitation, two-photon, studies[3] it is found that durene–3-MP states in this energy range exhibit quantum yields of the order of unity for generating ground-state duryl radical (whether or not this occurs *via* excited duryl radical is unknown). These high yields are not seen for the recombinational generation of duryl radical and certainly not for its formation in an excited state. The fact that direct excitation (*via* the durene triplet state) necessarily catches durene in a different equilibrium geometry (that of the triplet state) than for the charge recombination step (that of the durene cation) may be important here.

A secondary observation that the duryl radical fluorescence builds up with repeated uv-photosensitization–ISCR cycles has led to the discovery of a new near-uv sensitivity (following the primary uv photosensitization) for producing these charge recombination events (a sensitivity which seems to favor excited duryl radical formation with increasing time). These observations supplement earlier findings of new near-uv photoconductometric and electrophotoluminescent sensitivity. Both sets of observations seem to speak for the emergence of some new photoionizable durene–3-MP species (apparently involving a partial charge separation) upon primary uv photosensitization. The identity of this species remains unknown.

There are reports in the literature in which benzyl radical type luminescence is seen as a result of charge recombination events in photosensitized or γ-irradiated rigid glasses. One of the earliest is by Gibbons, *et al.*,[9] where the benzyl radical luminescence is seen as a component of the thermoluminescence obtained upon heating a solution of toluene in 3-MP after it had been photoionized at 77°K.

When, instead, similar solids are γ-irradiated their thermoluminescence also reveals a radical luminescence component. In fact Deniau, *et al.*,[10] report this for durene in methylcyclohexane. Their thermal resolution of the glow curve is able to distinguish cation–electron recombinational events from cation–anion events where some molecular diffusion is called for. At low doses the radical luminescence results from cation–anion recombination, but at high doses the isothermoluminescence itself reveals radical luminescence. However, here it seems that the electron is recombining with the radical cation to give excited duryl states. Such work, especially at low doses, was recently extended by Brocklehurst, *et al.*,[11] where ion recombinational thermoluminescence was seen from several methyl-substituted benzyl radicals. Common to most of these studies is their qualitative nature, as well as the absence of any sign of the sort of infrared-induced radical luminescence being studied in the present work. Very likely under more severe conditions of energy deposition than those used here, ion recombinational mechanisms (or electron recombinations with radical cations) for producing radical luminescence must prevail.

Apart from the specific results of studies, it is hoped that they do serve as an interesting example of quantitative charge recombinational chemistry in a condensed phase and invite further studies along these lines both as a supplement to and a contrast with charge recombinational chemistries occurring in ionized gas-phase systems.

References and Notes

(1) (a) This work has been supported primarily by NIH Grant No. GM 10865. Additional support by the material Science Center at Cornell University is gratefully acknowledged. (b) Taken in part from the Ph.D. Thesis of F. P. S., Cornell University, 1970.

(2) See, for example, G. E. Johnson and A. C. Albrecht, *J. Chem. Phys.*, **44**, 3162, 3179 (1966).

(3) F. P. Schwarz and A. C. Albrecht, submitted for publication.

(4) P. M. Johnson and A. C. Albrecht, "The Chemistry of Ionization and Excitation," C. R. A. Johnson and G. Scholes, Ed., Taylor and Francis Ltd., 1967, p 91.

(5) F. P. Schwarz and A. C. Albrecht, *Chem. Phys. Lett.*, **9**, 163 (1971).

(6) P. M. Johnson and A. C. Albrecht, *J. Chem. Phys.*, **48**, 851 (1968).

(7) W. M. McClain and A. C. Albrecht, *J. Chem. Phys.*, **43**, 465 (1965).

(8) R. Devonshire and A. C. Albrecht, Proceedings of the International Conference on Luminescence, Leningrad, 1972.

(9) W. A. Gibbons, G. Porter, and M. I. Savadatti, *Nature (London)*, **206**, 1355 (1965).

(10) C. Deniau, A. Deroulece, F. Kieffer, and J. Rigaut, *J. Lumin.*, **3**, 325 (1971).

(11) B. Brocklehurst, J. S. Robinson, and D. N. Tawn, *J. Phys. Chem.*, **76**, 3710 (1972).

Evidence for Ion–Molecule Reaction of Hydrogen Transfer in γ-Irradiated 2,3-Dimethylbutane at 77 K as Studied by Electron Spin Resonance Spectroscopy

Yoshiyuki Saitake, Tetsuo Miyazaki,* and Zen-ichiro Kuri

Department of Synthetic Chemistry, Faculty of Engineering, Nagoya University, Chikusa-ku, Nagoya, Japan
(Received May 25, 1973)

The occurrence of an H_2 transfer reaction in the solid phase was confirmed by the detection of product cation directly by esr spectroscopy. When SF_6 is added to 2,3-dimethylbutane (DMB), tetramethylethylene (TME) cation is formed in the radiolysis at 77 K. Yields of TME cation produced in γ-irradiated DMB containing SF_6 at 77 K increase upon the addition of ethylene, propylene, cyclopropane, or isobutene. The increase of the yields of TME cation is due to H_2 transfer from the parent ion of DMB to olefin or cyclopropane. Apparent efficiencies of ethylene, propylene, cyclopropane, and isobutene for the H_2 transfer reaction were different. The yield of TME cation in the γ-irradiated DMB–SF_6 (0.55 mol %)–C_3H_6 (0.55 mol %) in crystal II is much lower than that in crystal I. When DMB containing SF_6 without olefin is γ-irradiated at 77 K, TME^+ is formed. Since the yield of TME^+ does not decrease upon the addition of 2-methyltetrahydrofuran, it is suggested that the ion may be formed by the fragmentation of DMB^+ ion in the solid phase.

Introduction

Though ion–molecule reactions have been studied by the direct detection of ions with a mass spectrometer in the gas phase, most of the studies in the condensed phases have been performed by the analysis of final products in the radiolysis. Williams[1] studied the proton transfer reaction by the analysis of hydrogen in the radiolysis of liquid cyclohexane containing deuterated ammonia. Ausloos, *et al.*,[2] studied the ion–molecule reaction by the analysis of final products in the radiolysis of a deuterated hydrocarbon mixture in the liquid phase. Miyazaki, *et al.*,[3] studied the reaction of the carbonium ion by the analysis of unsaturated hydrocarbons in the radiolysis of liquid alkane containing ammonia and sulfur hexafluoride. Hamill, *et al.*,[4] studied the reaction of carbonium ion by the analysis of ether in the radiolysis of liquid neopentane containing alcohol.

The ion–molecule reactions by a positive ion in the solid phase have been studied by a few investigators. It was reported by the analysis of final products that the H_2 transfer reaction occurs in the radiolysis of alkane containing olefin in the solid phase,[2] but the analysis of final neutral product has a drawback for the study of the reaction in the solid phase at 77 K. The method cannot distinguish the reaction in the solid phase at 77 K from the reaction which occurs when the irradiated sample is warmed and diffusion becomes possible.

In order to study the solid-state kinetics, the observation of the product ion at 77 K is very useful to prove the occurrence of the H_2 transfer reaction in the solid phase. In this work, we observed the TME cation by esr spectroscopy in the γ-irradiated DMB containing olefin or cyclopropane at 77 K.

Experimental Section

2,3-Dimethylbutane (DMB), >99%, supplied by Tokyo Kagaku Seiki Co., was passed through a 50-cm column packed with activated silica gel and distilled on a vacuum line after being dried over a sodium mirror. Gas chroma-tographic analysis showed that the concentration of impurities, which were considered as some hydrocarbons of smaller molecular weight than DMB, was less than 10^{-2} mol %. Propylene, cyclopropane, ethylene, and isobutene supplied by Takachiho Chemical Industrial Co. and sulfur hexafluoride supplied by Matheson Co. were of high purity and were used without further purification. Phenyl bromide was used after distillation. 2-Methyltetrahydrofuran (MTHF) was distilled and then dried over a sodium mirror.

Samples were sealed into a quartz cell and irradiated with γ rays from ^{60}Ca at 77 K. The dose and dose rate were 9.2×10^{18} eV/g and 3.8×10^{19} eV/g hr, respectively. The esr measurements were made on a JES-3BX esr spectrometer.

According to a calorimetric study, 2,3-dimethylbutane has several crystalline forms in the solid state.[5] When it is cooled rapidly to 77 K, it forms a supercooled crystal I which is a transparent solid. When the supercooled crystal I is warmed up to some temperature lower than its melting point (145 K) and then cooled to 77 K and when this kind of annealing is repeated several times, it forms a crystal II which is the stable phase at 77 K.

Results and Discussion

Occurrence of H_2 Transfer Reaction in the Solid Phase. The esr spectrum of γ-irradiated DMB in the supercooled crystal I is shown in Figure 1a. The spectrum, which consists of five lines with a splitting of 22 G, is assigned to the $(CH_3)_2CHCH(CH_3)CH_2\cdot$ radical.[6] A quite different spectrum, shown in Figure 1b, was obtained by γ irradiation of DMB containing 0.8 mol % SF_6. The new absorption is superimposed on that of the solvent radical. Addition of propylene enhanced the intensity of the new absorption, which may be assigned to the tetramethylethylene (TME) cation for the following reasons. (1) The spectrum consists of at least nine equally spaced lines separated by 16.6 G and coincides well with the spectrum of the TME cation produced in γ-irradiated 3-methylpen-
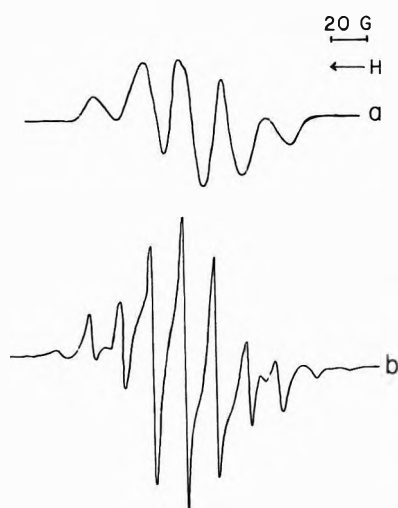
Figure 1. Esr spectra of γ-irradiated DMB in supercooled crystal I at 77 K: a, pure DMB; b, DMP–SF$_6$ (0.8 mol %). Spectrometer gain settings of a and b are approximately the same.
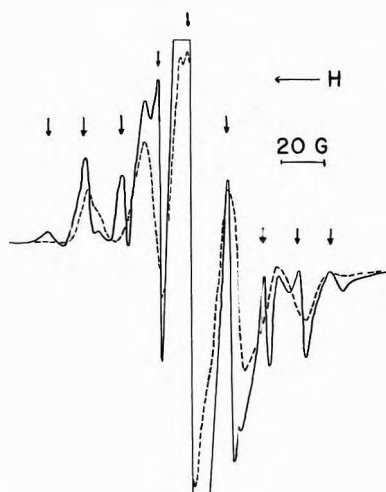

Figure 2. Esr spectra of γ-irradiated DMB–mesitylene (0.4 mol %) in supercooled crystal I at 77 K. Solid line, before photobleaching. The arrows indicate the nine absorption peaks. The central absorption with high intensity is due to mesitylene anion. Dashed line, after photobleaching with visible light for 0.5 min.

tane containing TME (0.3 mol %) and CO_2 (0.1 mol %).[7] The value of 16.6 G is also equal to that for the TME cation produced by the oxidation of TME.[8] (2) Though a spectrum of nine lines is clearly observed in the presence of an electron scavenger, it cannot be observed in pure DMB without any electron scavenger. (3) The spectrum of nine lines was obtained at lower intensity by γ irradiation of DMB containing 0.4 mol % mesitylene, where the formation of the mesitylene anion was also observed via esr spectroscopy (solid line in Figure 2). The central absorption with high intensity is due to the mesitylene anion. The nine absorption lines, indicated by arrows in Figure 2, were easily photobleached by illumination with visible light and the mesitylene anion disappeared at the same time (dashed line in Figure 2). This result indicates that the absorption is due to a cation. (4) Addition of MTHF, which is known as a positive charge acceptor, diminished the intensity of nine lines produced in the γ-irradiated DMB containing SF$_6$ and propylene (see ●—● in Figure 3). The result also supports the conclusion that the absorption is due to a cation.

As shown in Figure 4, yields of TME cation increase upon the addition of olefin or cyclopropane. Ausloos, *et*
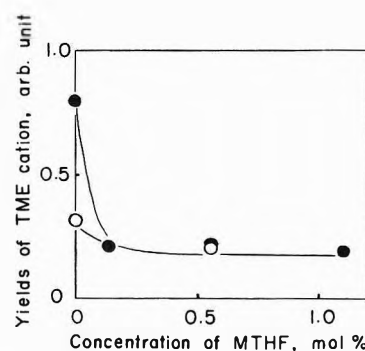

Figure 3. Effect of MTHF on the yields of TME cation in the radiolysis of DMB in supercooled crystal I at 77 K: O—O, DMB–SF$_6$ (0.55 mol %)–MTHF; ●—●, DMB–SF$_6$ (0.55 mol %)–C$_3$H$_6$ (0.55 mol %)–MTHF.
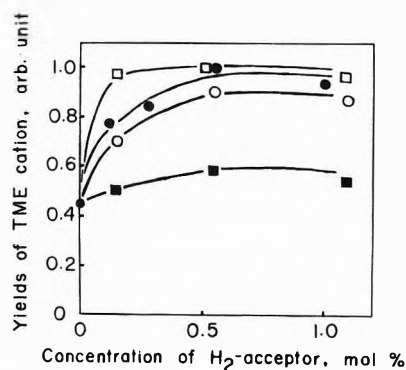

Figure 4. Effect of H_2 acceptors on the yields of TME cation in the radiolysis of DMB–SF$_6$ (0.55 mol %)–acceptor system in the supercooled crystal I at 77 K: ■, DMB–SF$_6$–C$_2$H$_4$; O, DMB–SF$_6$–c-C$_3$H$_6$; ●, DMB–SF$_6$–C$_3$H$_6$; □, DMB–SF$_6$–i-C$_4$H$_8$.
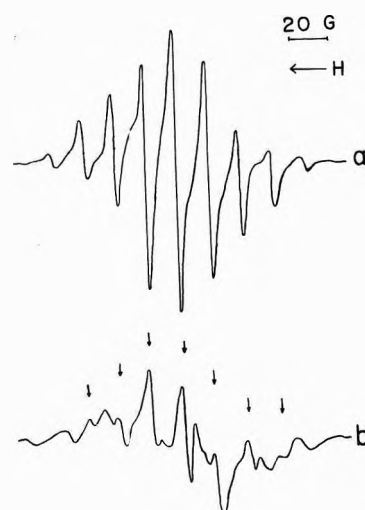

Figure 5. Effect of phase on esr spectra of γ-irradiated DMB–SF$_6$ (0.55 mol %)–C$_3$H$_6$ (0.55 mol %) at 77 K: a, in supercooled crystal I; b, in crystal II. The arrows indicate the signal of TME cation. Spectrometer gain settings of a and b are approximately the same.

al., reported the occurrence of an H_2 transfer reaction in the radiolysis of alkane containing olefin by the analysis of final neutral products.[2,9] It is reasonable to conclude that the increase of the yields of TME cation is due to an H_2 transfer reaction between olefin and DMB cation.

$$DMB \xrightarrow{SF_6} DMB_m^+ + SF_6^- \qquad (1)$$

$$DMB_m^+ + C_nH_{2n} \rightarrow TME^+ + C_nH_{2n+2} \quad (2)$$
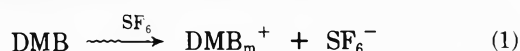
where DMB_m^+ represents a hole which can migrate through the DMB matrix. The apparent efficiencies of H_2 transfer from DMB_m^+ to various additives are different. It is uncertain, however, whether the difference is caused by the difference of actual concentrations of the additives in the crystal or by the different efficiencies of the H_2 transfer reaction of the additives.

Phase Effect on H_2 Transfer Reaction. Esr spectra of a γ-irradiated DMB-SF_6 (0.55 mol %)-propylene (0.55 mol %) system in crystal I and crystal II at 77 K are given in Figure 5a and b, respectively. The spectrum in Figure 5b is superimposed by two components; one is the spectrum of the TME cation, indicated by arrows, and the other is that of the solvent radical, assigned to the $(CH_3)_2CH\overset{\cdot}{C}(CH_3)_2$ radical.[6] Obviously, the yields of TME cation in crystal II are lower than those in crystal I.

Formation of TME^+ in the Radiolysis of DMB. When DMB containing SF_6 is γ-irradiated at 77 K, TME^+ is formed in an appreciable amount (Figure 1b). TME was not detected at all in pure DMB by gas chromatographic analysis and the concentration of TME as an impurity is less than 2×10^{-5} mol %. Therefore, TME^+ produced in γ-irradiated DMB containing SF_6 is not formed by a charge transfer from DMB^+ to TME as an impurity. As shown by the plots (O—O) in Figure 3, the formation of the TME cation in the radiolysis of DMB-SF_6 (0.55 mol

%) is not suppressed by the addition of MTHF which is an efficient charge acceptor. Therefore, the migrating hole does not participate in the formation of TME^+ in the DMB-SF_6 system. One plausible mechanism for the formation of TME^+ is the fragmentation of DMB^+ ion.

$$DMB \xrightarrow{SF_6} DMB^+ + SF_6^- \quad (3)$$

$$DMB^+ \rightarrow TME^+ + H_2 \quad (4)$$
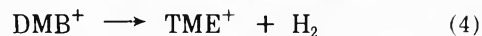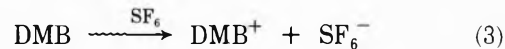
The ionic fragmentation of reaction 4 is scarcely observed by mass spectrometry, but since it is an exothermic reaction and the heat of its reaction is about 34 kcal/mol, its occurrence may be possible.

References and Notes

(1) F. Williams, *J. Amer. Chem. Soc.*, **86**, 3954 (1964).
(2) (a) A. A. Scala, S. G. Lias, and P. Ausloos, *J. Amer. Chem. Soc.*, **88**, 5701 (1966); (b) P. Ausloos, A. A. Scala, and S. G. Lias, *ibid.*, **89**, 3677 (1967).
(3) (a) T. Miyazaki, *J. Phys. Chem.*, **71**, 4282 (1967); (b) K. Tanno, T. Miyazaki, K. Shinsaka, and S. Shida, *ibid.*, **71**, 4290 (1967).
(4) J. A. Ward and W. H. Hamill, *J. Amer. Chem. Soc.*, **89**, 5116 (1967).
(5) K. Adachi, H. Suga, and S. Seki, *Bull. Chem. Soc. Jap.*, **44**, 78 (1971).
(6) M. Fukaya, T. Wakayama, T. Miyazaki, Y. Saitake, and Z. Kuri, *Bull. Chem. Soc. Jap.*, **46**, 1036 (1973).
(7) T. Ichikawa and P. K. Ludwig, *J. Amer. Chem. Soc.*, **91**, 1023 (1969).
(8) R. M. Dessau, *J. Amer. Chem. Soc.*, **92**, 6356 (1970).
(9) P. Ausloos and S. G. Lias, *J. Chem. Phys.*, **43**, 127 (1965).

Reaction of Hydroxyl Radicals with Polyethylene Oxide in Aqueous Solution

Max S. Matheson,*[1] A. Mamou, J. Silverman,[2] and J. Rabani

Department of Physical Chemistry, The Hebrew University of Jerusalem, Jerusalem 91000, Israel (Received April 13, 1973)

In aqueous solutions the rate constant for OH + polyethylene oxide depends upon the concentration and upon the molecular weight of the polymer. If the rate is expressed as "k_M"(OH)(M), where (M) is the concentration of polymer in monomer units, "k_M" varies with $x^{-0.4}$ (x = degree of polymerization) in dilute solutions where polymer molecules are isolated from each other. In concentrated solutions ((M) $\gtrsim 1$ M) where polymer molecules essentially fill all of the solution, "k_M" is independent of x and is the same as the rate constant "k_M" for polymer of $x = 3$ or 4. For polymer of $x = 3$ or 4 "k_M" is independent of (M). Experimentally, "k_M" has been evaluated for polyethylene oxide polymers of different x's and concentrations in pulse radiolysis competition experiments using ferrocyanide and iodide as OH scavengers. An equation has also been developed from polymer solution theory and probability theory which gives the appropriate correlation of "k_M" with (M) and with x.

Introduction

It has been pointed out previously[3] that the rate constant for a reaction involving a polymer molecule in solution as a reactant depends both upon the concentration and upon the degree of polymerization of the polymer. The reactions investigated were OH with polyethylene oxide or with polyvinylpyrollidone or with dextran. At high concentration where polymer molecules touch or in-

terpenetrate it was noted that the concentration approximates a uniform solution of monomer units and the rate constant "k_M" (expressed in terms of moles of monomer units per liter) is independent of molecular weight. In dilute solutions the polymer molecules are widely separated and, for the case where OH reacts at a rate which is diffusion controlled or nearly so, the rate constant, k_{p2}, in liters moles^{-1} sec^{-1} can be represented by the Smoluchow-

ski expression

$$k_{p2} = \frac{4\pi D_{OH} \mathfrak{N}_a}{10^3} r(x) \qquad (1)$$

where D_{OH} is the diffusion constant of OH, $\mathfrak{N}_a$ is Avogadro's number, and $r(x)$ is the effective radius of reaction of the polymer molecule containing x monomer units. $D_{OH} \gg D_p$, the diffusion constant of the polymer, and $r(x) \gg r_{OH}$, the reaction radius of OH. From the theory of linear polymers in solution $r(x)$ may be expected to be proportional to $x^{0.5}$. Behzadi, et al.,[3] find that for x greater than about 50, $k_{p2} \propto x^{0.57}$ for polyethylene oxide; that is "k_M" $\propto x^{-0.43}$ in dilute solutions.

We have with the technique of pulse radiolysis reinvestigated the reaction of OH radicals with polyethylene oxide in aqueous solution. We communicate our results for two reasons. First, we find values for "k_M" $= (k_p/x)$ about 3.5-fold greater than those reported by Behzadi, et al. Repeated tests of our technique both with polymer and with test compounds of known rate constants for reaction with OH lead us to believe our results are correct. Thus, for example, in experiments involving competition for OH between ferrocyanide and ethanol we measured k(OH + ethanol) $= 1.65 \times 10^9$ M^{-1} sec^{-1} when k(OH + ferrocyanide) was taken as 0.93×10^{10} M^{-1} sec^{-1}, whereas Willson, et al.,[4] give 1.85×10^9 and 0.93×10^{10}, respectively. Second, we have applied the theory of solutions of linear polymers to rationalize the dependence of "k_M" upon concentration in terms of just two constants which are closely related.

Experimental Section

The pulse radiolysis apparatus and syringe technique were essentially the same as described before.[5-8] Further details on the specific conditions of our set-up have been described elsewhere.[9] In the present work, an 1P 28 photomultiplier, a Bausch and Lomb high-intensity monochromator and a Tektronix 556 dual-beam oscilloscope were used. A xenon 150-W lamp with water cooling of the light enclosure served as a light source. Appropriate light filters were employed in order to minimize photochemistry of the solutions. Also a shutter between the lamp and the irradiation cell operated mechanically by air pressure, was opened $\sim$1 sec before irradiation. A 5-MeV electron beam (200 mA average pulse current) from the Hebrew University linear accelerator was used for most of the pulse irradiations; 1.5- and 0.5-μsec electron pulses were used for the ferrocyanide experiments; 0.2-μsec pulses were used for the I$^-$ experiments.

Matheson ultra pure argon and O_2 were used for the preparation of solutions. N_2O was purified by the procedure previously described.[10] All experiments were carried out with triply distilled water. Potassium ferrocyanide (Mallinckrodt) and iodide (BDH "analar") were used as received. Ethylene glycol and polyethylene glycols were obtained from Merck and generally used without further purification. Some of the samples were recrystallized from ethanol and dried in vacuo. They gave identical results. In some experiments a different sample of polyethylene glycol (Fluka) was irradiated and also gave identical results.[11] Finally, ethylene glycol either Koch-Light (high-purity) or Fluka (purum) was used in several experiments to check the accuracy of our rate constant measurements. We do not have data on the polydispersity ratio of the polymers; however, from the general method of synthesis (anionic polymerization with very rapid initiation) we infer that the ratio is less than 1.1.

A 4-cm cell with 12.3-cm light path was used for all the experiments, except those in Bethesda for which a 4-cm path was used. The temperature was 25 $\pm$ 2°.

Discussion and Results

Our results and those of Behzadi, et al.,[3] show that if the rate of reaction of OH with polyethylene oxide is expressed as

$$-d(OH)/dt = "k_M"(OH)(M) \qquad (2)$$

then "k_M" is a function of both (M) (the molar concentration of monomer units) and x (the degree of polymerization) such that at high concentrations ((M) $\simeq$ 1 M) "k_M" is independent of x and is approximately equal to k_M for OH + monomer, while at low concentrations ((M) $\simeq$ 10^{-3} M) "k_M" is approximately proportional to $x^{-1/2}$. Using the theory of solution of linear polymers we find that these results can be rationalized together with the dependence of "k_M" on (M) and x at intermediate values of (M).

Since the polymer radicals formed by the reaction of OH with polyethylene oxide do not absorb strongly in an easily accessible part of the spectrum, the rate constants for reaction have been determined by competition with an OH scavenger. The OH scavengers used by us were ferrocyanide and iodide ions, while Behzadi, et al.,[3] used p-nitrosodimethylaniline, potassium thiocyanate, and sodium benzoate. The competition with scavenger, S$^-$, may be expressed as

$$OH + S^- \xrightarrow{k_s} OH^- + S \qquad (3)$$

$$OH + P \xrightarrow{k_p} H_2O + P\cdot \qquad (4)$$
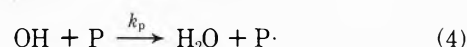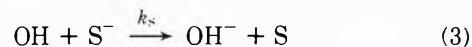
where, for example, S$^-$ could be Fe(CN)$_6^{4-}$ and S would then be Fe(CN)$_6^{3-}$. Then for the total rate of reaction of OH

$$-d(OH)/dt = k_S(OH)(S^-) + k_p(OH)(P) \qquad (5)$$

where (P) is the molar concentration of polymer molecules. Since S$^-$ and P are in excess the fraction reacting with S$^-$ is

$$\frac{(S)}{(S)_0} = \frac{k_S(S^-)}{k_S(S^-) + k_p(P)} = \frac{A}{A_0} = \frac{k_S(S^-)}{k_S(S^-) + "k_M"(M)} \qquad (6)$$

where (S) is the ferricyanide produced by a pulse with polymer present and (S)$_0$ is the ferricyanide produced by a pulse of the same intensity in the absence of polymer, but with the same concentration of ferrocyanide. A and A_0 are the absorbance values associated with (S) and (S)$_0$. To proceed, (1) the reaction volume is divided into two fractions: (a) the volume fraction, Φ, occupied by polymer molecules, including the solvent enclosed within the randomly oriented polymer coils, and (b) the volume fraction, 1 $- \Phi$, outside the polymer molecules. (2) We assume that (S$^-$) is uniform throughout the reaction system as is also the initial concentration of OH, that OH does not migrate between Φ and 1 $- \Phi$ in significant amounts, and that within the polymer the average concentration (P)/Φ can be used. Inside the polymer molecules the OH reacts with either scavenger or polymer in a homogeneous manner. In the region outside the polymer molecules S$^-$ competes for OH as it diffuses toward the reactive surface of the polymer molecules.

We will distinguish items related to volume fraction Φ by subscript 1 and items related to volume fraction 1 $- \Phi$

TABLE I: "k_M" from Competition Experiments with Ferrocyanide[a]

x	[M][b]	[F]	No. of Expt	Experimental A/A₀	Experimental "k_M"	Eq 18 (a = 0.2, b = 2.9) A/A₀	Eq 18 (a = 0.2, b = 2.9) "k_M"	Eq 20 (a = 0.369, b = 1.57) A/A₀	Eq 20 (a = 0.369, b = 1.57) "k_M"
1	2×10^{-3}	10^{-3}	3	0.71	19.4[c]			0.585	33
1	4×10^{-3}	10^{-3}	3	0.52	22.0[c]			0.413	33
1	8×10^{-3}	2×10^{-3}	3	0.50	24.0[c]			0.260	33
1	1×10^{-2}	10^{-3}	1	0.29	23.0[c]			0.360	33
4	8×10^{-3}	10^{-3}	3	0.38	19.0			0.379	19
4	1.5×10^{-2}	10^{-3}	1	0.25	18.6			0.245	19
460	10^{-3}	10^{-4}	3	0.764	2.87	0.76	2.9	0.763	2.88
460	10^{-2}	2×10^{-4}	5	0.385	3.0	0.384	2.98	0.384	2.98
460	10^{-2}	5×10^{-4}	3	0.624	2.79	0.60	3.1	0.600	3.09
460	10^{-2}	10^{-3}	9	0.741	3.31	0.738	3.3	0.738	3.3
460	2×10^{-2}	10^{-3}	8	0.572	3.50	0.580	3.36	0.580	3.36
460	3×10^{-2}	6×10^{-4}	6	0.326	3.83	0.280	3.18	0.280	3.18
460	3×10^{-2}	1.5×10^{-3}	5	0.608	2.97	0.562	3.62	0.562	3.62
460	4×10^{-2}	10^{-3}	3	0.38	3.87	0.40	3.5	0.400	3.49
460	4×10^{-2}	2×10^{-3}	4	0.50	4.66	0.54	3.9	0.545	3.88
460	5×10^{-2}	10^{-3}	3	0.324	3.87	0.34	3.6	0.343	3.55
460	0.1	2×10^{-3}	5	0.276	4.92	0.301	4.32	0.301	4.32
460	0.1	5×10^{-3}	8	0.488	4.89	0.460	5.45	0.460	5.45
460	0.1	10^{-2}	6	0.610	5.95	0.568	7.06	0.568	7.05
460	0.3	6×10^{-3}	6	0.198	7.57	0.192	7.82	0.192	7.82
460	0.3	1.5×10^{-2}	6	0.339	9.1	0.306	10.57	0.306	10.57
460	0.3	3×10^{-2}	6	0.456	11.5	0.411	13.3	0.411	13.3

[a] $k(OH + \text{ferrocyanide}) = 0.93 \times 10^{10} M^{-1} sec^{-1}$, $k(OH + M) = 2.1 \times 10^9 M^{-1} sec^{-1}$. All "$k_M$" in units $10^8 M^{-1} sec^{-1}$. [b] Moles monomer per liter. [c] Willson, et al.,[4] report $k(OH + \text{ethylene glycol}) = 1.5 \times 10^9 M^{-1} sec^{-1}$.

by subscript 2. Now in fraction Φ we use the average polymer concentration $(P)/\Phi$ which use corresponds to the high or uniform concentration results where "k_M" is independent of molecular weight. Therefore $k_{p1} = xk_M$ and since $(P) = (M)/x$

$$k_{p1}(P) = k_M(M) \tag{7}$$

Thus the competition in volume fraction Φ is written

$$\frac{(S)_1}{(S)_0} = \frac{k_S(S^-)}{k_S(S^-) + k_{p1}(P)/\Phi} = \frac{k_S(S^-)}{k_S(S^-) + k_M(M)/\Phi} \tag{8}$$

$(S)_0$ is the same for either volume.

For the competition outside the polymer

$$\frac{(S)_2}{(S)_0} = \frac{k_S(S^-)}{k_S(S^-) + k_{p2}(P)_2} \tag{9}$$

where k_{p2} is given by eq 1 and $(P)_2$ will be estimated as seen below.

For $r(x)$ in eq 1 we choose the root-mean-square displacement length, $(\overline{r^2})^{1/2}$. Flory[12] considers a tetrahedrally bonded chain consisting of n bonds each of length l in the absence of long-range (excluded volume) effects. With $\overline{r^2} = C_n n l^2$, then for large n and free rotation about the bonds $C_n = 2$. However, if one takes into account the rotational potentials and other short-range interactions, then for polyethylene glycol

$$\overline{r^2} = 4nl^2 \tag{10}$$

in the limit of large n, while at $n = 25$, C_n is already 3.5. For polyethylene oxide $n = 3x$, so

$$r(x) = (\overline{r^2})^{1/2} = (12x)^{1/2}l \tag{11}$$

Substituting (11) in eq 1 and taking[13] $D_{OH} = 2.8 \times 10^{-5}$ cm² sec^{-1} and taking $l = 1.47 \times 10^{-8}$ cm, one finds that

$$k_{p2} = 10.8 \times 10^9 x^{1/2} \tag{12}$$

Thus, k_{p2} is the rate constant for the reaction in which OH diffuses toward and reacts on every encounter with the surface of the polymer molecules whose radii are given by eq 11. Using the value for ferrocyanide of $k_S = 0.93 \times 10^{10} M^{-1} sec^{-1}$ of Willson, et al.,[4] we obtain from our results for low molecular weight polymer (e.g., $x = 1$ and $x = 4$, Table I) $k_M = 2.1 \times 10^9 M^{-1} sec^{-1}$, so that

$$k_{p2} = 5.1k_M x^{1/2} \tag{13}$$

(Note that k_M is constant but "k_M" varies.) If one takes[14] $D_{OH} = 2.0 \times 10^{-5}$ cm² sec^{-1}, then $k_{p2} = 3.7k_M x^{1/2}$.

One does not expect OH to be identically reactive toward a monomer unit in a chain and toward ethylene glycol. The difference in reactivity does not appear to be large, however, if one compares "k_M" in Table I for $x = 1$ and $x = 4$. The theory being developed does not apply to small molecules and the "k_M" found for $x = 4$ should be close to the correct value for k_M, the rate constant for reaction of OH with monomer unit in a hypothetical solution of homogeneously distributed $-CH_2-CH_2-O-$ units.

To evaluate Φ we use probability theory. The probability that m cells remain empty as z balls are distributed among N cells is[15]

$$P_m(z,N) = e^{-\lambda}\frac{\lambda^m}{m!} \tag{14}$$

where $\lambda = Ne^{-z/N}$. Further, the Poisson distribution, eq 14, has a mean value, $\overline{m} = \lambda$. Thus $1 - \Phi = \overline{m}/N = \lambda/N = e^{-z/N}$. We take $z = $ number of polymer molecules per liter $= \mathfrak{N}_a(P) = 6.02 \times 10^{23} (M)/x$, and since we take the volume of a cell as equal to the volume of a polymer molecule, V_p, then $N = $ number of cells in 1 l. $= 10^3/V_p = 10^3/(\frac{4}{3} \pi[(12x)^{1/2}l]^3) = 1.81 \times 10^{24}x^{-3/2}$. This gives $z/N = 0.333(M)x^{1/2}$. For the large molecules for which the theory is valid ($x \gtrsim 50$) more than one polymer molecule can occupy a cell since the concentration is low. For one

polymer molecule in a cell the molar concentration of monomer units is $3.01x^{-1/2}$.

We return to the evaluation of $(P)_2$ in eq 9. If two or more polymer molecules occupy the same cell, the effective radius will only be slightly larger than for one molecule and to a first approximation we will use the number of occupied cells as the effective concentration of polymer molecules. The number of occupied cells in one liter is $N\Phi = N(1 - e^{-z/N})$

$$(P)_2 = N\Phi \mathcal{R}_a = 3.01x^{-3/2}(1 - e^{-0.333(M)x^{1/2}}) \quad (15)$$

(Note that 3.01 and 0.333 are reciprocals.) If the exponential is expanded for low values of (M)

$$k_{p2}(P)_2 = 5.1k_M(M)x^{-1/2} \quad (16)$$

with the appropriate dependence found for dilute solutions.

It can be shown from simple considerations that the overall A/A_0 observed in the cell is

$$\frac{A}{A_0} = \frac{(S)_1}{(S)_0}\Phi + \frac{(S)_2}{(S)_0}(1 - \Phi) \quad (17)$$

In the exponential in Φ and $1 - \Phi$ 0.333 is based on the effective volume of the dissolved polymer molecule and for k_{p2} (eq 13) 5.1 is based on the effective radius of reaction (and on D_{OH}). The actual effective volume and radius may not be exactly those we have calculated, so we substitute a for 0.333 and b for 5.1, then substituting from eq 8 and 9 into eq 17 we get

$$\frac{A}{A_0} = \frac{k_S(S^-)}{k_S(S^-) + k_M(M)/(1 - e^{-a(M)x^{1/2}})}(1 - e^{-a(M)x^{1/2}}) +$$
$$\frac{k_S(S^-)}{k_S(S^-) + bk_M(1 - e^{-a(M)x^{1/2}})/ax}e^{-a(M)x^{1/2}} \quad (18)$$

This equation contains two closely related parameters, $a \simeq 0.33$ and $b \simeq 3.7$–5.1, which can be adjusted to give a best fit to the experimental results.

However, eq 18 is based on eq 10 in which the long-range, excluded-volume effect was ignored. This effect results from the fact that two segments of a polymer molecule cannot occupy the same space, and, therefore, the root-mean square displacement length, $(\bar{r^2})^{1/2}$, increases more rapidly than the square root of the degree of polymerization, x.[16] Equation 10 is obeyed in a poor solvent where polymer-polymer attraction exactly counteracts the excluded volume effect. For polyethylene oxide aqueous 0.45 M K_2SO_4 at 35° is such a solvent and Bailey and Callard[17] find the intrinsic viscosity–molecular weight relation for polyethylene oxide in this solvent is

$$[\eta] = 1.3 \times 10^{-3}(MW)^{0.5} \quad (19)$$

From this Mark and Flory[18] conclude $(\bar{r^2}/nl^2) = 4.1 \pm 0.4$ for polyethylene oxide in the absence of excluded volume effects in good agreement with theory. On the other hand, pure water is a better solvent than 0.45 M K_2SO_4 and in H_2O at 35° $[\eta] = 6.4 \times 10^{-5}(MW)^{0.82}$. Behzadi, et al.,[3] note that this latter dependence indicates $(\bar{r^2})^{1/2} \propto x^{(1+0.82)/3}$ or $x^{0.61}$. (Actually, these authors[3] from similar data give $x^{0.58}$). Recently, Grishman[19] treated the root-mean-square endpoint separation for self-avoiding walks without angular restrictions and found $(\bar{r^2})^{1/2} \propto x^{0.60}$. Further, Behzadi, et al., found experimentally in dilute solution that k_{p2} is proportional to $x^{0.57}$, so that "k_M" is proportional to $x^{-0.43}$. In addition, our own data indicate

that in dilute solution we should use "k_M" $\propto x^{-0.4}$ rather than $x^{-0.5}$.

Finally, the factor $x^{1/2}$ in the exponentials in eq 18 causes "k_M" to rise to the limiting high concentration value 2.1 $\times$ 10^9 at lower concentrations for the higher values of x. This causes the curves for different values of x to cross at high concentrations. This effect arises from the fact that in the theory, the volume of a cell was chosen as equal to the volume of a polymer molecule, so that there are fewer cells in a liter for the larger polymer molecules. In reality the larger molecules will interpenetrate at intermediate concentrations, which is equivalent to having a constant number of cells, but having a larger number of contiguous cells occupied by a larger polymer molecule.[20] In this case the power of x in the exponential will be lower. Empirically, we adjust eq 18 for the larger dependence of $r(x)$ on x, and the lesser dependence of occupied volume on x by rewriting eq 18 as

$$\frac{A}{A_0} = \frac{k_S(S^-)}{k_S(S^-) + k_M(M)/(1 - e^{-a(M)x^{0.4}})}(1 - e^{-a(M)x^{0.4}}) +$$
$$\frac{k_S(S^-)}{k_S(S^-) + bk_M(1 - e^{-a(M)x^{0.4}})/ax^{0.8}}(e^{-a(M)x^{0.4}}) \quad (20)$$

In eq 18 and 20 x refers to the number average degree of polymerization, and the equations are strictly applicable only to polymers having a narrow distribution of molecular weights.

To test the theory as expressed in eq 20 we first compared it with the results of Behzadi, et al.[3] (see their Figure 7). To do this, theoretical curves for "k_M" were calculated. It was assumed that in experiments values of A/A_0 near 0.5 were most likely and preferable. Therefore a computer program was written,[21] which for each value of (M) from 10^{-3} to 3 used eq 20 to determine a value of (M)/ (S^-) which would give $(A/A_0)_{theor} = 0.5$. The program then used this (M)/(S$^-$) ratio for each (M) and also the $(A/A_0)_{theor} = 0.5$ in eq 6 to calculate "k_M" as a function of (M). In this computation the following values were used: $a = 0.24$, $b = 2.1$ and $(k_M/k_S) = (2.1 \times 10^9)/(9.3 \times 10^9) = 0.226$.[22] Finally, the experimental points from Figure 7 of ref 3 were measured on a blown-up image and then all were multiplied by 3.5, the ratio of k_M measured by us to the k_M of ref 3. Increasing a moves the curves toward lower values of (M), while increasing b raises proportionally the limiting value of "k_M" in dilute solution. The above cited values of $a = 0.24$ and $b = 2.1$ in eq 20 gave the best fit to the data of ref 3, and that fit is shown in Figure 1.

We had previously found $a = 0.2$ and $b = 2.9$ gave the best fit to our own results using eq 18. For use in eq 20 a and b were chosen so that for $x = 460$ the theoretical results for eq 20 were identical with those obtained from eq 18 using $a = 0.2$ and $b = 2.9$. That is, in eq 20 $a = 0.2(460)^{0.1} = 0.369$ and $b = 2.9(460)^{-0.1} = 1.57$ were used.

Our experimental results using ferrocyanide to compete for OH are presented in Table I[23] and Figure 2 and there compared with theoretical results calculated from eq 18 and 20. Similarly, our experimental results using iodide as the competitor are compared with the theoretical results in Figure 3.[23] The fit is quite reasonable.

It was found in using the theory that increasing (S$^-$) for a given (M) increased the "k_M" calculated. Examining experiments on $x = 460$ in Table I it seems that experimentally this trend is found for (M) = 10^{-2}, 4×10^{-2}, 0.1, and 0.3. At (M) = 3×10^{-2} the apparent experimental
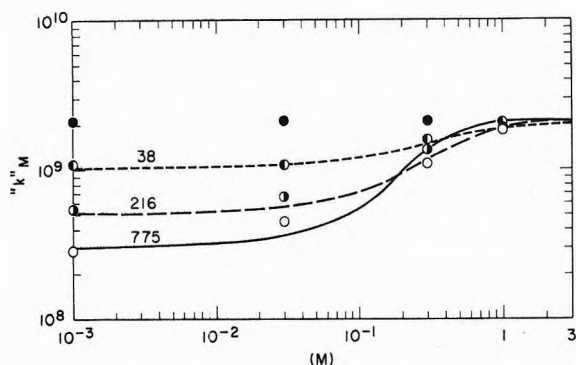
Figure 1. Points from Figure 7 of ref 3. Theoretical curves calculated from eq 20 and 6 (see text): ●, $x = 3$; ◐ and - - -, $x = 38$; ◑ and - - -, $x = 216$; O and —, $x = 775$.
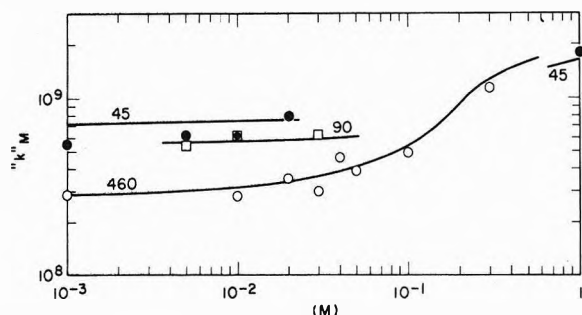

Figure 2. Comparison of "k_M" from eq 20 with "k_M" from experiment for competition experiments of ferrocyanide with polyethylene oxide. Curves are based on eq 20, using the values of "k_M" in column 10 for Table I.[23] For $x = 460$ where more than one value of (S) was used for a given value of (M), the curve was based on "k_M" theoretical corresponding to the experimental A/A_0 nearest to 0.5: ●, "k_M" experimental for $x = 45$; □, "k_M" experimental for $x = 90$; O, "k_M" experimental for $x = 460$. One point for $x = 45$ at 1 M (M) is from competition with iodide.
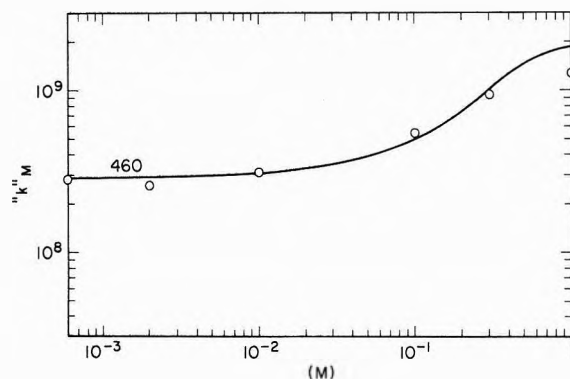

Figure 3. Comparison of "k_M" from eq 20 with experimental "k_M" for competition experiments of iodide with polyethylene oxide. Curve is based on eq 20, using the values of "k_M" in column 10 of Table II:[23] experimental "k_M": O, $x = 460$.

trend is opposite. Although a better correlation could be wished, on the whole within experimental error the observed trend agrees with theory.

We may conclude then that the dependence of k(OH + polyethylene oxide) on polymer or on monomer unit concentration in aqueous solutions is generally in agreement with a theory based on simple assumptions and the use of polymer solution theory and probability theory. In the foregoing we have assumed an ideal solution of polymer in water. In a poor solvent (weak polymer-solvent interaction) $r(x)$ will be smaller than we have estimated, while in

a good solvent (polymer-solvent interaction stronger than polymer-polymer attraction) $r(x)$ will be larger.

Acknowledgment. One of us (M. S. M.) is grateful to The Hebrew University, whose generous invitation to serve as a visiting Professor enabled his participation in this work. Two of us (M. S. M. and J. S.) are also grateful for partial support by the U. S. Atomic Energy Commission during this research. The authors gratefully acknowledge the expert operation and maintenance of the pulse radiolysis equipment by Mr. Yechiel Ogdan.

Supplementary Material Available. A more complete version of Table I including some data on polymers with $x = 8.5, 22, 45, 90$, and 225 plus a similar table for the iodide results of Figure 3 will appear following these pages in the microfilm edition of this volume of the journal. Photocopies of the supplementary material from this paper only or microfiche (105 × 148 mm, 20× reduction, negatives) containing all of the supplementary material for the papers in this issue may be obtained from the Journals Department, American Chemical Society, 1155 16th St., N.W., Washington, D. C. 20036. Remit check or money order for $3.00 for photocopy or $2.00 for microfiche, referring to code number JPC-73-2420.

References and Notes

(1) Address correspondence to: Chemistry Division, Argonne National Laboratory, Argonne, Ill. 60439.
(2) Present address, Laboratory for Radiation and Polymer Science, University of Maryland, College Park, Md. 20742.
(3) A. Behzadi, U. Borgwardt, A. Henglein, E. Schamberg, and W. Schnabel, *Ber. Bunsenges. Phys. Chem.*, **74**, 649 (1970).
(4) R. L. Willson, C. L. Greenstock, G. E. Adams, R. Wageman, and L. M. Dorfman, *Int. J. Radiat. Phys. Chem.*, **3**, 211 (1971). This reports a careful interlaboratory effort to establish accurate values for OH rate constants.
(5) M. S. Matheson and L. M. Dorfman, *J. Chem. Phys.* **32**, 1870 (1960).
(6) L. M. Dorfman, I. A. Taub, and R. E. Bühler, *J. Chem. Phys.*, **36**, 3051 (1962).
(7) S. Gordon, E. J. Hart, M. S. Matheson, J. Rabani, and J. K. Thomas, *Discuss. Faraday Soc.*, **36**, 193 (1963).
(8) E. J. Hart, S. Gordon, and J. K. Thomas, *J. Phys. Chem.*, **68**, 1271 (1964).
(9) D. Zehavi and J. Rabani, *J. Phys. Chem.*, **75**, 1738 (1971).
(10) J. Rabani and M. S. Matheson, *J. Phys. Chem.*, **70**, 761 (1966).
(11) For these latter samples experiments were carried out using the linear accelerator at the Armed Forces Radiobiology Institute, Bethesda, Md. We wish to thank Dr. M. Meaburn for his help in carrying out these experiments.
(12) P. J. Flory, "Statistical Mechanics of Chain Molecules," Interscience, New York, N. Y., 1969, pp 17, 170.
(13) H. A. Schwartz, *J. Phys. Chem.*, **73**, 1928 (1969).
(14) A. Kuppermann in "Radiation Research, 1966," G. Silini, Ed., North Holland Publishing Co., Amsterdam, 1967, p 212.
(15) W. Feller, "An Introduction to Probability Theory and Its Applications," Vol. I, 3rd ed, Wiley, New York, N. Y., 1968, pp 101–105 and 224.
(16) P. J. Flory, "Principles of Polymer Chemistry," Cornell University Press, Ithaca, New York, N. Y., 1953, p 600.
(17) F. E. Bailey, Jr., and R. W. Callard, *J. Appl. Polym. Sci.*, **1**, 56 (1959).
(18) J. E. Mark and P. J. Flory, *J. Amer. Chem. Soc.*, **87**, 1415 (1965).
(19) R. Grishman, *J. Chem. Phys.*, **58**, 220 (1973).
(20) Reference 12, p 35. Flory points out that the expansion of linear macromolecules owing to long-range interactions will be suppressed at higher concentrations where the random coils overlap copiously. This effect should tend to reduce the amount of crossover.
(21) The authors are grateful to C. D. Jonah for the calculations for Figure 1.
(22) In eq 20 only relative values of rate constants are involved. This is also true in eq 6; however, the absolute value of "k_M" obtained depends upon the value used for k_S. Recently, one of us reported k(OH + ferrocyanide) = 1.25×10^{10} M^{-1} sec^{-1} (D. Zehavi and J. Rabani, *J. Phys. Chem.* **76**, 3703 (1972)). Nevertheless, in this paper we use the value of Willson, *et al.*,[4] of k(OH + ferrocyanide) = 0.93×10^{10} M^{-1} sec^{-1}, because it gives "k_M" values more consistent with the iodide results, the latter of course being determined by the k(OH + I$^-$) rate constants that are used.
(23) See paragraph at end of paper regarding supplementary material.

Hydroxyl Radical Reaction with Phosphate Esters and the Mechanism of Phosphate Cleavage[1]

A. Samuni and P. Neta*

Radiation Research Laboratories and Center for Special Studies, Mellon Institute of Science, Carnegie-Mellon University, Pittsburgh, Pennsylvania 15213 (Received May 24, 1973)

The reaction of hydroxyl radicals with several phosphate esters in irradiated aqueous solutions has been followed by esr observation of the radicals and by determination of the yield of inorganic phosphate. The initial step of hydrogen abstraction takes place at all available C–H positions and, as expected, the site of reaction was found to be affected by the state of protonation of an amino group. In most cases the radicals produced by abstraction were observed by esr and in certain cases the radicals subsequently produced by elimination of H_2O or H_3PO_4 were also observed. The results for phospho glycols indicate that α-phospho radicals are the most stable toward phosphate elimination but that β-phospho radicals undergo elimination of H_3PO_4 very rapidly. Elimination of H_2O from these and other radicals appears to be slower than that of H_3PO_4. The results for ethanolamine and serine phosphates indicate that the elimination of H_3PO_4 from the radicals is slower than in the case of glycol phosphates and probably does not take place at all when the amino group is protonated.

Introduction

The mechanism of radiolytic phosphate ester cleavage has been the subject of numerous investigations because this process is believed to play a key role in the radiation induced damage to DNA. Potentially, phosphate esters can react with all the primary radicals of water radiolysis, e_{aq}^-, H, and OH, and partially release phosphate ions. The reaction of e_{aq}^- causing phosphate release by dissociative attachment

$$ROPO_3H_2 + e_{aq}^- \longrightarrow \dot{R} + H_2PO_4^- \qquad (1)$$

has been suggested by esr observations[2,3] on γ-irradiated alkyl phosphates at 77°K and by product analysis of irradiated aqueous solutions of trimethyl phosphate.[4] However, this reaction will be unimportant when biological systems are considered, because its rate constant is very low[4] and the electrons will be preferentially scavenged by the DNA bases which are $\sim 10^5$ times more reactive.
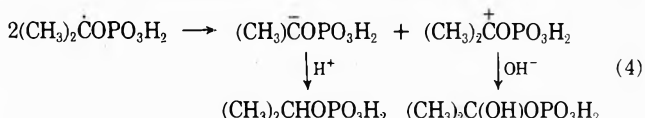
The reaction of H atoms with phosphate esters, although it can lead indirectly to partial cleavage, cannot have a major contribution because of the lower yield of H. The mechanism, however, is expected to be similar to that with OH radicals since in both cases the initial reaction is hydrogen abstraction. In fact, all the radicals that can abstract hydrogen from deoxyribose can induce single strand breaks by phosphate cleavage, as was shown for the uracilyl radical.[5]

The reaction of OH with aliphatic phosphate esters is expected to take place with a rate constant somewhat similar to that of the corresponding alcohol as was found, for example, for di- and trimethyl phosphate.[4] The initial step of reaction is also similar, i.e., abstraction of a hydrogen atom

$$RCH_2OPO_3H_2 + OH \longrightarrow \dot{R}CHOPO_3H_2 + H_2O \qquad (2)$$
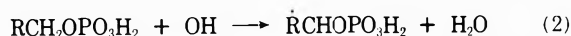
The mechanism of the subsequent release of inorganic phosphate is still controversial.[4,6–8] In previous studies a general mechanism for the phosphate release has been sought without reference to the nature of the alkyl group.

It seems, however, that such a generalized approach is not valid and may well have caused some of the controversies in the literature. Based on the results with alcohols it can be assumed that primary radicals will tend to dimerize whereas secondary or tertiary radicals will tend to disproportionate, e.g.

$$2\dot{C}H_2OPO_3H_2 \longrightarrow H_2PO_3OCH_2CH_2OPO_3H_2 \qquad (3)$$

$$2(CH_3)_2\dot{C}OPO_3H_2 \longrightarrow (CH_3)\bar{C}OPO_3H_2 + (CH_3)_2\overset{+}{C}OPO_3H_2$$
$$\qquad \qquad \downarrow H^+ \qquad \qquad \downarrow OH^- \qquad (4)$$
$$(CH_3)_2CHOPO_3H_2 \quad (CH_3)_2C(OH)OPO_3H_2$$

The resulting dimers can be stable whereas the species formed by oxidation can be expected to hydrolyze rapidly, either directly or after neutralization.

$$(CH_3)_2C(OH)OPO_3H_2 \longrightarrow (CH_3)_2CO + H_3PO_4 \qquad (5)$$
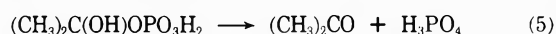
This mechanism is in line with the findings that radiosensitizers increase the yield of inorganic phosphate, most probably by oxidizing the radicals.[7]

$$R_2\dot{C}OPO_3H_2 + S \longrightarrow R_2\overset{+}{C}OPO_3H_2 + S^- \qquad (6)$$
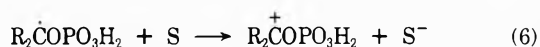
In competition with the radical reactions 3 and 4 direct hydrolysis of the radical can take place, probably catalyzed by base as suggested recently.[4]

$$R_2\dot{C}OPO_3H_2 + OH^- \longrightarrow R_2\dot{C}OH + H_2PO_4^- \qquad (7)$$
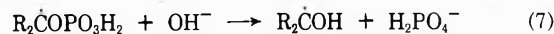
The contribution of this reaction depends on pH and dose rate indicating that it is not very rapid.

When considering phosphate cleavage in the biologically important ribose phosphate or glycerol phosphate, however, one should bear in mind that the behavior of the glycols can be quite different from that of alcohols and so can be the mechanism of phosphate release from their esters. It is known that hydrogen abstraction from glycols can be rapidly followed by elimination of water[9–11]

$$HOCH_2\dot{C}HOH \longrightarrow \dot{C}H_2CHO + H_2O \qquad (8)$$

and it is reasonable to assume that a similar elimination

of phosphoric acid can also be rapid in certain radicals derived from glycol phosphates.

It is the purpose of the present study to test this assumption and to evaluate its importance with the various radicals from glycerol phosphates. Some aspects of the mechanism of phosphate cleavage have been studied both by analysis of phosphate production and by esr observation of the radicals produced in irradiated aqueous solutions.

Experimental Section

Most of the organic compounds used were obtained from Sigma Chemical Co. and were used without further purification. Monomethyl phosphate was obtained from K and K and triethyl phosphate from Aldrich. Glycerol and all the inorganic compounds were Baker Analyzed reagents. Solutions in triply distilled water were bubbled with the desired gas, irradiated in a Gammacell 220 source (5×10^{19} eV g^{-1} hr^{-1}), and analyzed for inorganic phosphate by the Molybdenum Blue method.[12] The *in situ* radiolysis esr experiments have been carried out as described by Eiben and Fessenden.[13]

In order to follow the reaction of OH radicals the solutions were saturated (2×10^{-2} M) with N_2O to convert the radiolytically produced e_{aq}^- into OH. In strongly acid solutions the reaction of H$^+$ with e_{aq}^- to produce H atoms becomes more important and one observes then the reaction of both OH and H. At pH >3 the contribution of H to the total radical reactions is only ~10%. Because most of the reactions observed involve hydrogen abstraction the organic radicals formed by either OH or H are expected to be the same.
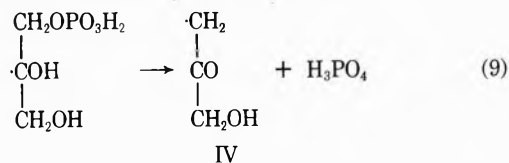
Results and Discussion

Radicals produced by the reaction of OH with phosphate esters have been studied in N_2O saturated aqueous solutions by the *in situ* radiolysis–esr technique. In order to facilitate the interpretation of the spectra some of the related alcohols have also been studied under similar conditions. The results of glycerol and its phosphates are summarized in Table I.

The spectrum recorded with irradiated solutions of glycerol at pH 4.6 consisted of lines of two radicals only. Radical I showed two proton splittings of 17.43 and 11.07 G which suggest that hydrogen abstraction took place at position 1 as shown in the table. The larger hyperfine constant is assigned to the α proton and the smaller to the β proton by comparison with previous findings with other glycols.[10] Splittings by the two equivalent γ protons and one hydroxyl proton were also observed. Radical II showed a 10.40-G splitting by four equivalent protons and must, therefore, be that produced by abstraction of the central hydrogen atom. Splittings by the central hydroxyl proton and by the two equivalent terminal OH protons were also observed and support the assignment in Table I. A previous study[14] of these radicals resulted in a misinterpretation owing to poor resolution.

Radicals I and II are expected to undergo elimination of water (reaction 8) as was previously found with acid solutions of glycerol[9] and similarly with other glycols.[10] Radicals III and IV are expected to be produced from I and II, respectively. The spectrum recorded with irradiated solutions of glycerol at pH 12.5 consisted of lines which are interpreted as those of radicals III and IV while no trace of I and II was found. The interpretation shown in Table I is based on the previous assignment.[9] The present esr pa-

rameters are in good agreement with the reported values[9] within the accuracy of those values. The assignment is also supported by the higher g factors which are characteristic of β-keto radicals. In the case of radical IV the central group of lines of the 19.73-G triplet was not observed, most probably as a result of line broadening caused by slow rotation around the $H_2\dot{C}$–CO bond. Some broadening has also been observed with $\dot{C}H_2COCH_3$.[10]
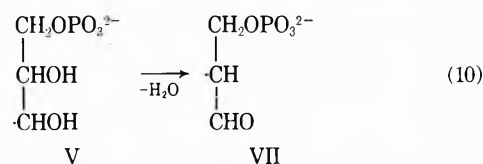
The esr spectra recorded with irradiated solutions of glycerol 1-phosphate at various pH values between 1 and 13 showed the presence of four different radicals under various conditions. The spectrum of radical IV was observed in all cases. This radical, the only one observed which does not contain the phosphate group, must be produced by elimination of H_3PO_4 from the radical resulting from abstraction of the central hydrogen

$$
\begin{array}{ccccc}
CH_2OPO_3H_2 & & \cdot CH_2 & & \\
| & & | & & \\
\cdot COH & \longrightarrow & CO & + H_3PO_4 & \quad (9) \\
| & & | & & \\
CH_2OH & & CH_2OH & & \\
& & IV & &
\end{array}
$$

The fact that radical IV has been observed at all pH values indicates that this type of elimination is very rapid. It should be also pointed out that the alternative elimination, *i.e.*, loss of water to produce $\cdot CH_2COCH_2OPO_3H_2$ was not observed and is probably a slower process.

The other two radicals that can be produced by abstraction from position 1 or 3 have been observed before undergoing elimination. At pH 5.4 a radical was observed which showed esr parameters very similar, but not identical with those of radical I, and was, therefore, assigned as radical V (Table I). The third possible radical (VI) was only observed in mildly alkaline solutions. The assignment is quite straightforward by comparison to radical V with all the proton hyperfine constants very similar and the α hydroxyl proton splitting of 1.25 G replaced by a 5.55-G ^{31}P splitting. The magnitude of this phosphorus hyperfine constant is supported by the parameters for $\dot{C}H_2OPO_3^{2-}$ (see below).
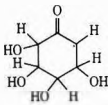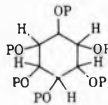
At pH 8.5–11 radical V was not observed and it was replaced by radical VII, the product of water elimination

$$
\begin{array}{ccccc}
CH_2OPO_3^{2-} & & CH_2OPO_3^{2-} & & \\
| & & | & & \\
CHOH & \xrightarrow[-H_2O]{} & \cdot CH & & \quad (10) \\
| & & | & & \\
\cdot CHOH & & CHO & & \\
V & & VII & &
\end{array}
$$

The assignment of radical VII is easily made by comparing its esr parameters with those of radical III. The g factors are identical, all the proton splittings are very similar, and the OH proton which was not observed (*i.e.*, $a^H < 0.1$ G) in radical III is replaced in radical VII by $a^P = 0.52$ G.
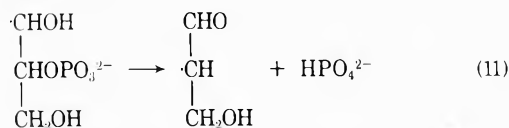
In summary of the results with glycerol 1-phosphate it is seen that the β-phospho radical undergoes rapid elimination of phosphate (compared with the time scale of the esr observation, *i.e.*, 100 μsec) even in neutral solution and was not observed. Radical IV produced from it was observed at all pH values. The γ-phospho radical V was observed at pH 5.4 and found to undergo water elimination in base to produce VII. And finally, the α-phospho radical VI which was observed at pH 8.5–11 does not undergo elimination of phosphate in the time scale of the esr measurements.

TABLE I: Esr Parameters and Suggested Structures of Radicals Produced by Reaction of OH with Phosphate Esters and Some Corresponding Alcohols

Solute	Radical	Structure	g factor[a]	Hyperfine constants[b]
Glycerol pH 4.6	I	CHOH | CHOH | CH$_2$OH	2.00301	a^H_α = 17.43, a^H_β = 11.07, a^H_γ = 0.34 (2), $a^H_{OH(\alpha)}$ = 0.81
	II	CH$_2$OH | COH | CH$_2$OH	2.00279	a^H_β = 10.40 (4), $a^H_{OH(\alpha)}$ = 0.44, $a^H_{OH(\beta)}$ = 0.19 (2)
pH 12.5	III	CHO | CH | CH$_2$OH	2.00414	a^H_α = 18.18, $a^H_{CH_2}$ = 25.98 (2), a^H_{CHO} = 1.50
	IV	CH$_2$ | CO | CH$_2$OH	2.00406	a^H_α = 19.73 (2)[c], a^H_γ = 2.33 (2)
Glycerol 1-phosphate pH 5.4	V	CH$_2$OPO$_3$H$^-$ | CHOH | CHOH	2.00303	a^H_α = 17.42, a^H_β = 11.66, a^H_γ = 0.24 (2), $a^H_{OH(\alpha)}$ = 1.25, $a^H_{OH(\beta)}$ = 0.49
pH 8.5–11	VI	CHOPO$_3^{2-}$ | CHOH | CH$_2$OH	2.00293	a^H_α = 18.25, a^H_β = 11.33, a^H_γ = 0.30 (2), $a^H_{OH(\beta)}$ = 0.60, a^P = 5.55
	VII	CH$_2$OPO$_3^{2-}$ | CH | CHO	2.00414	a^H_α = 18.34, $a^H_{CH_2}$ = 27.17 (2), a^H_{CHO} = 1.58, a^P = 0.52
pH 1–13	IV	d		
Glycerol 2-phosphate pH 11	III	d		
3-Phosphoglyceric acid pH 6–13	VIII	CHOPO$_3^{2-}$ | CHOH | CO$_2^-$	2.00301	a^H_α = 18.20, a^H_β = 11.32, $a^H_{OH(\beta)}$ = 0.32, a^P = 4.37
	IX	CH$_2$ | CO | CO$_2^-$	2.00435	a^H_α = 18.86 (2)[c]
Inositol (hexahydroxycyclohexane) pH 11.4	X		2.00428	a^H_α = 17.59, a^H_β = 37.21, a^H = 2.90[e], a^H = 0.73[f], a^H = 0.16[f]
Phytic acid (inositol hexaphosphate) pH 10	XI[h]		2.00322	$a^H_{\beta 1}$ = 14.35, $a^H_{\beta 2}$ = 11.41, a^P_α = 2.29, a^H_γ or a^P_β = {1.78[g], 0.88[g], 0.88[g]}
Ethanolamine phosphate pH 7.6	XII	CHOPO$_3^{2-}$ | CH$_2$NH$_3^+$	2.00306	a^H_α = 19.00, a^H_β = 13.11 (2), a^P = 4.90, a^N = 9.51, a^H_{NH3} = 0.30 (3)
Serine phosphate pH 7.3	XIII	CHOPO$_3^{2-}$ | CHNH$_3^+$ | CO$_2^-$	2.00307	a^H_α = 18.29, a^H_β = 13.51, a^P = 4.69, a^N = 7.15, a^H_{NH3} = 0.14 (3)
pH 10.8, 14	XIV	CH$_2$OPO$_3^{2-}$ | CNH$_2$ | CO$_2^-$	2.00326	$a^H_{CH_2}$ = 10.85 (2), a^N = 5.69, $a^{H1}_{NH_2}$ = 2.85, $a^{H2}_{NH_2}$ = 1.87, a^P = 0.97
Methyl phosphate pH 6–13	XV	CH$_2$OPO$_3^{2-}$	2.00311	a^H = 18.62 (2), a^P = 5.70

[a] Measured relative to the peak from the silica cell and accurate to ±0.00005. Second-order corrections have been made [R. W. Fessenden, *J. Chem. Phys.*, **37**, 747 (1962)]. [b] Given in gauss and accurate to ±0.03 G. The number of nuclei displaying the splitting is given in parentheses if different than one. [c] The central line or group of lines of this triplet was not observed because of broadening. [d] See structure and parameters of same radical above. [e] This splitting can be possibly assigned to the γ proton beyond the carbonyl group. [f] This splitting can be assigned either to a γ CH or a β OH proton. [g] Assignment of these three splittings to specific nuclei cannot be made with certainty. [h] In the structure of this radical OP stands for the phosphate group.
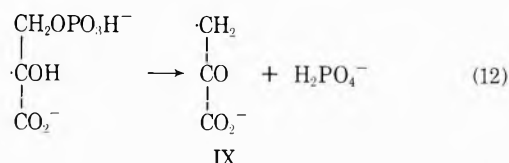
The spectrum recorded with irradiated alkaline solutions of glycerol 2-phosphate showed the presence of radical III. This radical can only be formed by elimination of phosphate from an initial radical produced by abstraction of a terminal hydrogen

$$
\begin{array}{ccc}
\cdot CHOH & CHO & \\
| & | & \\
CHOPO_3^{2-} & \longrightarrow \cdot CH & + HPO_4^{2-} \qquad (11) \\
| & | & \\
CH_2OH & CH_2OH &
\end{array}
$$

This reaction is in line with reaction 9 found in the case of glycerol 1-phosphate. In both cases β-phospho radicals eliminate phosphate rapidly.

The other radical expected to be formed from glycerol 2-phosphate is $HOCH_2\dot{C}(OPO_3^{2-})CH_2OH$, which is not expected to undergo elimination in parallel to the behavior of radical VI. However, this radical was not observed and was probably produced with a low yield.

Solutions of 3-phosphoglyceric acid have also been irradiated and the recorded esr spectra showed the presence of a mixture of radicals. Only two radicals have been successfully characterized and their parameters are given in Table I. The unidentified radicals seem to be produced by secondary reactions. Radical VIII shows coupling constants which parallel those of radical VI, except for the small CH_2 splitting which is absent because this group is replaced by a carboxyl group. By this analogy radical VIII is easily identified as shown in Table I. The second radical observed resembles radical IV produced from glycerol and from glycerol 1-phosphate and, therefore, the structure and the mechanism of its production must also be the same

$$
\begin{array}{ccc}
CH_2OPO_3H^- & \cdot CH_2 & \\
| & | & \\
\cdot COH & \longrightarrow CO & + H_2PO_4^- \qquad (12) \\
| & | & \\
CO_2^- & CO_2^- &
\end{array}
$$

IX

Only the external lines of radical IX have been observed, similar to the case of radical IV, where the central group of lines was not detected because of broadening. The results with 3-phosphoglyceric acid support the findings with the glycerol phosphates, namely, that the β-phospho radicals eliminate phosphoric acid very rapidly whereas the α-phospho radicals do not. To further examine this behavior we chose to study the reaction of OH with phytic acid (inositol hexaphosphate) where only α-phospho radicals can be produced (although they are β-phospho as well).

The results for inositol and phytic acid are also summarized in Table I. Radical X observed with solutions of inositol at pH 11.4 has been previously observed in acid solutions using Fenton's reagent,[9] and the hyperfine constants determined in both cases are in good agreement. In the present work two additional small splittings were observed which can be assigned to a β-OH and a γ-CH protons. The initial radical formed by abstraction from inositol, which has been observed in acid solutions,[9] was not detected at pH 11.4.

Radical XI observed with solutions of phytic acid at pH 10 shows $g = 2.00322$. This value indicates the absence of a β-keto group, i.e., as expected elimination of phosphate did not take place from this α-phospho radical. The β proton hyperfine constants are much smaller than those observed with inositol itself (30.5 G)[9] indicating that the geometrical conformation is quite different. This differ-

ence is also demonstrated by the lack of symmetry in radical XI in contrast to the case of inositol.[9] It should be pointed out that the phosphorus splitting is smaller here than in all the other cases of α-phospho radicals. The three additional small splittings cannot be assigned with certainty to specific protons or phosphorus nuclei. At pH 13.5 the spectrum of radical XI was not observed. Several lines were found which could not be given a clear interpretation.

Ethanolamine and serine phosphates have also been studied by comparison with the glycol phosphates. The esr spectrum recorded with irradiated neutral solutions of ethanolamine phosphate consisted of lines of one radical only. The parameters calculated are given in Table I and their assignment to radical XII is straightforward. The magnitude of the large proton splittings and the nitrogen splitting are somewhat similar to those observed with ethanolamine itself.[10] The magnitude of a_P is similar to that observed for the other α-phospho radicals in Table I. The site of the hydrogen abstraction from ethanolamine phosphate in neutral solution is in line with the expectation that the protonated amino group will strongly deactivate its neighboring hydrogen atoms. It is expected that in alkaline solution, when the amino group is not protonated, abstraction will take place to a large extent α to this group. Unfortunately, however, no esr lines were detected in alkaline solutions, indicating that a different radical with a shorter lifetime is produced.

Similar experiments with serine phosphate support the above argument and show a change with pH in the site of abstraction. In neutral solutions radical XIII was observed and its parameters are somewhat similar to those of XII. The presence of the carboxyl group causes an appreciable decrease in a^N but smaller changes in the other coupling constants. In alkaline solutions a different spectrum was found. The assignment in Table I was easily made on the basis of results with several amino acids.[15,16] The structure of radical XIV shows, indeed, that abstraction takes place from position α to the free amino group as was also found with the amino acids.[15,16]

The magnitude of the phosphorus splitting in most of the α-phospho alkyl radicals in Table I is in the range of 4.4–5.5 G. These values are much lower than those observed previously with dialkyl and trialkyl phosphates.[17,18] Because it was previously found that a_P for $R\dot{C}HO-P(O)(OH)OCH_2R$ is smaller than that for $R\dot{C}HO-P(O)(OCH_2R)_2$ (e.g., 10.5 and 7.8 G for the radicals from tri- and dimethyl phosphate, respectively)[17] it is reasonable to assume that a^P for monoalkyl phosphate will be even lower. To substantiate this assumption we studied monomethyl phosphate. The results for radical XV in Table I show that the phosphorus splitting is lower for this radical and should be similarly low for radicals from other monoalkyl phosphates.

According to one suggested mechanism[4] for phosphate cleavage the phosphomethyl radical XV can be expected to hydrolyze in base as shown in reaction 7. In an attempt to support this mechanism we searched for the esr lines of the hydroxymethyl radical. However, the fact that they were not observed does not indicate their absence because they are known[13] to be broad in the alkaline region and, therefore, more difficult to detect under our experimental conditions. It should be easier to detect the spectrum of the $CH_3\dot{C}HOH$ or $CH_3\dot{C}HO^-$ radical, which can be produced from triethyl phosphate by abstraction and hydrolysis. We have irradiated alkaline solutions of triethyl

TABLE II: Yield of Inorganic Phosphate in Irradiated Aqueous Solutions of Ethanolamine Phosphate[a]

Additives	G		
	pH 4.0	pH 7.3	pH 12.0
None	0.9 (0.9)[b]	1.4	2.3
$2 \times 10^{-2} M$ N_2O	1.9 (1.6)[b]	2.7	4.2
$1.5 \times 10^{-2} M$ $N_2O + 5 \times 10^{-4} M$ O_2	4.0	4.5	4.4
$2 \times 10^{-2} M$ $N_2O + 2.5 \times 10^{-3} M$ Cu^{2+}	5.1		

[a] Solutions containing $1 \times 10^{-2} M$ ethanolamine phosphate were deoxygenated by bubbling with nitrogen or saturated with the desired gas or gas mixture and were irradiated in a Gammacell 220 (Atomic Energy of Canada Limited) with doses of $10^{18}-10^{19}$ eV g^{-1}. The amount of inorganic phosphate present in solution before irradiation was determined and corrected for with each solution and was always <1% of the phosphate ester. [b] From ref 7.

phosphate at various pH values and could not detect the lines of the α-hydroxyethyl radical. It can be, therefore, concluded that if the hydrolysis shown in reaction 7 contributes to the radiolytic phosphate cleavage it must be taking place on a time scale slower than the millisecond range of the esr observation.

As a supplement to the esr findings we have measured the yield of inorganic phosphate from γ-irradiated solutions of several phosphate esters. The yield from the glycerol phosphates was found to be very close to $G(OH) + G(H)$ at all pH values and over a wide range of concentrations. For example, with $10^{-2} M$ glycerol 2-phosphate solution saturated with N_2O G(inorganic phosphate) was 5.7, 6.2, and 6.7 at pH 2.3, 7.9, and 12.4, respectively. These results are in agreement with the previously reported values for deaerated solutions[6] and both indicate that most of the radicals produced by hydrogen abstraction release inorganic phosphate. Combined with the esr observations these results suggest that the α-phospho radical also releases phosphate, but on a time scale longer than that of the esr experiments.

In contrast to the full yield found for the glycerol phosphates the yield from methyl and ethyl phosphate is much lower.[4,7] We have also examined ethanolamine phosphate and the results are shown in Table II. Two of the values in this table have been reported previously[7] and both results are in agreement. It is evident from Table II that despite the similarity between ethanolamine and glycol the mechanism of phosphate release is quite different, at least when the amino group is protonated. In the latter case, i.e., at neutral or acid pH much of the abstraction takes place α to the phosphate as shown by the esr results. The resulting radicals do not eliminate phosphoric acid but instead they probably disproportionate to a certain extent to produce inorganic phosphate with a yield of $\sim\frac{1}{2}G(OH)$. When oxygen or copper ions are added to the solution the yield of phosphate is increased by about a factor of 2 as the result of oxidation of the organic radicals as discussed above. In alkaline solutions the majority of the OH radicals react at position α to the free amino group and the resulting radical appears to behave similarly with the glycols and to eliminate phosphoric acid rapidly. Therefore, the yield is found to be higher at pH 12 than at pH 4 and 7 and oxygen is found to affect the former yield. The value of $G = 4.2$ at pH 12 indicates, though, that the elimination process is not as efficient with ethanolamine phosphate as with the glycerol phosphates.

Summary and Conclusions

The esr spectra obtained with irradiated aqueous solutions of glycerol phosphates and related compounds showed the presence of two kinds of radicals: those pro-

duced directly by the initial abstraction reaction showing g factors ~ 2.003 and those produced subsequently by elimination of H_2O or H_3PO_4 showing g factors ~ 2.004. The initial radicals undergo phosphate elimination at different rates. The α-phospho radicals are stable in the millisecond time scale of the esr observation but they undergo elimination of phosphate at longer times as shown by the final yield of phosphate. The β-phospho radical can potentially undergo elimination of either H_2O or H_3PO_4, but the latter was found to eliminate rapidly even in neutral solutions so that the initial radicals were not observed in esr experiments. The γ-phospho radicals can eliminate H_2O only and because these radicals were observed in neutral solutions and their elimination products in alkaline solutions this process is not as rapid as the elimination of H_3PO_4.

Ethanolamine and serine phosphates react with OH radicals in neutral solutions to undergo H abstraction mainly at the position α to the phosphate because the other position is deactivated by the neighboring protonated amino group. The resulting α-phospho radicals have been observed by esr and are somewhat stable. The final yield of phosphate shows that these radicals do not lose their phosphate quantitatively by elimination but probably disproportionate and cleave half of their phosphate. In alkaline solutions the free amino group directs most of the abstraction to its α position and the β-phospho radicals produced undergo elimination of phosphate, although not as rapid as in the corresponding case with glycols.

References and Notes

(1) Supported in part by the U. S. Atomic Energy Commission.
(2) C. M. L. Kerr, K. Webster, and F. Williams. *J. Phys. Chem.*, **76**, 2848 (1972).
(3) A. Begum, S. Subramanian, and M. C. R. Symons, *J. Chem. Soc. A*, 1334 (1970).
(4) C. V. Sonntag, G. Ansorge, A. Sugimori, T. Omori, G. Koltzenburg, and D. Schulte-Frohlinde, *Z. Naturforsch. B*, **27**, 471 (1972).
(5) J. D. Zimbrick, J. F. Ward, and L. S. Myers, Jr., *Int. J. Radiat. Biol.*, **16**, 525 (1969).
(6) G. Scholes, W. Taylor, and J. Weiss, *J. Chem. Soc.*, 235 (1957).
(7) J. A. Raleigh, C. L. Greenstock, and W. Kremers, *Int. J. Radiat. Biol.*, in press.
(8) See also references cited in ref 4 and 6.
(9) R. E. Florin, F. Sicilio, and L. A. Wall, *J. Res. Nat. Bur. Stand., Sect. B*, **72**, 49 (1968).
(10) B. C. Gilbert, J. P. Larkin, and R. O. C. Norman, *J. Chem. Soc., Perkin Trans. 2*, 794 (1972).
(11) K. M. Bansal, M. Gratzel, A. Henglein, and E. Janata, *J. Phys. Chem.*, **77**, 16 (1973).
(12) D. F. Boltz, Ed., "Colorimetric Determination of Nonmetals," Interscience, New York, N. Y., 1958, p 32.
(13) K. Eiben and R. W. Fessenden, *J. Phys. Chem.*, **75**, 1186 (1971).
(14) P. J. Baugh, O. Hinojosa, and J. C. Arthur, Jr., *J. Phys. Chem.*, **71**, 1135 (1967).
(15) H. Paul and H. Fischer, *Ber. Bunsenges. Phys. Chem.*, **73**, 972 (1969).
(16) P. Neta and R. W. Fessenden, *J. Phys. Chem.*, **75**, 738 (1971).
(17) E. A. C. Lucken, *J. Chem. Soc. A*, 1354 (1966).
(18) A. R. Metcalfe and W. A. Waters, *J. Chem. Soc. B*, 340 (1967).

Electrical Conductivity of Nickel Oxide–Magnesium Oxide Single Crystals

Jae Shi Choi,* Hoo Young Lee, and Keu Hong Kim

Department of Chemistry, Yonsei University, Seoul, Korea   (Received March 2, 1973)

Publication costs assisted by Yonsei University

The electrical conductivities of MgO single crystals doped with 0.375, 0.75, 1, and 5% NiO were measured from 900 to 1200° under oxygen partial pressures, P_{O_2}, of 10^{-1} to 10^{-7} atm. As P_{O_2} is increased from 10^{-7} atm, conductivities increase up to a maximum occurring in the region between 10^{-4} and 10^{-3} atm and then decrease as P_{O_2} is further increased higher than 10^{-3} atm. The point of maximum conductivity can be explained as the point at which there is a change in the current carrier type. It is suggested that the current carriers are O^{2-} at P_{O_2} greater than that corresponding to maximum conductivity and Mg^{2+} at lower P_{O_2}'s.

Introduction

The conduction mechanism in doped metal oxides is complex, involving both ionic and electronic flow, and dependent on surface pressure. In general metal oxides fall into two groups on the basis of oxide density in relation to the density of the metal. For those with oxide density greater than that of the metal, the distance between metal ions in the oxide is less than that in the metal, and such oxides are truly ionic oxides—alkali metal oxides, aluminum oxide, and the alkaline earth metal oxides (magnesium oxide is a member of this group). Included in the other group, in which the oxide density is less than that of the metal, are the transition metal oxides such as NiO, FeO, CoO, and MnO, in which electronic conductivity predominates.

In this research a mixture of the two types was used, MgO single crystals doped with NiO. As indicated above, MgO is an ionic semiconductor and NiO is known as an electronic p-type semiconductor at high temperatures. The system of NiO–MgO single crystals as a solid solution has the following characteristics. (1) Both components are cubic oxides. (2) Complete solid solubility exists in this system. (3) Replacement of Mg^{2+} by Ni^{2+} in the oxide lattice does not introduce a strain in the lattice since the cation radii are similar ($\gamma Ni^{2+} = 0.670$ Å, $\gamma Mg^{2+} = 0.650$ Å). (4) Both oxides possess relatively good stability against decomposition in the temperature range 900–1500°.

The most fundamental thing to find out about the conductivity of ionic compounds is whether the charge carriers are electrons or ions. In the case of magnesium oxide this point has not been settled. In fact, there are apparently conflicting observations and analyses of the type of charge carriers important at various temperatures and oxygen pressures. Most analyses[1-8] of the mechanism of conductivity have been made on the assumption that the charge carriers were electrons. Mittoff obtained experimental results indicating electronic conduction and analyzed the results of conductivity measurements made over a range of oxygen partial pressures on crystals of varying purity.[9] His major conclusions were that (1) impurities of variable valence dominated the conductivity and were responsible for changes in conductivity with changing gas pressures surrounding the crystals; (2) conductivity is electronic; and (3) the nature of the charge carriers in pure samples and in any samples at higher temperatures is not known.

On the other hand, Schmalzried[10] and Sambongi and Omori[11] reported ionic conduction from electrochemical solid cell measurements. By maintaining a different oxygen partial pressure on each side of the crystal. Mittoff[12-14] determined the ionic transference number and obtained results indicating that conduction is ionic at temperatures lower than 1300° and electronic above 1300°.

However, the ionic conduction mechanism proposed by Davies[15] is the most progressive theory reported recently. According to him the conduction carriers in MgO are O^{2-} and Mg^{2+} and their mobilities are dependent upon the oxygen partial pressures surrounding the crystal. Davies, however, used a poly-crystal of MgO as a sample, so there might be error due to grain boundaries in the sample, and there were no quantitative data on the dependence of conductivity on oxygen pressure.

The samples used in this investigation were MgO–NiO single crystals and the electrical conductivities were measured at different oxygen partial pressures; for in order to determine the conduction mechanism of semiconductor metal oxides, it is helpful to consider the oxygen pressure dependence. This investigation has been carried out to find and explain the dependence of electrical conductivity on oxygen partial pressure and the point at which the current carriers of MgO–NiO single crystals change.

Experimental Section

The samples used in this experiment are MgO single crystals from Saxonberg Co. doped with 0.375, 0.75, 1, and 5, mol % NiO. Samples were cut into rectangular forms with dimensions of $0.592 \times 0.408 \times 0.369$ cm, $0.75 \times 0.404 \times 0.161$ cm, $0.652 \times 0.429 \times 0.201$ cm, and $0.684 \times 0.412 \times 0.198$ cm, respectively. A quartz sample container in a furnace was connected with a vacuum system through a glass joint, and four platinum probes provided contact with the sample. Figure 1 shows a four-probe contact model and the conductivity measurement circuitry. Conductivity may be computed according to Valdes' theory.[16] When all the distances between adjacent probes are equal ($S_1 = S_2 = S_3 = S$) and the value of L/S is greater than 2, conductivity is calculated as

$$\sigma = \frac{1}{2\pi S} \frac{I}{V}$$

Here σ is the conductivity (ohm^{-1} cm^{-1}), I is the current through the sample, and V is the floating potential across the inner probes. B is a dc current source and current
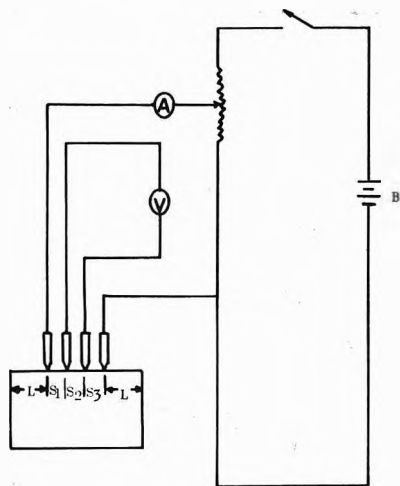
Figure 1. Measurement circuit of conductivity and four-probe model.

through the sample is maintained from 10^{-6} to 10^{-4} A; also the potential across the inner probes is maintained between 0.5 and 1.5 V. The potential difference V was measured by a Leeds and Northrup 7554 Type-K4 potentiometer connected to the inner probes, and the current through the sample was measured by a Keithley Instruments 610B electrometer. In the measurements, it was found to be essential to (1) test ohmic contact, (2) shield the entire circuit and ground the shielding at the electrometer, and (3) keep the entire circuit, including the current supply, well isolated from the ground. Therefore, the quartz sample container was covered by a grounded stainless steel pipe to provide shielding from the electric and magnetic fields from the furnace.

Conductivity has been measured in the region of temperatures from 900 to 1200° and oxygen partial pressures from 10^{-1} to 10^{-7} atm. The various oxygen partial pressures required were established using pure oxygen (research purity) obtained from Matheson gas products or a mixture of 0.001% oxygen in nitrogen from the Matheson Co. The sample container was evacuated to a pressure of 6.72×10^{-6} mm and then the temperature of the sample was increased immediately to 850° at this pressure. Pure oxygen or a mixture of oxygen–nitrogen was then allowed into the sample container and evacuated to the required oxygen partial pressures. The pressure in the evacuated sample container, pure oxygen gas pressure, and the gas pressure of oxygen–nitrogen mixtures were read on an ultrahigh-vacuum ionization gauge, a manometer, and a thermocouple gauge, respectively.

Results

To determine the electrical conductivity dependence on the oxygen partial pressure over NiO–MgO single crystals, doped with 0.375, 0.75, 1, and 5% NiO, conductivities were measured at different oxygen partial pressures in the region of 10^{-1} to 10^{-7} atm at constant temperature for 900, 1000, 1100, and 1200°. The results of the electrical conductivity measurements are shown in Figures 2–5. The conductivity of the NiO–MgO system studied as a function of oxygen pressure at 1200° is presented in Figure 6.

Log σ values of various samples are plotted against log P_{O_2}. Conductivities increased with increasing oxygen pressures for oxygen partial pressures up to a maximum in the pressure region between 10^{-4} and 10^{-3} atm and then
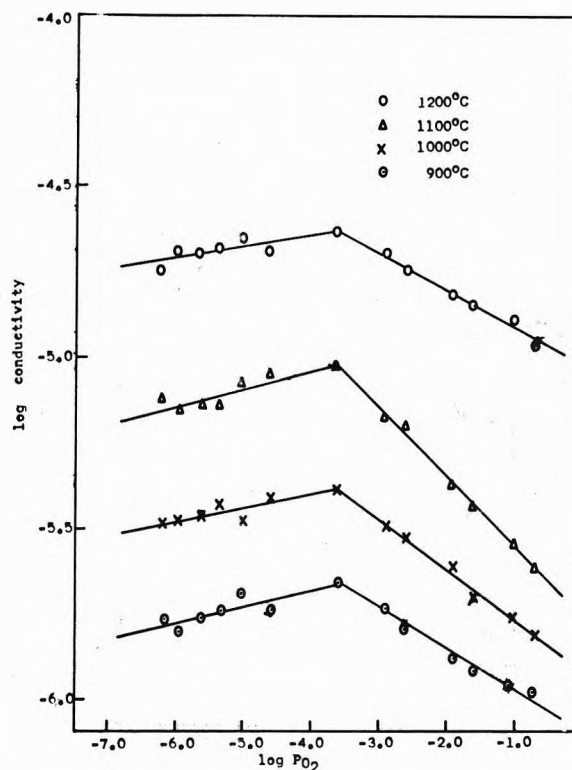

Figure 2. Conductivity of 0.375% NiO–MgO single crystal as a function of oxygen partial pressure at constant temperatures.
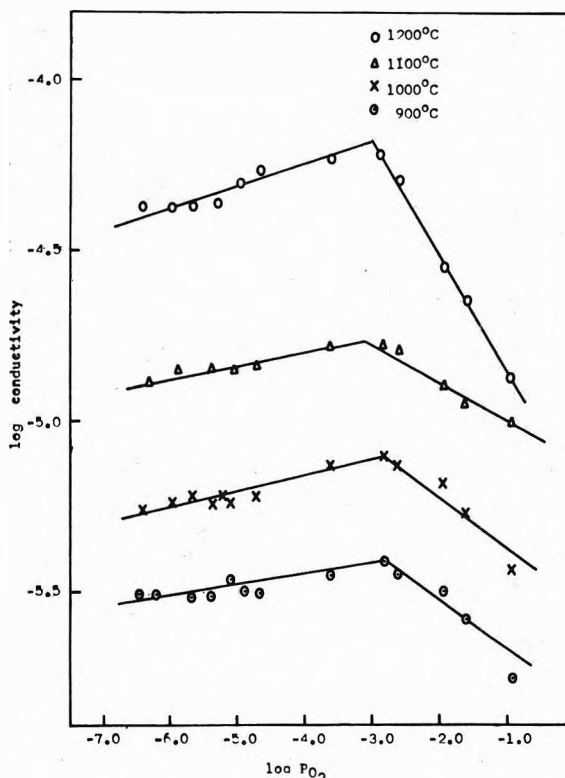

Figure 3. Conductivity of 0.75% NiO–MgO single crystal as a function of oxygen partial pressure at constant temperatures.

decreased as pressure was increased beyond that corresponding to the conductivity maximum. Conductivity dependence upon oxygen partial pressure is similar regardless of temperature or mol % of doped NiO. It presents a
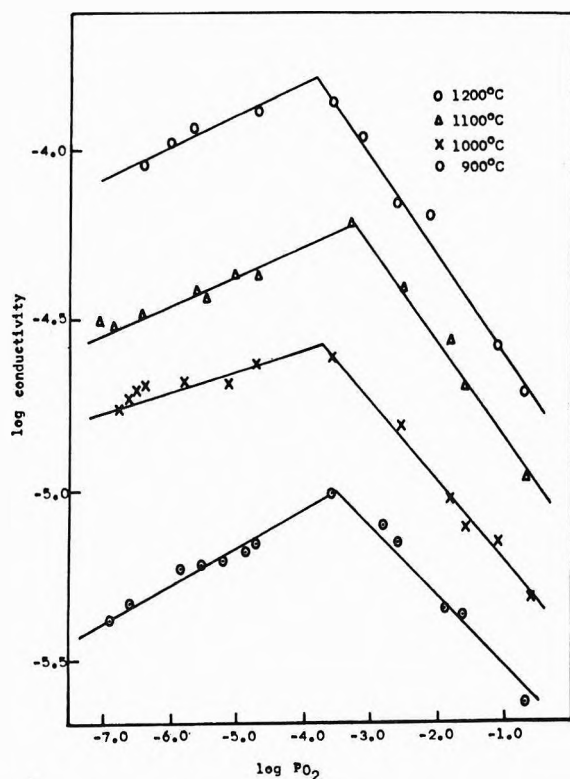
Figure 4. Conductivity of 1% NiO–MgO single crystal as a function of partial pressure at constant temperatures.
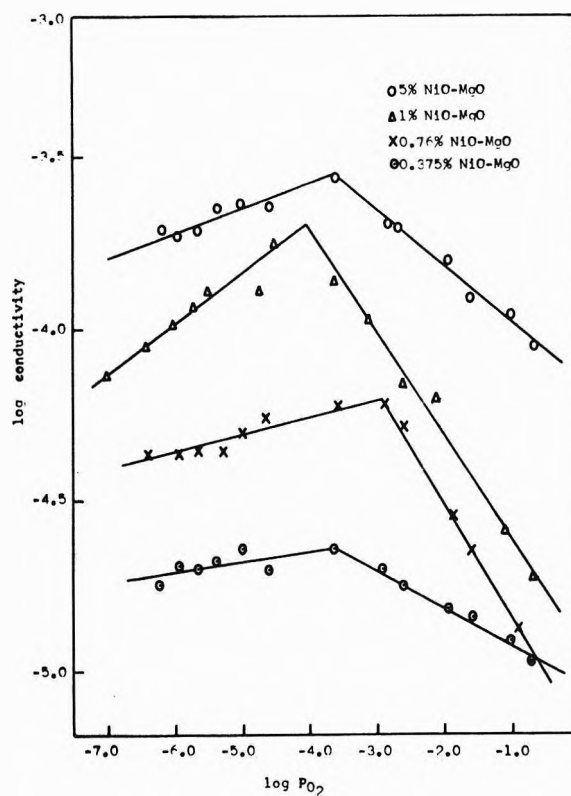

Figure 6. Conductivity of NiO–MgO system as a function of oxygen partial pressure at 1200°.
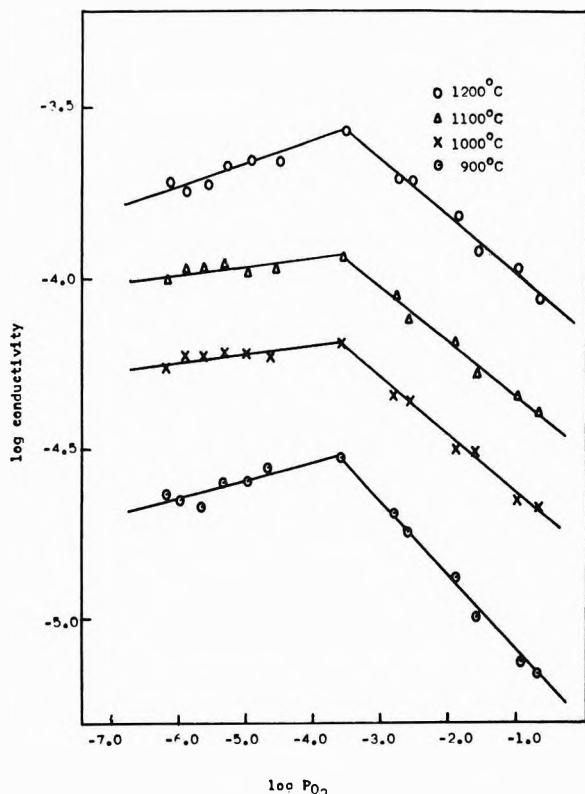

Figure 5. Conductivity of 5% NiO–MgO single crystal as a function of oxygen partial pressure at constant temperatures.

striking contrast to Mittoff's[9] conductivity data for MgO single crystals containing small amounts of FeO impurity. It is a very interesting and remarkable result.

Discussion

The conduction mechanism of ionic compounds may be thought of as (a) the motion of electrons in the conduction band, (b) the motion of electron holes in the valence band, (c) the diffusion of cations, or (d) the diffusion of anions.[17] The first two mechanisms are classified as electronic conductivity and the last two as ionic conductivity. Electrons or electron holes generally diffuse rapidly through the crystal, if present in the conduction and valence bands respectively, and give rise to a high conductivity. Cations and anions will be attracted to the cathode and anode, respectively, upon application of an electric field, but the diffusion of these species is generally slow, since ionic diffusion depends upon the existence of atomic defects in the crystal. If cation interstitials are major defects in a crystal, cation diffusion will be relatively fast, since the interstitial ion is surrounded by empty interstitial sites in which to move. On the other hand, if the major type of defect is the cation or anion vacancy (or both) diffusion will be much slower, since, for example, in order for a cation to move toward the cathode, a cation vacancy must move into a nearest neighbor position. The possible types of conductivity are shown schematically in Figure 7. Therefore, the total conductivity σ_t is $\sigma_t = \sigma_i + \sigma_e$ where σ_i and σ_e are ionic and electronic conductivity, respectively. The transference number t_i for ions will then be

$$t_i = \frac{\sigma_i}{\sigma_t} = \frac{\sigma_i}{\sigma_i + \sigma_e}$$

The t_i is a function of temperature, oxygen pressure, and mole per cent of impurities contained. The transfer of charge through an ionic compound may be reduced to the electrical equivalent circuit represented in Figure 8. In the
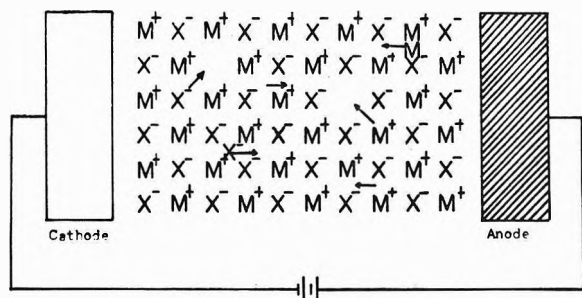
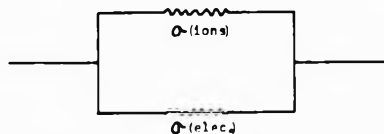**Figure 7.** Illustration of possible mechanism of electrical conductivity.

Figure 8. Conduction mechanism of ionic compounds.

equivalent circuit σ_e represents the conductivity path for electrons and σ_i represents the independent path for ions to transfer charge.

As was mentioned in the Introduction, the ionic character of MgO was investigated by Schmalzried[10] and Sambongi and Omori.[11] They measured the emf developed in an electrochemical solid cell of MgO and obtained a value similar to that for ZrO_2, which is an ionic semiconductor.

Parfitt[18] found that the activation energies for self-diffusion of Mg^{2+} in the intrinsic and extrinsic regions are 3.5 and 0.92 eV, respectively. Oisch and Kingery[19] obtained 2.7 eV for O^{2-} self-diffusion in the extrinsic region. Davies[15] reported that the activation energies for the conduction of MgO are 5.2 eV for the intrinsic region and 2.7 eV for the extrinsic region at higher oxygen partial pressures and 3.5 eV for the intrinsic region and 0.92 eV for the extrinsic region at lower oxygen partial pressures.

Davies suggested that the current carriers in MgO are oxygen ions at higher oxygen partial pressures and magnesium ions at lower oxygen partial pressures. This is because the activation energy obtained from conductivity data at high oxygen pressures is equal to the value for O^{2-} self-diffusion, and at low oxygen partial pressures is equal to the Mg^{2+} self-diffusion measurement. Davies' theory seems to be reasonable. However, his theory has a fault in that it cannot show the conductivity dependence upon oxygen pressure and does not discuss the conversion point of conduction carrier type.

For data of conductivity dependence upon oxygen pressure we may introduce Mittoff's result,[9] where the electrical conductivity of MgO single crystals containing small amounts of Fe in the temperature region of 1300° is observed to depend upon the partial pressure of oxygen surrounding the sample. The conductivity increases at oxygen pressures both higher and lower than 10^{-5} atm. At this pressure the conductivity is a minimum. He explains the dependence of conductivity on oxygen pressure by changes in stoichiometry and thus lattice defects in MgO and mentions an electronic mechanism rather than an ionic one.

This is a very different result from our measurement. In our result for NiO–MgO single crystals, conductivity increases with increasing P_{O_2} up to a maximum in the region between 10^{-4} and 10^{-3} atm and decreases with increasing P_{O_2} in the pressure region higher than that of the maximum. This behavior cannot be explained by an electronic mechanism. Therefore we conclude that the mechanism of conduction in NiO–MgO single crystals must be ionic rather than electronic. According to Davies' report[15] and self-diffusion data for O^{2-} and Mg^{2+}, we suppose that at oxygen pressures higher than that at the conductivity maximum, the conduction is via O^{2-} and at P_{O_2} lower than that at the conductivity maximum, conduction is carried out by the Mg^{2+} ion. For higher oxygen partial pressures, oxygen is adsorbed on the crystal surface

$$\tfrac{1}{2}O_2 + V(-) = V_O(ads)$$
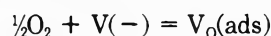
where $V(-)$ is oxygen vacancy and $V_O(ads)$ is adsorbed oxygen atom in a vacancy site (MgO has a structure of oxygen deficiency). The number of anion vacancies would then decrease, and the diffusion of O^{2-} ions through the crystal and the electrical conductivity would also decrease.

In this experiment, we used a four-probe contact method and the conductivity is surface conductivity rather than bulk conductivity. Therefore, the conductivity was very sensitive to oxygen pressure. However, in the region of low oxygen pressure conduction is carried out by Mg^{2+}, and this Mg^{2+} ion diffuses through cation vacancies. Ni has variable valences as Fe does. At low oxygen pressures Ni has a $+2$ rather than a $+3$ oxidation state. Thus, at oxygen pressures lower than about 10^{-3} atm, that corresponding to the conductivity maximum, the cation vacancies decrease with decreasing P_{O_2}

$$2Ni^{3+} + O^{2-} + V(+) = 2Ni^{2+} + \tfrac{1}{2}O_2$$
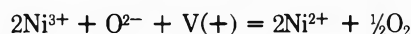
where $V(+)$ is cation vacancy and, as the Mg^{2+} diffuses through cation vacancies, the electrical conductivity increases with increasing P_{O_2}.

References and Notes

(1) A. Lempicki, *Proc. Phys. Soc., London, Sect. B*, **66**, 281 (1953).
(2) E. Yamaka and K. Sawamoto, *Phys. Rev.*, **95**, B48 (1954).
(3) R. Mansfield, *Proc. Phys. Soc., London, Sect. B*, **66**, 614 (1953).
(4) N. A. Surplice, *Brit. J. Appl. Phys.*, **15** (6), 639 (1964).
(5) E. Yamaka and K. Sawamoto, *J. Phys. Soc. Jap.*, **10**, 176 (1956).
(6) H. F. John, *Phys. Rev.*, **91**, 822 (1953).
(7) E. Yamaka and K. Sawamoto, *Phys. Rev.*, **101**, 565 (1956).
(8) T. J. Lewis and A. J. Wright, *Brit. J. Appl. Phys.*, (2) 1 (4), 441 (1968).
(9) S. P. Mittoff, *J. Chem. Phys.*, **31**, 1261 (1959).
(10) H. Schmalzried, *J. Chem. Phys.*, **33**, 940 (1960).
(11) K. Sambongi and Y. Omori, *Tohuko Univ. Sci. Rept.*, **11A**, 244 (1959).
(12) S. P. Mittoff, *J. Chem. Phys.*, **33**, 941 (1960).
(13) S. P. Mittoff, *J. Chem. Phys.*, **36**, 1385 (1962).
(14) S. P. Mittoff, *J. Chem. Phys.*, **41**, 2561 (1964).
(15) M. O. Davies, *J. Chem. Phys.*, **38**, 2047 (1963).
(16) L. B. Valdes, *Proc. IRE*, **42**, 420 (1954).
(17) R. A. Swalin, "Thermodynamics of Solids," Wiley, New York, N. Y., 1961, pp 298–300.
(18) R. Lindner and G. D. Parfitt, *J. Chem. Phys.*, **26**, 182 (1957).
(19) Y. Oisch and W. D. Kingery, *J. Chem. Phys.*, **33**, 905 (1960).

Photoconductivity in an Argon Matrix Containing Sodium and Tetracyanoethylene

Alan Snelson

IIT Research Institute, Chicago, Illinois 60616 (Received April 30, 1973)

A matrix-isolation cryostat was modified to allow photoconductivity measurements to be made. Argon matrices were deposited containing alternate layers of trapped sodium atoms and tetracyanoethylene molecules. These matrices on illumination exhibited photoconductivity. The photoconductivity mechanism is believed to be associated with the formation of donor–acceptor complexes between the trapped sodium and tetracyanoethylene.

Introduction

The matrix isolation technique is now a well-established method for obtaining spectroscopic data for atomic, molecular, and radical species. Recently the method has been extended[1-5] so that the spectra of trapped ionic species may also be obtained. In this latter technique, suitable electron-donating and electron-accepting species are isolated within the same inert gas matrix and electron transfer between the donors and acceptors is promoted by photoexcitation.[1,2] Electron spin resonance techniques have been used to characterize the isolated anionic and cationic species[1-3] and infrared spectra of a variety of matrix-isolated negative ions have been reported.[4,5] The most commonly used electron donors have been alkali metal atoms. A variety of electron-accepting species have been used, NO_2,[5] NO,[5] SO_2,[4] B_2H_6,[3] tetracyanoethylene,[3] and furan.[3]

To date there does not appear to have been any attempt to detect photoconductivity in matrices containing electron-donating and -accepting species and it was the purpose of this study to determine if this phenomenon could be observed. Sodium (IP = 5.18 eV) and tetracyanoethylene (EA = 3.25 eV) were selected as the electron-donating and -accepting species, respectively.

Experimental Section

The basic matrix-isolation cryostat and molecular beam furnace used in this study has been described previously[6] and only those details pertinent to the present experiments will be described. Liquid helium was used as the refrigerant. Matheson Research Grade argon was used as the matrix gas and was deposited at the rate of 1.5×10^{-2} mol/hr^{-1}. The infrared transmitting window on which matrices were normally deposited was replaced by a piece of glass with an electrical conducting surface (a deposit of tin oxide). This conducting surface formed one electrode of the photoconductor and matrices were deposited on this surface. The surface area of the window available for matrix deposition was rectangular, 0.75 in. × 0.5 in. A second rectangular electrode, 0.4 in. × 0.4 in., made of stainless steel 0.010 in. thick could be positioned directly in front of, and parallel to, the matrix on the conducting window after its deposition. This electrode was mounted in an insulated high-vacuum feed-through and its distance from the matrix surface could be varied from 0 to 1.5 in.

Two Knudsen cells were constructed of steel to contain the sodium and TCNE (tetracyanoethylene). Both cells had orifices of 0.025 in. diameter and were mounted on separate arms on a shaft which could be rotated *via* a vac-

uum feedthrough, so that one Knudsen cell at a time could be aligned with the window on which the matrix was deposited. The Knudsen cells were heated electrically and their temperatures measured with chromel–alumel thermocouples. The orifices of both Knudsen cells when aligned with the cooled window were about 2.5 in. from the surface on which the matrices were formed. Sodium was vaporized at about 320° and TCNE at 70°. These temperatures correspond to vaporization rates of 1.9×10^{-4} mol hr^{-1} for sodium[7] and 3.7×10^{-4} mol hr^{-1} for TCNE.[8] From these vaporization rates and the geometry of the system, the matrix dilution factors may be estimated at about 1300:1 for the sodium and 670:1 for the TCNE. Matrices were formed over a period of 10 min with alternate layers of sodium and TCNE being isolated. Each individual layer during the matrix formation was deposited over equal time periods, always starting with sodium and ending with TCNE. In various experiments deposition times for the individual layers of 10, 20, and 30 sec were used.

At the end of the matrix deposition period, the liquid helium cold finger was rotated to a position at which the matrix could be illuminated through the window on which it was deposited. A commercial 150-W tungsten filament light bulb was used for this purpose. The movable electrode was positioned a suitable distance from the matrix surface, separations of 0.25, 0.5, and 0.75 in. being typically used. A variable dc potential of from 0 to 2000 V was applied across the electrodes, and photocurrents were measured on a Keithley 601A electrometer. The latter instrument had a range of 10^{-3}–10^{-11} A.

Results

The first series of experiments performed with the equipment were made to determine if any photoconductivity could be detected under the following conditions of illumination: (a) the matrix window alone at 4.2°K, (b) the matrix window covered with argon at 4.2°K, (c) the matrix window covered with argon containing isolated sodium atoms at a dilution of approximately 1600:1, (d) the matrix window covered with argon containing isolated TCNE molecules at a dilution of approximately 670:1, (e) the matrix window covered with a thin layer of sodium, (f) the matrix window covered with a thin layer of TCNE, (g) the matrix window covered with alternate layers of pure sodium and TCNE. Applied voltages of up to 2000 V dc were tried, but no detectable photocurrents were observed.
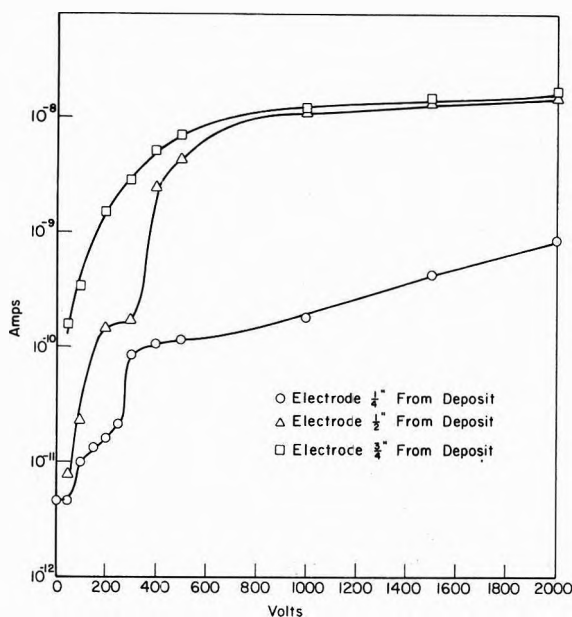
Figure 1. Photoconductivity curves for sodium and tetracyanoethylene in an argon matrix, 30 layers of each.

TABLE I: Photocurrent with 30 Layers Each of Matrix-Isolated Sodium and TCNE

V	Current, A[a]		
	A[b]	B[c]	C[d]
0	0	0	0
10	0.7×10^{-11}	e	e
50	0.7×10^{-11}	0.9×10^{-11}	2.8×10^{-10}
100	1.0×10^{-11}	4.3×10^{-11}	5.7×10^{-10}
150	2.1×10^{-11}	e	e
200	2.9×10^{-11}	1.5×10^{-10}	2.6×10^{-9}
250	4.0×10^{-11}	e	e
300	9.3×10^{-11}	3.1×10^{-10}	5.1×10^{-9}
400	1.3×10^{-10}	4.6×10^{-9}	7.4×10^{-9}
500	1.6×10^{-10}	6.7×10^{-9}	8.6×10^{-9}
1000	3.4×10^{-10}	1.4×10^{-8}	1.8×10^{-8}
1500	6.6×10^{-10}	2.1×10^{-8}	2.6×10^{-8}
2000	9.4×10^{-10}	2.6×10^{-8}	3.1×10^{-8}

[a] In these measurements, the movable electrode was held in a fixed position and the voltage varied. No measurements were made in which the voltage was held constant and the electrode repositioned. [b] Electrode 0.25 in. from matrix surface (see footnote a). [c] Electrode 0.5 in. from matrix surface. [d] Electrode 0.75 in. from matrix surface. [e] No measurements made.

Several experiments were then tried in which alternate matrix isolated layers of sodium and TCNE were deposited and attempts were made to detect photocurrents under illumination. The results from two typical "well-behaved" experiments are given in Table I and II and are presented graphically in Figures 1 and 2. Photoconductivity measurements made in the well-behaved experiments had the following characteristics. The photocurrent values were reproducible, stable, and did not show hysteresis effects. In order to obtain the photoconductivity it was necessary that the potential be applied so that the electrode adjacent to the first sodium layer was negative, and the movable electrode nearest the last TCNE layer was positive. If this polarity was reversed, no photocurrents were observed.
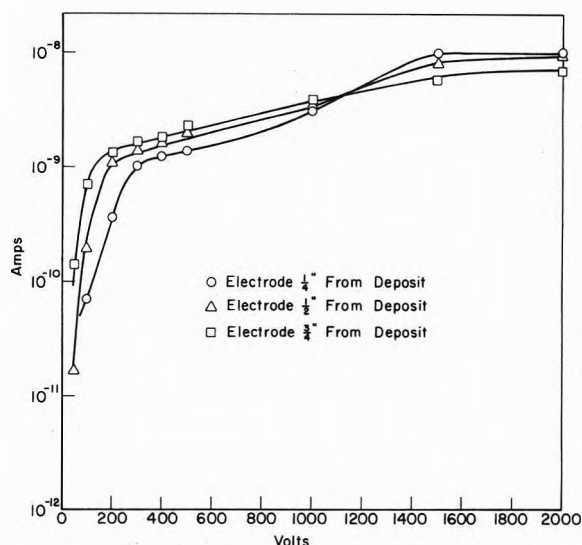

Figure 2. Photoconductivity curves for sodium and tetracyanoethylene in an argon matrix, 15 layers of each.
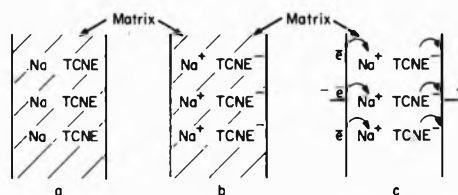

Figure 3. Schematic of photoconductivity process: (a) matrix-isolated layers of sodium and TCNE without illumination; (b) matrix-isolated layers of sodium and TCNE ions formed on illumination; (c) photoconductivity due to charge transfer under the influence of an applied electric field.

TABLE II: Photocurrent with 15 Layers Each of Matrix-Isolated Sodium and TCNE

V	Current, A		
	A[a]	B[b]	C[c]
0	0	0	0
10	0	0	0
50	0	2.9×10^{-11}	2.2×10^{-10}
100	8.6×10^{-11}	3.6×10^{-10}	8.6×10^{-10}
200	6.0×10^{-10}	1.4×10^{-9}	2.1×10^{-9}
300	1.1×10^{-9}	2.3×10^{-9}	3.1×10^{-9}
400	1.8×10^{-9}	2.9×10^{-9}	3.7×10^{-9}
500	2.3×10^{-9}	3.6×10^{-9}	4.3×10^{-9}
1000	5.5×10^{-9}	5.9×10^{-9}	6.3×10^{-9}
1500	1.0×10^{-8}	9.3×10^{-9}	8.0×10^{-9}
2000	1.2×10^{-8}	1.0×10^{-8}	8.7×10^{-9}

[a] Electrode 0.25 in. from matrix surface. [b] Electrode 0.5 in. from matrix surface. [c] Electrode 0.75 in. from matrix surface.

In a few experiments matrices containing sodium and TCNE were prepared in which the resulting photocurrents were not very stable or reproducible. When this was the case relatively high photocurrents were recorded, some in the 10^{-5}–10^{-4} range. In some cases a greenish glow appeared to emanate from the matrix and the photocurrent persisted for several seconds after the illumination was removed. It was also observed that the photocurrent occurred irrespective of the electrode polarity, though the magnitudes for a given potential difference were not equal.

Discussion

On the basis of the experimental evidence there can be little doubt that photocurrents can be obtained in inert gas matrices containing layers of isolated sodium atoms and TCNE molecules. The source of this effect will be considered. Spectral response curves for the photocurrent were not obtained. However, the spectral response curve for the light source was crudely measured. Its output at the shortest wavelength started at about 3700 Å, with the bulk of the radiation being emitted between 5300 and 7000 Å. The generation of photocurrents must therefore be justified in terms of this incident photon energy. The possibility that the photocurrents arise from the simple photoionization of solid argon, trapped sodium atoms, or trapped TCNE molecules is negated by the preliminary experimental data and also by the known magnitudes of the photoionization potentials for argon (≈ 13 eV < 950 Å),[9] sodium (5.8 eV < 2380 Å),[1] and TCNE (EA $= 3.25$ eV,[1] IP $\ll 3790$ Å). Of the various materials used in the equipment only metallic sodium, with a work function of 2.28 eV < 5400 Å, could possibly be an electron source under the experimental conditions of illumination. That no photocurrent was observed in the preliminary experiments when a layer of metallic sodium was illuminated is not surprising, since the rear surface of the layer was illuminated remote from the collecting electrode. The possibility that small aggregates of trapped sodium atoms, which could possibly be formed during the matrix isolation process, could have an ionization energy low enough to produce electrons under illumination was disproved by the preliminary experiments.

The experimental evidence and above considerations strongly indicate that the photocurrents observed in matrix isolated layers of sodium atoms and TCNE molecules must arise from some cooperative phenomenon involving the two species. The epr studies of Kasai[1] and others have shown that in a mixed argon matrix of sodium atoms and TCNE molecules, electron transfer from the metal to the electron acceptor, TCNE, can be accomplished with photon energies of >5000 Å or ≈ 3.20 eV. This latter quantity is markedly lower than the ionization potential of sodium atoms (5.8 eV). The light source used in this study would have sufficient energy, therefore, to cause the formation of matrix-isolated ion pairs. With the production of ion pairs, photoconductivity can be visualized as shown schematically in Figure 3. The experimental observation that photoconductivity could only be observed in the well-behaved experiments when the electrode adjacent to the first sodium layer was negative supports the proposed conductivity mechanism. Photoconductivity data presented in Tables I and II indicate that somewhat larger photocurrents were measured in the matrix containing a total of 30 layers of sodium and TCNE than in the matrix containing 15 layers. Qualitatively, this behavior would be expected, since more ion pairs and hence current carrying centers are formed in the former than in the latter matrix. The increase in photocurrent with applied voltage probably reflects the effect of the increasing electric field reducing the effective number of electron traps within the matrix. In this connection it has been shown in solid argon that oxygen impurities markedly affect electron mobilities and lifetimes.[9] Obviously, doping the matrix in the present study with an excess of a strong electron acceptor, TCNE, is liable to produce many electron-trapping sites. A curious aspect of the photocurrent vs. applied voltage curves is the apparently larger currents that were often obtained when one of the electrodes was farther from the matrix surface than closer to it. There does not seem to be any simple explanation for this behavior. Similarly, the production of large currents and greenish light emanations in the non-well-behaved experiments is not open to obvious interpretation.

Summary

This preliminary study has clearly shown that photocurrents can be obtained from matrices containing isolated sodium atoms and TCNE molecules. The photoconduction mechanism almost certainly involves electron injection to an electron donor–acceptor complex formed by the trapped species. The system clearly requires further study, since some of the experimental observations are difficult to explain. From a practical point of view, it is possible that a matrix isolated donor–acceptor complex could be used as a memory device since it has been shown that once the complex is formed it is quite stable.[1] A second interesting aspect of the device might be in the area of detection of electron-accepting and -donating materials in special cases. From data obtained in this study for the well-behaved matrix it may be estimated that the presence of at least 10^{12} donor–acceptor complexes can be detected. With a more thorough understanding of the photoconduction process, this already high sensitivity could possibly be increased.

References and Notes

(1) P. H. Kasia, Phys. Rev. Lett., 21, 67 (1968).
(2) P. H. Kasai and D. McLeod, Jr., J. Chem. Phys., 51, 1250 (1969).
(3) P. H. Kasai, Accounts Chem. Res., 4, 329 (1971).
(4) D. E. Milligan and M. E. Jacox, J. Chem. Phys., 55, 1003 (1971).
(5) D. E. Milligan and M. E. Jacox, J. Chem. Phys., 55, 3404 (1971).
(6) A. Snelson, J. Phys. Chem., 73, 1919 (1969).
(7) W. T. Hicks, J. Chem. Phys., 38, 1873 (1963).
(8) R. H. Boyd, J. Chem. Phys., 38, 2529 (1963).
(9) L. S. Miller, S. Howe, and W. E. Spear, Phys. Rev., 166, 871 (1968).

Spectrophotometric and Electrochemical Studies of Flash-Photolyzed Trioxalatoferrate(III)

J. I. H. Patterson and S. P. Perone*

Department of Chemistry, Purdue University, Lafayette, Indiana 47907 (Received July 18, 1972; Revised Manuscript Received February 26, 1973)

Spectrophotometric and electrochemical monitoring techniques have been used to follow the intermediates generated by the flash photolysis of trioxalatoferrate(III). The results indicate that there are competing initial photolytic processes followed by a sequence of three secondary reactions. In the first, an oxidizable iron(III) diradical species, formed by the flash, disappears by a rapid first-order reaction. The rate of disappearance of the second intermediate is dependent on the iron(III) oxalate concentration. The third step in the mechanism produces the final product, dioxalatoferrate(II). Of the three sequential steps, only the reaction of the second intermediate can be followed photometrically and has been reported previously. The initial and final reactions can be monitored conveniently electrochemically. The reaction sequence proceeds to completion in less than 1 sec.

Recently, from this laboratory, Jamieson and Perone[1] reported a flash photolytic study of iron(III) oxalate using electrochemical detection methods. They proposed a mechanism involving initial formation of a diradical intermediate which could be monitored electrolytically. The overall mechanism suggested was not in agreement with proposals of other workers[2,3] who have used spectrophotometric monitoring in similar flash photolysis studies. A review of other workers' results was provided previously.[1]

Because the earlier flash photolysis studies utilizing kinetic spectroscopy[2,3] employed solution and photolytic conditions different than for our earlier work[1] using electrochemical monitoring, the purpose of the work reported here was to apply both electrochemical and spectrophotometric monitoring techniques under identical conditions. Moreover, the instrumentation employed here allowed simultaneous monitoring by both techniques. Thus, it was possible to obtain a more complete outline for the mechanism of the trioxalatoferrate(III) photoreduction than had been postulated when considering either electrochemical or spectrophotometric data alone.

Experimental Section

Apparatus and Procedures. The apparatus and general procedures for photometric and electrochemical measurements have been described previously.[4] Photometric determination of the final concentration of iron(II) oxalate produced was made at 430 nm. Electrochemical determination of the concentration of electroactive intermediates was done with time-delay potentiostatic current measurements.[5]

Reagents. All solutions were prepared as in ref 1. Except as noted in the text, all data are reported for trioxalatoferrate(III) in 0.4 M oxalate solution at pH 6.0.

Results

Spectrophotometric Monitoring. The absorbance *vs.* time behavior following the flash photolysis of iron(III) oxalate solution is qualitatively the same at all wavelengths as that reported previously.[2,3] In no case was an increase in absorbance observed after the slow decay, in contrast to the report of Cooper and Degraff[3] that a slow increase was noted at 334 and 313 nm. This, however, may be caused by the slightly different conditions of the experiments reported here.

The majority of the experiments in this work were monitored at the isosbestic point, 410 nm, to eliminate the contribution of the changing absorbances of trioxalatoferrate(III) and dioxalatoferrate(II). The absorbance here rises instantaneously with the flash and then decreases until the final absorbance is equal to the initial absorbance. The decrease in absorbance was plotted according to first-order kinetics from data which spanned at least one-and-a-half to two half-lives of the reaction. Standard deviations were the order of 2–5%. The observed rate constants agreed within experimental error regardless of the monitoring wavelength used over the range 315–640 nm. At long times (greater than 25 msec), there were no absorbance changes noted which would correspond to the long-lived electrochemically monitored reaction reported below.

The dependence of the first-order rate constant on the concentration of iron(III) oxalate was studied, varying the initial concentration of trioxalatoferrate(III) over the range of 1×10^{-4}–2×10^{-3} M. Figure 1 shows a log–log plot of the observed first-order rate constants *vs.* the concentration of excess trioxalatoferrate(III). The range covered in this study is somewhat larger than that used by Cooper and DeGraff[3] and shows that the dependence is more complex than they have suggested. At low concentrations, the rate constant shows no dependence on the iron(III) oxalate concentration, while at higher concentrations the dependence appears half-order as Cooper and DeGraff observed.

Electrochemical Monitoring. Potentiostatic analysis of flash-photolyzed trioxalatoferrate(III) was performed and confirmed the data reported previously by Jamieson and Perone.[1] However, more detailed studies of certain features were conducted as discussed below.

Figure 2 shows a typical plot of the total oxidation current, measured at -0.1 V *vs.* sce, *vs.* time (τ) for 2×10^{-4}
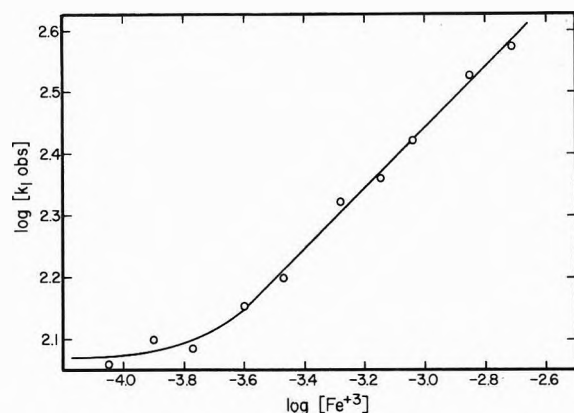
Figure 1. Log–log plot of photometrically observed first-order rate constant vs. the concentration of excess iron(III) after the flash.

Figure 2. Current vs. log (τ) after the flash for 2×10^{-4} M $FeOX_3{}^{3-}$: $E_{appl} = -0.10$ V vs. sce.

M trioxalatoferrate(III) in 0.4 M oxalate at pH 6.0. (The data in Figure 2 and all other electrochemical currents referred to in this work were measured by time-delay potentiostatic analysis.)[5] Reduction currents measured at -1.5 V vs. sce 300 μsec after the flash show a decrease from the initial level which is equal, within experimental error, to the minimum oxidation current observed after the flash (see Figure 2). This indicates that there may be a small amount of iron(II) oxalate formed initially by the flash. (This observation contrasts with the earlier report[1] that no significant instantaneous decrease in the reduction current at -1.5 V occurred with the flash. Because the decrease only slightly exceeds the range of experimental error, it was not recognized earlier.)

The observation of the initial decrease in reduction current led to a closer examination of the initial decay in oxidation current at -0.1 V vs. sce. The measured minimum oxidation current, due to initial production of iron(II) oxalate, can be subtracted from each of the short-time current measurements. Then, when this corrected current is plotted in the standard first-order manner, good linear plots are obtained with a standard deviation of about 6%. The first-order rate constant observed for this reaction was found to be independent of iron(III) oxalate concentration and has a value of $(2.8 \pm 0.2) \times 10^3 \, \text{sec}^{-1}$.

The slow *increase* of oxidation current measured at -0.1 V vs. sce was plotted using the standard first- and second-order plotting techniques, and both cases were found to display some curvature, with neither order giving an appreciably better fit. The calculated rate constants for both orders are given in Table I. These rate constants display a dependence on iron(III) oxalate concentration which probably reflects the effect of a preceding reaction.

Simultaneous Monitoring. In order to determine that the reactions being monitored photometrically and electrochemically were results of the same photolytic process, the reactions were monitored simultaneously using time-delay potentiostatic analysis at -0.1 V vs. sce and photometric monitoring at 430 nm. The final observed concentrations of dioxalatoferrate(II) were calculated with the results shown in Table II. It can be seen that the two different systems are monitoring very similar final concentrations, indicating that they are monitoring the same segment of solution. This conclusion allows the pooling of kinetic data obtained from both measurements into a digital simulation of the complete photolytic process as described below.
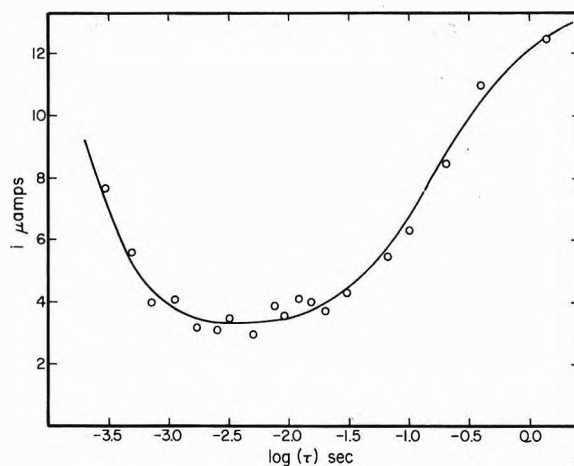
TABLE I: Rate Constants for Long Time Increase in Oxidation Current at -0.1 V vs. Sce

$[Fe(OX)_3{}^{3-}]$, M	k (first order), sec^{-1}	k (second order), $M^{-1}\,\text{sec}^{-1}$
2×10^{-4}	2.4	7.8×10^4
6×10^{-4}	3.3	11.1×10^4
1×10^{-3}	9.5	13.5×10^4

TABLE II: Comparison of $[Fe^{2+}]_{final}$ Monitored Electrochemically at -0.1 V vs. Sce and Photometrically at 430 nm

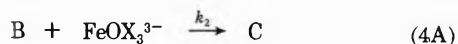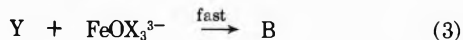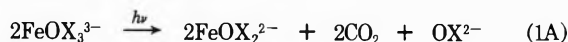| $[Fe^{3+}]_{initial}$, M	$[Fe^{2+}]_{final}$, M Electrochemical	Photometric
2×10^{-4}	0.98×10^{-4}	0.91×10^{-4}
4×10^{-4}	1.3×10^{-4}	1.4×10^{-4}
6×10^{-4}	1.6×10^{-4}	1.8×10^{-4}
8×10^{-4}	1.8×10^{-4}	2.0×10^{-4}
1×10^{-3}	2.0×10^{-4}	2.1×10^{-4}

Effects of pH and Oxalate. In addition to the experiments outlined above, studies were made of the various reactions observed with varied pH and oxalate concentration. The concentration of oxalate had no measurable effect on any of the reactions observed over the range 0.1–0.4 M. Likewise, the solution pH had no effect over the range 5.0–6.5.

Discussion

It is appropriate here to emphasize the new information available from the combined studies described above. From the photometric kinetic study, the dependence on ferrioxalate concentration was established over a broader range, with a zero-order dependence showing up at the lowest concentrations. From the electrochemical studies, detection of a small amount of iron(II) oxalate produced initially with the flash allowed the more accurate kinetic analysis of subsequent data. Finally, the results of simultaneous monitoring allowed the pooling of kinetic data to characterize the complete photolytic process.

The work reported here provides a more complete picture of the kinetic pathway for the photolytic reduction of ferric oxalate. It is clear, for example, that at least three

sequential reactions occur. Thus, the results presented in the preceding section, and the very restrictive fact that the quantum yield of iron(II) oxalate is not affected by either the concentration of iron(III) or iron(II), suggests the following basic mechanism.

$$2FeOX_3{}^{3-} \xrightarrow{h\nu} 2FeOX_2{}^{2-} + 2CO_2 + OX^{2-} \quad (1A)$$

$$FeOX_3{}^{3-} \xrightarrow{h\nu} A \quad (1B)$$

$$A \xrightarrow{k_1} B + Y \quad (2)$$

$$Y + FeOX_3{}^{3-} \xrightarrow{fast} B \quad (3)$$

$$B + FeOX_3{}^{3-} \xrightarrow{k_2} C \quad (4A)$$

$$B \xrightarrow{k_3} C \quad (4B)$$

$$C \xrightarrow{k_4} FeOX_2{}^{2-} \quad (5)$$

Although the data do not allow an explicit assignment of all the intermediate species, spectroscopic and electrochemical characteristics of each can be specified. In this mechanism, A is a species which is electrochemically oxidizable at −0.1 V vs. sce and is so short lived that it was not observed photometrically in this work. B is not oxidizable at −0.1 V vs. sce and is the intermediate which is responsible for the first-order decay observed photometrically; C is a species which is not oxidizable at −0.1 V vs. sce and has a spectrum very similar to dioxalatoferrate(II). Therefore, C is not detected photometrically or electrochemically but is inferred from the long-term production of iron(II) oxalate as observed electrochemically. Y is a reactive intermediate which disappears in a very rapid step and, therefore, is not observed electrochemically or photometrically.

The competitive photolytic steps (1A and 1B) are suggested by the fact that there is a small amount of iron(II) oxalate generated initially by the flash. This reaction must have a quantum yield which is independent of the concentration of iron(III) oxalate, as the overall reaction has a quantum yield which is independent of iron(III) oxalate. Jamieson and Perone[1] suggested that the initial photolytic intermediate A is an iron(III) oxalate diradical species. The predicted electrochemical features of this species agree well with the observed photoelectrochemical data.[1] Also, the suggestion of intermediate A, is supported by other work.[6,7]

A
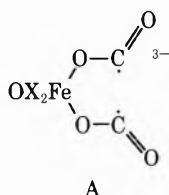
The second reaction (2) represents the rapid first-order reaction which is observed electrochemically. This reaction shows no dependence on iron(III) oxalate concentration; it has a first-order rate constant (k_1) of 2.8×10^3 sec^{-1}, which is an order of magnitude faster than the reaction monitored photometrically. The most probable unimolecular reaction of A would be an intramolecular oxidation–reduction reaction producing iron(II) dioxalate, CO_2, and a $CO_2\cdot^-$ radical. However, iron(II) dioxalate is oxidizable at −0.1 V vs. sce, while experimental data show that intermediate B is not. Thus, it appears that the
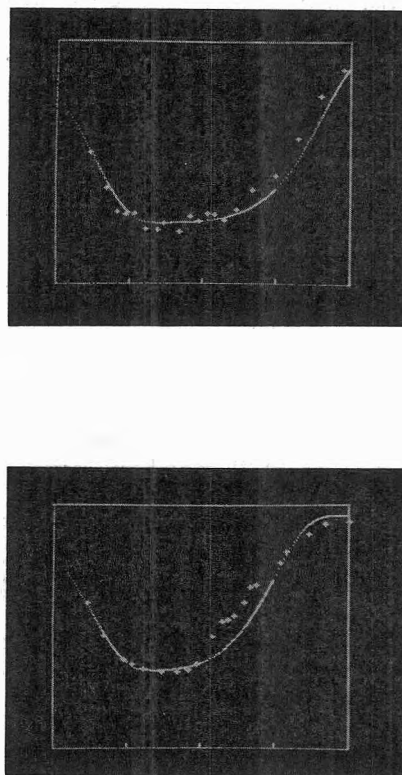

Figure 3. Digital simulation of concentration vs. log (τ) after the flash. Time scale is 100 μsec to 1 sec: (upper photo) 2×10^{-4} M FeOX$_3{}^{3-}$, rate constants: $k_1 = 2.8 \times 10^3$ sec^{-1}, $k_2 = 1.4 \times 10^5$ M^{-1} sec^{-1}, $k_3 = 121$ sec^{-1}, $k_4 = 2.4$ sec^{-1}; initial concentrations: $A = 4.1 \times 10^{-5}$ M, FeOX$_3{}^{3-} = 1.4 \times 10^{-4}$ M, FeOX$_2{}^{2-} = 2.9 \times 10^{-5}$ M; (lower photo) 1×10^{-3} M FeOX$_3{}^{3-}$, rate constants: $k_1 = 2.8 \times 10^3$ sec^{-1}, $k_2 = 1.4 \times 10^5$ M^{-1} sec^{-1}, $k_3 = 121$ sec^{-1}, $k_4 = 9.5$ sec^{-1}; initial concentrations: $A = 7.6 \times 10^{-5}$ M, FeOX$_3{}^{3-} = 8.6 \times 10^{-4}$ M, FeOX$_2{}^{2-} = 7.5 \times 10^{-5}$ M.

redox reaction may proceed through an intermediate (B) in which electron transfer is incomplete. For example, B might be a species where one $CO_2\cdot^-$ radical acts as a bidentate ligand allowing delocalization of the odd electron. Such a complex would be more difficult to oxidize and could account for the observed loss of oxidation current as reaction 2 proceeds. It would also be unstable, decomposing as indicated by reactions 4A and 4B which are observed photometrically.

Species Y could be a free $CO_2\cdot^-$ radical released by the intramolecular reaction 2. It should react very rapidly with excess iron(III) oxalate (reaction 3), presumably to form the same product, B, as in reaction 2. Species Y is apparently too short lived to be detected here, although reaction 3 accounts for the fact that the overall quantum yield can be greater than one;[8] i.e., a second molecule of iron(III) oxalate must be reduced in the reaction sequence.

It is possible that reactions 4A and 4B involve the competition of intra- and intermolecular steps which result in the reduction of a central iron(III) atom to iron(II) and oxidation of the radical ligand to CO_2. Rapid solvolysis could then occur to form a carbonate or bicarbonate complex (C). Experimental data indicate that the product, C, is not oxidizable at −0.1 V vs. sce. Moreover, it must have an absorption spectrum very similar to iron(II) oxalate, as no absorbance change is observed over the range 315–640

nm during the final step, reaction 5 These observations are not inconsistent with a carbonate complex.

The set of competitive reactions (4A and 4B) involving B, the photometrically observed intermediate, are suggested by the nature of the dependence of the photometrically observed first-order rate constant on the concentration of excess iron(III) oxalate (Figure 1). It is possible to reproduce the data presented in Figure 1 by assuming that reaction 4A is a pseudo-first-order reaction in iron(III) oxalate, while reactions 4A and 4B show first-order dependence on B. Then the photometrically observed first-order rate constant (k_{obsd}) will be

$$k_{obsd} = k_3 + k_2[FeOX_3{}^{3-}]$$

From the data in Figure 1, k_3 and k_2 were calculated to be 121 ± 6 sec^{-1} and $(14.0 \pm 0.8) \times 10^{+4}$ M^{-1} sec^{-1}, respectively. The reaction of B seen here corresponds to the "normally observed" photolytic process reported by others.[2,3]

The final reaction in this sequence (5) is probably a ligand exchange process. This could involve the slow displacement of carbonate or bicarbonate ion, which is equivalent to one of the final products, carbon dioxide. This results in the formation of dioxalatoferrate(II) giving rise to the slow increase in oxidation current which is noted at long times. The apparent dependence of this final reaction on the concentration of iron(III) oxalate is probably a result of the preceding reactions (4A and 4B) which show a definite dependence on iron(III) oxalate.

It is interesting to note that the data obtained indicate that the mechanism is divided into three distinctly different time segments following the initial photolysis. The first segment is the rapid first-order reaction 2 which is followed electrochemically. The next segment, which is followed photometrically, involves the "normally observed" reactions (4A and 4B). The final time range is represented by reaction 5 and is followed electrochemically.

In order to further substantiate the mechanism proposed above, digital simulation was performed. In these simulations, all rate constants used are those which were directly observed for each of the three reaction times. Figure 3 shows the results of the simulation of the electrochemical data obtained at 2×10^{-4} and 1×10^{-3} M iron(III) oxalate. In these simulations, the crosses represent oxidation currents due to intermediates oxidizable at -0.1 V vs. sce. The line represents the simulated results for the two-electron oxidation of A plus the one-electron oxidation of iron(II) oxalate. The excellent agreement between the simulated and real electroanalytical data is all the more significant because the rate constants used in the simulation were obtained necessarily from the two different monitoring techniques.

References and Notes

(1) R. A. Jamieson and S. P. Perone, *J. Phys. Chem.*, **76**, 830 (1972).
(2) C. A. Parker and C. J. Hatchard, *J. Phys. Chem.*, **63**, 22 (1959).
(3) G. D. Cooper and B. A. DeGraff, *J. Phys. Chem.*, **75**, 2897 (1971).
(4) J. I. H. Patterson and S. P. Perone, *Anal. Chem.*, **44**, 1978 (1972).
(5) S. P. Perone and J. R. Birk, *Anal. Chem.*, **38**, 1589 (1966).
(6) F. R. Dukes, *J. Amer. Chem. Soc.*, **69**, 2885 (1947).
(7) V. V. Boldyrev, I. S. Nev'yantsev, Yu I. Mikhailov, and E. F. Khalretdinov, *Kinet. Katal.*, **11**, 367 (1970).
(8) C. A. Parker, *Proc. Roy. Soc., Ser. A*, **220**, 104 (1953).

Brillouin Spectra of Solutions. III.[1] Excess Free Energy of Some Relaxing Binary Liquid Mixtures

George A. Miller* and Ching S. Lee

School of Chemistry, Georgia Institute of Technology, Atlanta, Georgia 30332 (Received March 21, 1973)

The intensity ratios have been measured in the Brillouin spectra of the binary systems benzene–toluene, benzene–ethylene dichloride, toluene–ethylene dichloride, acetone–chloroform, acetone–carbon disulfide, and benzene–methanol, at 25°, and naphthalene–dodecane at 85°. In the first four systems, scattering from concentration fluctuations was sufficiently weak to allow the first term of the intensity ratio equation to be evaluated and compared with a simplified relaxation theory. The theory appeared to be adequate and was used with the remaining three systems to determine activity coefficients and excess free energies from the concentration dependence of the intensity ratio. The results showed satisfactory agreement with vapor composition data at the same temperature for the systems C_3H_6O–CS_2 and C_6H_6–CH_4O, giving additional support to the simplified theory. For the system $C_{10}H_8$–$C_{12}H_{26}$, intensity ratio results at 85° could be combined with vapor composition data at about 140° to give an apparently reasonable heat of mixing. Further simplification of the intensity ratio equation is suggested which removes the dependence of the method on certain subsidiary data.

Rayleigh scattering exhibits a fine structure of three closely spaced peaks, called the Brillouin spectrum. Our particular interest is in the use of the ratio of intensities of central to side peaks to obtain thermodynamic activity coefficients of nonideal, binary solutions (or solute molecular weights in dilute solutions). For both pure liquids and solutions, thermodynamic fluctuation averages and qualitative notions of the dynamics of fluctuation decay give straightforward expressions for the peak intensities.[2] However, these formulas must be significantly modified if there is relaxation of sound at the hypersonic frequencies corresponding to the peak separation. We were able to incorporate relaxation in the intensity ratio formula for dilute solutions, again using qualitative arguments.[3] Subsequently, Fishman and Mountain[4] filled in our incomplete theory with a detailed dynamical calculation which showed the relation of the spectrum line shape to the relaxation parameters of the solution. They suggested that, to obtain activity coefficients from intensity ratios, it would be necessary to determine the relaxation parameters by recording Brillouin spectra at several scattering angles.

In this paper we show that, by using a simple, albeit less rigorous relaxation theory, we may introduce in turn several additional approximations which greatly simplify the intensity ratio equation. The result is to reduce the dependence of our method on subsidiary data to the point that, in addition to recording the Brillouin spectra, only refractive index measurements need be made. To test our approach we have measured intensity ratios and Brillouin shifts of some thermally relaxing systems. First, four systems for which the concentration scattering is small or negligible have been studied to test the concentration dependence of that part of the intensity ratio coming from fluctuations (the quantity a in eq 2). These systems are benzene–toluene, benzene–ethylene dichloride, toluene–ethylene dichloride, and acetone–chloroform. The strongly relaxing components here are C_6H_6 and $CHCl_3$. Second, two systems have been studied for which the concentration scattering is large enough to be useful for determining

activity coefficients and excess free energy, and for which these data are available from vapor equilibrium measurements. These systems are acetone–carbon disulfide and benzene–methanol, the strongly relaxing components being CS_2 and C_6H_6. Finally, we have determined the excess free energy for naphthalene–dodecane at 85°, for which system vapor equilibrium data are available only at about 140°.

Theory

For a nonrelaxing binary solution, of mole fractions x_1 and x_2, the intensity ratio of central to side peaks, J, is related to the chemical potential, μ_2, and activity coefficient, γ_2, of component 2 by

$$J = a' + a'KRTx_1/(\partial \mu_2/\partial x_2)_{T,P} =$$
$$a' + a'Kx_1x_2/[1 + x_2(\partial \ln \gamma_2/\partial x_2)] \quad (1)$$

where $a' = (\gamma - 1)/(1 + f\gamma)$, γ is the ratio of specific heats, C_p/C_v, and f is a quantity defined earlier[3] which is generally unknown. In eq 1 the subscripts 1 and 2 may be interchanged because of the Gibbs–Duhem relation. The quantity K is given by

$$K = \frac{C_p}{RT^2}\left(\frac{\partial n/\partial x_2}{\partial n/\partial T}\right)^2$$

where C_p is the heat capacity per mole of solution, R is the gas constant, T is the absolute temperature, and n is the refractive index of the solution. On limited evidence[3] we will assume that f is small enough so that $a' \cong \gamma - 1$. This is the Landau–Placzek relation for pure fluids.

In a relaxing solution, a fraction, Δ, of the intensity of the side peaks is transferred to a new, unshifted relaxation peak. This peak can be counted as part of the central peak, since it is generally narrow enough not to overlap seriously with the side peaks. The result is

$$J(k) = a + bKx_1x_2/[1 + x_2(\partial \ln \gamma_2/\partial x_2)] \quad (2)$$
$$a = (a' + \Delta)/(1 - \Delta), \quad b = a'/(1 - \Delta)$$

Here, $J(k)$ implies that, due to relaxation, J is now dependent on the change in wave vector of the scattering pro-

cess producing the Doppler shifted side peaks. According to Fishman and Mountain, there is a slight coupling of relaxation with concentration fluctuations so that Δ depends slightly on J. For a single relaxation mechanism, they find $\Delta = A(k)J(0) + B(k)$, where $J(0)$ is the low-frequency or nonrelaxing limit of $J(k)$ given by eq 1, and

$$A(k) = \frac{r(p - r)v^2k^2\tau^2 + 1 - r}{r^2v^2k^2\tau^2 + 1}$$

$$B(k) = \frac{r(p - 1)v^2k^2\tau^2 + 1 - r}{r^2v^2k^2\tau^2 + 1}$$

where $r = v^2/v_0^2$, $p = v_\infty^2/v_0^2$, and v is the velocity of the hypersound, τ is the relaxation time, and v_0 and v_∞ are the limiting low or ultrasonic and high-frequency sound velocities. Using carbon tetrachloride-like parameters ($v_0 = 10^5$ cm/sec, $v_\infty = 1.15 \times 10^5$ cm/sec, $n = 1.5$, and $\tau = 5 \times 10^{-11}$ sec), these authors show $B(k)$ as being slightly negative for small k but otherwise positive and dominating in the expression for Δ, and $A(k)$ as being always negative and small. The negative values of $A(k)$ and $B(k)$ appear to be due to their using one of the standard, approximate dispersion formulas for the hypersound. Going back to their original dispersion equation

$$-i\omega^3\tau - \omega^2 + i\omega v_\infty^2 k^2 + v_0^2 k^2 = 0$$

we find, for the same parameters, that $A(k)$ and $B(k)$ are positive with $0 < A(k) < 0.005$. In the limit of large k, $B(k)$ approaches 0.24. For typical binary systems, we can expect that $J(0) < 10$, hence $A(k)$ will have a small, almost negligible effect on $J(k)$.

Therefore, we will turn to a simplified relaxation theory which does not include the above-mentioned coupling between Δ and $J(0)$. Following Pinnow, et al.,[5] we write, for a pure liquid

$$J_0 = \gamma r - 1 \qquad (3)$$

Taking the previous CCl$_4$ parameters and $\gamma = 1.4$ we find at $\omega\tau = 1$ (middle of the relaxation range) that J_0 is 0.62 by eq 3 and 0.52 by the theory of Fishman and Mountain. The two theories give the same values of J_0 in the low- and high-frequency limits, if it is assumed as before that $J(0) = \gamma - 1$ for a pure liquid. Introducing eq 3 into our relations for solutions we have

$$a = \gamma r - 1$$

$$\Delta = (r - 1)/r$$

$$b = (\gamma - 1)r$$

The intensity ratio equation is, thus

$$J = (\gamma r - 1) + (\gamma - 1)rKx_1x_2/$$
$$[1 + x_2(\partial \ln \gamma_2/\partial x_2)] \qquad (4)$$

The hypersonic velocity contained in r can be determined from the peak separation in the Brillouin spectrum according to the relation

$$\Delta\nu = 2\nu(v/c) \sin (\theta/2) \qquad (5)$$

where c is the velocity of the incident light of frequency ν in the medium and θ is the scattering angle.

Experimental Section

The procedure for obtaining Brillouin spectra at 6328 Å and $\theta = 90°$ has been described.[3] Naphthalene rich solutions were clarified at elevated temperatures through very fine sintered glass filters; otherwise, various submicron porous membrane filters were used. Intensity ratios were

determined in the vertically polarized spectrum after subtracting the scattering from orientation fluctuations ($\frac{4}{3}$ the depolarized intensity). The Brillouin peaks were integrated by measuring the area under the outside half of each peak and multiplying by 2 in order to minimize the problem of overlap with the central peak at large J. The reproducibility in J was ±0.05.

Eastman Spectrograde dodecane and Highest Purity naphthalene were used. The remaining liquids were Fisher Certified reagent grade.

Hypersonic velocities were obtained with a reproducibility of ±0.5% from the ratio of the Brillouin shift to the interferometer free spectral range and the corresponding ratio for a standard liquid (viz., eq 5). Standards used were benzene,[6] $v = 1.453 \times 10^5$ cm/sec, and acetone,[6,7] $v = 1.168 \times 10^5$ cm/sec (hypersonic value = ultrasonic value) both at 25°.

Results and Discussion

The data were evaluated with our simplified relaxation theory as given by eq 4. Of the basic experimental quantities appearing in eq 4, those measured by us are J, the hypersonic velocity v, and the T and x_2 dependence of n; those derived from the literature are the ultrasonic velocity v_0, C_p, and the T dependence of the density, from which γ could be calculated by the relation

$$\gamma - 1 = Tv_0^2\alpha^2M/C_P \qquad (6)$$

where α is the thermal expansivity and M is the weight of 1 mol of solution.[8] When the required data were available only for the pure components, linearity with mole fraction was assumed. However, both v_0 and C_p disappear in the second term of eq 4 since

$$(\gamma - 1)rK = \frac{v^2\alpha^2M}{RT}\left(\frac{\partial n/\partial x_2}{\partial n/\partial T}\right)^2 \qquad (7)$$

For those systems of small refractive increment, hence weak excess scattering, the small concentration scattering term in eq 2 was readily calculated and subtracted from J to give the experimental values of a shown in Figure 1. The agreement with the simplified relaxation theory is satisfactory for our purposes. Mostly the calculated a's are a bit low. However, there are several sources of experimental error to be weighed against the approximate nature of our relaxation theory. Small amounts of dust in the scattering medium plus instrument scattering increase J. Peak overlap also remained a minor source of error. We tended to get values of J slightly higher than some other workers. For example, we obtained for benzene a value 0.87, compared with reported values of 0.84[9] and 0.80.[10]

The data for those systems with large excess scattering were used in eq 4 to calculate the quantity $\partial \ln \gamma_2/\partial x_2$.[8] Activity coefficients and excess Gibbs free energies, given in Table I, were obtained from the standard relations

$$\frac{\partial \ln \gamma_1}{\partial x_1} = \frac{x_2}{x_1}\frac{\partial \ln \gamma_2}{\partial x_2}$$

$$\ln \gamma_i = \int_1^{x_i}\left(\frac{\partial \ln \gamma_i}{\partial x_i}\right) dx_i$$

$$G^E = RT(x_1 \ln \gamma_1 + x_2 \ln \gamma_2)$$

Our excess free energies from Brillouin scattering agree well with values from vapor equilibrium data. In the case of dodecane–naphthalene, a comparison of our results with those from vapor equilibrium shows that G^E de-

TABLE I: Activity Coefficients and Excess Gibbs Free Energy (cal/mol) from Brillouin Spectra

X_2	Acetone(1)–carbon disulfide(2) at 25°				Benzene(1)–methanol(2) at 25°				Dodecane(1)–naphthalene(2) at 85°			
	$\ln \gamma_1$	$\ln \gamma_2$	G^E	Lit. values	$\ln \gamma_1$	$\ln \gamma_2$	G^E	Lit. values	$\ln \gamma_1$	$\ln \gamma_2$	G^E	Lit. values
0	0		0		0		0	0	0		0	
0.1	0.013	1.219	79	110[a]	0.043	1.886	135	145,[c] 141[d]	0.009	0.642	52	37[e]
0.2	0.053	0.991	142	165,[a] 136[b]	0.141	1.279	218	225,[c] 227[d]	0.031	0.507	90	70[e]
0.3	0.119	0.792	190	198,[a] 176[b]	0.261	0.906	269	275,[c] 277[d]	0.061	0.418	120	99[e]
0.4	0.215	0.616	222	222[a]	0.400	0.644	295	299,[c] 301[d]	0.103	0.340	141	114[e]
0.5	0.347	0.457	238	235[b]	0.562	0.444	298	301,[c] 301[d]	0.165	0.265	153	128[e]
0.6	0.522	0.314	235		0.754	0.287	281	283,[c] 284[d]	0.256	0.193	155	136[e]
0.7	0.753	0.191	213	211[a]	0.980	0.164	242	245,[c] 246[d]	0.386	0.124	144	131[e]
0.8	1.054	0.091	168	170,[a] 180[b]	1.245	0.076	183	186,[c] 186[d]	0.573	0.064	118	104[e]
0.9	1.438	0.024	98	100[a]	1.567	0.020	103	100,[c] 105[d]	0.845	0.018	72	58[e]
1	0		0		0		0		0		0	

[a] A. N. Campbell, E. M. Katzmark, and S. C. Anand, *Can. J. Chem.*, **49**, 2183 (1971). [b] F. Michaud, *Ann. Phys.*, **6**, 265 (1916). [c] G. Scatchard and L. B. Ticknor, *J. Amer. Chem. Soc.*, **74**, 3724 (1952). [d] I. Brown, W. Fock, and F. Smith, *J. Chem. Thermodyn.*, **1**, 273 (1969). [e] Over the range 140–145°, H. I. Lyvers and M. Van Winkle, *J. Chem. Eng. Data*, **3**, 6 (1958).

creases with increasing temperature with an enthalpy of mixing of roughly 300 cal/mol for an equimolar mixture. This is in line with the behavior of the system n-hexane–benzene, where measurements at 25° show also that the enthalpy of mixing and G^E are positive and that the enthalpy of mixing is about twice as large as G^E.[11]

It is of interest at this point to see how further approximations can be introduced to lessen the dependence of our method on data from other sources. First we note that a may be assumed to vary linearly with mole fraction with little loss in accuracy, since we are considering solutions with large excess scattering; a will be defined then by the J_0's of the pure components, $a = x_1 J_{0,1} + x_2 J_{0,2}$. As eq 7 shows, we have now eliminated v_0 and C_p from eq 4.

Then, we note the occurance of $[\alpha/(\partial n/\partial T)]^2$ in eq 7. This parameter is predicted by the Lorentz–Lorenz relation as follows

$$\frac{n^2 - 1}{n^2 + 2} = C_1 \rho, \qquad \rho = \text{density}$$

$$-\frac{1}{\alpha}\frac{\partial n}{\partial T} = \rho \frac{dn}{d\rho} = \frac{(n^2 - 1)(n^2 + 2)}{6n} \qquad (8)$$

Equation 8 predicts values of $-(\partial n/\partial T)/\alpha$ that are typically 10% high. Let us suppose there is a function $F(n)$ which predicts this parameter accurately enough so that we can reduce eq 7 to

$$(\gamma - 1)rK = \frac{v^2 M}{RT}\left(\frac{\partial n/\partial x_2}{F(n)}\right)^2$$

For example, following Rosen[12] we might write

$$\frac{n^2 - 1}{n^2 + 2} = \frac{C_1 \rho}{1 + C_2 \rho}$$

for which

$$\rho \frac{dn}{d\rho} = \frac{(n^2 - 1)(n^2 + 2)}{6n} - \frac{(n^2 - 1)^2}{6n}\frac{C_2}{C_1} = F(n)$$

where C_2/C_1 is to be considered an adjustable constant. In seeking a best fit we might absorb the term $1 + f\gamma$ of eq 1 which was dropped because it is generally unknown. Equation 7 would then be

$$\frac{(\gamma - 1)rK}{1 + f\gamma} = \frac{v^2 \alpha^2 M}{(1 + f\gamma)RT}\left(\frac{\partial n/\partial x_2}{\partial n/\partial T}\right)^2$$

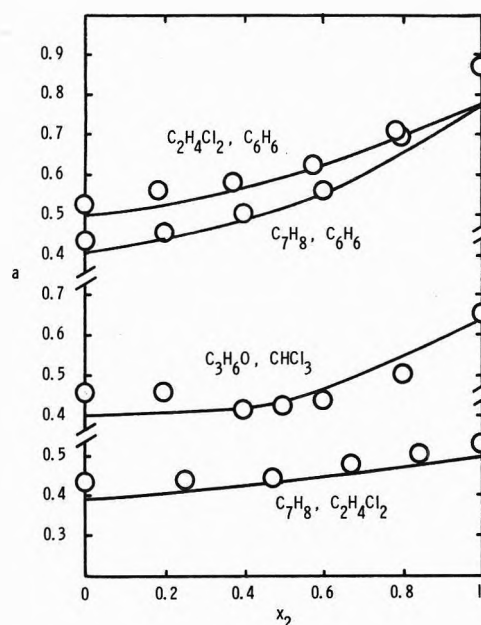and C_2/C_1 would be adjusted to fit

Figure 1. Experimental values of a (circles) compared with $a = \gamma(v/v_0)^2 - 1$ from approximate relaxation theory.

$$F(n) = (1 + f\gamma)^{1/2}\frac{-1}{\alpha}\frac{\partial n}{\partial T}$$

Of the quantities needed to calculate f, it is principally $\partial n/\partial P$ for which experimental values are lacking. As a preliminary test we find $C_2/C_1 \simeq 0.20$ for eleven liquids studied by Coumou, *et al.*,[13] at 5460 Å. This yields

$$F(n) = \frac{(n^2 - 1)(4n^2 + 11)}{30n}$$

With the above simplifications we may now estimate G^E solely from J, v, n, and $\partial n/\partial x_2$. For equimolar mixtures we get 250 cal/mol for $(CH_3)_2CO$–CS_2, 298 for C_6H_6–CH_3OH, and 142 for $C_{12}H_{26}$–$C_{10}H_8$, which suggests that the Brillouin scattering method in simplified form will yield equimolar excess free energies to about ±10 cal. However, in order to apply with confidence any semiempirical approximation of $F(n)$, it would be preferable to test it against a larger number of liquids than we have been able to. Moreover, the accuracy of the method depends on how appreciable the excess scattering is. As a rough rule, the

two components should not differ by much less than 0.2 units in refractive index.

The Brillouin scattering method provides a useful alternate for the study of the nonideality of solutions of low vapor pressure. However, such solutions can be very viscous and exhibit structural relaxation not well characterized by a single relaxation time. We have not tried to adapt our simplified relaxation theory to viscous solutions but feel that this would be a useful exercise.

Supplementary Material Available. Listings of the basic experimental quantities for all systems studied will appear following these pages in the microfilm edition of this volume of the journal. Photocopies of the supplementary material from this paper only or microfiche (105 × 148 mm, 20× reduction, negatives) containing all of the supplementary material for the papers in this issue may be obtained from the Journals Department, American Chemical Society, 1155 16th St., N.W., Washington, D. C. 20036. Remit check or money order for $3.00 for photocopy or $2.00 for microfiche, referring to code number JPC-73-2441.

References and Notes

(1) Part II: F. I. San Filippo, G. A. Miller, and J. A. Bertrand, *Inorg. Chem.*, **11**, 1433 (1972).
(2) G. A. Miller, *J. Phys. Chem.*, **71**, 2305 (1967).
(3) G. A. Miller and C. S. Lee, *J. Phys. Chem.*, **72**, 4644 (1968).
(4) L. Fishman and R. D. Mountain, *J. Phys. Chem.*, **74**, 2178 (1970).
(5) D. A. Pinnow, S. J. Candau, J. T. LaMacchia, and T. A. Litovitz, *J. Acoust. Soc. Amer.*, **43**, 131 (1968).
(6) D. P. Eastman, A. Hollinger, J. Kenemuth, and D. H. Rank, *J. Chem. Phys.*, **50**, 1567 (1969).
(7) E. B. Freyer, J. C. Hubbard, and D. H. Andrews, *J. Amer. Chem. Soc.*, **51**, 759 (1929).
(8) See paragraph at end of text regarding supplementary material.
(9) H. Z. Cummins and R. W. Gammon, *J. Chem. Phys.*, **44**, 2785 (1966).
(10) C. L. O'Connor and J. P. Schlupf, *J. Acoust. Soc. Amer.*, **40**, 663 (1966).
(11) K. R. Harris and P. J. Dunlap, *J. Chem. Thermodyn.*, **2**, 805 (1970).
(12) J. S. Rosen, *J. Chem. Phys.*, **17**, 1192 (1949).
(13) D. J. Coumou, E. L. Mackor, and J. Hijmans, *Trans. Faraday Soc.*, **60**, 1539 (1964).

Studies of Dimethyl Sulfoxide Association in Dimethyl Sulfoxide–Pyridine Mixtures. Infrared and Light Scattering Spectroscopy

Jack B. Kinsinger,* Mary M. Tannahill, Mark S. Greenberg, and Alexander I. Popov

Department of Chemistry, Michigan State University, East Lansing, Michigan 48824   *(Received April 11, 1973)*

Mixtures of dimethyl sulfoxide (DMSO) with pyridine over the full composition range were studied by Brillouin scattering and infrared spectroscopy. The density, refractive index, and molar refractivity were also determined. The data are consistent with the concept of an onset of association of DMSO in its mixtures with pyridine in the 5–15 mol % DMSO composition range. As the concentration of DMSO is increased there is evidence for rearrangement and new associated species. The compositional regions in which the various aggregated species occur are influenced by temperature.

Introduction

It has been shown in previous publications that the solvating abilities of solvents can be empirically related to (a) the enthalpy of formation of their 1:1 complexes with antimony pentachloride[1] and (b) the downfield chemical shift of the sodium-23 resonance of sodium perchlorate and tetraphenylborate solutions in these solvents when compared to an aqueous sodium chloride solution as external reference.[2] Both types of measurements indicate that neat pyridine has a somewhat stronger solvating ability than dimethyl sulfoxide (DMSO). When nmr measurements were performed in solvent mixtures, however, the solvating abilities were found to be reversed,[3] and dimethyl sulfoxide was found to preferentially solvate sodium ions in DMSO-pyridine mixtures. Similar results were obtained when the respective donor abilities of DMSO and

of pyridine were compared against solvents such as nitromethane, acetonitrile, or benzonitrile.[3]

Since DMSO is reported to be a highly associated liquid,[4] the enhancement of its donor ability in solvent mixtures may result from rupture of the DMSO structure by the second liquid component. In liquid mixtures, therefore, the DMSO molecules would be less rigidly bound than in pure solvent and could interact better with the ions of dissolved salts. In order to investigate this phenomenon several physicochemical studies of DMSO-pyridine mixtures have been initiated.

As an indication of microscopic interactions, the S–O stretching frequency of the DMSO molecule was determined at 22° over the complete compositional range from pure pyridine to pure DMSO. Submacroscopic structural changes were probed by measuring the velocity of sound *via* Brillouin scattering over a similar set of samples and a

broad temperature. The density at 22° and the refractive index at several different temperatures were also determined.

Experimental Section

A. Reagents. Dimethyl sulfoxide (reagent grade, J. T. Baker) was dried over Linde Type 4A molecular sieves and then vacuum distilled at 50°. The first 20% of the distillate was discarded and only the middle 60% fraction was collected and stored over 4A sieves. Karl Fischer titration showed less than 0.077% water by weight (0.33 mol %).

Pyridine (Fischer Certified) was purified by refluxing the solvent over granular BaO for 24 hr followed by fractional distillation at 112°. The middle 60% fraction of the distillate was collected and stored over molecular sieves. Karl Fischer titration showed less than 0.05% water.

B. Preparation of Solutions. Pyridine-DMSO mixtures were prepared by weighing appropriate amounts of the two solvents in a volumetric flask. Thirteen solutions ranging from 0.00 to 1.00 mole fraction DMSO were prepared and stored over molecular sieves. Solutions for scattering measurements were passed through an ultrafine and a millipore filter into tubes of 10 mm diameter which served as light scattering cells. After filtration each solution appeared to be free of dust when viewed at low angle with the laser source used in the scattering experiments. The tubes were sealed to prevent dust and moisture from entering the solutions.

C. Instrumentation. Infrared spectra were obtained on the Perkin-Elmer Model 225 spectrometer. Barnes standard demountable cells with KBr windows were used. Refractive indices were determined on a Bausch and Lomb refractometer equipped with a Haake temperature control unit. Measurements were made with a sodium lamp. Corrections for other wavelengths were made from a set of dispersion tables supplied for this instrument by the Bausch and Lomb Co.

Density measurements were made with a Sargent Welsh pycnometer calibrated with distilled water.

D. Brillouin Scattering. The Brillouin spectrometer was designed and constructed by Gaumer. The instrumental details are contained in his thesis.[5] The optical source for the spectrometer is a single mode, frequency stabilized Spectra Physics 165 argon ion laser. Vertically polarized incident light at 5145 Å was used for all scattering measurements. The scattering cell was housed at the center of a rotating table and vertically polarized scattered light was collected at 90°. The cell holder which is constructed of copper constitutes a thermostatic jacket which is maintained at constant temperature (±0.1°) by a proportional controller. A very small cone of scattered light is taken into the optical detection system by passing the scattered light through two variable apertures (~1 mm each). The scattered light is collimated by a 500-mm focal length achromatic lens, is filtered through a third aperture, and is passed into the mirrors of a Lansing Fabry-Perot interferometer which is scanned piezoelectrically. The interferometer mirrors are 1 in. in diameter and have inside surfaces polished to λ/100 flatness. The resolved light is passed from the interferometer through another achromatic lens (100-mm focal length) where it is collimated and focused onto a pinhole (~2 mm). The light then travels to a photomultiplier tube where it is detected. The output of the photomultiplier is amplified with a Keithley picoammeter and the signal is fed into a Sargent recorder. As the linear ramp voltage is increased to the piezoelectric

driven mirrors, the spectrum of the scattered light is traced by the recorder. During a single scan, five spectral orders are obtained. The resolution (finesse) of the Fabry-Perot interferometer fell between 30 and 45 for the large series of measurements reported in this paper.

Results and Discussion

The fact that DMSO is a highly associated liquid is evident from a variety of experimental information. It has a high entropy and enthalpy of vaporization (29.0 cal deg^{-1} mol^{-1} at 189°[6] and 12.64 kcal mol^{-1} at 25°,[7] respectively). In benzene solutions its dipole moment varies with concentration, decreasing from 3.88 D in dilute solutions to a minimum value of 3.45 D in 1.49 M DMSO solution, rising to a constant value of 3.89 D in the 4.9-9.1 M concentration range, and finally progressing to 4.11 D for neat solvent.[8] Likewise, the frequency of the S-O stretch varies from 1102 cm^{-1} in the gas phase to ~1080-1070 cm^{-1} in nonpolar liquids to 1013 cm^{-1} in water.[4] Several other physicochemical measurements such as cryoscopic[9] studies and refractive index studies[8] of DMSO in benzene also indicate strong associative forces between the DMSO molecules. There is no evidence that DMSO is an H-bonding species. Formation of charge-transfer complexes in pyridine-DMSO mixtures is quite unlikely since DMSO and Py are both electron donors. On the other hand, it has been reported that the Kirkwood g factor for neat DMSO is ~1.0 and this fact has been taken as evidence for the absence of specific dipole-dipole interactions in DMSO.[10] Recent theoretical study[11] shows that in highly polar liquids long-range correlations have an important role in the theory of dielectric phenomena. This important development raises serious doubts as to the validity of the Kirkwood g factor as a measure of association.

Infrared Studies. The S-O stretching frequency was examined in neat DMSO and in DMSO-pyridine mixtures at 22°. The data are presented in Figure 1 and Table I. It is seen that the addition of small amounts of pyridine to DMSO result in a sharp increase in the ν_{S-O} frequency to ~5 mol % pyridine. In the region from 10 to 80 mol % pyridine, the increase in frequency is much more gradual. Above 80% pyridine, however, the slope of the curve once again becomes quite steep.

These results are in agreement with the infrared studies of Szmant and coworkers[12] on solutions of DMSO in carbon tetrachloride at room temperature. These authors conclude that in the concentration range from pure carbon tetrachloride to 0.008 M DMSO, dimethyl sulfoxide exists in the form of monomers. As the concentration is increased to 0.3 M, the DMSO molecules gradually associate to dimers; above this concentration higher DMSO aggregates are formed. Naturally, one would not expect a strict parallelism between DMSO behavior in carbon tetrachloride and in pyridine mixtures. Pyridine is a relatively polar liquid with a dipole moment of 2.2 D. It would be expected, therefore, that it would be more effective in breaking up the DMSO structure than carbon tetrachloride. Thus, the addition of small amounts of pyridine could result in the disruption of aggregates, resulting in the initial sharp increase in the ν_{S-O} frequency.

Refractive Index and Density. The refractive indices of the two neat solvents and of the DMSO-pyridine mixtures were determined in the 22-39° temperature range (Table II). Densities were also evaluated at 22° so that the molar refractivity could be calculated. Within experimental limits the density-composition values at 22° can be repre-
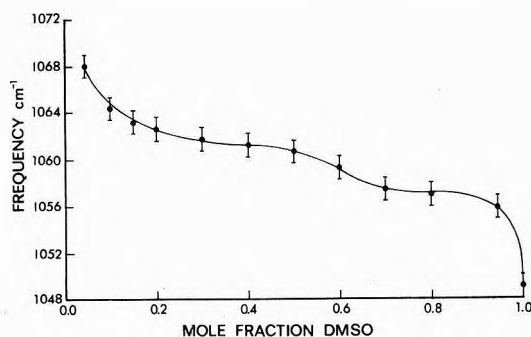
Figure 1. Variation in the ν_{S-O} stretch in DMSO-pyridine mixtures at 22°.

TABLE I: Variation of the S–O Stretching Frequency in DMSO as a Function of Solvent Composition for DMSO–Pyridine Mixtures

Mole fraction DMSO	ν_{S-O}, cm^{-1}	Mole fraction DMSO	ν_{S-O}, cm^{-1}
0.050	1068 ± 1	0.500	1061
0.010	1064	0.598	1059
0.150	1063	0.700	1057
0.198	1063	0.800	1057
0.300	1062	0.946	1056
0.400	1061	1.000	1049

TABLE II: Refractive Index Study for DMSO–Pyridine Mixtures as a Function of Temperature[a]

Mole fraction DMSO	n_D			
	22.0°	26.4°	30.1°	39.0°
1.000	1.4784	1.4763	1.4748	1.4709
0.946	1.4802	1.4785	1.4768	
0.800	1.4852	1.4831	1.4809	
0.700	1.4880	1.4863	1.4846	
0.598	1.4915	1.4894	1.4877	1.4827
0.501	1.4942	1.4917	1.4901	1.4858
0.400	1.4962	1.4942	1.4923	
0.300	1.4979	1.4962	1.4941	
0.198	1.5044	1.5010	1.4993	1.4931
0.151	1.5052	1.5020	1.5003	1.4942
0.099	1.5056	1.5035	1.5017	1.4947
0.050	1.5073	1.5053	1.5031	
0.000	1.5090	1.5064	1.5046	1.4988

[a] λ = 5890 Å (sodium D line). The average standard error for these measurements is ±0.0005.

sented by $d = 0.116X_{DMSO} + 0.956$, where X_{DMSO} = mole fraction of DMSO.

Brillouin Scattering. The interaction of an incident beam of light with a thermally propagated pressure wave (sound wave) in a liquid gives rise to an intensity-frequency distribution known as a Brillouin scattering spectrum. A Brillouin spectrum consists of three peaks, the central Rayleigh peak centered about the frequency of the incident radiation and two symmetrical side bands which are shifted according to the expression suggested by Brillouin[13] in 1922

$$\Delta\nu = \pm 2\nu_0\langle\eta\rangle \frac{V_s}{C} \sin(\theta/2)$$

Here $\Delta\nu$ is the shift of the Brillouin peaks, ν_0, the frequency of the incident light, C, the speed of light *in vacuo*, $\langle\eta\rangle$ the average refractive index of the medium, V_s,

the speed of sound in the medium, and θ, the viewing angle. With a stable interferometer at a finesse of 30, the Brillouin shift can be measured to within 1% precision. The velocity of sound, which depends only on the Brillouin shift for a given medium under a specific set of experimental conditions, can be calculated with the same degree of precision.

The isentropic pressure fluctuations which produce the characteristic Brillouin shift course over distances as large as $10\lambda_0$ in the medium under conditions of constant external temperature and pressure. The incident radiation scatters inelastically from the moving pressure wave when the Bragg condition is satisfied.

An approximate but useful theory for Brillouin scattering in mixtures was first proposed by Miller and Lee[14] and later placed on a firmer hydrodynamic foundation by Mountain and his coworkers.[15,16] Both theories, however, require the knowledge of temperature- and concentration-dependent thermodynamic and optical properties, few of which have been determined for mixtures. Consequently, no experimental test of Mountain's theory for mixtures has been accomplished, whereas Miller and Lee's approximate theory has been tested and found adequate for dilute solutions. We are left, therefore, to explore the qualitative information contained in the velocity of sound data for the DMSO-pyridine mixtures over a wide temperature range.

Brillouin scattering can be employed to study structural changes in liquids in much the same manner in which ultrasonic experiments have been used in the past. One common denominator in both experiments is the determination of the velocity of sound. The velocity of sound varies with the compressibility of the medium and the compressibility, in turn, depends on liquid structure. The velocity of sound, therefore, is a direct measure of the strength of intermolecular forces, or degree of association, in a liquid.

Velocity of sound data gathered by light scattering experiments and by ultrasonics for a variety of liquids have been found to be in good agreement.[17,18] A logical consequence, therefore, would be to assume that one can use documented ultrasonic experiments on mixtures to aid in the interpretation of data obtained from Brillouin scattering measurements.

Ultrasonic physicists identify three classes of liquids, based on their acoustical properties: (1) the classical fluids, (2) Knesser fluids, and (3) associated liquids.[19] This classification is determined by measuring the sonic attenuation coefficient, α, as a function of temperature. When $d\alpha/dT$ is negative, the fluids fall into category 3. Although our data are not reported in this paper, $d\alpha/dT$ for the pure fluids and all their mixtures were found to be negative.

If there were no structural changes occurring in the composition region from pure pyridine to pure DMSO, one would expect to observe two phenomena: (1) the change in the velocity of sound in going from one pure fluid to the other would be a smooth, continuous curve;[20] (2) the change in dV_s/dT with composition would also be a smooth, continuous curve.

In Table III are displayed the measured frequency shifts and the refractive indices for the DMSO-pyridine mixtures as a function of temperature. By numerical least-squares analysis the sonic velocity-temperature curves for each composition are fit by a straight line relationship, $V_s = A + BT$ where $T = °C$. These linear temperature relationships are consistent with data taken by

TABLE III: Brillouin Shift and Velocity of Hypersound for Mixtures of DMSO and Pyridine[a]

T, °C	Δν, GHz	n_{5145} Å	T, °C	Δν, GHz	n_{5145} Å	T, °C	Δν, GHz	n_{5145} Å	T, °C	Δν, GHz	n_{5145} Å
Pure C_5H_5N			05 mol % DMSO			60 mol % DMSO			70 mol % DMSO		
21.6	6.39	1.5168	21.6	6.29	1.5149	21.6	6.00	1.4977	21.6	6.05	1.4940
29.5	6.27	1.5121	29.5	6.17	1.5107	29.5	5.91	1.4936	29.5	5.92	1.4903
34.5	6.19	1.5091	34.5	6.08	1.5080	34.5	5.84	1.4910	34.5	5.83	1.4880
39.4	6.11	1.5061	39.4	6.01	1.5053	39.4	5.78	1.4885	39.4	5.75	1.4856
44.5	6.03	1.5031	44.5	5.92	1.5026	44.5	5.72	1.4859	44.5	5.66	1.4832
49.3	5.95	1.5002	49.3	5.85	1.5000	49.3	5.66	1.4834	49.3	5.57	1.4810
54.2	5.87	1.4974	54.2	5.77	1.4974	54.2	5.60	1.4809	54.2	5.49	1.4787
59.0	5.79	1.4944	59.0	5.69	1.4948	59.0	5.54	1.4784	59.0	5.41	1.4764
10 mol % DMSO			15 mol % DMSO			80 mol % DMSO			95 mol % DMSO		
21.6	6.27	1.5134	21.6	6.28	1.5125	21.6	6.04	1.4912	21.6	6.13	1.4857
29.5	6.12	1.5087	29.5	6.14	1.5075	29.5	5.95	1.4870	29.5	6.00	1.4823
34.5	6.02	1.5058	34.5	6.05	1.5043	34.5	5.88	1.4843	34.5	5.92	1.4802
39.4	5.92	1.5029	39.4	5.97	1.5012	39.4	5.82	1.4818	39.4	5.83	1.4781
44.5	5.82	1.5000	44.5	5.88	1.4979	44.5	5.75	1.5791	44.5	5.75	1.4759
49.3	5.73	1.4971	49.3	5.80	1.4948	49.3	5.69	1.4765	49.3	5.67	1.4738
54.2	5.63	1.4942	54.2	5.71	1.4917	54.2	5.63	1.4739	54.2	5.59	1.4717
59.0	5.54	1.4914	59.0	5.63	1.4887	59.0	5.57	1.4714	59.0	5.51	1.4696
20 mol % DMSO			30 mol % DMSO			Pure DMSO					
21.6	6.17	1.5115	21.6	6.22	1.5047	21.6	6.11	1.4837			
29.5	6.05	1.5063	29.5	6.08	1.5015	29.5	5.99	1.4803			
34.5	5.97	1.5030	34.5	5.98	1.4994	34.5	5.91	1.4781			
39.4	5.89	1.4998	39.4	5.89	1.4974	39.4	5.84	1.4760			
44.5	5.81	1.4965	44.5	5.79	1.4953	44.5	5.75	1.4737			
49.3	5.74	1.4933	49.3	5.70	1.4934	49.3	5.68	1.4716			
54.2	5.66	1.4901	54.2	5.61	1.4914	54.2	5.60	1.4695			
59.0	5.59	1.4870	59.0	5.52	1.4894	59.0	5.53	1.4674			
40 mol % DMSO			50 mol % DMSO								
21.6	6.11	1.5027	21.6	6.02	1.5005						
29.5	5.99	1.4990	29.5	5.90	1.4966						
34.5	5.90	1.4967	34.5	5.82	1.4942						
39.4	5.82	1.4944	39.4	5.75	1.4918						
44.5	5.73	1.4921	44.5	5.67	1.4893						
49.3	5.65	1.4899	49.3	5.59	1.4869						
54.2	5.57	1.4876	54.2	5.51	1.4846						
59.0	5.49	1.4854	59.0	5.44	1.4822						

[a] Average standard deviations for the temperature and Brillouin shift are $\sigma_T = \pm0.1°$ and $\sigma = \pm0.05$ GHz respectively.

ultrasonic interferometry for organic solvents in lower frequency regions.[21]

The parameters A and B obtained for each composition and their standard deviations are exhibited in Table IV. The sonic velocities as a function of composition at each temperature are shown in Figure 2. The parameter B, (dV_s/dT), as a function of composition is shown in Figure 3. Within experimental precision in the measurements, neither the V_s vs. x_1 curve nor the dV_s/dT vs. x_1 curve is a smooth, continuous function, indicating that there are structural changes in the mixture as one progresses from pure pyridine to pure DMSO.

It is especially noteworthy that the data in Figure 2 show large variations in the 5-15 mol % DMSO region at all temperatures. The variation at 22° corresponds with the striking decrease in the S-O stretching frequency observed at this temperature (Figure 1). Our interpretation of this information is that a significant structural change occurs in this region. Lindberg, et al.,[8] suggest that in a similar compositional range at 25° for benzene–DMSO mixtures, DMSO dimers are formed. If we use the principles of "structural comparison" from the ultrasonic investigations of Lutskii and Solon'ko[22,23] on a series of pure

liquids of varying molecular structure, we would conclude that in the region from 15 to 30 mol % DMSO at 22°, dimeric structures are rearranging into higher associated species. At the higher temperatures it appears that dimer formation occurs between 5 and 10 mol % DMSO, and that between 10 and 20 mol %, rearrangement of these aggregates proceeds. These assumptions are supported further by the oscillatory nature of the V_s and dV_s/dT curves between 5 and 20% DMSO (Figures 2 and 3). We note that these oscillations and changes with composition and temperature could result also from the various mixtures and neat fluids being subject to a dispersion in V_s. Since no V_s-frequency data were taken and none is available on these mixtures, we cannot rule out the possible explanation. However, limited ultrasonic data on dispersion as a function of composition show this to be an unlikely explanation of our data.

A randomization of structure appears to carry the solutions into the 50-50 mol % region where V_s reaches a minimum at all temperatures. The sonic wave apparently is more sensitive to the supramicroscopic structure in this region than the S-O stretching frequency, which is sensitive to shorter range interactions and thereby remains on
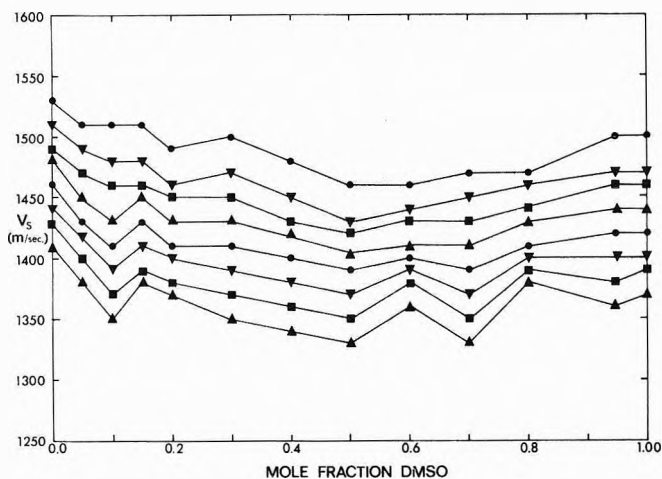
Figure 2. Velocity of sound in DMSO-pyridine mixtures at different temperatures; from top to bottom: ●, 21.6°; ▼, 29.5°; ■, 34.5°; ▲, 39.4°; ●, 44.5°; ▼, 49.3°; ■, 54.2°; ▲, 59.0°.
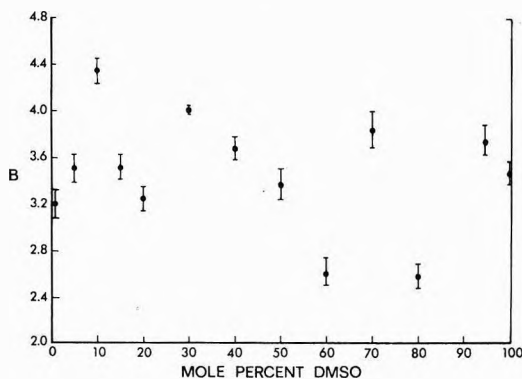

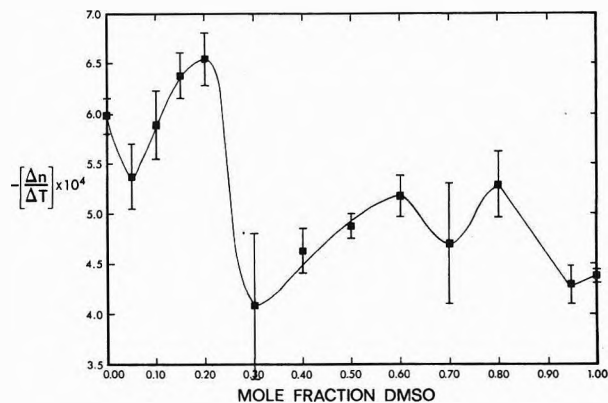Figure 3. Plot of parameter B as a function of composition for DMSO-pyridine mixtures.

Figure 4. Temperature coefficient of the refractive index for DMSO-pyridine mixtures.

TABLE IV: Linear Parameters of $V_s = A + BT$ in DMSO-Pyridine Mixtures

Mole fraction DMSO	A, m/sec	B, m/sec/deg
0.00	1603 ± 10	−3.23 ± 0.1
0.05	1589	−3.51
0.10	1606	−4.36
0.15	1585	−3.52
0.20	1558	−3.25
0.30	1588	−4.02
0.40	1560	−3.67
0.50	1534	−3.38
0.60	1516	−2.59
0.70	1559	−3.84
0.80	1529	−2.56
0.95	1583	−3.73
1.00	1575	−3.47

a plateau. Finally, there is some variation of V_s vs. x_1 in the 50–96 mol % region, especially at the higher temperatures. This phenomenon is noted as well in the S–O stretching frequency at 22°. We interpret this as further evidence of structural rearrangements and possible formation of a chain-like structure. The extreme vacillations exhibited by the V_s vs. x_1 curves at the highest temperatures probably connote the formation, partial breakdown, and rearrangement of the DMSO aggregates under the influence of thermal motion in the liquid. The 70–95 mol % region also shows anomalous behavior in the dielectric constant in mixtures of benzene and DMSO at 25°.[8]

The depolarized spectra of pure pyridine and pure DMSO showed no spectral peak associated with orientational scattering but only a broad background ordinarily identified with dipole–induced-dipole effects in the liquid.[24] The lack of an orientational relaxation component supports the general concept of molecular association in DMSO. We further note that several Brillouin spectra of the neat liquids and mixtures were fit to a Lorentzian curve for both the Rayleigh and Brillouin peaks. In view of the excellent fit we see no evidence for any additional contributions which may arise from mode coupling.

Conclusion

Most physical evidence shows that DMSO is an associated fluid. The new S–O stretch data, coupled with data for the velocity of sound and its temperature derivative as a function of composition, show agreement with the con-

cept of association. It is our analysis that the published value of $g = 1$ for neat DMSO[10] is in error since recent work supports the concept that liquids with a large dipole moment are not adequately treated for long-range forces by the Onsager–Kirkwood theory.[11]

Our data uniformly show structural changes in the 5–30 mol % DMSO region for all temperatures examined. The data are consistent with the concept of association and rearrangement of species over the full compositional range. The most disordered region at the 50–50 mol % mixture, and at higher concentrations, evidence for further association and rearrangement of DMSO species appears.

The microscopic data (ir) clearly show the effect of local variation in interactions. The velocity of sound data appear even more sensitive to the aggregated structures than the S–O stretching frequency.

On the submicroscopic and essentially atomic scale the effect of association is manifested in the temperature coefficient of the refractive index (Figure 4). Once more the regions from 0 to 30 and 60 to 95 mol % DMSO exhibit the striking discontinuities, demonstrating unequivocally that significant structural changes are occurring in the liquid in these composition regions.

Since the structure of liquid DMSO is extensively disrupted by the addition of pyridine, it seems reasonable to conclude that the solvating ability of the former is enhanced by this process. The selective solvation process in liquid mixtures is a function of solvent–solvent interaction as well as solvent–solute interaction.

References and Notes

(1) V. Gutmann, "Coordination Chemistry in Nonaqueous Solvents," Springer-Verlag, Vienna, 1968.
(2) R. H. Erlich and A. I. Popov, *J. Amer. Chem. Soc.*, **93**, 5620 (1971).
(3) R. H. Erlich, M. S. Greenberg, and A. I. Popov, *Spectrochim. Acta, Part A*, **29**, 543 (1973).
(4) H. H. Szmant in "Dimethyl Sulfoxide," S. W. Jacob, E. E. Rosenbaum, and D. C. Wood, Ed., Marcel Dekker, New York, N. Y., 1971, pp 1–98.
(5) S. J. Gaumer, Ph.D. Thesis, "A Brillouin Spectrophotometer," Department of Chemistry, Michigan State University, 1973.
(6) H. L. Schlafer and W. Schaffernicht, *Angew. Chem.*, **72**, 618 (1960).
(7) W. S. MacGregor, *Ann. N. Y. Acad. Sci.*, **141**, 3 (1967).
(8) J. J. Lindberg, J. Kenttamaa, and A. Nissema, *Suom. Kemistilehti B*, **34**, 156 (1961).
(9) J. J. Lindberg, J. Kenttamaa, and A. Nissema, *Suom. Kemistilehti B*, **34**, 98 (1961).
(10) R. L. Amey, *J. Phys. Chem.*, **72**, 3358 (1968).
(11) J. D. Ramshaw, *J. Chem. Phys.*, **57**, 2684 (1972).
(12) R. Figueroa, E. Roig, and H. H. Szmant, *Spectrochim. Acta, Part A*, **22**, 587 (1966).
(13) L. Brillouin, *Ann. Phys. (Paris)*, **17**, 88 (1922).
(14) G. A. Miller and C. S. Lea, *J. Phys. Chem.*, **72**, 4644 (1968).
(15) R. D. Mountain and C. M. Deutch, *J. Chem. Phys.*, **50**, 1103 (1969).
(16) L. Fishman and R. D. Mountain, *J. Phys. Chem.*, **74**, 2178 (1970).
(17) I. L. Fabelinskii, "Molecular Scattering of Light," translated by R. T. Beyer, Plenum Press, New York, N. Y., 1968.
(18) R. S. Krishnan, "The Raman Effect," A. Anderson, Ed., Marcel Dekker, New York, N. Y., 1971, Chapter 6.
(19) K. F. Herzfeld and T. A. Litovitz, "Absorption and Dispersion of Ultrasonic Waves," Academic Press, New York, N. Y., 1959.
(20) E. G. Richardson, "Ultrasonic Physics," Elsevier, Amsterdam, 1952.
(21) G. W. Marks, *J. Acoust. Soc. Amer.*, **41**, 103 (1967).
(22) A. E. Lutskii and V. N. Solon'ko, *Russ. J. Phys. Chem.*, **38**, 217 (1964).
(23) A. E. Lutskii and V. N. Solon'ko, *Russ. J. Phys. Chem.*, **39**, 414 (1965).
(24) V. Volterra, J. A. Bucaro, and T. A. Litovitz, *Ber. Bunsenges. Phys. Chem.*, **75**, 309 (1971).

Spectroscopic Studies of Ionic Solvation. XIV. A Sodium-23 Nuclear Magnetic Resonance and Electrical Conductance Study of Contact Ion Pairs in Nonaqueous Solvents

Mark S. Greenberg, Richard L. Bodner, and Alexander I. Popov*

Department of Chemistry, Michigan State University, East Lansing, Michigan 48824   *(Received May 17, 1973)*

Publication costs assisted by the National Science Foundation

Sodium-23 nuclear magnetic resonance measurements have been carried out on several sodium salts in 1,1,3,3-tetramethylurea, 1,1,3,3-tetramethylguanidine, sulfolane, tetrahydrofuran, dimethylformamide, formamide, ethanol, methanol, pyridine, and ethyl acetate. Chemical shifts were measured relative to aqueous 3.0 M sodium chloride solution. The direction, magnitude, and concentration dependence of the chemical shifts are strongly influenced by the "donicity" (or solvating ability) of the solvents. Formation of contact ion pairs depends not only on the dielectric constants of the solvents but also on their solvating abilities. Electrical conductance studies of NaI solutions in pyridine and tetramethylguanidine yield ion pair dissociation constants of 3.91×10^{-4} and 6.2×10^{-5}, respectively. The interpretations obtained from the ^{23}Na chemical shifts correlate well with the data obtained from electrical conductance measurements.

Introduction

It is becoming increasingly obvious that the mechanisms and rates of most reactions in solutions are strongly dependent on the nature and physicochemical properties of the solvent. In order to elucidate the role of the solvent in chemical reactions it is necessary to have a sound knowledge of solvent–solute, solvent–solvent and solute–solute interactions in the given medium. Yet such data are seldom available and even the knowledge of the ionic species and the equilibria in solutions of simple salts in water or in nonaqueous solvents is in a very rudimentary state.

In recent years it has been shown that the alkali metal nmr, and particularly sodium-23 nmr, is a very sensitive probe of the immediate chemical environment of alkali metal ions.[1-5] The magnitude and the direction of ^{23}Na chemical shifts in various solvents have been related either to the Lewis basicity[2] of the solvents or to their donor (or solvating) abilities.[1a]

The purpose of this investigation is to extend our earlier studies of ion–ion and ion–solvent interactions in nonaqueous solutions of various sodium salts by sodium-23 nmr.[1a] The solvents were selected so as to vary as much as possible their dielectric constants and solvating abilities.

Experimental Section

Chemicals. Sodium salts used in this study were of reagent grade quality and were not further purified before use except for drying. Solvents, 1,1,3,3-tetramethylurea (Aldrich) and 1,1,3,3-tetramethylguanidine (Eastman), were purified by refluxing over granulated barium oxide for 24 hr followed by fractional distillation under vacuum. Sulfolane (Shell) was purified by fractional freezing followed by vacuum distillation over sodium hydroxide pellets. Tetrahydrofuran (Matheson Coleman and Bell) was fractionally distilled over calcium hydride. Dimethylformamide (Fisher) was vacuum distilled over phosphorus pentoxide. Commercially available absolute ethanol and reagent grade ethyl acetate (Baker) were used without further purification. Methanol (Baker) was fractionally distilled over calcium sulfate. Formamide (Fisher) was purified by fractional freezing. Pyridine (Fisher) was refluxed over barium oxide for 24 hr and fractionally distilled. Dimethyl sulfoxide (Baker) was dried over molecular sieves and vacuum distilled. Purified solvents were stored over Linde 4A molecular seives. Stock solutions of sodium salts (0.500 M) were prepared by weighing out the desired amount of a salt into a 5-ml volumetric flask and diluting to the mark with solvent. The remaining solutions were prepared by appropriate dilutions of the stock solutions.

Measurements. Nmr. Sodium-23 nuclear magnetic measurements were made at ambient temperature on a modified NMRS MP-1000 spectrometer at 60 MHz (53.3 kG). The experimental details are described in a previous publication.[1d] The Kontes K-897155, 5-mm o.d. polished nmr sample tube was fitted with a Wilmad precision coaxial 520-2 nmr tube for the reference solution. The reference for ^{23}Na measurements was 3.0 M aqueous sodium chloride solution. When the chemical shifts were so small that the sample resonance was masked by the reference, a secondary reference of 2.5 M sodium perchlorate in methanol was used. In the latter case, the shifts were corrected so as to apply to the same sodium chloride reference solution.

Magnetic Susceptibility Corrections. Bulk diamagnetic susceptibility measurements of the solutions were made on a Gouy balance employing the Alpha Magnetic Susceptibility System Model 4520. It should be noted that when the applied field is transverse to the long axis of the cylindrical sample, the correction to the observed chemical shift due to different bulk diamagnetic susceptibilities of the sample and reference is given by

$$\delta_{corr} = \delta_{obsd} + \frac{2\pi}{3}(X_v^{ref} - X_v^{sample}) \tag{1}$$

Live and Chan[6] have shown that for high-field nmr spectrometers with superconducting solenoids, where the applied field is parallel the long axis of the cylindrical sample, the correction to the observed chemical shift is

$$\delta_{corr} = \delta_{obsd} - \frac{4\pi}{3}(X_v^{ref} - X_v^{sample}) \tag{2}$$

All of the data presented in this paper have been corrected according to eq 2. In general the corrections were of the order of <1 ppm and varied with the solvent.

In an earlier study[1b] data obtained on the Varian DA-60 were not corrected. Because of the greater sensitivity and accuracy available on NMRS MP-1000 spectrometer, we repeated some of these earlier studies to more carefully observe the ^{23}Na resonance as a function of electrolyte concentration. If the earlier data are corrected by eq 1, they agree, within experimental error, with the data presented in this paper. We assume the contribution of the salt to the susceptibility of the solution to be negligible with respect to that of the solvent; hence, the corrections simply reflect susceptibilities between the sample and reference solvents. It can be seen from the evidence of Templeman and Van Geet[5a] that neglect of salt contribution to the diamagnetic susceptibility of the solution is negligible (<0.05 ppm) especially for dilute solutions of electrolytes.

Conductance. The conductance bridge has been previously described[7] and was operated at 1000 Hz. The cells, constructed similarly to those of Daggett, Bair, and Kraus,[8] were steamed for at least 1 hr followed by oven drying at 110°. Calibration with standard aqueous potassium chloride solutions gave cell constants of 0.0826 ± 0.0001, 1.442 ± 0.001, and 3.916 ± 0.001 cm^{-1}. All measurements were made at 25.00 ± 0.02° utilizing a Sargent S-84805 thermostatic bath assembly filled with light mineral oil. Specific conductances of the pure solvents were found to be negligible as compared to the conductances of the solutions even at the lowest concentrations.

The stock solutions were prepared by weighing solvent into a flask containing previously weighed solute. All solution transfers to the cell were made by means of a weight buret. To maximize accuracy over the entire concentration range ($\sim 10^{-5}$–5 × 10^{-1} m), the final solutions were prepared by one of the following methods. Method A involved progressive addition of the stock solution to the cell which contained a previously weighed amount of solvent. Conversely, method B involved progressive additions of the solvent to the stock solution in the conductance cell. In both methods, the cell contents were thoroughly mixed, temperature equilibrated, and resistance measurements obtained.

Results and Discussion

The chemical shift of the sodium-23 resonance with respect to 3.0 M aqueous sodium chloride was determined for NaBPh$_4$, NaClO$_4$, NaSCN, NaI, and NaBr at several concentrations in various solvents. The data are presented in Table I. Confirming the results of our earlier study,[1a] the chemical shifts for sodium thiocyanate, bromide, and iodide solutions exhibit marked concentration dependence whereas concentration independence is observed for solutions of sodium perchlorate and tetraphenylborate. The results obtained in 1,1,3,3,-tetramethylurea (TMU) and N,N-dimethylformamide (DMF), which are shown in Figures 1 and 2, illustrate this behavior.

The dielectric constants (D) of DMF and TMU are 36.7 and 26.0, respectively. Since the ^{23}Na chemical shifts reflect changes in the inner solvation sphere of the cation, it seems reasonable to assume that the downfield shift occurring with increasing concentration for sodium thiocyanate, bromide, and iodide is due to the formation of contact ion pairs. The frequency of ^{23}Na resonance of Na$^+$ ion in solutions is affected primarily or exclusively by the nearest neighbors of the ion. Hence, chemical shift measurements can differentiate between contact ion pairs and free solvated ions and/or solvent separated ion pairs, but apparently not between free solvated ions and solvent separated ion pairs.

TABLE I: ^{23}Na Chemical Shifts vs. 3.0 M Aqueous NaCl^a

Solvent	Concn, M						
	0.50	0.40	0.30	0.20	0.10	0.05	0.01
			NaClO$_4$				
Pyridine	0.70	0.45	0.45	0.15	−0.10	−0.05	−0.04
Methanol	4.20	4.15	4.10	4.05	3.95	3.90	3.90
Ethanol	2.10	1.85	1.75	1.55	1.30	1.15	0.50
Tetramethylurea	3.30	3.20	3.15	3.15	3.10	3.10	
Tetramethylguanidine	−7.35	−7.30	−7.10	−7.10	−7.05	−6.55	−6.65
Tetrahydrofuran	8.60	8.55	8.50	8.30	8.15	8.10	7.85
Formamide	4.25	4.40	4.25	4.25	4.25	4.25	4.35
Sulfolane	9.25	9.15	9.20	9.25	9.35	9.85	
Dimethylformamide	5.05	5.10	5.10	4.95	4.95	5.10	
Ethyl acetate	9.70	9.60	9.45	9.30	9.20	8.95	8.65
			NaSCN				
Pyridine	−3.20	−3.30	−3.10	−3.20	−3.10	−3.05	
Methanol	3.35	3.40	3.45	3.50	3.55	3.60	3.55
Ethanol	−0.10	0.05	0.05	0.20	0.15	0.20	0.45
Tetramethylurea	0.75	0.85	0.95	1.25	1.45	1.75	2.55
Tetramethylguanidine	−9.60	−9.50	−9.40	−9.15	−9.35	−9.35	−8.75
Tetrahydrofuran	I	I	I	I	2.50	2.50	
Formamide	3.95	4.10	4.15	4.25	4.30	4.25	4.15
Sulfolane							I
Dimethylformamide	3.65	3.80	3.95	4.10	4.40	4.60	4.85
Ethyl acetate	3.45	3.50	3.55	3.60	3.55	3.80	4.65
			NaBPh$_4$				
Pyridine	−1.25	−1.25	−1.30	−1.25	−1.30	−1.25	−1.25
Methanol	3.80	3.80	3.75	3.75	3.75	3.80	3.75
Ethanol	1.00	0.80	0.65	0.55	0.40	0.35	0.45
Tetramethylurea	2.80	2.85	2.90	2.95	2.95	2.95	
Tetramethylguanidine	−10.05	−9.99	−10.20	−9.70	−9.95	−9.85	−9.55
Tetrahydrofuran	7.45	7.30	7.15	7.15	7.15	7.10	7.10
Formamide	I	I	4.25	4.30	4.25	4.30	4.25
Sulfolane	8.95	8.75	8.85	8.85	8.90	9.00	
Dimethylformamide	5.00	4.95	4.95	4.95	4.95	4.95	4.90
Ethyl acetate	8.90	8.75	8.70	8.50	8.20	8.20	7.70
			NaI				
Pyridine	−9.00	−9.50	−9.10	−9.00	−8.25	−8.25	−7.45
Methanol	3.20	3.30	3.35	3.40	3.50	3.55	3.65
Ethanol	−0.25	−0.25	−0.10	−0.15	−0.10	0.00	0.60
Tetramethylurea	−0.30	0.05	0.40	0.80	1.40	1.80	2.50
Tetramethylguanidine	−14.55	−13.95	−14.00	−13.75	−13.80	−13.60	−13.20
Tetrahydrofuran	I	I	I	−7.05	−6.40	−6.25	−5.35
Formamide	4.05	4.15	4.10	4.15	4.20	4.25	4.25
Sulfolane	6.30	6.85	7.05	7.45	8.10	8.90	
Dimethylformamide	I	4.35	4.55	4.55	4.70	4.85	4.95
Ethyl acetate							I
Acetone	1.30	1.80	2.10	2.60	4.25	4.75	6.30
Dimethyl sulfoxide	0.85	0.85	0.80	0.85	0.75	0.80	0.90
			NaBr				
Methanol	3.30	3.30	3.35	3.40	3.55	3.60	3.65
Formamide	4.10	4.05	4.10	4.15	4.25	4.20	4.15
Dimethylformamide	0.65	1.00	1.45	1.85	2.50	3.10	4.20
Dimethyl sulfoxide	−1.35	−1.20	−1.05	−0.80	−0.50	−0.30	−0.05

^{a} In order to convert to aqueous NaCl at infinite dilution subtract 0.38 ppm. I = insoluble.

It is interesting to note that in formamide (D = 109.5) (Table I) the chemical shifts of all the salts used, do not show concentration dependence and that the positions of the ^{23}Na resonance for each salt are almost identical. These results indicate that over the concentration range studied (0.01–0.50 M) contact ion pairs do not exist. Such

behavior is to be expected in solvents of high dielectric constant.

However, the ^{23}Na chemical shifts in solvents of very low dielectric constant such as tetramethylguanidine (TMG) (D = 11.0) and tetrahydrofuran (THF) (D = 7.6) also show little or no concentration dependence over the
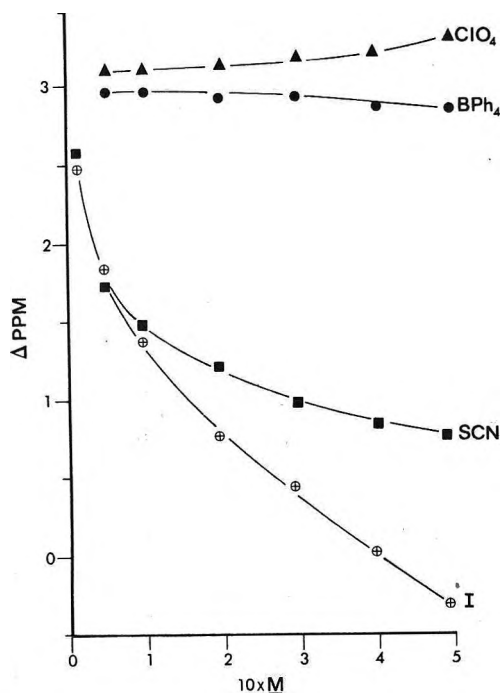
Figure 1. Sodium-23 chemical shift of various sodium salts in 1,1,3,3-tetramethylurea.
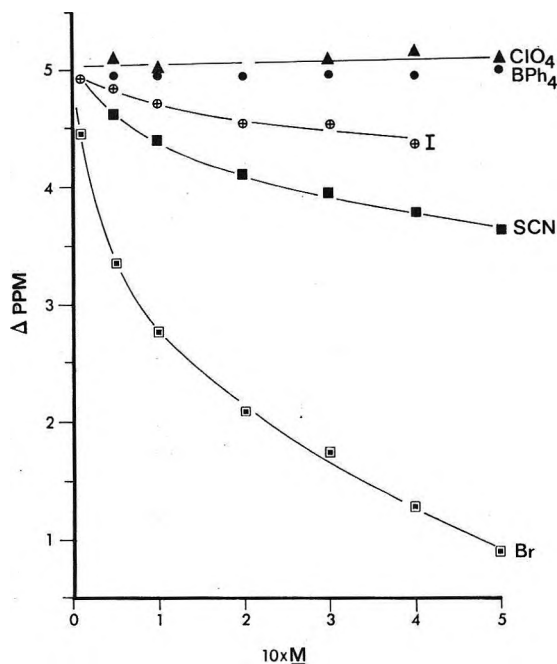

Figure 2. Sodium-23 chemical shift of various sodium salts in N,N-dimethylformamide.
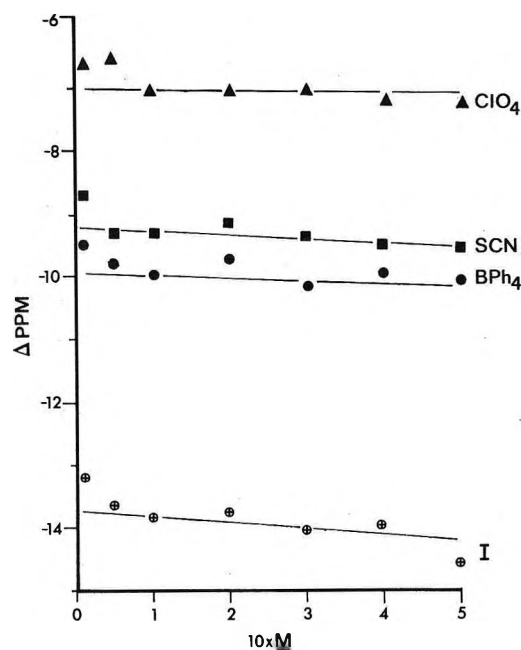

Figure 3. Sodium-23 chemical shift of various sodium salts in 1,1,3,3-tetramethylguanidine.
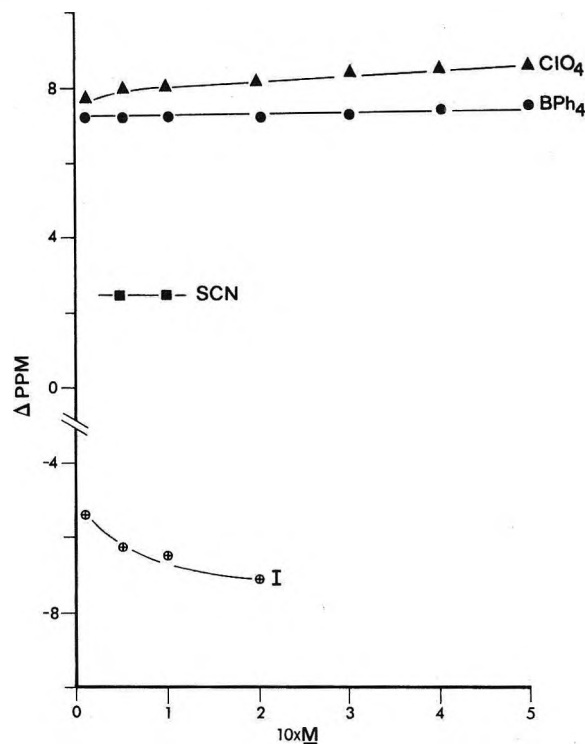

Figure 4. Sodium-23 chemical shift of various sodium salts in tetrahydrofuran.

concentration range studied. The data are presented in Figures 3 and 4. It should be noted, however, that in these solvents the chemical shifts do not converge at lower concentrations as they do in solvents of medium and high dielectric constant. Our measurements could be carried out only down to 0.01 M solutions. In solvents of low dielectric constant, the concentration of *free* ions is vanishingly small in the 0.01–0.50 M concentration range, and the predominant species must be contact ion pairs. It should be noted that in TMG the plots of chemical shifts *vs.* concentration (Figure 3) begin to curve upward in the 0.1–

0.01 M concentration range, where one would expect ion pair dissociation to become observable.

The conductance of NaI solutions in TMG (D = 11.0) and pyridine (D = 12.3) was determined in the 1×10^{-5}–5×10^{-1} m concentration range. The data are shown in Figures 5 and 6. It is seen that the ion pair dissociation is negligible in solutions with concentrations above $\sim 10^{-2}$ m. The conductance data were analyzed by the Fuoss–Shedlovsky technique.[9] For TMG, Λ_0 = 51.6 and the ion pair dissociation constant K_d = 6.2×10^{-5}. In pyridine, Λ_0 = 73.4 and K_d = 3.91×10^{-4}. The latter value agrees
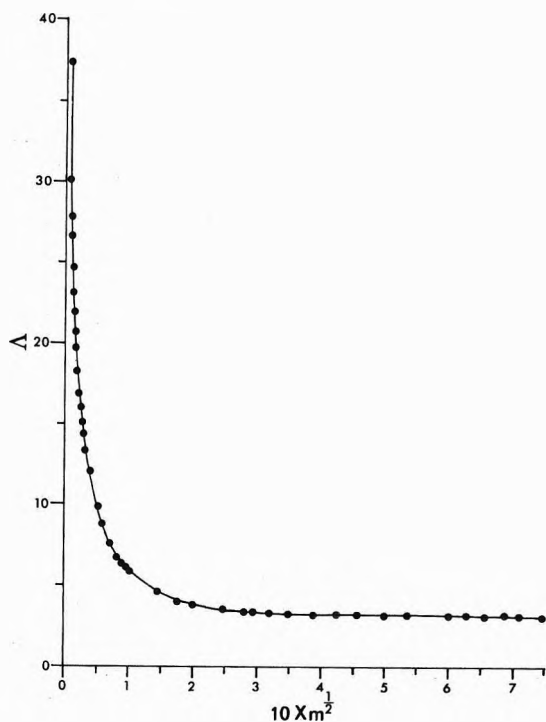
Figure 5. Conductance curve for sodium iodide in 1,1,3,3,-tetramethylguanidine.

Figure 6. Conductance curve for sodium iodide in pyridine.

with K_d = 3.7 × 10^{-4} as determined by Burgess and Kraus.[10] No literature data seem to be available for conductance of sodium iodide in TMG.

Results obtained in hydrogen bonding solvents such as methanol and ethanol show one significant difference as compared to other solvents we studied. As shown in Figure 7 the ^{23}Na resonance observed for NaClO$_4$ and to a lesser extent for NaBPh$_4$ shifts upfield with increasing concentration while in the case of NaI and NaSCN the corresponding shifts are downfield. Upfield shifts have been previously observed for aqueous alkali nitrate solutions.[4] With increasing concentration the alkali metal resonances of the nitrate solutions shifted upfield while those in alkali halide solutions shifted downfield. Similar behavior has been recently observed by Van Geet[5] again, in aqueous solution. While both upfield and downfield shifts with increasing salt concentration are due to increasing cation-anion interaction, it has been postulated[4,5] that the upfield shifts occur when the replacement of a water molecule in the cation solvation shell by an anion results in a decreased electron density around the alkali cation. It is possible that the same explanation applies to the chemical shifts observed in ethanol and methanol solutions.

As we earlier reported[1a] the magnitude of the ^{23}Na chemical shift for solutions of sodium tetraphenylborate and perchlorate exhibit a *linear* relationship with Gutmann's donor number for these solvents[11] provided that the chemical shift is unperturbed by ion–ion interactions. The chemical shift data for two new solvents in this investigation, namely, TMU and sulfolane, fall on this straight line. The donor numbers of methanol, ethanol, and formamide have not been determined experimentally but from the above plot they can be predicted to be 25.7, 31.5, and 24.7, again provided that the chemical shifts are unperturbed by ion–ion interactions.

It should be noted that, while the solvation process involves electrostatic ion–dipole interactions, the donor numbers represent the enthalpy of formation of a covalent
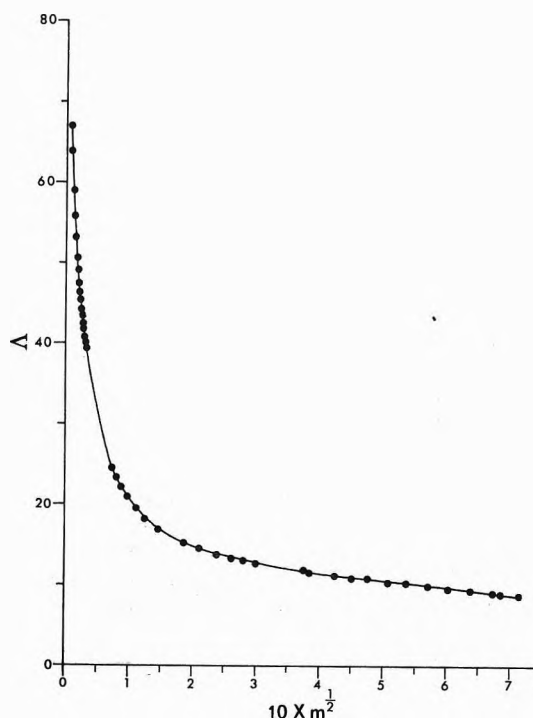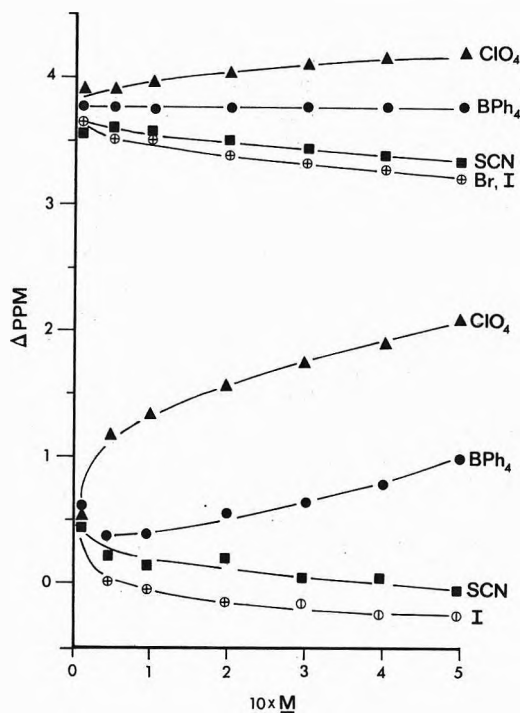
Figure 7. Sodium-23 chemical shift of various sodium salts in methanol and ethanol.

bond between a given solvent and antimony pentachloride.[11] *A priori* it seems, therefore, that one should not expect a parallelism between the solvating abilities of solvents toward alkali metal cations and their tendency to form covalently bonded complexes with SbCl$_5$. As Gutmann points out,[12] however, the fact that such parallelism exists strongly suggests that some covalent interaction is involved in the solvation of Na$^+$ ion by donor solvents and that the extent of covalency in the solvation bonds increases with the solvent donicity.
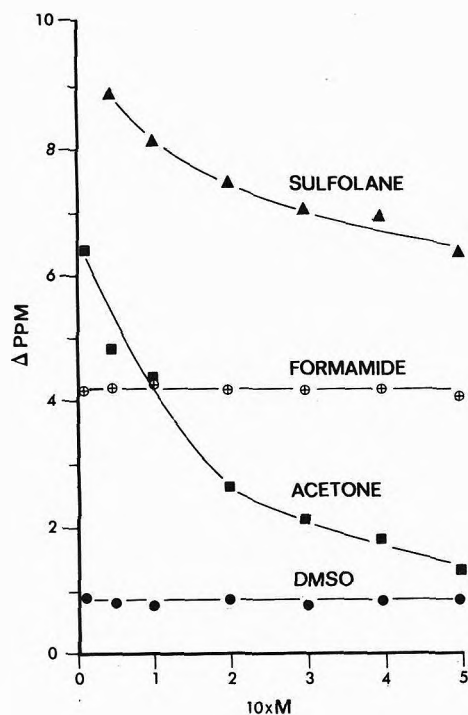
Figure 8. Sodium-23 chemical shift of sodium iodide in sulfolane, formamide, acetone, and dimethyl sulfoxide.

The fact that the donor properties of solvents can strongly influence ion pair dissociation has been shown by Gutmann.[12,13] Our data clearly show such dependence. For example, formamide (D = 109.5, DN = 24.7) has a high dielectric constant and a medium donor number, so that the formation of ion pairs in the 0.01–0.50 M concentration range would not be expected. This conclusion seems to be confirmed by our data (Figure 8). The comparison of dimethyl sulfoxide, sulfolane, and acetone with the dielectric constants of 46.7, 44, and 20.7 and the donor numbers of 29.8, 14.8, and 17.0, respectively, shows the importance of the donicity of the solvent in contact ion pair formation. While dimethyl sulfoxide and sulfolane have nearly identical dielectric constants, the former is a much better solvation agent. We would expect, therefore, that contact ion pair formation would be more probable in the latter solvent. Indeed, the [23]Na chemical shift for NaI shows no concentration dependence in dimethyl sulfoxide

but marked concentration dependence in sulfolane. On the other hand, acetone and sulfolane have nearly the same donicity but the latter has a much higher dielectric constant. Qualitative indications from our data are that the tendency toward ion pair formation in acetone is much higher than in sulfolane. Additional evidence has been obtained in propylene carbonate solutions.[14] This solvent has a high dielectric constant of 65.0 but a relatively low donor number of 15.1. The [23]Na chemical shifts for sodium iodide solutions are strongly concentration dependent thus indicating that despite the high dielectric constant, the formation of contact ion pairs occurs to a considerable extent.

While at the present time only qualitative indications of contact ion pair formation have been obtained from [23]Na chemical shifts, it seems reasonable to assume that these data can be used for the determination of the ion pair formation constants. It would be interesting to compare the nmr results with the values obtained from conductance measurements where it is often quite difficult to distinguish between contact ion pairs and solvent-separated ion pairs. Such studies are now in progress in our laboratory.

References and Notes

(1) (a) R. H. Erlich, E. Roach, and A. I. Popov, *J. Amer. Chem. Soc.*, **92**, 4989 (1970); (b) R. H. Erlich and A. I. Popov, *ibid.*, **93**, 5620 (1971); (c) M. Herlem and A. I. Popov, *ibid.*, **94**, 1431 (1972); (d) R. H. Erlich, M. S. Greenberg, and A. I. Popov, *Spectrochim. Acta, Part A*, **29**, 543 (1973).

(2) E. G. Bloor and R. G. Kidd, *Can. J. Chem.*, **46**, 3425 (1968).

(3) R. E. Richards and B. A. Yorke, *Mol. Phys.*, **6**, 289 (1963).

(4) C. Deverell and R. E. Richards, *Mol. Phys.*, **10**, 551 (1966).

(5) (a) G. J. Templeman and A. L. Van Geet, *J. Amer. Chem. Soc.*, **94**, 5578 (1972); (b) A. L. Van Geet, *ibid.*, **94**, 5583 (1972).

(6) D. H. Live and S. I. Chan, *Anal. Chem.*, **42**, 791 (1970).

(7) H. B. Thompson and M. T. Rogers, *Rev. Sci. Instrum.*, **27**, 1079 (1956).

(8) H. M. Daggett, E. J. Bair, and C. A. Kraus, *J. Amer. Chem. Soc.*, **73**, 799 (1951).

(9) T. Shedlovsky, *J. Franklin. Inst.*, **225**, 739 (1938).

(10) D. A. Burgess and C. A. Kraus, *J. Amer. Chem. Soc.*, **70**, 706 (1948).

(11) (a) V. Gutmann and E. Wychera, *Inorg, Nucl. Chem. Lett.*, **2**, 257 (1966); (b) V. Gutmann, "Coordination Chemistry in Nonaqueous Solvents," Springer Verlag, Vienna, 1968.

(12) U. Mayer and V. Gutmann, *Struct. Bonding (Berlin)*, **12**, 113 (1972).

(13) V. Gutmann, "Chemische Functionslehre," Springer-Verlag, Vienna, 1971, pp 65–67.

(14) M. S. Greenberg, D. M. Weid, and A. I. Popov, in press.

Lasing Action and the Relative Populations of Vibrationally Excited Carbon Monoxide Produced in Pulse-Discharged Carbon Disulfide–Oxygen–Helium Mixtures

S. Tsuchiya,[1] N. Nielsen, and S. H. Bauer*

Department of Chemistry, Cornell University, Ithaca, New York 14850 (Received November 27, 1972; Revised Manuscript Received June 18, 1973)

Lasing was initiated by a fractional microsecond pulse discharge (≈ 15 kV) in flowing CS_2-O_2-He mixtures, maintained at about 3 Torr. Two types of cavities were tested: one with two spherical mirrors and the other with a grating for wavelength selection. In the first configuration we determined the optimum discharge voltage to maximize laser power. When the impressed voltage was higher than the optimum, CS and O generated by fragmentation of the CS_2 and O_2 apparently were directly involved in the lasing reaction. When the discharge voltage was lower, a chain reaction was the principal mechanism for lasing. In the turned cavity, the measured τ_d's (intervals between termination of the discharge and initiation of lasing) followed a characteristic sequence; the minimum delay (≈ 10 μsec) occurred for the $12 \rightarrow 11$ transition, with longer times for higher and lower vibrational states. The recorded delay sequence was explained on the basis of the initially generated distribution of vibrationally excited CO. The relative populations were also estimated from chemiluminescence intensities recorded under conditions identical with laser operation but in the absence of mirrors; these are $\varphi_{17}/.../\varphi_1 = 0.13/0.34/0.56/0.77/1.00/0.97/0.89/0.80/0.71/0.67/0.62/0.58/0.55/0.52/0.82/1.13/2.38$, in general agreement with the laser delay measurements. While this distribution is close to that reported from other laboratories for $v > 8$, there is a significant difference for the $v \leq 7$ range, in that our data show that substantial fractions are also generated in the low v states.

Introduction

The reaction between carbon disulfide and oxygen which, under suitable conditions, generates inverted populations of vibrationally excited CO, has many intriguing aspects. While this process has been investigated assiduously during the past 5 years, and a concensus has been reached regarding the principal reactions, as yet no clear identification of all the essential steps has been presented, nor has any detailed study been made of the lifetimes and concentrations of intermediates in the chain which must be present in the flame laser.[2] Only a few quantitative measurements of the reaction rates have been published.[3-6] For computer modeling of CS_2-O_2 lasers it is essential to establish the partition of vibrational energy among the wide range of states as initially produced in the pumping reaction. We have no knowledge of any proposed three-center potential energy surface for the S-C-O system nor of trajectory calculations on such a surface which would provide from a theoretical analysis some inkling of how the exothermicity is distributed in the product species.

In this manuscript we report on the deduction of the vibrational population distribution for the nascent species from measurements of delay times for lasing (τ), at specified frequencies, subsequent to initiation of the reaction by a pulsed electrical discharge. We have also measured relative chemiluminescence intensities under conditions identical with the above but in the absence of cavity mirrors. In the meantime the reports by Hancock and Smith[6,7] provided complementary data on this distribution, based on their measured chemiluminescence intensities in a flow apparatus. Dawson and Tam[8] developed laser models based on Hancock and Smith's distribution. The results of these investigations are compared with ours. Also, we made preliminary measurements on CS level populations *via* uv absorption spectra. While these data are as yet qualitative, their implications regarding the mechanism were unexpected and significant.

Apparatus

The laser tube is 1 m long and 2.54 cm in diameter. Two aluminum ring electrodes are placed at each end, and between them the charge from a capacitor (0.01 μF) is released through an ignitron (WL-7703), which is triggered at a rate of 6 Hz. The current pulse width depends on the pressure and composition of the gas, as well as the voltage; shorter pulse widths and larger peak currents result from higher discharge voltages. A typical combination has a half-width of 0.3 μsec, a peak current of 550 A in a mixture consisting of 0.05 Torr of CS_2, 0.35 Torr of O_2, and 1.8 Torr of He, for a discharge voltage of 15 kV.

Fine needle valves (vernier settings) were used to control the flow of each gas. The flow rates were calibrated by measuring the rate of decline of pressure in a vessel of known volume. Most of the experiments were done with mixtures of CS_2 0.015 $\sim$ 0.05 Torr, O_2 0.01 $\sim$ 0.8 Torr, and He 2 $\sim$ 3 Torr, and a linear flow velocity of 8 m/sec.

Two types of cavities were tested. In the first, two gold-coated spherical Ge mirrors with a radius of 4 m were used. The mirrors were placed 1.5 m apart, and one had an uncoated hole in the center of 0.75 mm diameter, for coupling out the laser emission. The total power generated in the laser was monitored by a Au-doped Ge detector through a tilted NaCl plate with rough surfaces used for attenuation, and an ir filter having a flat response between 4.1 $\sim$ 5.6 μ. The output from the detector passed through an FET impedance reducer, and was displayed on an oscilloscope (Tektronix 535). For dispersed wavelength studies, an ir grating monochromator, Perkin-Elmer 88G, with a Bausch and Lomb, 150 lines/mm grating blazed at

6 μ, and a Au-doped Ge detector (Santa Barbara Research Lab, 70R) were used. The monochromator was calibrated by measuring several lines of a low-pressure mercury lamp in high orders. The wavelength response of the monochromator and detector system was calibrated by recording the emission of a Nernst glower whose temperature was measured with an optical pyrometer, assuming the emissivity was constant over the 0.65-5-μ region. In order to measure integrated power the vertical signal output from the oscilloscope was passed through a pulse stretcher in which the signal was integrated by a 0.47-μF capacitor through a Ge diode, and lead to the input of a lock-in amplifier (PAR Model 120); the reference signal was synchronized with the trigger pulse that initiated the discharge. The accuracy of response of the lock-in amplifier output was compared with the total power obtained by integration of the laser pulse as displayed on the oscilloscope. The proportionality between the two measured outputs was good except for very weak laser signals.

In the second arrangement a wavelength controlled cavity was used. A grating (Bausch and Lomb, 300 lines/mm, blazed at 3.5 μ) was set at one end, replacing the totally reflecting spherical mirror. The measuring system remained the same as for the conventional cavity. Since the laser transitions of CO are close to each other, it was difficult to isolate a single transition by tuning the grating. Most of the tuned laser lines were accompanied by two or three weak satellite lines. Usually, an effort was made to reduce the intensity of these satellite lines to less than 10% of the main oscillating lines. Thus cascading due to stimulated transitions had little effect on the measured delay times of the laser pulses.

Chemiluminescence intensities at the CO fundamental were measured from one end of the laser tube. The brewster angle window was replaced with a NaCl plate set perpendicular to the axis, and the region close to the end of the tube was imaged onto the slit plane of the monochromator with a spherical mirror, focal length = 10 cm. Emissions that originate in the farther portions of the discharged gas made only small contributions to the recorded intensities. The signal from the monochromator was sampled with a Boxcar integrator, PAR 160, for a duration of 2.5 μsec using a constant preset delay after the discharge. The monochromator was scanned very slowly over the wavelength region 4.5-5.8 μ. Thus the emission spectrum by $CO^{(v)}$ at a given delay time could be obtained. The recorded spectrum did not change when the discharge pulse rate was reduced from 6 to 3 Hz. Hence 1/6 sec was long enough to sweep out the reaction products prior to the subsequent initiation, and if any products did remain in the tube, they did not contribute significantly to the chemiluminescence.

Experimental Results

Studies with a Conventional Cavity. Figures 1a and 1b are oscilloscope records of the laser pulses. These clearly show delays after initiation by the discharge. In the O_2-rich case, the laser power peaks very rapidly and then decreases in an oscillatory manner. In contrast, for low O_2 content, the laser pulse delays are longer, and the pulses attain their maximum more gradually. Low discharge voltages in mixtures with excess O_2 show pulse shapes very similar to the case of low O_2 content. Thus, two types of pulse shapes were found: one for high discharge voltage and O_2-rich mixtures, and the other for low discharge voltages and either low or high O_2 content. The
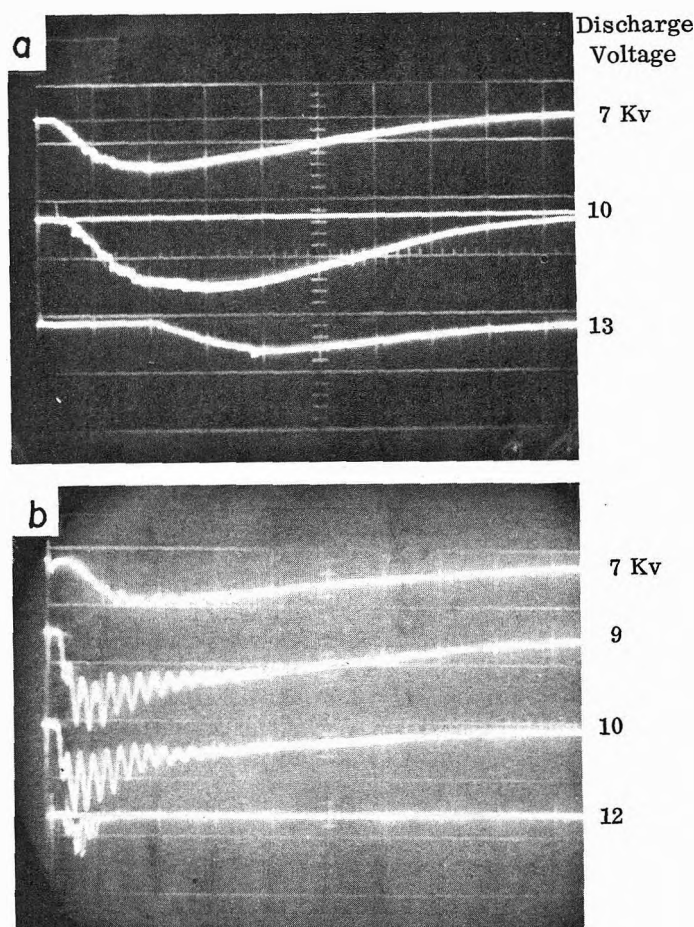

Figure 1. Signal profiles as a function of discharge voltage and O_2 content. Time progresses from left to right: (a) abscissa 200 μsec/cm; ordinate 0.1 V/cm; CS_2 = 0.018 Torr, O_2 = 0.037 Torr, He = 1.85 Torr, total = 1.90 Torr; (b) abscissa 100 μsec/cm; ordinate 0.2 V/cm; CS_2 = 0.018 Torr, O_2 = 0.36 Torr, He = 1.79 Torr, total = 2.16 Torr.

observed time dependence of laser emission intensity on mixture composition and discharge conditions reflects the effect of differing levels of reactive fragments initially generated in the lasing medium. The oscillations of the laser pulse may be related to radially propagating acoustic waves. The period of oscillation does not depend on the discharge voltage. However, the addition of He to the system while maintaining constant CS_2 and O_2 content results in a reduction of the period of oscillation as well as of its amplitude. This correlates with the higher sound velocity and the more homogeneous appearance of the discharge when additional He was present; note Figure 2.

The dependence of the integrated laser power on the discharge voltage and O_2 concentration is shown in Figure 3. The optimum discharge voltage depends on the O_2 content. One can account for the indicated trend if it is assumed that there is an optimum discharge voltage for the formation of CS from CS_2 and that the concentration of O atoms increases with the discharge voltage; the former is supported by the uv absorption measurements of CS. At high discharge voltages the laser power increases monotonically with CS_2, as does the optimum discharge voltage. This is reasonable, because a larger amount of energy is required to decompose the CS_2 to CS.

The overall effect of added He is small. With increasing He pressure, the optimum discharge voltage for laser power shifts slightly to the high side, but the power does
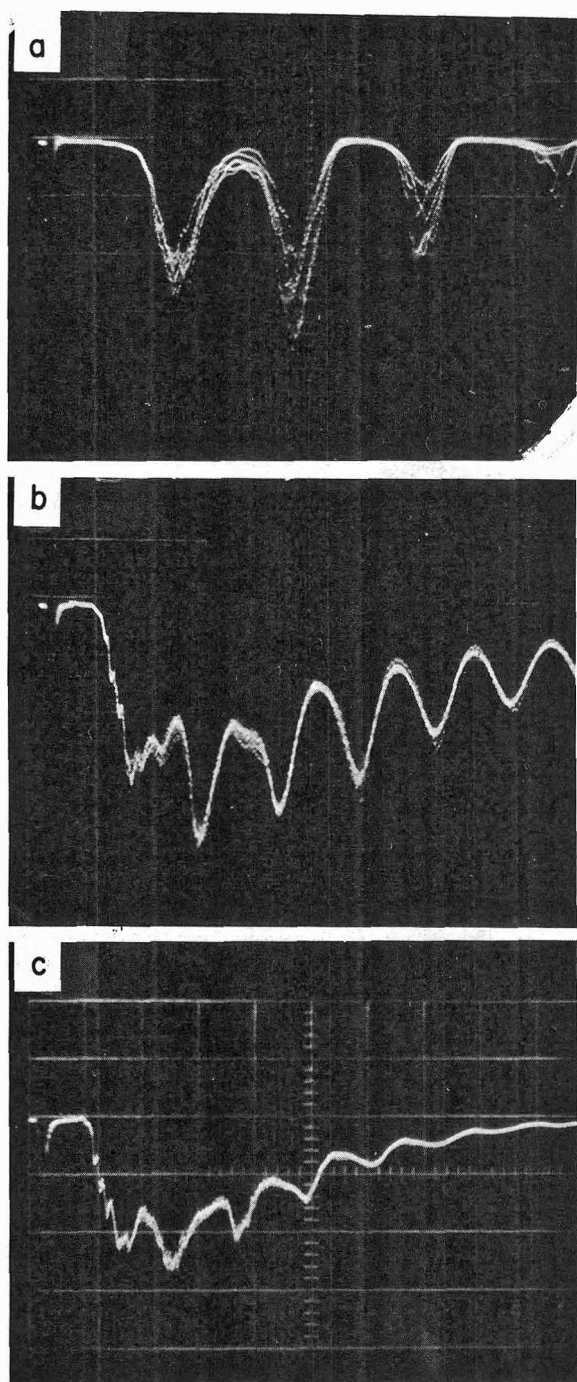
Figure 2. Signal profiles as a function of He content: (a) CS_2 = 0.02 Torr, O_2 = 0.85 Torr, He = 0 Torr, 20 μsec/division, 10 kV; (b) CS_2 = 0.02 Torr, O_2 = 0.6 Torr, He = 3.1 Torr, 20 μsec/division, 10 kV; (c) CS_2 = 0.02 Torr, O_2 = 0.6 Torr, He = 6.6 Torr, 20 μsec/division, 12 kV.

		CS$_2$	O$_2$	He
○	#1	.017	.68	1.69
△	#2	.017	.35	1.75
□	#3	.018	.18	1.76
●	#4	.018	.11	1.81
▲	5	.018	.018	1.82

Figure 3. Integrated power dependence on O_2 partial pressure.
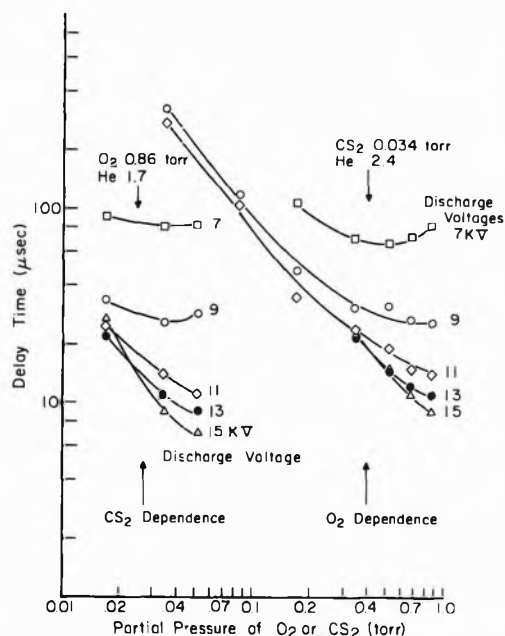
Figure 4. Dependence of delay times on operating conditions.

not change. Apparently, the He atoms act as decelerators for the electrons. A shift of the optimum discharge voltage was also observed when the size of the discharge capacitor was changed. With 0.01 μF, a mixture of (0.016 Torr of CS_2, 0.68 Torr of O_2, and 1.7 Torr of He) produces peak power at 9.5 kV; with a 0.0036-μF capacitor, the peak power for the same gas mixture was observed at 14.5 kV. The two cases have almost the same electrical energy: 0.45 and 0.38 J, respectively.

The delay times for the initiation of laser pulses are determined by the discharge voltage as well as the CS_2 and O_2 concentrations. As shown in Figure 4, the dependence is complex. This is not unexpected since the nature of the discharge depends on the amount of CS_2 and O_2 present. In this respect, some information was obtained from measured current pulses. For voltages higher than 10 kV, the half-width was generally constant, at about 0.3 μsec, and was not affected by small changes in CS_2 or O_2. However, for discharge voltages below 10 kV the half-width was larger, and an increase in CS_2 or O_2 produced an increase in the half-width. This implies that the addition of CS_2 or O_2 to the system reduced the discharge peak current, i.e., the resistance of the discharge gas was larger. Thus, when the system has sufficient discharge energy, the extent of dissociation is proportional to the CS_2 and O_2 content, and the lasing process is accelerated. From Figure 4, it
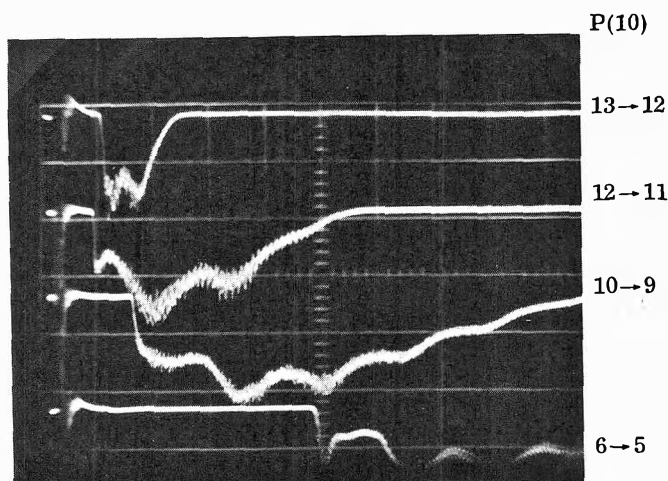
Figure 5. Change of time delay for initiation of P(10) laser pulse, as a function of vibrational level (abscissa: 20 μsec/ division; ordinate for $v = 13 \to 12$ through $v = 6 \to 5$ transitions: 0.01, 0.05, 0.05, 0.02 V/division).
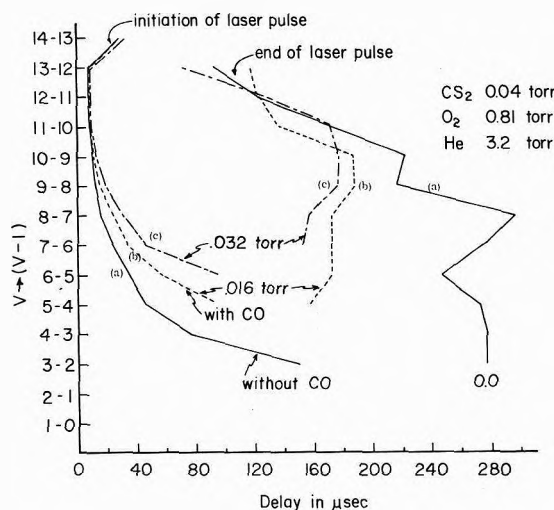
Figure 6. Time history of P(9) lasing line, for no added CO (a); 0.016 Torr of CO added (b); 0.032 Torr of CO added (c).

appears that when the discharge voltage is $11 \sim 15$ kV the inverse of the delay time (τ) is proportional to the O_2 and CS_2 concentrations: $(1/\tau) \propto [CS_2][O_2]$.

Ninety vibration–rotation lines were recorded; these were assigned to various transitions from $v = 14 \to 13$ to $v = 2 \to 1$. The spectra were taken for a gas mixture consisting of (0.017 Torr of CS_2, 0.68 Torr of O_2, and 1.7 Torr of He); the discharge voltages were 7, 9, and 12 kV. For 7-kV discharges, the recorded laser transitions were mostly P(16) $\sim$ P(11) of $v = 14 \to 13$ to $v = 4 \to 3$. The spectrum initiated by 12 kV showed P(19) $\sim$ P(14) of $v = 13 \to 12$ to $v = 6 \to 5$ transitions; that produced with 9-kV discharges exhibited characteristics of both the low and high voltage initiations. Possibly the higher J transitions are favored for the higher voltage discharges because the corresponding rotational temperatures of the system are higher. When the sums of intensities of the various rotational transitions for each vibrational transition were plotted vs. ($v \to v - 1$), maxima appeared at $v = 11 \to 10$ for the high voltage and at $v = 9 \to 8$ for the low voltage discharges. This suggests that in higher voltage discharges there is a larger contribution to the emitted intensity from chemical pumping in contrast to secondary effects, such as collisional or stimulated transitions.
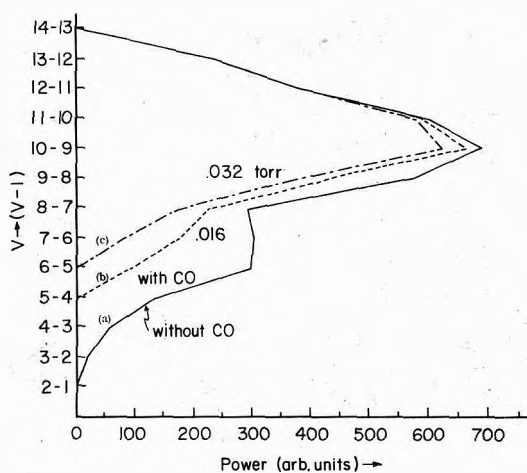
Figure 7. Dependence of integrated power for P(9) on vibrational transition and the amount of added CO. (Conditions same as in Figure 6.)

Measurements with a Tuned Cavity. To eliminate the effect of stimulated transitions, laser oscillations for specific rotation–vibration transitions were selected with the aid of a grating. These measurements were carried out mostly with a 15-kV discharge because the former experiments suggested that under high voltage conditions the species produced by the discharge contributed directly to lasing.

Typical oscilloscope traces that show a sequence of delay times for lasing on the P(10) transition, as these depend on $v \to v - 1$, are reproduced in Figure 5. Each transition starts with a sharp rise at a distinct delay time $\tau_{v,v-1}(J)$. The graphs in Figure 6 show the dependence of $\tau_{v,v-1}(J)$ on $v \to v - 1$, and indicate the effect of added CO. Also shown are the estimated termination times for the corresponding laser pulses. It is evident that the addition of a small amount of CO has little effect on $\tau_{v,v-1}(J)$ for the initiation of lasing for $v \geq 9$, but produces progressively increasing delays, up to about a factor of 2, for the lower v's down to $v = 5$. Depending on the CO content the intensities for the lower transitions diminish. At a partial pressure of CO half of that of the initial CS_2 the effect is marked. Added CO also reduces the duration of lasing for transitions from levels lower than $v = 9$ (Figure 6), thus accounting for the decrease in measured total integrated intensities at P(9) for each vibrational transition; the effect is marked for transitions from $v \leq 9$, as shown in Figure 7. The decrement is monotonic with the amount of gas added. This effect will be discussed further below.

Measurement of Spontaneous Emission. The emission spectra of the CO fundamental were recorded at specified delay times after the discharge pulse to establish the time dependence of the population distribution for each vibrational level. The emission was too weak to permit measurement of individual rotation–vibration lines, and the higher vibrational transitions overlap appreciably. The monochromator slits were set so that the equivalent triangular slit function had a width of 2.9 cm^{-1} at half-height. A computer program was written to select by a least-squares method the "best" vibrational distribution that simulated the observed spectrum. The procedure is similar to that described by Horn and Ottinger.[9] The wave numbers for the lines were calculated from the molecular constants reported by Mantz, *et al.*;[10] values for the spontaneous emission coefficients and for the vibration–rotation interaction factors were given by Fisher,[11] and by
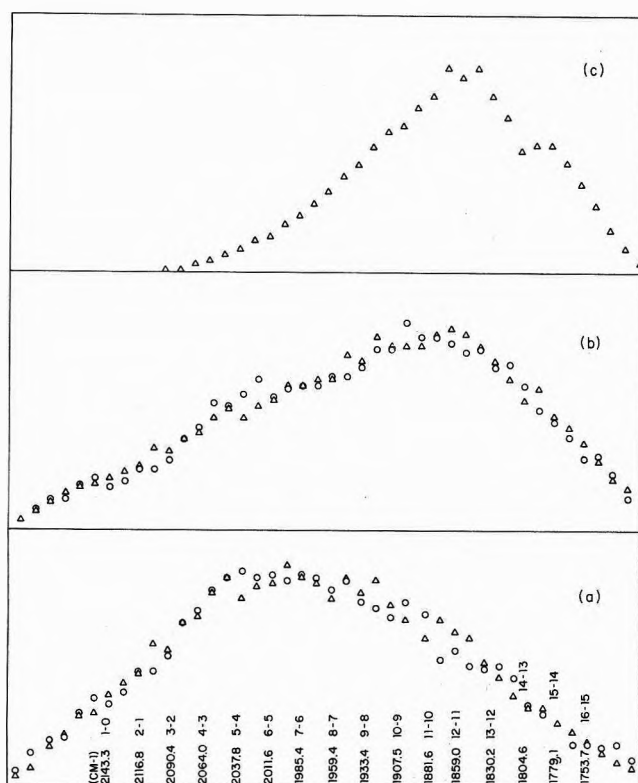
Figure 8. Observed ($\circ$) vs. calculated ($\triangle$) superposed spectral intensities of CO spontaneous emissions: 0.045 Torr of CS_2 plus 0.76 Torr of O_2 plus 3.0 Torr of He; 15 kV discharge; (a) 148 μsec after the discharge pulse, (b) 23 μsec, (c) calculated spectrum on the basis of the Hancock, Morley, and Smith distribution (ref 7).

Figure 9. Normalized vibrational population at selected delay times. The experimental conditions are those for Figure 8.

Toth, et al.,[12] respectively. Figure 8 shows three examples of the observed and calculated spectra.

To estimate the rotational temperature, a small amount of HCl (0.14 Torr in 3.8 Torr total pressure) was introduced to serve as a trace radiator, and the relative intensities of the R(0)-R(6) lines of the fundamental band for HCl were measured. The data were corrected for self-absorption by the method of Ladenburg and Levy.[13] The estimated temperatures were 440 and 450°K at 11.5 and 26.5 μsec, respectively, after a 15-kV discharge pulse. These values are lower limits, because the added HCl does extract some portion of the discharge energy. However, the temperatures so deduced were used in the analysis of the delay data and the CO fluorescence results because tests showed that ±50°K does not lead to significantly different results.

The principal sources of inaccuracy in the above procedure are lack of a precise rotational temperature, absorption by water vapor in the region of the higher vibrational transitions, and overlap of the CO emission by that of OCS. The first was readily checked by recalculation, using 400 and 500°K as trial temperatures. The changes in the resulting distributions were less than 10%. Regarding interference by water, the monochromator was flushed with dry N_2, while the light path of about 30 cm from the laser tube to the spectrometer slit was left open to the air. Absorption by water was clearly indicated. Therefore, our deduced distribution at the *high vibrational states* $v = 12$ ~ 17 may be somewhat *underestimated*. With respect to OCS absorption, Hancock and Smith[6] in their study of the O-CS_2 system found that emission by OCS did overlap the CO fundamentals. However, we found that when a
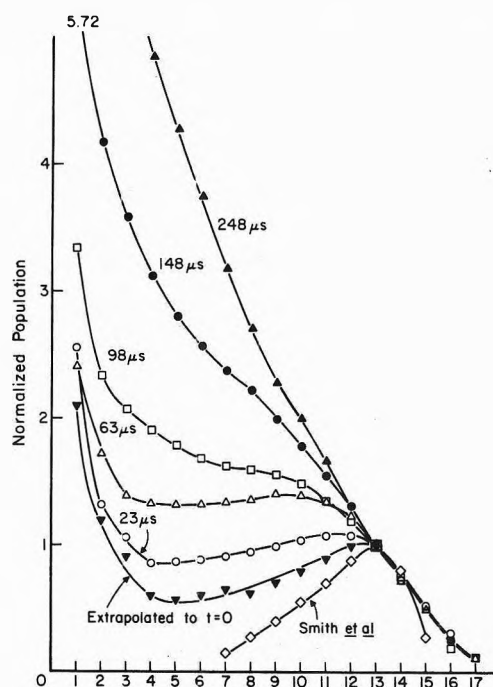
cell 10 cm in length filled with OCS at 1 Torr was placed in front of the entrance slit of the monochromator, no change in the spectrum was observed. Hancock and Smith suggested that at most 1.5% of the CS_2 is converted to OCS in O_2-rich mixtures. Hancock and Smith[14] showed that the v-v transfer probability between CO in $v = 7 \sim 4$ levels and OCS was of the order of 10^{-1}, but this estimate also includes collisions with CO in any state. If the excitation of OCS is due to collisions with CO, 10 collisions require about 40 μsec. Note that the pressure of CO cannot exceed the initial pressure of CS_2 (which in these experiments is less than 0.05 Torr) and CO starts at zero and increases exponentially (following the initiation discharge pulse) with a first-order rate constant $\approx 10^4$ sec^{-1}. Therefore, the contribution of OCS emission to the spectrum cannot be large during the first 100 μsec after the discharge. Were *excited* OCS *generated directly*, an overestimate of CO population at $v = 5 \sim 3$ may occur, depending on the rate of OCS* formation.

In Figure 9 the relative population distributions, normalized to unity at $v = 13$, are shown for a range of delay times after the discharge pulse. At a delay of 23 μsec a peak in the population appears at $v = 11$ or 12 and a minimum occurs at $v = 4$. As the delay time increases, the peak shifts to lower v values and the distribution becomes more Boltzmann-like. The "initial distribution" was estimated by graphical linear extrapolation to $t = 0$. Figure 9 shows the results of Hancock, Morley, and Smith.[7]

To obtain the rate of formation of CO, the observed relative populations in levels $v = 1$ to $v = 17$ were summed; this is shown in Figure 10. Since the population in the $v = 0$ level cannot be observed, and the relaxation process produces a significant amount of CO in the ground state during the latter stages, we were forced to estimate CO ($v = 0$) by linear extrapolation from the higher levels; this is subject to considerable uncertainty. The *estimated* total CO was also plotted in Figure 10. Carbon monoxide accumulates exponentially

$$[CO] \propto (1 - e^{-k_0 t}) \tag{1}$$

S. Tsuchiya, N. Nielsen, and S. H. Bauer

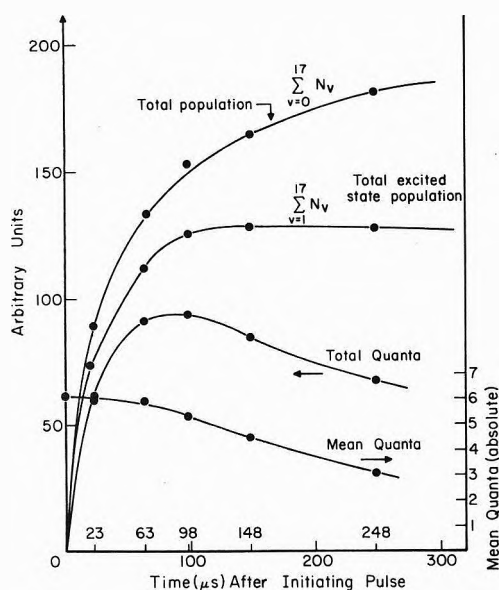**Figure 10.** Total population, total excited state population, total vibrational quanta, and average quanta per $CO^{(v)}$ as a function of time. The data are from Figure 9.

where $k_0 = 2.3 \times 10^4 \text{ sec}^{-1}$, when the initial pressures of He, O_2, and CS_2 are 3.1, 0.75, and 0.046 Torr, respectively, and the discharge voltage is 15 kV. It is interesting to note (Figure 11) that the decrease of [CS] follows a decay rate that closely parallels the growth of CO.[15] The concentration of $CS^{(0)}$ in the ground electronic state was estimated from the decline in absorption at λ 2511 [1,0 band head at λ 2507.3]. The characteristic radiation for these measurements was generated by a discharge through CS_2-O_2-He mixtures in a TEA configuration. The relative populations in states $v = 0$ to 4 were obtained from absorption intensities at λ 2511, 2523, 2539, 2555, and 2710; these indicated a vibrational temperature for CS^* of 12,300°K for 15-kV discharges.

Of the two types of relaxation processes that deactivate excited CO, v-v energy transfers are near-resonant exchanges which can efficiently modify the initial distribution of $CO^{(v)}$ generated in the reaction. An upper limit for the collision number of $CO^{(v)}$ with CO, during a time (τ) after the initiation of reaction, can be calculated from

$$Z = \int_0^\tau \sigma^2 (8\pi kT/\mu)^{1/2} N(1 - e^{-k_0 t}) dt \qquad (2)$$

where σ is a collision diameter (3.7 A), μ the reduced mass of a CO-CO pair, and N is assumed to be the initial concentration of CS_2 at 0.05 Torr, since this limits the amount of CO produced. Numerical estimates show that a $CO^{(v)}$ generated chemically makes on the average 2.4 collisions with another CO during the first 23 μsec. However, the v-v collision probability divided by the vibrational quantum number for CO (P_{v-v}/v) is less than 10^{-2}.[14] Hence, the mean collision number of 2.4 during 23 μsec is too small to produce a significant deviation from the initial distribution. At somewhat longer times, the vibrational population is altered by v-v transfers, but not the total number of vibrational quanta, in contrast with v-T transfers which reduce that number. The average number of vibrational quanta per CO generated in the initial distribution is estimated to be 6.0, which corresponds to 42% of the exothermicity of the pumping reaction: CS + O $\rightarrow$ $CO^{(v)}$ + S. The total number of quanta is conserved during the first 60 μsec after the discharge; then it gradually

The ordinate is either $\left\{ 1 - \dfrac{[CO]}{[CO]_\infty} \right\}$ or $\left\{ \dfrac{[CS] - [CS]_\infty}{[CS]_0 - [CS]_\infty} \right\}$
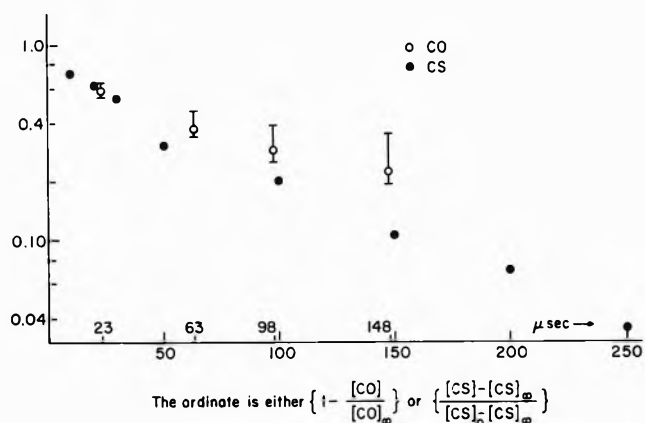
Figure 11. Time history of total CO and $CS^{(0)}$ concentrations subsequent to initiation by a 15-kV pulse. From the absorption intensities at the indicated band head locations ($\Delta\lambda = 15$ Å), relative populations were estimated for CS($v = 0 \ldots 4$). These were extrapolated to $t \rightarrow 0$ and plotted to deduce an effective vibrational temperature ($\approx 12,300°$K).

decreases. The decrement rate after 60 μsec is about $4 \times 10^3 \text{ sec}^{-1}$, which is much larger than the spontaneous emission rate for $v = 6 \rightarrow 5$ [$1.61 \times 10^2 \text{ sec}^{-1}$]. v-T relaxation of CO in collisions with He or O_2 is very inefficient at room temperature, so that the CO is effectively deactivated either at the walls of the tube or by collision with the "active" species, such as O, S, or CS.

Interpretation of τ_v's. Since the total CO concentration increases exponentially before relaxation processes become dominant, the population of level v may be expressed by

$$N_v = \varphi_v N(1 - e^{-k_0 t}) \qquad (3)$$

where N is the steady-state concentration and $\varphi_v = k_v / \Sigma_v k_v$ is the fraction channeled to that level. Even though the distribution of CO changes rapidly, as shown in Figure 9, the above analysis shows the v-v relaxation is not significant during the first 20 μsec after the discharge pulse. We recorded delay times of less than 20 μsec, except for the lower vibrational transitions. The latter were disturbed by v-v relaxation, because the addition of a small amount of CO significantly affected their delay times. However, laser pulse delays from 14-13 to 7-6 can be interpreted in terms of the initially generated distribution.

To deduce population ratios for adjacent levels from laser delay data an additional assumption was made, that the loss in the cavity was independent of a small change in the grating angle, which is in the range of 7°. The theoretical gain for a P-branch transition, $(v, J - 1) \rightarrow (v - 1, J)$ is

$$\alpha_{v,v-1}(J) = [8\pi^3 c^4 A_{v,v-1}/3kT(2\pi kT/m)^{1/2}]J\bigg[N_v B_v \times$$

$$\exp\bigg\{ -F_v(J - 1)\frac{hc}{kT} \bigg\} - N_{v-1}B_{v-1} \exp\bigg\{ -F_{v-1}(J)\frac{hc}{kT} \bigg\} \bigg] \qquad (4)$$

where $A_{v,v-1}$ = transition matrix element for $v \rightarrow v - 1$, N_v = molecule density of CO in level v, m = mass of CO, T = translational = rotational temperature, $F_v(J)$ = rotational term value for vibrational level v [$= B_v J(J + 1) - D_v J^2(J + 1)^2$]. For a sequence of transitions $(v, J - 1) \rightarrow (v - 1, J)$, with J *fixed*, the time-dependent relative gain after the discharge pulse, may be written in terms eq 3

$$\alpha_{v,v-1}(J) = \alpha_{v,v-1}^\infty(J)(1 - e^{k_0 t}) \qquad (5)$$

where

$$\alpha_{v,v-1}^{\infty}(J) = \text{const } A_{v,v-1}\left[\varphi_v B_v \exp\left\{-F_v(J - 1)\frac{hc}{kT}\right\} - \right.$$

$$\left. \varphi_{v-1}B_{v-1} \exp\left\{-F_{v-1}(J)\frac{hc}{kT}\right\}\right] \quad (6)$$

which is the maximum gain were the chemically produced excited species not to make transitions to lower levels. Laser oscillations start when the gain exceeds the cavity loss. Therefore, the delay time $\tau_{v,v-1}(J)$ may be defined by

$$\tau_{v,v-1}(J) = -(1/k_0) \ln\left[1 - (L/\alpha_{v,v-1}^{\infty}(J))\right] \quad (7)$$

where L is the loss in the cavity (equal to α at threshold). When a value for k_0 is available it is more convenient to work with the equation

$$T_{v,v-1}(J) = L/\alpha_{v,v-1}^{\infty}(J) \quad (8)$$

where $T_{v,v-1}(J) \equiv 1 - \exp[-k_0\tau_{v,v-1}(J)]$. When relative values for adjacent φ_v's are available one may compare $T_{v,v-1}(J)$ with that of $T_{v-1,v-2}(J)$

$$\frac{T_{v-1,v-2}(J)}{T_{v,v-1}(J)} =$$

$$\frac{A_{v,v-1}}{A_{v-1,v-2}} \frac{(\varphi_v/\varphi_{v-1})B_v \exp\{-F_v(J - 1)(hc/kT)\} - B_{v-1} \exp\{-F_{v-1}(J)(hc/kT)\}}{B_{v-1} \exp\{-F_{v-1}(J - 1)(hc/kT)\} - (\varphi_{v-2}/\varphi_{v-1})B_{v-2} \exp\{-F_{v-2}(J)(hc/kT)\}} \quad (9)$$

Once a population ratio for one pair of adjacent vibrational levels is specified, the population ratios for other pairs may be derived.

Additional information on population ratios may be derived from the dependence of $\tau_{v,v-1}(J)$ on J. From eq 6 and 8, the following relation is obtained for a *fixed vibrational* transition at *different J's*

$$1/T_{v,v-1}(J) \propto J\left[1 - \frac{\varphi_{v-1}}{\varphi_v}\frac{B_{v-1}}{B_v} \exp\left\{-\left[F_{v-1}(J) - \right.\right.\right.$$

$$\left.\left.\left. F_v(J - 1)\right]\frac{hc}{kT}\right\}\right] \quad (10)$$

Relative values of $1/T_{v,v-1}(J)$ for P(3) to P(22) of the 12 $\rightarrow$ 11 transition for a range of population ratios $\varphi_{11}/\varphi_{12}$ at $T = 450°K$ are plotted *vs.* J in Figure 12. Superimposed on these are $1/T_{v,v-1}$ from observed τ's for $k_0 = 2.86 \times 10^4 \sec^{-1}$. Although there is considerable scatter, on comparing the experimental points with the calculated curves best agreement is indicated for $(\varphi_{11}/\varphi_{12})$ in the range of $0.85 \sim 0.95$. This is consistent with the value of 0.92 derived from the CO spontaneous emission measurements.

To estimate population ratios within this range of $(\varphi_{11}/\varphi_{12})$'s, eq 9 was applied, assuming 0.80, 0.85, and 0.90. The results are shown in Table I. They are compared with the relative population distributions deduced from the spontaneous emission measurements obtained in this laboratory and those reported by Hancock, Morley, and Smith.[7] The assumption $\varphi_{11}/\varphi_{12} = 0.8$ gives a ratio for (φ_7/φ_6) which is negative; this is physically unacceptable. However, for $(\varphi_{11}/\varphi_{12}) = 0.85 \sim 0.9$ the relative populations derived from the τ values are in general agreement with those from the spontaneous emission measurements, except for the low v's, $7 \sim 5$. As shown in Figure 6, for transitions lower than $8 \rightarrow 7$ the relatively long delays are significantly affected by added CO. Hence it is not valid to assume that the population of levels lower than $v = 8$ are predominantly determined by the chemical production
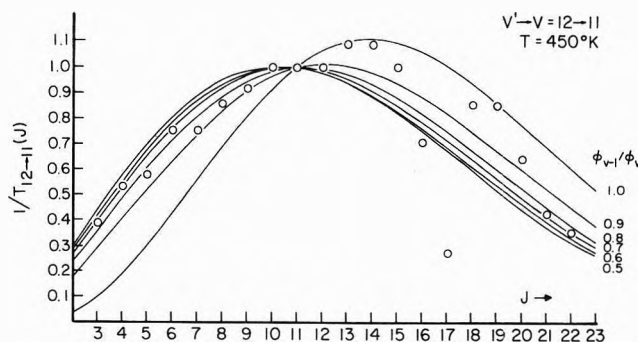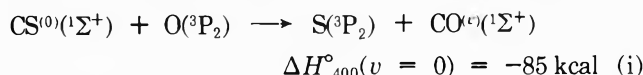

Figure 12. Dependence of $1/T_{12,11}(J)$ on φ ratio. The observed (O) were normalized to the calculated curves at P(11).

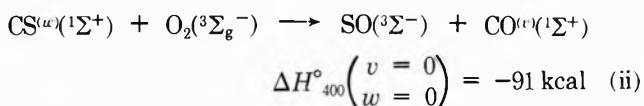step at a time when the laser begins to oscillate at these transitions.

One may compare the gain calculated from the distribution based on the spontaneous emission measurements with the laser delay data shown in Figure 6. Reasonable estimates of the gain-time relation can be made using eq 4, since N_v is now a known function of time. The results show for the P(9) transitions that $13 \rightarrow 12$ to $5 \rightarrow 4$ have positive gains which initially increase with time, attain maxima, and then decrease to negative values. The gain for the $8 \rightarrow 7$ transition remains positive for the longest time, while that for $9 \rightarrow 8$ is largest. Gains for the $4 \rightarrow 3$ and $3 \rightarrow 2$ transitions are initially negative; these increase to a positive value before decreasing again to become negative. From Figures 6 and 7, the maximum power appears at $10 \rightarrow 9$ and the laser duration is longest for $8 \rightarrow 7$.

Discussion

Remarks on the Reaction Mechanism. There is a general concensus that the dominant pumping reaction is
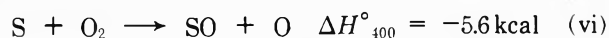
$$CS^{(0)}(^1\Sigma^+) + O(^3P_2) \longrightarrow S(^3P_2) + CO^{(v)}(^1\Sigma^+)$$

$$\Delta H°_{400}(v = 0) = -85 \text{ kcal} \quad (i)$$

The indicated exothermicity is based on Okabe's redetermination[16] of the heat of dissociation of CS_2. Whether the reaction

$$CS^{(u)}(^1\Sigma^+) + O_2(^3\Sigma_g^-) \longrightarrow SO(^3\Sigma^-) + CO^{(v)}(^1\Sigma^+)$$

$$\Delta H°_{400}\begin{pmatrix} v = 0 \\ w = 0 \end{pmatrix} = -91 \text{ kcal} \quad (ii)$$

contributes to any significant extent, when w is greater than some as yet unspecified critical value, is still being debated.[17,18] The following is a minimal set of reactions needed to account for the production of the essential fragments

$$O_2 \xrightarrow{e} O + O \quad \Delta H°_{400} = -119 \text{ kcal} \quad (iii)$$

$$CS_2 \xrightarrow{e} CS + S \quad \Delta H°_{400} = -102 \text{ kcal} \quad (iv)$$

initiation (either or both)

$$CS_2 + O \longrightarrow CS + SO \quad \Delta H°_{400} = -21 \text{ kcal} \quad (v)$$

$$S + O_2 \longrightarrow SO + O \quad \Delta H°_{400} = -5.6 \text{ kcal} \quad (vi)$$

chain propagation

An exhaustive listing of all possible reactions that could occur in this complex system led to about 70,[19] exclusive of distinctive reactions by vibrationally excited species and of vibrational energy transfer steps. Obviously, the search for a tractable mechanism involves the identifica-

TABLE I: Relative Populations of CO Vibrational Levels

	Laser delay measurements						Ir emission measurements		
	Assumed $\varphi_{11}/\varphi_{12} = 0.9$		0.85		0.8		This work	Hancock, et al.	
v	φ_{v-1}/φ_v	$\varphi_v^{n\ a}$	φ_{v-1}/φ_v	φ_v^n	φ_{v-1}/φ_v	φ_v^n	$\varphi_v^{n\ b}$	$\varphi_v^{n\ b}$	$\varphi_v^{n\ c}$
17							0.13	0	0.18
16							0.34	0	0.32
15							0.56	~0.2	0.58
14	1.07	0.93	1.06	0.94	1.02	0.98	0.77	0.64	0.90
13	0.93	1.00	0.90	1.00	0.87	1.00	1.00	1.00	1.00
12	0.90	0.93	0.85	0.90	0.80	0.87	0.97	0.87	0.85
11	0.88	0.84	0.83	0.77	0.75	0.70	0.89	0.80	0.65
10	0.89	0.74	0.81	0.64	0.69	0.52	0.80	0.66	0.55
9	0.88	0.66	0.78	0.51	0.55	0.36	0.71	0.61	0.41
8	0.87	0.58	0.73	0.40	0.18	0.20	0.67	0.27	0.32
7	0.90	0.50	0.72	0.29	−2.9	0.036	0.62	~0.06	0.17
6	0.89	0.45	0.60	0.21			0.58		0.05
5	0.87	0.40	0.29	0.13			0.55		
4		0.35		0.037			0.52		
3							0.82		
2							1.13		
1							2.38		

^{a} $\varphi^n \equiv$ relative population normalized to $v = 13$. ^{b} Derived from O + CS$_2$ system. ^{c} Derived from flash-photolyzed CS$_2$ + O$_2$.

tion of a minimal set of auxiliary steps; i.e., those reactions which if omitted would affect to a measurable extent the concentrations of the species $CO^{(v)}$, O, S, and CS. That selection (a list of ≈ 15) can be made on the basis of an evaluation of the product of measured (or estimated) rate constants and corresponding estimated local concentrations. In turn the latter depend on the details of the initiation process which is determined by the experimental configuration. Our observations on the effect of discharge voltage on laser output thus can be qualitatively explained. When the voltage of the initiating pulse was high, the electrical energy was sufficient to dissociate a large portion of the CS$_2$ as well as the O$_2$, so that the pumping reaction i quickly produced an inverted $CO^{(v)}$ population, and the level of stimulated emission exceeded cavity losses. For the lower voltage discharges initiation occurred predominantly through iii and the critical rate of $CO^{(v)}$ production required steps v and vi as well as i. That the initiating voltage determines the relative importance of these two paths is supported by our observation of CS absorption in the ultraviolet. Subsequent to a high voltage discharge the concentration of CS decays exponentially approaching a constant value, while after a low voltage discharge the concentration of CS remains almost constant for more than 1 msec.[15] The latter indicates that CS is a reaction intermediate which attains a stationary state concentration, whereas in the former case, the decay rate of CS agrees with the observed rate of production of CO. Also, an optimum discharge voltage to generate CS in [CS$_2$-He] mixtures was found which corresponds to the observed optimum discharge voltage for laser power production. Apparently, when discharge voltages greater than the optimum are used, the level of CS$_2$ is partly depleted by the production of species other than CS.

As yet there is no cogent evidence that reaction ii contributes significantly to pumping. Sadie, et al.,[18] proposed that it may be important under the following conditions. When a dilute mixture of CS$_2$ and He (0.1 + 4.2 Torr, respectively) was rapidly passed through a discharge and

mixed with O$_2$ [at ≈ 1 Torr] 30 cm downstream, lasing was observed over the lowest six vibrational levels and for $v \geq 14$. In this configuration initiation must occur via reaction iv. However, this does not limit pumping to step ii, since reaction vi is known to be very fast[20] [$k_{vi} = 2.35 \times 10^{13} \exp(-2300/RT)$ mol^{-1} cm^3 sec^{-1}] and as many S atoms are generated in the discharge as CS radicals. More direct evidence is provided by our uv absorption studies. These indicate that a rapid reaction between CS and O$_2$ does not occur, since the concentration of CS ($v = 0 \ldots 4$) remains constant long after the end of CO formation, even when O$_2$ is present in excess. That the lifetime of CS produced by flash photolysis was not affected by the presence of O$_2$ was also reported by Callear.[21] The low probability for reaction ii was also discussed by Hancock and Smith.[6] This is a four-center process which requires the concerted breaking of two strong bonds, for which an activation energy of ≈ 50 kcal is anticipated. The rates of such reactions are augmented when either or both of the reagents are in vibrationally excited states.[22] However, it has been shown that in reaction v, of the 21 kcal of exothermicity, on the average no more than about 2 kcal is channeled into the CS vibrations, and about 4 kcal into SO vibrations;[23] most of the rest goes into rotations.[24] Nevertheless, reaction ii cannot be completely eliminated for those experimental configurations in which the CS$_2$ is passed through a high voltage discharge. As noted above, equivalent vibrational temperatures of $\approx 12,000°$K are indicated by our uv absorption spectra.

Comparison with Other Experiments. The only published data on the delay sequence for CO lasing are those of Gregg and Thomas.[25] They observed laser pulses in flash photolyzed CS$_2$-O$_2$ mixtures using a cavity with a grating and a rotating mirror and found two minima in delay times, associated with 13 → 12 and 10 → 9 transitions. This led them to the conclusion that the $CO^{(v)}$ was produced chemically as well as by collisions with electronically excited SO$_2$. The latter part of their conclusion is doubtful. Hancock and Smith[26] found only a weak CO

emission associated with the slow recombination reaction: $SO + O \rightarrow SO_2^*$. Also, the correlation we found between the CS and CO concentrations indicates that the main source of CO is the reaction between CS and O. Gregg and Thomas' τ's are roughly in agreement with our values, except for our finding a single minimum in the delay time sequence, at $12 \rightarrow 11$.

Literature reports on the effect of added CO on laser power suggest that the manner of excitation is a controlling factor. That the excitation and mixing sequence plays a significant role was demonstrated by Sadie, et al.[18] Pollack,[27] who initiated lasing in [CS$_2$-O$_2$-He] mixtures by flash photolysis, and Arnold and Kimbell,[28] who used an axial spark discharge, found that the addition of CO to the mixture *decreased* the output power. On the other hand, Suart, Arnold, and Kimbell[29] observed enhanced lasing when they added cold CO to a CS$_2$-He flow, and mixed it with discharged oxygen; the same result was reported by Foster.[30] They attributed this effect to an increase in the population inversion density through selective depopulation by v-v exchange between the cold CO and the lower vibrational states produced *via* chemical excitation. Similarly, Jeffers[31] reported a factor of 2 increase in power in a transverse flow configuration when he added CO to the CS$_2$ flow and subsequently mixed that with discharged [O$_2$-He]. A positive effect due to carbon monoxide was also reported by Searles and Djeu[32] in a CS$_2$-O$_2$ flame laser. Our experimental configuration is similar to that used by Arnold and Kimbell; in agreement with their observation, we found that the addition of CO to the mixture resulted in a decrease of laser power both in grating tuned and in conventional cavities. Qualitatively, one may argue that for an initial distribution such as shown in Figure 9 the chemically unexcited diluent merely raises the relative population in the low v states to produce a distribution with a shallow minimum; *i.e.*, one that resembles a somewhat relaxed system. This accelerates relaxation to an equilibrium state and accounts for the observed shortening of laser duration for each transition, as shown in Figure 6. We considered the possibility that the added CO may be excited by the pulsed discharge. Other experiments and theoretical predictions[33,34] indicate that the populations thus generated in the higher levels are smaller than in the ground state by several orders of magnitude.

Recent measurements of relative magnitudes for $k_i{}^{(v)}$ by Hancock, Morley, and Smith[7] and by Foster[30] provide no information for vibrational levels $v < 6$; where their data overlap ours the agreement is good, particularly with the latter, in view of the assigned error limits. Hancock, Morley, and Smith made two types of measurements. In one they estimated the stationary distribution of CO$^{(v)}$ in a flowing [CS$_2$-O] mixture. The recorded light intensities were interpreted in terms of specific chemical excitation rates, using the relative spontaneous emission intensities and collisional relaxation rates. They indicated the possible presence of large errors in the rates for $v < 7$, because the latter were given by the *difference* between deactivating rates of CO from v to lower levels, and from higher levels to v. In their second method they directly monitored the population of excited CO$^{(v)}$ in flash-photolyzed [CS$_2$-O$_2$-Ar] mixtures, using the CO continuous wave laser lines $20 \rightarrow 19$ to $5 \rightarrow 4$ transitions as a light source. They concluded that $\varphi_4 \approx \varphi_5 \approx 0$ from the analysis of gain coefficients, assuming $\varphi_{19} = 0$. However, errors thus accumulate in estimating populations of the lower levels.

The values in the last column of Table I give the distribution derived under the assumption $\varphi_4 = 0$.

Our measurements of CO chemiluminescence are not compatible with the Hancock, Morley, and Smith distribution. Note that whereas the scanning time of the monochromator (which required 2 hr to cover the CO fundamental region) limits the integration time of the signal, and the signal-to-noise ratio is not as good as desired for the weak bands, the lower transitions, with small radiative transition probabilities, do not overlap each other as much as do the higher transitions. To account for the observed spectrum one must introduce contributions from the low v transitions; it is quite different from the one calculated using the distribution given by Hancock, et al., as seen from Figure 8c. In this respect, an interesting analysis was presented by Dawson and Tam[8] who calculated the stationary vibrational state distribution of CO, including chemical production of CO$^{(v)}$ in each level, v-v and v-T energy transfers, spontaneous radiation loss, and removal of CO by pumping. They could explain the two sets of experimental CO distributions reported by Hancock and Smith[14] by using the initial formation rates proposed by Hancock, Morley, and Smith.[7] However, the results of Arnold, et al., which called for a distribution appropriate to a large rate of CO formation, were difficult to simulate without assuming CO$^{(v)}$ production in the low levels. Since the distribution developed under a high production rate of CO would be more sensitive to the form of the initial distribution of CO, this conclusion supports the v dependence given by our experiments. However, the analysis by Dawson and Tam was made on the basis of v-v rates calculated according to the modified SSH theory, which leads to transition probabilities for the low v levels that are smaller by a factor of about 6 than those of Hancock and Smith, or the ones estimated from the Sharma-Brau theory. Therefore, the conclusion derived by Dawson and Tam requires further analysis.

Vibrational excitation of CO$^{(v)}$ in up to $v = 17$ were seen in the present system. Using the new value for the heat of formation of CS,[16] the exothermicity for i is 84.6 kcal/mol; this permits excitation to $v = 15$. Additionally, since CS in levels $v = 0 \sim 4$ were detected in our uv absorption experiments it is reasonable to assume that CS ($v = 4$) can supply up to 14.6 kcal, so that $v = 17$ for CO can be pumped.

References and Notes

(1) Permanent address, Department of Pure and Applied Science, University of Tokyo.
(2) (a) H. S. Pilloff, S. K. Searles, and N. Djeu, *Appl. Phys. Lett.*, **19**, 9 (1971); (b) M. J. Linevsky and R. A. Carabetta, *ibid.*, **22**, 288 (1973).
(3) A. B. Callear and I. W. M. Smith, *Nature (London)*, **213**, 382 (1967).
(4) A. A. Westenberg and N. deHaas, *J. Chem. Phys.*, **50**, 707 (1969).
(5) I. W. M. Smith, *Trans. Faraday Soc.*, **64**, 378 (1968).
(6) G. Hancock and I. W. M. Smith, *Trans. Faraday Soc.*, **67**, 2586 (1971).
(7) G. Hancock, C. Morley, and I. W. M. Smith, *Chem. Phys. Lett.*, **12**, 193 (1971).
(8) P. H. Dawson and W. G. Tam, *Can. J. Phys.*, **50**, 889 (1972).
(9) K. P. Horn and P. E. Ottinger, *J. Chem. Phys.*, **54**, 3040 (1971).
(10) A. W. Mantz, E. R. Nichols, B. D. Alpert, and K. N. Rao, *J. Mol. Spectrosc.*, **35**, 325 (1970).
(11) G. Abraham and E. R. Fisher, Report from Wayne State University, No. RIES 71-39, Oct 1971.

(12) R. A. Toth, R. H. Hunt, and E. K. Plyler, *J. Mol. Spectrosc.*, **32**, 85 (1969).
(13) R. Ladenburg and S. Levy, *Z. Phys.*, **65**, 185 (1930).
(14) G. Hancock and I. W. M. Smith, *Appl. Opt.*, **10**, 1827 (1971).
(15) Investigation still in progress.
(16) H. Okabe, *J. Chem. Phys.*, **56**, 4381 (1972).
(17) S. Rosenwaks and S. Yatsiv, *Chem. Phys. Lett.*, **9**, 266 (1971).
(18) F. G. Sadie, P. A. Büger, and O. G. Malan, *J. Appl. Phys.*, **43**, 5141 (1972).
(19) S. H. Bauer and N. Nielsen, unpublished report.
(20) Estimated on basis of data by D. D. Davis, *Int. J. Chem. Kinet.*, **4**, 367 (1972).
(21) A. B. Callear, *Proc. Roy. Soc.*, *Ser. A*, **276**, 401 (1963).
(22) S. H. Bauer, D. R. Lederman, E. L. Resler, and E. R. Fisher, *Int. J. Chem. Kinet.*, **5**, 93 (1973).

(23) I. W. M. Smith, *Disc. Faraday Soc.*, **44**, 194 (1967).
(24) P. L. Moore, P. N. Clough, and J. Geddes, *Chem. Phys. Lett.*, **17**, 608 (1972).
(25) D. W. Gregg and S. J. Thomas, *J. Appl. Phys.*, **39**, 4399 (1968).
(26) G. Hancock and I. W. M. Smith, *Chem. Phys. Lett.*, **3**, 573 (1969).
(27) M. A. Pollack, *Appl. Phys. Lett.*, **8**, 237 (1966).
(28) S. J. Arnold and G. H. Kimbell, *Appl. Phys. Lett.*, **15**, 351 (1969).
(29) R. D. Suart, S. J. Arnold, and G. H. Kimbell, *Chem. Phys. Lett.*, **7**, 337 (1970).
(30) K. D. Foster, *J. Chem. Phys.*, **57**, 2451 (1972).
(31) W. Q. Jeffers and C. E. Wiswall, *Appl. Phys. Lett.*, **17**, 67 (1970).
(32) S. K. Searles and N. Djeu, *Chem. Phys. Lett.*, **12**, 53 (1971).
(33) J. W. Rich and H. M. Thompson, *Appl. Phys. Lett.*, **19**, 3 (1971).
(34) W. Q. Jeffers and C. E. Wiswall, *IEEE J. Quantum Electron.*, **QE-7**, 407 (1971).

Relative Reactivities of Carbon–Carbon Single Bonds in Normalized Recoil Tritium Systems[1]

J. L. Williams, S. H. Daniel, and Y.-N. Tang*

Department of Chemistry, Texas A & M University, College Station, Texas 77843   (Received August 28, 1972; Revised Manuscript Received May 30, 1973)

Recoil tritium atoms were allowed to react with 14 different hydrocarbons, including alkanes, alkenes, and alkynes, in hexafluorocyclobutene-normalized systems. The relative CH_3T yields per bond from the hot tritium abstraction of end methyl groups were correlated inversely with the R–CH_3 bond dissociation energies. The electron density around the reaction site showed no obvious effect on CH_3T yields. The reaction time for this type of interaction is likely to be less than $2\text{-}5 \times 10^{-14}$ sec. Possible mechanisms for the formation of CH_3T are discussed.

Introduction

Recent studies on recoil tritium reactions have revealed the importance of chemical parameters in controlling the reaction probabilities of hot atom interactions.[2-14] Among these factors, the presence of a bond strength effect has been convincingly established for three fundamental types of hot tritium reactions: (1) H abstraction;[5-9] (2) T*-for-X substitution;[2,10] and (3) T*-for-R substitution.[11]

$$T^* + RH \longrightarrow HT + R \qquad (1)$$

$$T^* + RX \longrightarrow RT + X \qquad (2)$$

$$T^* + R_1\text{-}R_2 \longrightarrow R_1T + R_2 \qquad (3)$$
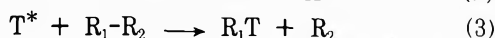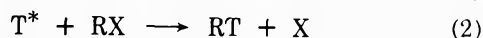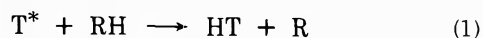
An excellent correlation between the HT yields from (1) in normalized systems and D(C–H) values has been shown by Rowland and coworkers.[5-9] A bond strength effect in T*-for-X substitution has also been observed in CH_3X systems.[2,10] Very recently, Root[11] has reported essentially linear correlations of the intrasample product ratios from (3) and T*-for-H substitution with the bond strength of the C–C bonds of C_2 to C_5 alkanes when these ratios are grouped according to the four degrees of branching (primary, secondary, tertiary, and quaternary) at the "at-tacked" carbon atom. For the attack at primary carbons in seven alkanes to give CH_3T, a dependence of the ratios on D(R_1–CH_3) is definitely observed, even though the variation of bond strengths covers only about 8 kcal/mol.

In the present work, we have also studied recoil tritium reactions in the gas phase at carbon–carbon single bonds, and have positively confirmed the role of the bond strength effect. The major advantages of this work over that of Root are (1) the recoil tritium reactions were carried out in a "normalized" system where a moderator is in large excess to ensure a nearly identical tritium energy spectrum for each parent hydrocarbon, which allows intersample comparisons; (2) CH_3T yields from alkenes and alkynes as well as alkanes were measured and, therefore, a bond strength range of about 40 kcal/mol was covered; (3) the normalized yields of R_1T were directly measured instead of using the ratios of the R_1T values relative to the T*-for-H substitution products, avoiding the possibility of canceling the common effects of some parameters.

Among other chemical factors, the presence of an electron density effect has also been convincingly established for the T*-for-H substitution.[2,4] In this work, the possible correlation between the C–C bond reactivities and the carbon-13 nmr chemical shifts is also explored.

Experimental Section

The standard techniques in studying recoil tritium reactions were employed. Helium-3 with a tritium content of less than 2×10^{-11} was obtained from the Monsanto Research Corp. Hexafluorocyclobutene (>99.5% purity, PCR, Inc.) and the hydrocarbon parent compounds (Matheson, >99% purity) were all used after bulb-to-bulb distillation. The nuclear reaction $^3He(n,p)^3H^*$ was used for the hot tritium production.

The normalized system comprised approximately 20 Torr of ^3He, 30 Torr of O_2, 150 Torr of parent hydrocarbon compound, and 600 Torr of hexafluorocyclobutene. A large excess of hexafluorocyclobutene was employed in every system to ensure exposing parent molecules to a nearly equivalent tritium energy spectrum.

The samples were irradiated for 50 min in a rotisserie at the Texas A & M University Nuclear Science Center reactor with a thermal neutron flux of 10^{12} neutrons/(cm^2 sec). Two of the samples were always neopentane monitors.

Standard radio-gas chromatography techniques were employed in separating and analyzing the irradiated samples.[15] Each sample was separated into two equal aliquots.

The first aliquots were assayed for HT activity, CH_3T activity, and ^3He mass. The separation was effected by a series of columns: first, a 25-ft glass beads column (to build up pressure), followed by a 10-ft activated alumina column (to absorb the hexafluorocyclobutene, which would have otherwise quenched the counter), and finally a 10-ft 5-Å molecular sieve column (to perform the actual separation). HT and CH_3T retention times differed by more than 30 min, allowing a complete separation.

The second aliquots were assayed for tritium-labeled hydrocarbons with two or more carbon atoms. Either a 50-ft PCA column (9.6% propylene carbonate on 30/50 mesh activated alumina, operated at 0°), or a 50-ft DMS column (35% dimethylsulfolane on 30/60 mesh firebrick, operated at room temperature) was used. The PCA column was used to separate hydrocarbons with three or less carbon atoms; the DMS column was used to separate heavier hydrocarbons. However, since hexafluorocyclobutene quenches the counter and has a retention time that interferes with the heavier hydrocarbons, most of the DMS column analyses were rendered useless.

Results

Normalized CH_3T Yields. Recoil tritium reactions in the hexafluorocyclobutene-normalized systems have been carried out with fourteen different hydrocarbons, including alkanes, alkenes, and alkynes. We have concentrated our effort on the hot tritium reaction with terminal methyl groups

$$T^* + R_1\text{-}CH_3 \longrightarrow \begin{array}{l} CH_3T + R_1 \quad (4) \\ R_1T + CH_3 \quad (5) \end{array}$$
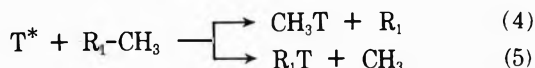
The CH_3T product was formed only from the attack of hot tritium on *end* carbon–carbon *single* bonds; this was shown by the fact that 1,3-butadiene samples gave essentially no CH_3T yield. The observed normalized CH_3T yields are included in Table I, listed in order of decreasing yield.

The quantitative numbers for the normalized yields were obtained using the equation

$$Y = \frac{[\text{activity}][\text{moderator pressure}]}{[^3He \text{ mass peak}][\text{parent pressure}] \times [\text{no. of } R_1\text{-}CH_3 \text{ bonds}]}$$

Each irradiation consisted of a set of ten samples in a rotisserie. Since the neutron flux could vary from set to set, it was necessary to "standardize" the different amounts of irradiation exposure each set received. To do this, two of the ten samples were always neopentane "standards;" the average CH_3T yields from these were arbitrarily adjusted to 100 and this same factor was applied to all samples in the set.

Correlation with C–C Bond Dissociation Energies. In Table I, the C–C bond dissociation energies[16-19] of several $R_1\text{-}CH_3$ molecules are also included. The corresponding values for the other molecules have not yet been well established. By comparing the CH_3T yields with the C–C bond dissociation energies as shown in Table I, it is obvious that they are inversely related to each other, *i.e.,* the CH_3T yields decrease by a factor of 3 over an increasing bond dissociation energy span of about 40 kcal/mol. This rough correlation is alternatively expressed in Figure 1. It is seen that a steep line can be drawn through the points of the saturated hydrocarbons.

The CH_3T yields are directly correlated with $D(R_1\text{-}CH_3)$ without making any correction for possible decomposition in the gas phase because (1) the degree of decomposition of CH_3T is expected to be small due to a high activation energy, and (2) since CH_3T is a common product from every parent compound, any decomposition is likely to be similar regardless of the system.

Correlation with Carbon-13 Nmr Chemical Shifts. In Table I the values of the carbon-13 nmr chemical shifts for the carbon atoms in the terminal methyl groups as well as those attached to the terminal methyl groups for all the listed hydrocarbons are also shown.[20] The correlation between the relative normalized yields of CH_3T per bond and the carbon-13 chemical shift for the terminal carbon is plotted in Figure 2. With the exception of 1-butene, the general trend appears to indicate that the higher the chemical shift, the higher the yield. In particular, a rather smooth correlation exists in the series ethane, propane, isobutane, and neopentane. A plot (not shown) similar to Figure 2 of CH_3T yields *vs.* carbon-13 nmr chemical shifts for the carbon atoms attached to the terminal methyl groups indicates that no correlation was obvious.

Other Products from Recoil Tritium Reaction at Carbon–Carbon Single Bonds. Although CH_3T is the most important product from recoil tritium reactions at carbon–carbon single bonds, other simple hydrocarbons are also expected to be formed. However, due to the fact that hexafluorocyclobutene quenches the counter, and that it possesses a retention time which is comparable to the C_4 and C_5 alkanes, any hydrocarbon product with four or more carbon atoms will be affected by the quenching action. Therefore, only the C_2 and the C_3 products can be quantitatively evaluated in this normalized system. The measured R_1T yields from (5) for the saturated hydrocarbon parent molecules, R_1CH_3, are also shown in Table I. The unsaturated systems are not included here because there are some additional sources of the product formation, such as the decomposition of excited radicals. For neopentane, *n*-pentane, and *n*-hexane, R_1T has four or five carbon atoms and thus is quenched. Since the CH_3T yield for these three molecules could be established independently, the R_1T yield was calculated from the $CH_3T/$

TABLE I: Relative Normalized Yields of CH_3T per Bond from Recoil Tritium Reactions at C–C Single Bonds

Parent (R_1–CH_3)	Relative[a] normalized yields per bond		$D(R_1$–$CH_3)$,[b] kcal/mol	^{13}C nmr chemical shifts, ppm[c]	
	CH_3T	R_1T		R_1–$^{13}CH_3$	^{13}C–CH_3
C\C/C (neopentane)	(100.0) ± 0.5	[12.0 ± 0.1]	80	31.5	27.9
C=C–C–C	97.7 ± 4.4		74.5	~13.2[d]	~27.5[d]
C=C–C(C)(C)	83.9 ± 4.2			~22.0[d]	~32.4[d]
C–C(C)(C)	76.1 ± 6.8	16.3 ± 1.5	84	24.3	25.2
C–C–C–C–C–C	71.9 ± 6.3	[32.8 ± 3.1]	85	13.9	22.9
C–C–C–C–C	68.4 ± 2.0	[25.6 ± 0.8]	85	13.7	22.6
C–C–C–C	64.0 ± 2.2	20.0 ± 0.9	85	13.2	25.0
C–C–C	61.0 ± 7.2	35.1 ± 1.9	85	15.6	16.1
C=C–C	60.6 ± 8.8		97	18.7	133.1
C=C(C)(C)	57.0 ± 1.2			23.3	141.2
C–C	47.0 ± 2.7	47.0 ± 2.7	88	5.9	5.9
C\C=C\C	46.1 ± 4.3			17.3	124.5
C/C=C\C	42.3 ± 3.2			10.6	123.3
C≡C–C	34.1 ± 4.2		112	2.1[e]	79.4[e]

[a] With the CH_3T yield from neo-C_5H_{12} as 100.0. [b] Values from ref 16–19. [c] Values from ref 20, ppm relative to TMS, increasing positive values indicating decreasing shielding. [d] Estimated values, based on statements of ref 20. [e] Values from R. J. Pugmire, quoted in Strong, Ikenberry, and Grant, *J. Magn. Resonance*, 9(1), 145 (1973), converted from original data using $\delta(C_6H_6)$ 128.7.
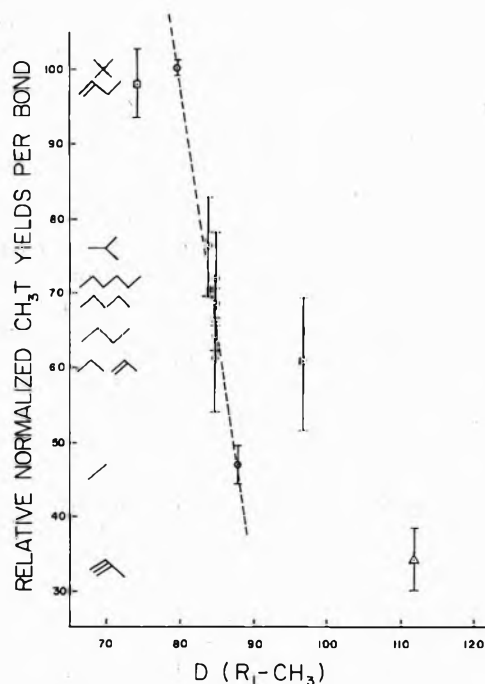
Figure 1. Relative normalized CH_3T yields per bond vs. R_1–CH_3 bond dissociation energies: ⊙, alkanes; ⊡, alkenes; △, alkynes.

R_1T ratios in the literature.[21] The yields thus calculated are in brackets in Table I.

The sum of the CH_3T yield from (4) and the R_1T yield from (5) appears to be approximately constant, with possibly a trend showing a slightly higher sum for a weaker bond. However, the observed values obtained here may differ considerably from the actual sums because R_1T in the gas phase may undergo considerable decomposition with the percentage of decomposition varying from molecule to molecule.
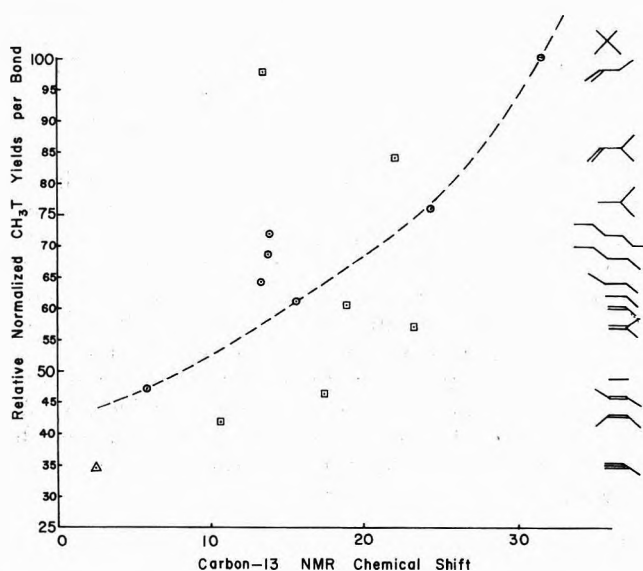
Figure 2. Relative normalized CH_3T yields per bond vs. R_1–$^{13}CH_3$ carbon-13 nmr chemical shifts: ⊙, alkanes; ⊡, alkenes; △, alkynes.

Variation of CH_3T Yields with Composition in a Normalized System. A composition study of the CH_3T yields has been carried out in hexafluorocyclobutene-moderated systems with propane, propene, and neopentane. For each of these parent molecules, a variation of the parent concentration from 2 to 20 mol % was studied with total pressure held constant. For the saturated compounds, the specific yield of CH_3T decreased slightly with increasing parent concentration and leveled off at a concentration of 10%. A similar plateau was also observed in the propene system; however, the initial drop was rather sharp. In the present set of experiments on C–C bond reactivities, a constant parent concentration of about 15% was used, and a plateau is likely to exist above 10% parent concentration

for every molecule studied. Although the reason for the initial decrease in the specific yield of CH_3T with increasing parent concentration is not certain, it is believed that the comparison of C–C reactivities in this work should still be meaningful because concentrations in the plateau region were used.

Discussion

Role of Chemical Factors in Hot Atom Reactions. The effect of bond energy, electron density, and electronegativity in hot atom reactions has already been well established by various studies.[2,13] The mechanism of these reactions is likely to involve collisional complexes with certain finite lifetimes.[22] The two fundamental processes involved in a reaction are bond breaking and bond forming, and these two processes are likely to occur simultaneously during the life span of the collisional complex. Among the possible chemical factors influencing a reaction, the major determinant for the bond-breaking process should be the bond dissociation energy, and the major determinant for the bond-forming process should be the electron density around the reaction site. As a result, it is not surprising that bond dissociation energy and electron density are the two most fundamental controlling parameters in hot atom reactions.

Bond Strength Effects in Recoil Tritium Reactions with Carbon–Carbon Single Bonds. From the general correlation shown in Figure 1, it is likely that the bond strength of carbon–carbon single bonds is one of the primary factors affecting their reactivities toward recoil tritium atoms. Among the data, the qualitative trend for the C_4-skeletal compounds is most noteworthy. The CH_3T yields are in the order $1\text{-}C_4H_8 > n\text{-}C_4H_{10} > 2\text{-}C_4H_8$. This trend strictly follows the order of increasing $D(R_1\text{–}CH_3)$[23] and not the trend of any other known parameters (*e.g.*, the ^{13}C nmr chemical shift values).

In Figure 1 the line drawn through the alkanes shows that the CH_3T yield is extremely sensitive to the C–C bond dissociation energies. In this figure, it is also seen that the CH_3T yields from propene and propyne lie above the alkane line while the CH_3T yield from 1-butene lies below. With reasonable estimates of the $D(R_1\text{–}CH_3)$ values for other olefins whose exact bond dissociation energies are unknown, it can be shown that the CH_3T yields from isobutene and *cis-* and *trans-*2-butene lie above the line while that of 3-methyl-1-butene lies below. This seems to indicate that vinyl methyl groups are more likely, while allyl methyl groups are less likely, to yield CH_3T than what would have been predicted by consideration of the bond dissociation energies alone. This observation reflects the possibility that certain factors relating to the structure of the molecule modify the reactivity of the C–C bonds. In the case of vinyl methyl groups the nature of this operating structure effect is unfortunately not certain, while for allyl methyl groups the lower than expected yield is likely due to incomplete operation of the allyl resonance which will be discussed later.

The straight chain alkanes, such as C_3H_8, $n\text{-}C_4H_{10}$, $n\text{-}C_5H_{12}$ and $n\text{-}C_6H_{14}$, all have a $D(R_1\text{–}CH_3)$ value of 85 kcal/mol; however, their relative normalized yields of CH_3T per bond increases from 61.0 to 71.9 in the order listed above. This difference may be due to either one of two possibilities. On one hand, the $D(R_1\text{–}CH_3)$ values may actually decrease slightly going down the series of alkanes and a 0.5 kcal/mol difference may be adequate to quantitatively explain the differences in yields. On the other

hand, it may again reflect a structure effect due to the differences in R_1 groups.

Reaction Time for Recoil Tritium Interactions in Carbon–Carbon Single Bonds. The presence of a structure effect has been suggested above. For unperturbed molecules the properties of the methyl group in 1-butene should be similar to those of the methyl groups in either *n*-butane or propene. This is supported by the fact that the carbon-13 nmr chemical shifts of these methyl carbon atoms have approximately the same values. As a result, the CH_3T yield from 1-butene is expected to either fall on or above the alkane line of Figure 1. That is, the expected value should be 140 or above.

The actual CH_3T yield of 97.7 ± 4.4 from 1-butene is large but not as large as the expected value of 140 considering its low $D(R_1\text{–}CH_3)$ value. In employing the alkane correlation line, an apparent bond dissociation energy of 82 kcal/mol instead of the literature value of 75 kcal/mol[18] is observed. These differences can be explained by the fact that the methyl abstraction leaves an allyl radical. The situation is exactly parallel to the hot tritium abstraction of a hydrogen atom from propene which also gives an allyl radical.[7] In both cases, the reaction is complete before complete allyl resonance occurs. This means that the reaction of recoil tritium atoms at C–C single bonds is faster than the vibrational displacement of the allyl radical. In other words, the reaction time is likely to be less than $2\text{-}5 \times 10^{-14}$ sec.

The Minor Role of Electron Density in Determining the CH_3T Yield. In addition to bond dissociation energy, electron density has also been shown to be a major controlling factor in hot atom interactions. The presence of the former in the H-abstraction reactions and the latter in the T^*-for-H substitution reactions has been unmistakenly demonstrated. However, these two factors are also closely related, as a low electron density generally corresponds to a weak bond.

The correlation shown in Figure 2 indicates that the CH_3T yield changes inversely with the electron density, that is, a high electron density around the carbon corresponds to a low CH_3T yield. This is just the opposite of what has been observed in T^*-for-H substitution.[2,4] Since increasing CH_3T yields, such as in the series C_2H_6, C_3H_8, $i\text{-}C_4H_{10}$ and $neo\text{-}C_5H_{12}$, correspond to decreasing $D(R_1\text{–}CH_3)$ values, it is concluded that bond dissociation energy is by far the most important factor determining the CH_3T yields, while electron density at most plays a minor role in this case.

The extremely high yield of CH_3T from 1-butene in comparison with those from other molecules of similar electron density as shown in Figure 2 again confirms the importance of bond dissociation energy.

Proposed Model for the CH_3T Formation. The presence of chemical factors in controlling hot atom reactions points to the presence of certain collisional complexes of finite lifetimes.[22] It is possible to postulate different types of complexes for the formation of each product.[10] In the case of CH_3T formation, two kinds of collisional complexes are possible: a linear complex, as shown in I, and a triangular complex, as shown in II. For the formation of
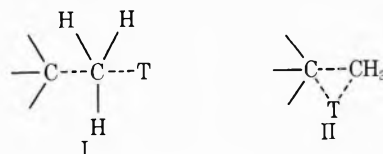
CH_3T from various compounds, the cleavage of the R_1–CH_3 bond should be the rate-differentiating step for the CH_3 abstraction in the linear complex I, while the electron-overlapping process and the C–T bond formation process are likely to be rate determining in the triangular complex II.

There are two different mechanisms that could be proposed to account for the basic experimental findings in this work. There is, however, no decisive evidence to prefer one or the other at the present moment.

The first proposed mechanism calls for I to be the major contributor of the CH_3T yield, while allowing II to account for a relatively minor portion. The major support for this CH_3 abstraction mechanism is the dependence of the CH_3T yields on $D(R_1$–$CH_3)$, as shown in Figure 1, as well as the minor role which electron density plays in determining the CH_3T yields, as shown in Figure 2. The analogous H-abstraction reactions by recoil tritium to give HT also show similar dependence on the dissociation energies of the cleaved bonds and similar independence on the electron density, while, on the other hand, the T-for-H substitution processes which may involve triangular complexes show a direct dependence on the electron density.[4-9] The proposal that a majority of the CH_3T yields come from I is also consistent with the observation that the CH_3T yield is normally much higher than the yields of other possible C–C bond products. It should be noted that an inversion of configuration is proposed for the product formation. Unfortunately, the test for inversion, which necessitates the conversion of the three hydrogen atoms into functional groups, may obscure this route.

The second proposed mechanism[24] calls for II to be the major contributor for the CH_3T yield with the C–T bond formation step to be rate determining. Since there are two possible C–T bonds, a competition results between the formation of the stronger CH_3–T (104 kcal/mol) bond and weaker R_1–T (85–98 kcal/mol) bond, and the stronger bond should always be formed in a larger abundance. As a result, the CH_3T yield is expected to be higher than the corresponding R_1T yield, and the variation of CH_3T yields for a series of compounds should be inversely related to the $D(R_1$–T) values. In practice, a plot of relative normalized CH_3T yields per bond as a function of $D(R_1$–H) gives a graph which is extremely similar to Figure 1. This is actually expected because of the exact parallel trends of the $D(R_1$–$CH_3)$ and $D(R_1$–H) values. Another support for this mechanism is the apparent lack of variation for the sum of CH_3T and R_1T as noted in Table I.

The two mechanisms proposed above differ in that different kinds of complexes are proposed, and in that whether the bond strength effect predominates during the bond-breaking or bond-forming step. The important point is that they both emphasize that a bond strength effect is definitely present during recoil tritium reactions with C–C single bonds, and that certain kinds of collisional complexes are involved in the product formation processes.

References and Notes

(1) This work has presented in part at the 161st National Meeting of the American Chemical Society, Los Angeles, Calif., March 1971.
(2) Y.-N. Tang, E. K. C. Lee, E. Tachikawa, and F. S. Rowland, *J. Phys. Chem.,* **75,** 1290 (1971).
(3) S. H. Daniel and Y.-N. Tang, *J. Phys. Chem.,* **75,** 301 (1971).
(4) F. S. Rowland, E. K. C. Lee, and Y.-N. Tang, *J. Phys. Chem.,* **73,** 4024 (1969).
(5) W. Breckenridge, J. W. Root, and F. S. Rowland, *J. Chem. Phys.,* **39,** 2374 (1963).
(6) J. W. Root, W. Breckenridge, and F. S. Rowland, *J. Chem. Phys.,* **43,** 3694 (1965).
(7) E. Tachikawa, Y.-N. Tang, and F. S. Rowland, *J. Amer. Chem. Soc.,* **90,** 3584 (1968).
(8) E. Tachikawa and F. S. Rowland, *J. Amer. Chem. Soc.,* **90,** 4767 (1968).
(9) E. Tachikawa and F. S. Rowland, *J. Amer. Chem. Soc.,* **91,** 559 (1969).
(10) Y.-N. Tang, Ph.D. Dissertation, University of Kansas, 1964.
(11) J. W. Root, *J. Phys. Chem.,* **73,** 3174 (1969).
(12) F. Schmidt-Bleek and F. S. Rowland, *Angew. Chem.,* **76,** 901 (1964).
(13) F. S. Rowland, "Proceedings of the International School of Physics, "Enrico Fermi" Course XLIV-Molecular Beam and Reaction Kinetics," Ch. Schlier, Ed., Academic Press, New York, N. Y. 1970.
(14) S. H. Daniel, G. P. Gennaro, K. M. Ranck, and Y.-N. Tang, *J. Phys. Chem.,* **76,** 1249 (1972).
(15) J. K. Lee, E. K. C. Lee, B. Musgrave, Y.-N. Tang, J. W. Root, and F. S. Rowland, *Anal. Chem.,* **34,** 741 (1962).
(16) S. W. Benson, *J. Chem. Educ.,* **42,** 502 (1965).
(17) J. A. Kerr, *Chem. Rev.,* **66,** 465 (1966).
(18) D. M. Golden and S. W. Benson, *Chem. Rev.,* **69,** 125 (1969).
(19) S. W. Benson, "Thermochemical Kinetics," Wiley, New York, N. Y., 1968.
(20) J. B. Stothers, "Carbon-13 NMR Spectroscopy," Academic Press, New York, N. Y., 1972.
(21) D. Urch and R. Wolfgang, *J. Amer. Chem. Soc.,* **83,** 2982 (1961).
(22) C. C. Chou and F. S. Rowland, *J. Phys. Chem.,* **75,** 1283 (1971).
(23) Reference 19 shows that $D(CH_2CH$–$CH_3)$ is 97 kcal/mol and $D(C_6H_5$–$CH_3)$ is 102 kcal/mol. Therefore the $D(CH_3CHCH$–$CH_3)$ value is expected to be in the order of 100 kcal/mol.
(24) We appreciate a reviewer of this paper for calling our attention to this possible mechanism.

Condensed-Phase Photochemistry of Formaldehyde

Samuel G. Thomas. Jr., and William A. Guillory*[1]

*Department of Chemistry. Drexel University. Philadelphia. Pennsylvania 19104 (Received May 11, 1973)*

Publication costs assisted by Drexel University

The ultraviolet and vacuum–ultraviolet photolyses of CH_2O and CD_2O in argon, CO, and CO-doped argon matrices have been performed between 8 and 10 K. The results of these experiments suggest that the photodecomposition mechanism of CH_2O is a function of photon energy. The major products of photolysis are CO, H_2, HCO, and H which presumably result from the two primary processes: $CH_2O + h\nu \rightarrow H + HCO$ (1) and $CH_2O + h\nu \rightarrow H_2 + CO$ (2). No infrared detectable products were observed as a result of photolysis with a medium-pressure Hg lamp from exciting wavelengths above ~ 3000 Å. Photolysis into the continuum between 3000 Å and the air cutoff (~ 1780 Å) with major lines at 2654 and 2537 Å resulted solely in the production of CO. Similar results were obtained from excitation into one of the Rydberg states with a hydrogen resonance lamp at 1215 Å; thus it appears that reaction 2 is the major primary photodissociative process occurring in these wavelength regions. Based on relative intensities, more CO than HCO was obtained from photolysis at 1634 Å; it appears that process 2 > 1 at this wavelength, although the possibility of secondary photolysis also exists ($HCO \rightarrow H + CO$). A discussion of the photophysical processes occurring as a function of specific electronic absorptions is presented based on the results obtained from excitation into their continua by various resonance and filtered multiline light sources.

I. Introduction

The photochemistry of formaldehyde (CH_2O) is important in the area of air pollution because it is a significant minor contaminant in certain urban atmospheres. Its significance arises from the fact that one of its primary dissociative paths involves the formation of H and HCO, both of which have been suggested to play an important role in the chain-catalyzed oxidation of NO to NO_2[2a] in polluted urban atmospheres. The relative rates of H and HCO formation resulting from the photochemical decomposition of CH_2O by the sunlight have recently been estimated from gas phase work by Calvert, *et al.*[2b] They suggested that the photolysis of CH_2O is an important source of H atoms in the lower atmosphere.

Many workers have studied the photodecomposition of CH_2O and have interpreted it in terms of two primary distinct processes

$$H_2CO + h\nu \longrightarrow H + HCO \qquad (1)$$

$$H_2CO + h\nu \longrightarrow H_2 + CO \qquad (2)$$
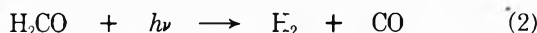
Gorin[3] studied the iodine-inhibited photolysis of CH_2O in the gas phase at 2537, 3130, and 3650 Å. He concluded that only process 1 occurred at 2537 and 3130 Å. He also suggested that (1) was still the predominate process at 3650 Å while (2) accounted for 30% of the CH_2O decomposition at this wavelength. Klein and Schoen[4] examined the photolysis of CH_2O–CD_2O mixtures and concluded that both processes 1 and 2 occurred at 3650 and 3130 Å, while (2) predominated. In later work Harrison and Lossing[5] used a mass spectrometer to observe the 2537-Å mercury-photosensitized decomposition of CH_2O. They estimated that process 2 was responsible for 40% of the CH_2O decomposition. DeGraff and Calvert[6] and McQuigg and Calvert[7] have recently studied the photolysis of CH_2O within the first absorption band using olefin inhibition in the former case and a flash photolytic technique in the latter. In the more recent work concerning the relative

importance of processes 1 and 2 at various wavelengths, McQuigg and Calvert[7] using isotopic exchange methods estimated that ϕ_1/ϕ_2 varied from almost zero at long wavelengths (3550 Å) to a number greater than one at shorter wavelengths (2800 Å).

The photochemistry of CH_2O has also been studied in an inert matrix at 4.2 K. Cochran and Adrian[8] and Adrian, Cochran, and Bowers[9] photolyzed CH_2O (1%) in an argon matrix with a hydrogen discharge lamp ($\lambda > 1450$ Å) and a low-pressure Hg lamp (2537 and 1849 Å), respectively. They observed esr signals consistent with the occurrence of process 1.

In view of the conflicting results obtained in the gas-phase work concerning the relative importance of processes 1 and 2 at various wavelengths, it seemed worthwhile to reexamine the photodecomposition processes in a matrix environment employing infrared analysis. We have previously demonstrated[10,11] the usefulness of the matrix photolysis technique in characterizing the relative importance of atom *vs.* molecular detachment processes. The power of this technique is based on the natural limitation of condensed-phase photolysis by preventing photochemical fragmented diffusion of all but relatively light atoms. The most significant shortcoming involves the secondary photolysis of primary dissociation products. However, this occurrence can be minimized by the use of monochromatic or band pass filtered sources. In this particular study, the photodecomposition products, the reactive HCO radical, and the CO molecule were easily identified from their known infrared spectra; this provided a direct means, based on relative intensities, to compare the relative importance of processes 1 and 2 as a function of photon energy.

II. Experimental Section

The CH_2O monomer was prepared by heating paraformaldehyde (Polysciences Inc.) to 110° and trapping the
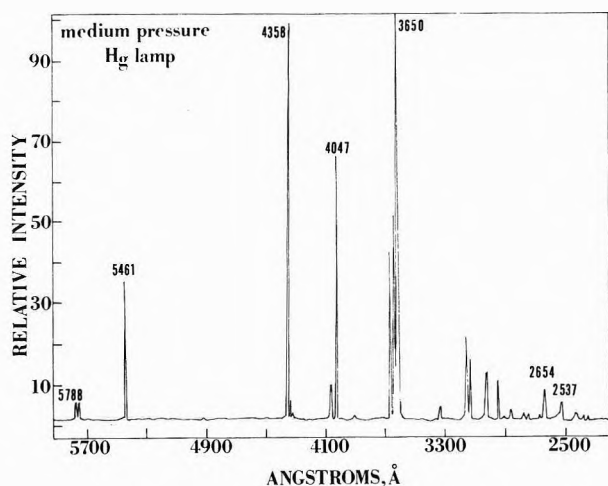
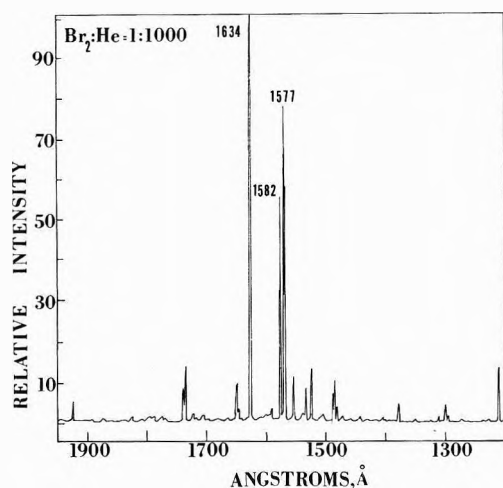**Figure 1.** Emission spectrum from the medium-pressure Hg lamp.

Figure 2. Emission spectrum from the bromine discharge lamp (Br_2:He = 1:1000).

vapor in liquid N_2. In order to purify the CH_2O, it was distilled from a Dry Ice–acetone trap ($-80°$) to a liquid N_2 trap (77 K) where it was stored. The CD_2O was prepared from deuterioparaformaldehyde (Merck Sharp and Dohme of Canada, stated purity, 99.2%) using the same procedure.

The matrix gas argon (99.99% purity) was used without further purification whereas the carbon monoxide matrix gas was passed through a P_2O_5 trap to remove traces of water. The ratios of the matrix to active materials (M:A) were 800:1. The CO-doped argon matrix experiments were conducted with ratios 800:1:1 of Ar:CH_2O:CO. Experiments were also performed with mixtures of CH_2O and CD_2O as the active materials (800:1:1 of Ar:CH_2O:CD_2O). Sample mixtures were prepared in a 2-l. bulb and delivered through a Granville-Phillips leak valve, generally at a rate of 1 mm/min or lower. These mixtures were condensed on a cold CsI window, below 10 K. The cryogenic instrument used was an Air Products closed-cycle helium Displex refrigerator.

The photolysis of the matrix isolated species was accomplished by subjecting the samples on the cold CsI window to direct radiation through a LiF ultraviolet window. A medium-pressure Hg lamp (Hanovia No. 30620) and microwave powered hydrogen and bromine flow discharge lamps[12] were used as photolysis sources. The spec-

tral emission from the Hg lamp and bromine discharge lamp are shown in Figures 1 and 2, respectively. The spectral characteristics of the hydrogen discharge lamp have been discussed in a previous publication.[13] These emission spectra were recorded using a McPherson 225 vacuum–ultraviolet monochrometer in conjunction with a McPherson Model 790A electronic detector system. The various wavelength regions of the Hg lamp were isolated by attaching calibrated glass filters (Esco Products) directly to the LiF ultraviolet transmitting window. The wavelength regions transmitted by these filters and their corresponding Esco numbers were the following: wavelengths >3000 Å, 0-54 0160; 3100-4500 Å, 7-59 5850; 3100-4000 Å, 7-60 5840. The transmission characteristics of these filters were also checked with the McPherson instrument and found to be consistent with the Esco published data.

The identification of the photochemically produced species was obtained from the infrared spectra after photolysis. A Perkin-Elmer 621 spectrophotometer was used for this purpose.

III. Results

The infrared spectrum of a film of Ar:CH_2O = 800:1 before photolysis is shown in the solid trace of Figure 3. The spectrum of the unphotolyzed sample agrees well with that reported by Khoshkhoo and Nixon.[14] When this film was subjected to radiation from an unfiltered medium-pressure Hg lamp, a single new absorption appeared at 2138 cm^{-1} as shown in the dashed trace of Figure 3 and summarized in Table I, column 1. This new absorption is indicative of CO as demonstrated by Leroi, Ewing, and Pimentel.[15] In order to obtain an estimation as to where the onset of photodissociation occurred under these conditions, the photolysis of matrix isolated Ar:CH_2O = 800:1 samples was performed by passing the Hg radiation through a series of ultraviolet filters. The transmission characteristics of each of the filters were matched to excite specific portions of the n → π* transition (3967-3600 and 3530-2300 Å). The results of simultaneous deposition and photolysis with each filtered Hg photolysis experiment showed no new features; this suggests that wavelengths less than 3000 Å were responsible for photodecomposition.

In order to gain a better understanding of the mechanism of photochemical decomposition, a Hg lamp photolysis of Ar:CH_2O:CD_2O = 800:1:1 was performed. The infrared spectrum of the unphotolyzed sample agreed with the individual spectra of matrix isolated CH_2O and CD_2O reported by Khoshkhoo and Nixon.[14] The results of 5 hr of simultaneous deposition and photolysis of this sample again resulted in a single new feature, the 2138-cm^{-1} absorption due to CO.

The next lowest electronic absorption of CH_2O leading to diffuse band structure at the short wavelengths is the 1750-1650-Å system. For this system, photolysis was performed with vacuum–ultraviolet radiation from the single 1634-Å resonance line of a microwave powered discharge bromine lamp. In Figure 4 the results of the bromine discharge lamp photolysis of the Ar:CH_2O = 800:1 film are presented (dotted line) along with one absorption of unphotolyzed sample (solid line). The new absorption at 2138 cm^{-1} is indicative of CO and those at 1863 and 1085 cm^{-1} are due to HCO, with the CO absorption being much stronger in intensity than those of HCO. The HCO assignment is based on work reported by Milligan and
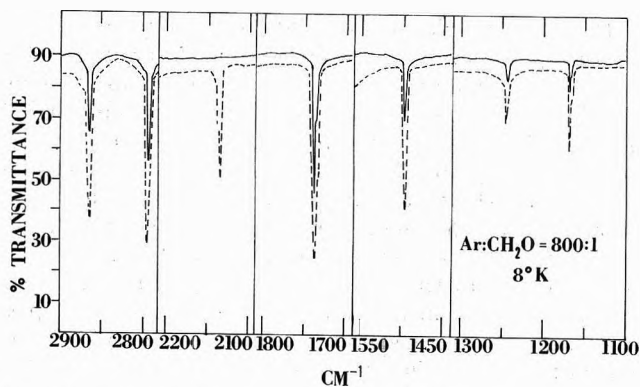
Figure 3. Infrared spectra of Ar:CH$_2$O = 800:1: (a) (——) deposition at 8 K, 1 mm/min for 1 hr from a 2.5-l. volume; (b) (-----) simultaneous deposition and photolysis for 5 hr with a medium-pressure Hg lamp.
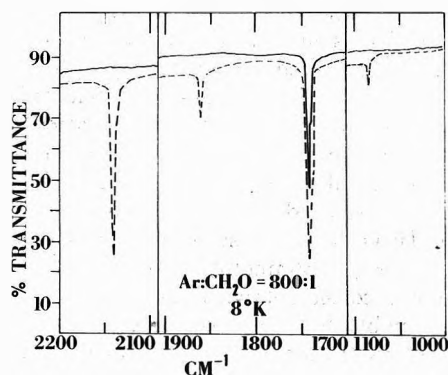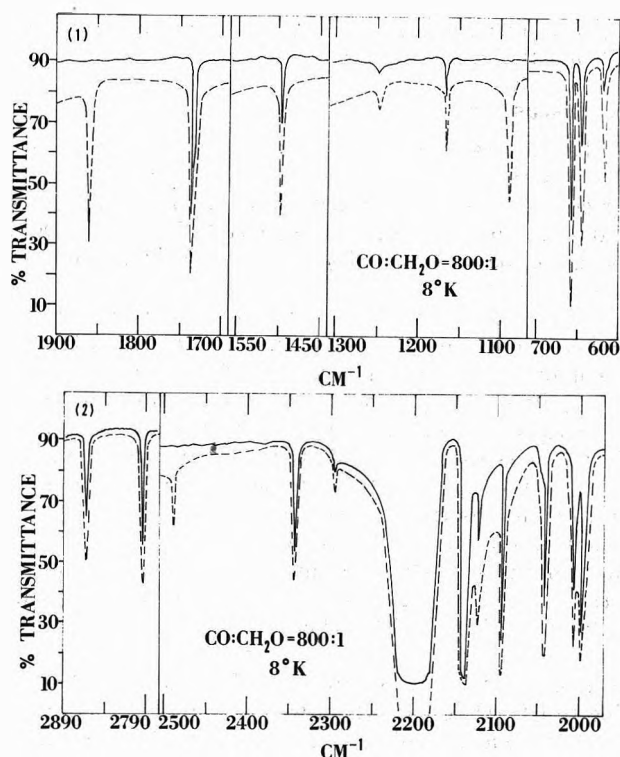

Figure 4. Infrared spectra of Ar:CH$_2$O = 800:1: (a) (——) unphotolyzed sample identical with that shown in Figure 3a with all absorptions omitted except one; (b) (- - - -) simultaneous deposition and photolysis for 5 hr with a bromine discharge lamp.

TABLE I: Summary of Absorptions (cm^{-1}) in the Ar:CH$_2$O = 800:1 Experiments

| Before photolysis | After photolysis[a] | | | Assignment |
	1	2	3	
		1085 w		HCO
1168 w				CH$_2$O
1245 w				CH$_2$O
1498 m				CH$_2$O
1742 s				CH$_2$O
		1863 w		HCO
	2138 ms	2138 s	2138 w	CO
2797 ms				CH$_2$O
2863 m				CH$_2$O

[a] After photolysis with the following lamps: (1) a medium-pressure Hg lamp; (2) bromine discharge lamp; (3) hydrogen discharge lamp.

Jacox,[16] taking into account the usual matrix shifts in going from the argon to the CO matrix. Upon controlled warming, the HCO features disappeared and the CO feature broadened while all others remained unchanged. The disappearance of the HCO absorptions upon warming is indicative of the reactivity of HCO. The results of photolysis are summarized in Table I, column 2.

Excitation into the CH$_2$O Rydberg series (1397–1161 Å) was also performed with radiation from a hydrogen discharge lamp. After 5 hr of simultaneous deposition and photolysis of this sample, a weak absorption appeared at

Figure 5. Infrared spectra of CO:CH$_2$O = 800:1: (a) (——) deposition at 8 K, 1 mm/min for 1 hr from a 2.5-l. volume; (b) (-----) simultaneous deposition and photolysis for 5 hr with a bromine discharge lamp: (1) 1900–1700, 1550–1450, 1300–1100, 700–600 cm^{-1}; (2) 2890–2790, 2500–1994 cm^{-1}.

TABLE II: Summary of Absorptions (cm^{-1}) in the CO:CH$_2$O = 800:1 Experiments

Before photolysis	After photolysis	Assignment
618 w		CO$_2$
645 m		CO$_2$
658 s		CO$_2$
	1089 s	HCO
1168 w		CH$_2$O
1249 w		CH$_2$O
1497 m		CH$_2$O
1736 s		CH$_2$O
	1860 s	HCO
1994–2300 vs		CO
2344 ms		CO$_2$
	2488 mw	HCO
2794 ms		CH$_2$O
2861 m		CH$_2$O

2138 cm^{-1} due to CO. This result is shown in Table I, column 3.

Photolysis experiments were also performed with CH$_2$O in carbon monoxide and CO-doped argon matrices. The results of Hg lamp photolysis of a CO:CH$_2$O = 800:1 film showed no new features. A Hg lamp *in situ* photolysis of Ar:CH$_2$O:CO = 800:1:1 was also performed. The results of this experiment simply revealed the increased growth of the CO absorption. However, after 5 hr of simultaneous deposition and bromine discharge lamp photolysis of CO:CH$_2$O = 800:1, new features appeared at 2488, 1860, and 1089 cm^{-1}. These new features are attributable to HCO.[16] Thus, further evidence for photodetachment of H atoms from the 1750–1650-Å system is presented. Some CO$_2$ is observed in the spectrum as an impurity from CO.

These results are presented in Figure 5 and summarized in Table II.

IV. Discussion

The sources used here to photolyze matrix isolated CH_2O were a medium-pressure Hg lamp (5788 Å, 2.1 eV–air cutoff), a hydrogen discharge lamp (1215 Å, 10.2 eV), and a bromine discharge lamp (1634 Å, 7.6 eV). Since the ionization potential of CH_2O is 10.88 eV, it is safe to assume that ion production is unimportant in the systems under consideration here. From gas-phase work, the energy necessary to dissociate the first H atom from CH_2O is estimated to be between 3.02 and 3.56 eV;[4,17,18] the energy required to remove both H atoms is estimated thermochemically[17] to be 4.53 eV. Based on these results, the light sources used in this study that lead to photodissociation of CH_2O are of sufficient energy to remove H, 2H, or H_2 from the absorption of a single photon.

The results of photolysis, with the full intensity of a medium-pressure Hg lamp and the H_2 discharge lamp, of CH_2O isolated in argon showed a single new absorption at 2138 cm^{-1} due to CO. When the same experiment was performed with a bromine discharge lamp, new absorptions appeared at 2138, 1863, and 1085 cm^{-1}; the first was due to CO while the others were due to HCO. Thus, the reactions which could be important in this system and serve as a basis of discussion are the following

$$H_2CO + h\nu \longrightarrow H + HCO \qquad (1)$$

$$H_2CO + h\nu \longrightarrow H_2 + CO \qquad (2)$$

$$HCO + h\nu \longrightarrow H + CO \qquad (3)$$

$$H + HCO \longrightarrow H_2 + CO \qquad (4)$$

$$H + H_2CO \longrightarrow \text{no reaction} \qquad (5)$$

$$H + HCO \longrightarrow H_2CO \qquad (6)$$

$$H + H \longrightarrow H_2 \qquad (7)$$

$$H + CO \longrightarrow HCO \qquad (8)$$
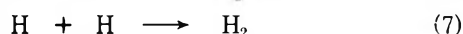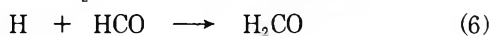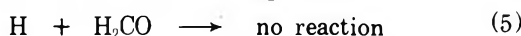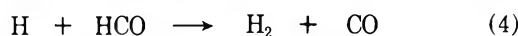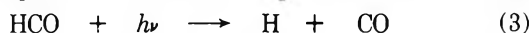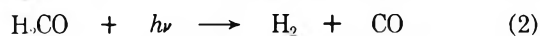
The Hg photolysis experiments using the various ultraviolet filters indicated no observable photodecomposition above 3000 Å. This is not an unexpected result since the 3967–3600-Å band is symmetry and spin forbidden with an $\epsilon_{max} \simeq 10^{-3}$ M^{-1} cm^{-1}, and the 3530–2300-Å band only symmetry forbidden with an $\epsilon_{max} \simeq 18$ M^{-1} cm^{-1}. Absorption into the latter gives well-defined structure to about 2800 Å, whereupon diffuseness sets in and extends to 2300 Å with decreasing intensity. It appears from the results of the Hg lamp photolysis experiments that process 2 clearly dominates in this case with practically no contribution from (1). The absence of HCO could possibly be the result of secondary photolysis. However, this process would have to be extremely efficient such that absolutely no net HCO would be observed. This possibility seems unlikely based on our previous experience with HCO in other systems.[10,11] In addition, CO is known to be a weak absorber in the infrared; thus, even a rather low concentration of HCO would be expected to be observed relative to CO, if reaction 1 were significant to any real extent. Processes 4 and 5 involving abstractions are expected to play a minimal role since any reactions they undergo would probably involve an activation energy greater than 2.0 kcal/mol.[19] Such processes are extremely improbable in condensed media below 20 K. The other competitive H atom processes (6, 7, and 8) should all have practically zero activation energy and depend simply on the concentration of the bimolecular reaction partner.

However, in order to more stringently test the hypothesis that process 2 > 1 and that (4) and (5) are not significant, an *in situ* photolysis with the Hg lamp involving the doped mixture Ar:CH_2O:CO = 800:1:1 was performed. In this situation any H atoms produced would have a much higher probability of encountering a CO molecule, and of the H atom diffusion processes 4–8, reaction 8 should clearly dominate. The results of this experiment revealed simply the increased growth of CO and no absorptions due to HCO. It might be argued that H atoms photodissociated inside of a matrix site might not have sufficient recoil translational energy to escape, thereby obviating its reaction with isolated CO molecules. This possibility is negated by the results obtained using CO as the matrix where no observable HCO was produced.

Previously, Adrian, Cochran, and Bowers[9] used a low-pressure Hg lamp (2537 and 1849 Å) to photolyze CH_2O (1%) in an argon matrix and reported the esr spectrum of HCO, which is indicative of the occurrence of reaction 1. From esr, which is more sensitive than ir by a factor of 10^2 or 10^3, they observed a large isotropic proton hyperfine splitting for HCO. They suggested that this splitting could be explained in terms of configuration interaction between the ground state and a low-energy excited state, consisting of an unbonded H atom interacting with a CO molecule. The esr study presents evidence for the weakness of the HCO bond and suggests that H atoms may be present in our Hg lamp photolysis study. These results are however not inconsistent with those of this study since they were unable to detect H_2 or CO. The implication from the interpretation of the combined results (ir and esr) based on sensitivity is that process 2 is greater than process 1 by at least a factor of 100.

A final experiment designed to test H atom production, assuming for the moment secondary photolysis of HCO to be 100% efficient, was performed with a one to one mixture of CH_2O:CD_2O in argon. In this case any significant amount of H or D atoms produced by photolysis should react to form the mixed isotopes, CHDO or HD *via* reactions 4, 6, and 7. The results of this photolysis showed only one new feature in the infrared, which was attributed to CO. The absence of new absorptions, HCO, DCO, HD, or CHDO due to photolysis, suggests that H atoms are not present in sufficient concentration to observe the occurrence of reactions 1 and 3 in the infrared.

Previous low-temperature irradiation of CH_2O (1%) in argon by Cochran and Adrian[8] with a hydrogen discharge lamp ($\lambda > 1450$ Å) produced esr signals consistent with the occurrence of reaction 1. These authors suggested that secondary photolysis of HCO (reaction 3) occurred resulting in the observation of highly excited H atoms. However, the results we obtained, upon photolysis with a hydrogen discharge lamp of CH_2O in argon, showed only a weak absorption in the infrared due to CO; this absorption was considerably weaker in intensity than that obtained with the Hg lamp and indicated that process 2 > 1 in this case. Again, the fact that secondary photolysis is occurring here (reaction 3) seems unlikely since no net HCO is found and the concentration of CO obtained from photolysis is low. It is surprising that the photodissociative yield in this case was not more efficient since this Rydberg series is reported to be very intense.[17,20,21] We assume the 1215-Å line is either weakly absorbed into the continuum or that predissociation is relatively inefficient.

Upon photolysis of Ar:CH_2O = 800:1 with a bromine discharge lamp, new absorptions appeared at 2138, 1863,

and 1085 cm^{-1}; the first absorption due to CO and the others due to HCO, suggesting the occurrence of reactions 1 and 2. The probability of reaction 3 occurring is rather remote since the photolytic source emitted principally the three bromine resonance lines at 1634, 1582, and 1577 Å, but (3) cannot be conclusively discounted. Since the CO feature was much stronger than those of HCO (Figure 4) and CO is a weak absorber in the infrared it is again suggested that process 2 > 1. The results of photolysis with a bromine discharge lamp of CH$_2$O isolated in carbon monoxide verified H-atom detachment as a photodecomposition mechanism by showing new features at 2488, 1860, and 1089 cm^{-1} due to HCO.

Since the possibility exists that process 4 might mask or reduce significantly HCO production in all wavelength regions and particularly at long wavelengths, it will be considered in detail at this point. Presuming first that process 1 occurs within the site and the H atom does not escape, then the recombination would most likely be process 4 or 6. The most important factor determining which will dominate is probably the activation energy. In the absence of known values for these processes, we cite the results of numerous studies[10,11] involving atom addition vs. atom abstraction processes in condensed media below 20 K performed in this laboratory, where the former has consistently been the dominant process and therefore assumed to have a lower activation energy.

If, on the other hand, the H atom does escape the photolytic site, then detection of its formation would have been accomplished by the experiments involving D$_2$CO-H$_2$CO, CO matrix, and CO-doped argon experiments.

V. Conclusions

The photodecomposition mechanism of matrix-isolated CH$_2$O is a function of photon energy. By matching the Hg lamp emission spectrum (Figure 1) with the 3967-2300-Å electronic absorption band[17,22] of CH$_2$O ($^1A_2$, $^3A_2$, $^1A_1{}^v$, etc.) it is concluded that the Hg lamp (major lines at 2654 and 2537 Å) excites CH$_2$O into the 2750-2300-Å continuum. This excitation process leads to dissociative products H$_2$ and CO. These observations suggest that reaction 2 is the major primary photodissociative process occurring between 3000 Å and the air cutoff. From gas-phase work, McQuigg and Calvert[7] have suggested that reaction 2 predominates at long wavelengths (3550 Å) and reaction 1 occurs at wavelengths near 3385 Å. However, H atoms or HCO are not observed as photolysis products in our Hg lamp experiments; this may be due to the matrix quenching of the predissociative state,[23-25] which leads to H and HCO. Another reason for the discrepancy between this work and that of McQuigg and Calvert[7] is in the nature of the different experiments. The recent laser-induced photochemical dissociation of formaldehyde by Yeung and Moore[26] clearly indicates that the gas-phase studies to date are collision-induced dissociation processes, whereas our experiments more nearly approach "zero pressure" photochemical dissociation. The relative yields of pro-

cesses 1 and 2 under these conditions are probably quite different.

It appears that the bromine discharge lamp (Figure 2; 1634, 1577 Å) excites CH$_2$O into the continuum of the diffuse 1750-1650-Å electronic absorption band[17,20,21] ($^1B_2$); this process leads to the photodissociative products CO, H$_2$, HCO, and H. Based on relative intensities, a greater amount of CO than HCO was obtained; therefore, it appears that reaction 2 > 1 at 1634 Å. The possibility of secondary photolysis of HCO also exists in this case, but appears to be rather remote.

Matching the hydrogen discharge lamp emission spectrum (10.2 eV, 1215 Å)[13] with the diffuse 1397-1161-Å (Rydberg series) electronic absorption band[17,20,21] of CH$_2$O suggests excitation into a predissociative state; this process leads to the photodissociative products CO and H$_2$. The results of this study suggest the occurrence of reaction 2 as the major primary photodissociative process at 1215 Å.

References and Notes

(1) Alfred P. Sloan Foundation Fellow.
(2) (a) J. Heicklen, K. Westenberg, and N. Cohen, Pennsylvania State Center Air for Environmental Studies, Publication No. 115-69 (1969); K. Westenberg, N. Cohen, and K. W. Wilson, *Science*, **171**, 1013 (1971); (b) J. G. Calvert, J. A. Kerr, K. L. Demerjian, and R. D. McQuigg, *ibid.*, **175**, 751 (1972).
(3) E. Gorin, *J. Chem. Phys.*, **7**, 256 (1939).
(4) R. Klein and L. J. Schoen, *J. Chem. Phys.*, **24**, 1094 (1956).
(5) A. G. Harrison and F. P. Lossing, *Can. J. Chem.*, **38**, 544 (1960).
(6) B. A. DeGraff and J. G. Calvert, *J. Amer. Chem., Soc.*, **89**, 2247 (1967).
(7) R. D. McQuigg and J. G. Calvert, *J. Amer. Chem. Soc.*, **91**, 1590 (1969).
(8) E. L. Cochran and F. J. Adrian, 5th International Symposium on Free Radicals, Uppsala, July, 1961; published in Preprints of Papers, Almquist and Wiksell, Stockholm, 1961, paper No. 12.
(9) F. J. Adrian, E. L. Cochran, and V. A. Bowers, *J. Chem. Phys.*, **36**, 1661 (1962).
(10) G. R. Smith and W. A. Guillory, *J. Chem. Phys.*, **56**, 1423 (1972).
(11) W. A. Guillory, R. J. Isabel, and G. R. Smith, *J. Mol. Struct.*, in press.
(12) D. Davis and W. Braun, *Appl. Opt.*, **7**, 2071 (1968).
(13) R. Isabel and W. A. Guillory, *J. Chem. Phys.*, **55**, 1197 (1971).
(14) H. Khoshkhoo and E. R. Nixon, *Spectrochim. Acta, Part A*, **29**, 603 (1973).
(15) G. E. Leroi, G. E. Ewing, and G. C. Pimentel, *J. Chem. Phys.*, **40**, 2298 (1964).
(16) D. Milligan and M. E. Jacox, *J. Chem. Phys.*, **41**, 3032 (1964).
(17) G. Herzberg, "Molecular Spectra and Molecular Structure. III. Electronic Spectra and Electronic Structure of Polyatomic Molecules," Van Nostrand, Princeton, N. J., 1966, p 612.
(18) R. I. Reed, *Trans. Faraday Soc.*, **52**, 1195 (1956).
(19) W. R. Brennen, I. D. Gay, G. P. Glass, and H. Niki, *J. Chem. Phys.*, **43**, 2569 (1965).
(20) W. C. Price, *J. Chem. Phys.*, **3**, 256 (1935).
(21) E. P. Gentieu and J. E. Mentall, *Science*, **169**, 681 (1970).
(22) J. G. Calvert and J. N. Pitts, "Photochemistry," Wiley, New York, N. Y., 1966, p 368.
(23) J. C. Brand, *J. Chem. Soc.*, 858 (1956).
(24) J. C. Brand and R. I. Reed, *J. Chem. Soc.*, 2386 (1957).
(25) G. W. Robinson and V. E. DiGiorgio, *Can. J. Chem.*, **36**, 31 (1958).
(26) E. S. Yeung and C. B. Moore, *J. Chem. Phys.*, **58**, 3988 (1973).

Hydrothermal Hydrolysis of Al^{3+} and the Precipitation of Boehmite from Aqueous Solution

Digby D. Macdonald,*[1a] P. Butler,[1b] and D. Owen

Research Chemistry Branch, Whiteshell Nuclear Research Establishment, Atomic Energy of Canada Limited, Pinawa, Manitoba, Canada (Received January 29, 1973)

Publication costs assisted by Atomic Energy of Canada Ltd.

The hydrothermal hydrolysis of Al^{3+} in aqueous KCl solutions and the precipitation of boehmite (γ-AlOOH) have been studied by *in situ* acidity measurements at temperatures to 200°. The effect of varying the initial solution pH and the total aluminum concentration was investigated. The hydrothermal hydrolysis behavior was found to be consistent with the equilibria $2Al^{3+} + 2H_2O = Al_2(OH)_2^{4+} + 2H^+$ and $14Al^{3+} + 34H_2O = Al_{14}(OH)_{34}^{8+} + 34H^+$ followed by the irreversible formation of boehmite from the polymeric species $Al_{14}(OH)_{34}^{8+}$.

Introduction

It has long been recognized that oxides and hydroxides can be precipitated hydrothermally from solutions containing dissolved metal ions. This phenomenon is of considerable scientific and practical interest since it is believed to occur in processes such as the formation of terrestrial ore deposits[2a] and the growth of oxide layers on corroding metal surfaces.[2b] Helgeson[2a] has recently reviewed previous work on the hydrothermal deposition of solid products from ionic solutions. These studies show that the deposition process is largely determined by the effect of temperature on the position of equilibria between metal ions and complexing species in solution. The equilibria of interest in the present study involve the hydrolysis of metal ions to form progressively higher hydrolyzed species and ultimately the solid oxide or hydroxide. While it is known that these equilibria shift in the general direction of the solid product with increasing temperature, few details of this process have been determined. For instance, almost no data are available on the identity of the hydrolyzed species in the system prior to precipitation or as to how temperature affects the pH of the solution and the average number of hydroxide ions bound per metal atom in the system. These data are required before a quantitative description of hydrothermal precipitation is possible.

In this study we have used recently developed potentiometric techniques[3,4] to measure the acidity of aluminum chloride-potassium chloride solutions at temperatures to 200°. The hydrolysis and precipitation phenomena have been studied as a function of initial solution pH, total aluminum concentration, and time of storage of the solution at 25°. Detailed X-ray diffraction studies of the precipitated phase were made to supplement the acidity-temperature measurements outlined above.

Experimental Section

High-Temperature Concentration Cell. The electrolyte concentration cell with liquid junction[3,4] used to measure acidities at elevated temperatures is shown in Figure 1. The cell consisted of a titanium autoclave (300 ml) which was gold plated on the inside surface to minimize contamination. The inner compartment was machined from Tef-

lon to a wall thickness of <1.5 mm which allowed rapid thermal equilibration of the contents of the two compartments. Both compartments contained Teflon-covered magnetic stirring bars to agitate the solutions. These stirring bars were activated by a rotating magnet located beneath the aluminum oil bath used to control temperature. The vapor spaces of the two compartments were connected *via* a 0.76-mm hole which allowed rapid pressure equilibration, yet was small enough to minimize distillation from one compartment to the other prior to thermal equilibration.

The reversible hydrogen electrodes consisted of pure platinum tubes (3 mm o.d., 1.5 mm i.d.) which were weld-sealed at the lower ends. The electrodes were insulated from the autoclave and from each other by Conax fittings containing Teflon sheaths and cones. The electrodes were lightly platinized before use by electrolysis in a dilute solution of chloroplatinic acid. Chromel–alumel thermocouples (0.8 mm diameter) were inserted into the platinum tubes to monitor the temperatures of the two compartments.

The liquid junction between the two compartments consisted of a porous Teflon disk (3 mm thick, 6.4 mm diameter, 10 μm pore size) as previously described.[3] Reliable liquid junctions were formed by wetting the porous Teflon with acetone and then forcing potassium chloride solution through the disk under pressure.

The entire autoclave was immersed in an oil bath which allowed temperatures (25–200°) to be controlled to ±0.1°. All potential measurements were made using a Beckman Research pH meter. This instrument was capable of detecting 0.1 mV changes in voltage between the two hydrogen electrodes. The cell was degassed by cyclic compression–decompression and finally pressurized to 0.6 Pa with pure hydrogen prior to heating. The temperature was increased in steps of 10–20° and potentials were recorded after they had become sensibly constant for at least 15 min (variation <0.1 mV.)

Solutions. Solutions of Al^{3+} in HCl–KCl media, where the concentration of chloride ion was held constant at 1 mol/kg, were prepared either by dissolving pure aluminum metal in concentrated HCl followed by dilution with the appropriate KCl solution or by dissolution of weighted
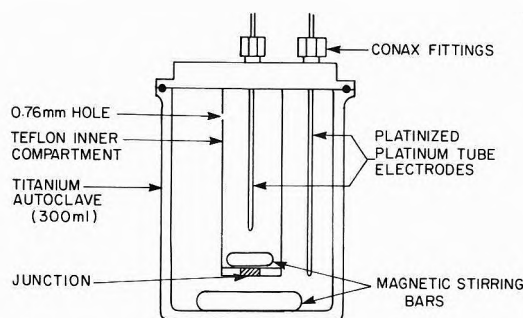
**Figure 1.** High-temperature potentiometric concentration cell.

amounts of reagent grade $AlCl_3$ and KCl in dilute HCl solution. Identical results were obtained using solutions prepared by both techniques. The exact concentration of Al^{3+} was determined by back titration of a sample of the solution in EDTA with Zn^{2+} using Eriochrome Black T indicator. Aluminum analyses were reproducible to $\pm 1\%$. The reference compartment contained a HCl-KCl solution with $[H^+] = 1.00 \times 10^{-3}$ mol/kg and $[Cl^-] = 1.00$ mol/kg. This solution was stored in polyethylene and glass containers and the pH was checked periodically against a glass electrode to detect any variations. None were found. All solutions were prepared from doubly distilled water, having a conductivity not greater than 0.5×10^{-8} S m^{-1}.

Results and Discussion

X-Ray Diffraction Studies. Powder diffraction patterns of precipitates formed on heating Al^{3+}-KCl solutions to 200° showed that the major constituent was boehmite, γ-AlOOH (ASTM 21-1307, 17-940). Four additional, but yet unidentified, lines with d spacings of 4.90 (w), 2.82 (vvw), 0.786 (w), and 0.784 (w), were also found. These lines do not correspond to any pattern listed in the ASTM index for aluminum oxides, oxychlorides, or hydroxides.

The formation of boehmite observed in the present study is in agreement with the findings of Mesmer and Baes[5] who observed the precipitation of this product from chloride solutions at 150°. This finding is also consistent with recent thermodynamic calculations[6] which show that boehmite is the stable oxide of aluminum in the temperature range of interest (*i.e.*, 150–200°).

High-Temperature Acidity Measurements. The concentration cell with liquid junction used to determine acidities at elevated temperatures can be represented formally as

$$Pt(H_2)\,|\,H^+(a_1)\,|\,H^+(a_2)\,|\,(H_2)Pt \qquad (I)$$
$$E$$
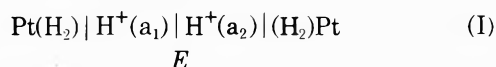
where subscripts 1 and 2 refer to the inner and outer compartments, respectively, and the potential (E) represents the potential difference between the outer and inner compartment platinum electrodes. Since the pressure of hydrogen is the same in both compartments, the potential difference, E, is given by

$$E = \frac{2.303RT}{F} \log \frac{(a_2)}{(a_1)} + E_j \qquad (1)$$

where E_j is the liquid junction potential. Liquid junction potentials were estimated using the Henderson equation

$$E_j = -\sum D_i[(m_i)_2 - (m_i)_1] \qquad (2)$$

The D_i coefficient for the ith species in solution is given by

$$D_i = RT|z_i|\lambda_i / (z_iF)\sum(|z_i|\overline{m}_i\lambda_i) \qquad (3)$$

where $\overline{m}_i$ is the average concentration of species i in the two compartments, z_i is the ionic charge, and λ_i is the equivalent conductance. Equivalent conductances for K^+, Cl^-, H^+, and OH^- at temperatures to 400° have been reported by Quist and Marshall[7] and were used here to estimate E_j. The junction potential contribution due to the diffusion of Al^{3+} was calculated using eq 2 and 3 and equivalent conductances for this species estimated from Stokes' law[8]

$$\lambda = 0.820|z|/r_s\eta \qquad (4)$$

where r_s is the "Stokes radius," taken as 3.95 Å for Al^{3+},[8] and η is the viscosity of water.[9] No corrections were possible for diffusional processes involving hydrolyzed ions since insufficient data are available on their identities and electrochemical properties. In the present study, however, liquid junction potentials rarely exceeded 1 mV. This represents a minor correction to the measured potential (typically 100 mV) and exclusion of hydrolyzed species in calculation of liquid junction potentials is unlikely to result in an error of greater than 0.1 mV.

Expansion of eq 1, and denoting pH $= -\log m_{H^+}$, results in

$$pH_2 = pH_1 - \frac{F(E - E_j)}{2.303RT} + \log \frac{\gamma_2}{\gamma_1} \qquad (5)$$

where γ_2 and γ_1 are activity coefficients for hydrogen ion in the outer and inner (reference) compartments, respectively. We assume that, although the ionic strengths of the solutions are well outside the Debye-Hückel range,[8] the *ratio* of activity coefficients can be approximated by the expression

$$\log \frac{\gamma_2}{\gamma_1} = -z^2 S \left[\frac{\sqrt{I_2} - \sqrt{I_1}}{(1 + \sqrt{I_2})(1 + \sqrt{I_1})} \right] \qquad (6)$$

where I is the ionic strength $[= \frac{1}{2}\sum m_i z_i^2]$ and the coefficient S is given by

$$S = 1.814 \times 10^6 / (\epsilon T)^{3/2} \qquad (7)$$

Dielectric constant (ϵ) data were taken from the work of Akerlof and Oshry.[10] Since $I_2 \approx I_1$, the contribution that the activity coefficient term (eq 6) makes to pH_2 in eq 5 is small (usually <0.01), and any error inherent in the above assumption is probably within the total experimental error.

The variation of hydrogen ion concentration with temperature for aluminum solutions having different initial acidities is plotted in Figure 2. The pH-temperature profiles were highly reproducible with variations of less than ± 0.01 in pH at temperatures to 200°. In the absence of hydrolysis, the molal concentration of hydrogen ion in the system is independent of temperature. Thus, for an initial pH of 1.75 no detectable hydrolysis occurs below 100°. However, for an initial pH of 2.58 hydrolysis occurs almost immediately on heating. A particularly interesting feature of the data plotted in Figure 2 is that the pH(T)-temperature curves converge at high temperatures, *i.e.*, the acidity of the solution at 200° is relatively insensitive to variation of pH at 25°. This buffering action of the hydrolysis equilibria is well demonstrated in Figure 3 in which pH(T) *vs.* pH(25°) profiles are plotted for eight different temperatures between 25 and 200°. Thus, only at the highest initial acidity is there any detectable dependence
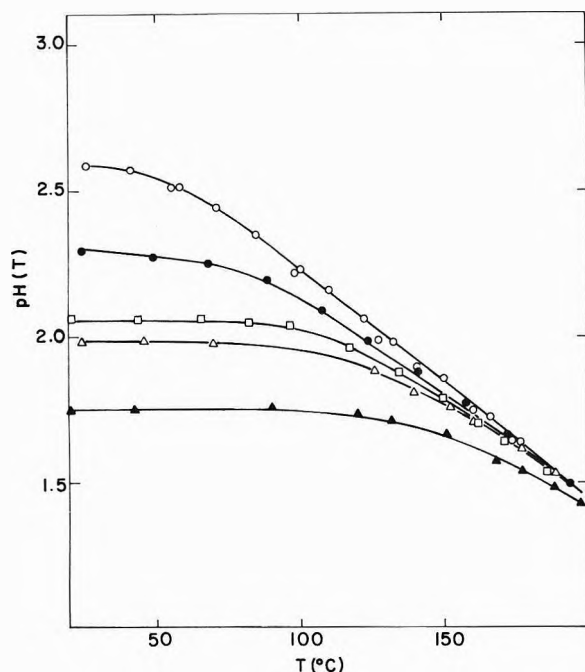
Figure 2. pH(T)-temperature profiles for the hydrolysis of Al^{3+} (0.038 mol/kg) in KCl solution. Total Cl^- concentration = 1 mol/kg. Initial pH values are as follows: ▲, 1.75; △, 1.97; □, 2.04; ●, 2.30; ○, 2.59.

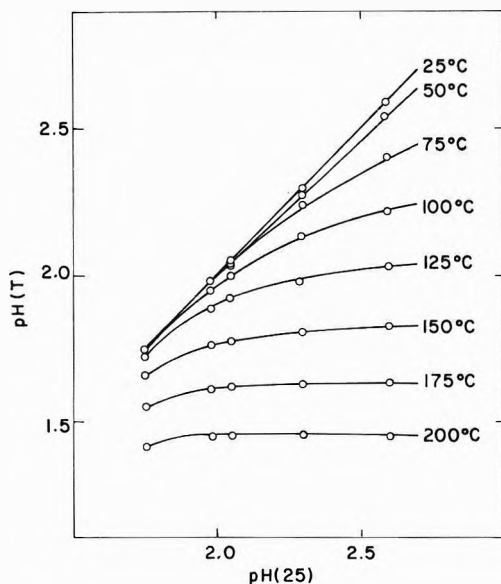**Figure 3.** Plot of pH(T) vs. pH(25) at various temperatures to 200°. Total aluminium concentration = 0.038 mol/kg.

of pH(T) on pH(25) at 200°. However, the dependence becomes more pronounced with decreasing temperature, as expected.

Hydrothermal Hydrolysis. The influence of temperature on hydrothermal hydrolysis and precipitation is best considered by defining a parameter $Z(T)$ equal to the average number of hydroxide ions bound to metal in the system. The total molal concentrations of hydrogen and oxygen in a system containing $H^+(m_1)$, $OH^-(m_2)$, $H_2O(m_3)$, and metal (M) are given by

$$[H]_{total} = (m_1)_T + (m_2)_T + 2(m_3)_T + Z_T(M)_T \quad (8)$$

$$[O]_{total} = (m_2)_T + (m_3)_T + Z_T(M)_T \quad (9)$$

where subscript T refers to temperature. Due to equilibration between H^+ and OH^-, the concentration of hydroxide ion in the system is given by

$$(m_2)_T = Q_{W,T}/(m_1)_T \quad (10)$$

where $Q_{W,T}$ is the ionic product of water at the temperature of interest.[3] Substitution of eq 10 into eq 8 and 9, followed by elimination of m_3 for two temperatures T and T_0, results in eq 11 for $Z(T) - Z(T_0)$. Thus, the change

$$Z(T) - Z(T_0) = [Q_{W,T_0}/(m_1)_{T_0} - Q_{W,T}/(m_1)_T]/$$
$$M + [(m_1)_T - (m_1)_{T_0}]/(M) \quad (11)$$

in Z with temperature is easily calculated from the corresponding change in pH of the solution. In the majority of experiments reported here, the initial pH (pH(25°)) of the solution was chosen such that $Z(T_0)$ is very small and the change in Z, i.e., $Z(T) - Z(T_0)$, can be equated to $Z(T)$.

Plots of $Z(T)$ vs. temperature for Al^{3+} (0.038 m)-KCl solutions having different pH(25) values are shown in Figure 4. These curves were calculated directly from the data plotted in Figure 3 using eq 11. As shown in Figure 4, hydrolysis begins almost immediately on heating for the solution with the highest starting pH (2.58) but not below 100° for the most acidic (pH(25) 1.75) solution. Above these temperatures, $Z(T)$ increases rapidly on heating so that by 190° the above solutions have $Z(T)$ values of 0.75 and 0.45, respectively.

The influence of varying the total aluminum concentration on the hydrothermal hydrolysis of Al^{3+} is shown in Figures 5 and 6. At both initial pH values, the more concentrated solution undergoes hydrolysis first on heating as shown by the pH(T) vs. temperature profiles plotted in Figure 5. Furthermore, the pH(T) vs. temperature profiles tend to become parallel at high temperatures. The $Z(T)$ vs. temperature profiles calculated from the data plotted in Figure 5 are shown in Figure 6. At temperatures greater than 130°, and for both initial pH values, the solution with the lowest Al^{3+} concentration has the highest Z values. At lower temperatures, the reverse appears to hold true, although the accuracy of the data is not sufficient to establish this phenomenon with certainty for the solutions with the lowest initial pH value (2.04$_2$). We suggest that this cross-over phenomenon is associated with the irreversible formation of boehmite since precipitation was only observed to occur at temperatures in excess of 150°. Also, if the pH of the solution was measured as a function of decreasing temperature then marked hysteresis in the $Z(T)$ vs. temperature plots (Figure 7) was found to occur if the maximum temperature attained was greater than the cross-over value shown in Figure 6.

A number of experiments were performed with a solution of high initial pH as shown in Figure 8. It was found that the initial pH decreased markedly on storage at room temperature (23 ± 2°) and is attributed to slow hydrolysis reactions occurring in this acidity range ($Z(25°) \neq 0$). This phenomenon has been previously noted[5a] and is most likely responsible for the lack of agreement between different authors as to the hydrolysis behavior of Al^{3+} at room temperature. At high temperatures (>140°) the curves converge as expected from the effect of temperature on rate processes, i.e., the rate of hydrolysis becomes sufficiently rapid that equilibrium is attained in a time which is short compared with that required to perform the measurements.
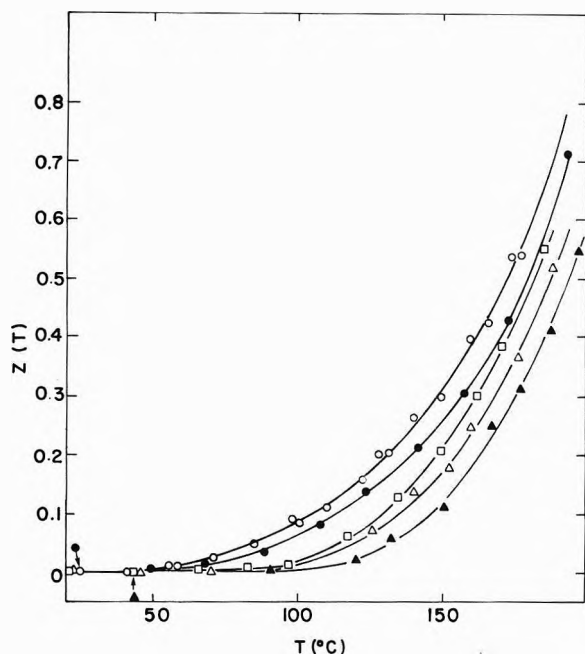
Figure 4. Variation of $Z(T)$ with temperature for the hydrolysis of Al³⁺ (0.038 mol/kg) in KCl solution. Total Cl⁻ concentration = 1 mol/kg. Initial pH values as listed in Figure 2.
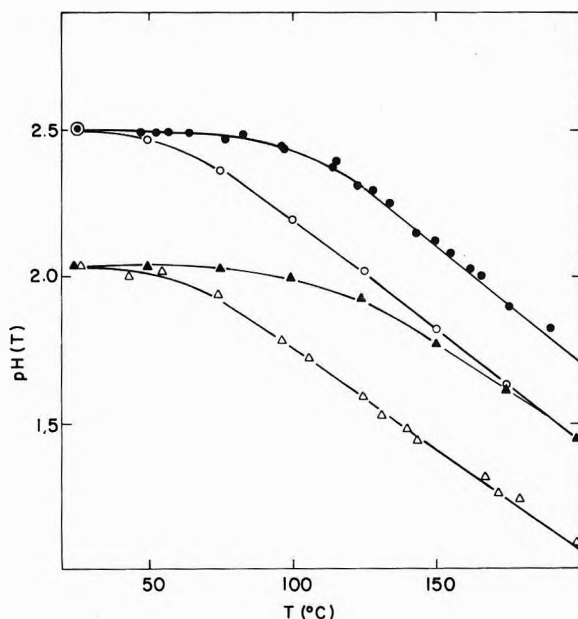

Figure 5. Influence of total aluminum concentration on the pH(T)-temperature profiles for the hydrolysis of Al³⁺ in KCl solution: $\triangle$, [Al] = 0.17 mol/kg, pH(25) = 2.04; $\blacktriangle$, [Al] = 0.038 mol/kg, pH(25) = 2.04; $\bigcirc$, [Al] = 0.038 mol/kg, pH(25) = 2.50; $\bullet$, [Al] = 0.0089 mol/kg, pH(25) = 2.50.

Hydrolysis Mechanism. While this work was in progress, Mesmer and Baes[5a] published a study of the hydrolysis of Al³⁺ in 1 m KCl solution at temperatures to 150°. These authors used a titration technique in which a known number of moles of hydroxide ion was added to the aluminum solution at the temperature of interest and, after equilibration, the pH measured. The difference between the actual pH and the pH expected in the absence of hydrolysis permitted determination of $Z(T)$. It was shown in the study by Mesmer and Baes[5a] that the hydrolysis behavior of Al³⁺ at temperatures to 124.8° is consistent with the existence of the following three polymeric
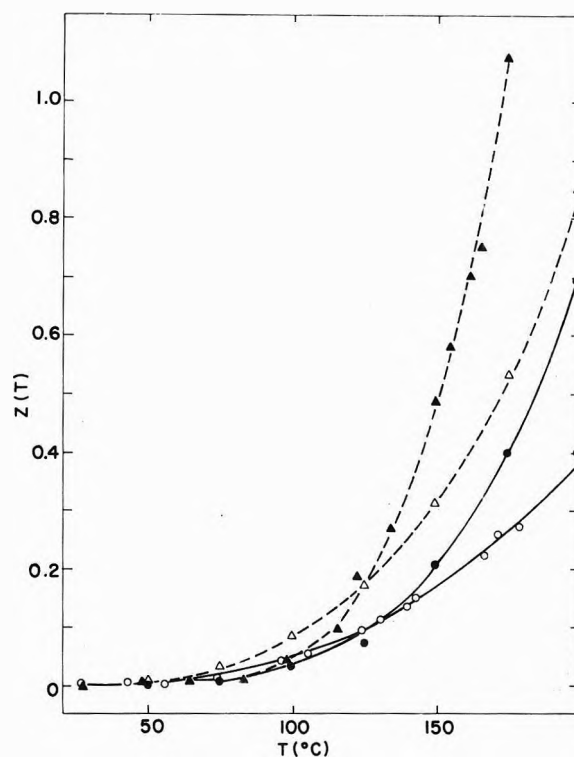
Figure 6. Variation of $Z(T)$ with temperature for the hydrolysis of Al³⁺ as a function of total aluminium concentration and initial pH. Total aluminium concentrations and initial pH values as listed for Figure 5.
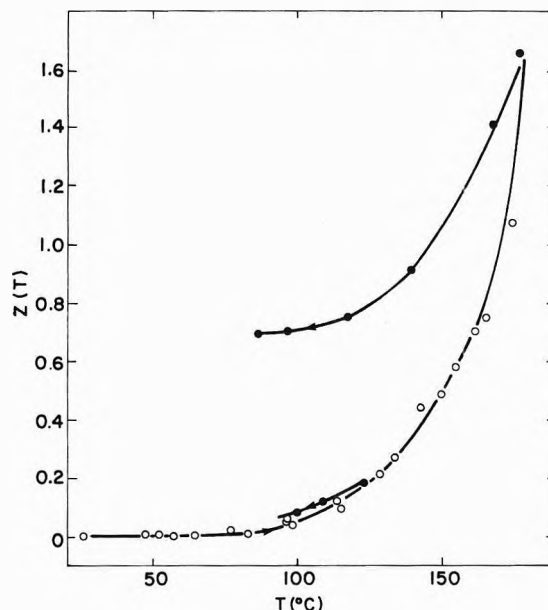
Figure 7. Influence of temperature scan reversal on the $Z(T)$ vs. temperature profile for the hydrolysis of Al³⁺ (0.0089 mol/kg) in 1 mol/kg KCl solution: initial pH 2.50.

species: $Al_2(OH)_2^{4+}$, $Al_3(OH)_4^{5+}$, and $Al_{14}(OH)_{34}^{8+}$. A two species scheme involving $Al_2(OH)_2^{4+}$ and $Al_{14}(OH)_{34}^{8+}$ was found to be somewhat less satisfactory but had the advantage of representing the hydrolysis behavior over a larger temperature range, *i.e.*, to 149.8°. In the following discussion we show that the above hydrolysis schemes also account for the $Z(T)$/temperature profiles observed in the present study over the same temperature range.
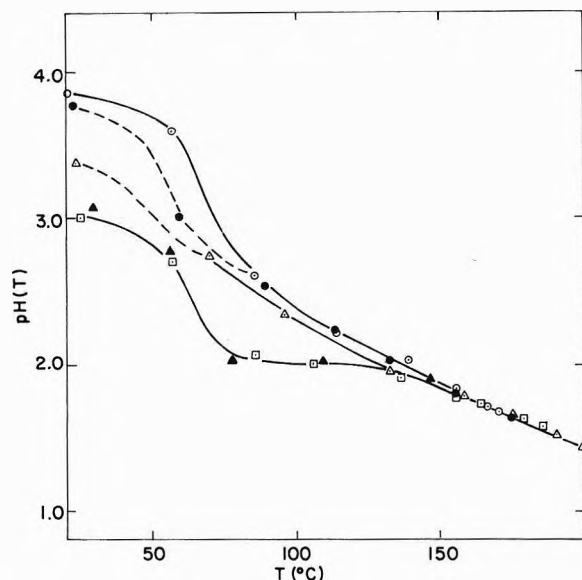
Figure 8. pH(T)-temperature profiles for high initial pH solutions of Al^{3+} (0.049 mol/kg). Times of storage of solutions at 25° as follows: O, 1 day; ●, 2 days; △, 7 days; ▲, 9 days; □, 14 days.
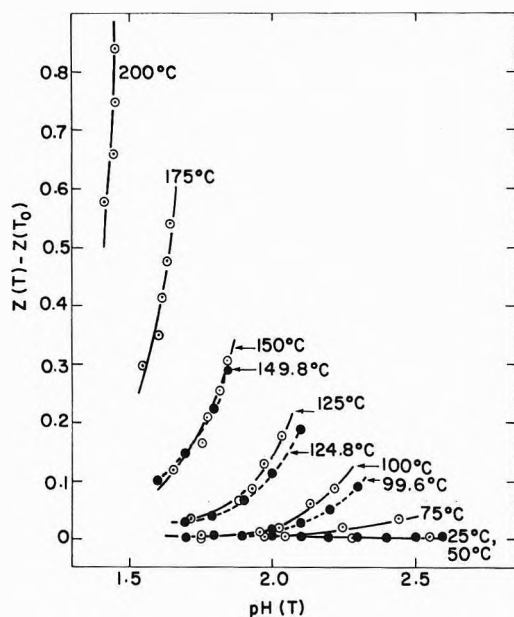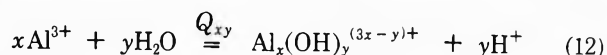

Figure 9. $Z(T)$-pH(T) profiles for Al^{3+} (0.038 mol/kg) hydrolysis in KCl solution (total [Cl$^-$] = 1 mol/kg) at various temperatures to 200°: O, this work; ●, calculated from the data of Mesmer and Baes.[5a]

The formation of species $Al_x(OH)_y^{(3x-y)+}$ is represented by

$$x Al^{3+} + y H_2O \overset{Q_{xy}}{=} Al_x(OH)_y^{(3x-y)+} + y H^+ \qquad (12)$$

The molal formation quotient, Q_{xy}, for the above equilibrium is related to the concentrations of the ions in solution by

$$Q_{xy} = m_{xy} m_1^y / m^x \qquad (13)$$

where m_{xy}, m_1, and m are the molal equilibrium concentrations of $Al_x(OH)_y$, H^+, and free metal ion, respectively. Thus, the concentration of species $Al_x(OH)_y^{(3x-y)+}$ is given by

$$m_{xy} = Q_{xy} m^x m_1^{-y} \qquad (14)$$

and the total metal in the system by

$$M = m + \sum_y \sum_x x Q_{xy} m^x m_1^{-y} \qquad (15)$$

For a given set of values for M, x, y, Q_{xy}, and m_1 at the temperature of interest eq 15 represents a polynomial in m and was solved for the positive root using the Newton-Raphson iterative technique. The value for m obtained by the above procedure was then used to calculate $Z(T)$. The average molal concentration of hydroxide ions bound to metal can be written as

$$m_{OH}(\text{bound}) = \sum_x \sum_y y Q_{xy} m^x m_1^{-y} \qquad (16)$$

and therefore

$$Z(T) = m_{OH}(\text{bound})/M \qquad (17)$$

Thus, the change in Z on heating a solution from T_0 to T°C is given by

$$Z(T) - Z(T_0) = \left\{ \left[\sum_x \sum_y y Q_{xy} m^x m_1^{-y} \right]_T - \left[\sum_x \sum_y y Q_{xy} m^x m_1^{-y} \right]_{T_0} \right\} / M \qquad (18)$$

Values for $Z(T)$ calculated as described above using Q_{xy} data listed by Mesmer and Baes[5a] are plotted in Figure 9 as a function of temperature and pH(T) together with experimental data obtained in the present study. Good agreement is obtained between the two sets of data and confirm the validity of the schemes proposed by Mesmer and Baes[5a] to describe the hydrolysis behavior of Al^{3+} in potassium chloride solution at temperatures to 150°.
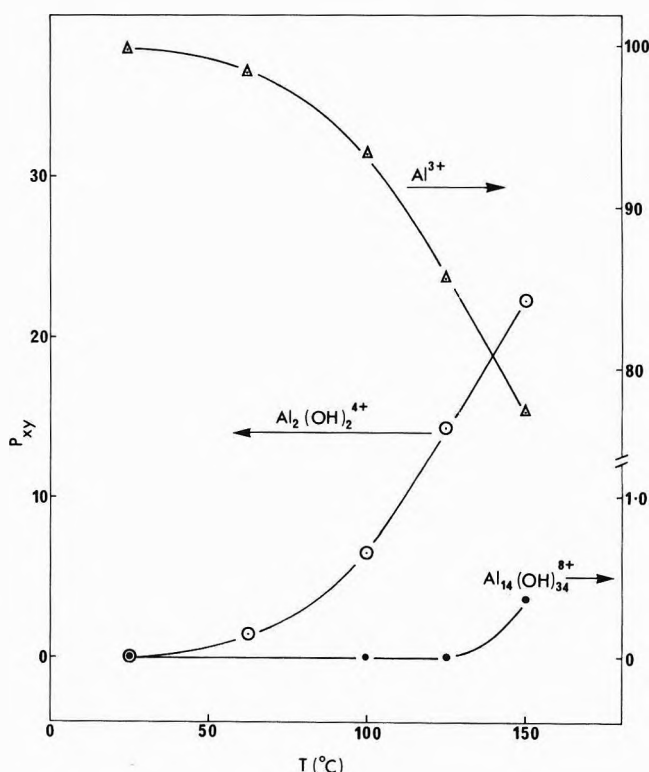

Figure 10. Plots of P_{xy} vs. temperature for the hydrolysis of Al^{3+} in 1 mol/kg KCl solution. Total aluminum concentration = 0.038 mol/kg, initial pH 2.59: △, Al^{3+}; O, $Al_2(OH)_2^{4+}$; and ●, $Al_{14}(OH)_{34}^{8+}$.

The hydrolysis schemes discussed above permit calculation of the concentrations of individual ions as a function of temperature. Thus, for a given total metal concentration of M, at temperature T, and acidity pH(T), the concentration of species $Al_x(OH)_y^{(3x-y)+}$ is given by eq 14 where m, the free metal in the system, is equal to the positive root obtained by solution of eq 15. For the present purpose, it is convenient to define of parameter P_{xy} equal to the percentage of total metal tied up as the complex $Al_x(OH)_y^{(3x-y)+}$. An analytical expression for this parameter is easily derived from eq 14 and results in the following equation for P_{xy}

$$P_{xy} = (100xQ_{xy}m^x m_1^{-y})/M \qquad (19)$$

In examining the variation of P_{xy} with temperature we have chosen to use pH(T)-temperature data for a 0.038 mol/kg Al^{3+} solution in 1 mol/kg KCl with a starting pH(25) of 2.59 (Figure 2). Also, the two species ($Al_2(OH)_2^{4+}$, $Al_{14}(OH)_{34}^{8+}$) hydrolysis scheme proposed by Mesmer and Baes[5a] was selected since it reproduces the experimental hydrolysis data to a higher temperature (149.8°) than do the three species schemes also listed (good to 124.8°). Plots of P_{xy} vs. temperature for Al^{3+} (i.e., free metal ion), $Al_2(OH)_2^{4+}$, and $Al_{14}(OH)_{34}^{8+}$ are shown in Figure 10. These curves demonstrate that at temperatures less than 125° the principal species involved in the hydrolysis of Al^{3+} are the free metal ion, Al^{3+}, and the dimer, $Al_2(OH)_2^{4+}$. At higher temperatures, however, the large polymer, $Al_{14}(OH)_{34}^{8+}$, becomes important. This species is probably the precursor to the formation of boehmite since precipitation was only observed to occur at

temperatures greater than 150°. Also, the $Z(T)$ vs. temperature plots shown in Figure 7 indicate that the formation of boehmite is irreversible with respect to changing temperature while at lower temperatures almost no hysteresis in the $Z(T)$ vs. temperature plot was observed. Therefore, the following scheme is proposed to provide a quantitative description of the hydrothermal hydrolysis of Al^{3+} in aqueous KCl solution at elevated temperatures

$$2Al^{3+} + 2H_2O = Al_2(OH)_2^{4+} + 2H^+ \qquad (20)$$

$$14Al^{3+} + 34H_2O = Al_{14}(OH)_{34}^{8+} + 34H^+ \qquad (21)$$
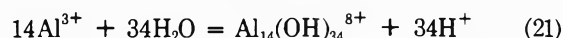
followed by the precipitation of boehmite according to

$$Al_{14}(OH)_{34}^{8+} \longrightarrow 14\gamma\text{-}AlOOH + 6H_2O + 8H^+ \qquad (22)$$

References and Notes

(1) (a) Present address, Department of Chemistry, Victoria University of Wellington, Wellington, New Zealand. (b) Summer student May–Sept 1972.
(2) (a) H. C. Helgeson, "Complexing and Hydrothermal Ore Deposition," Macmillan, New York, N. Y., 1964; (b) G. Kortüm, "Treatise on Electrochemistry," 2nd ed, Elsevier, Amsterdam, 1965.
(3) D. D. Macdonald, P. Butler, and D. Owen, to be submitted for publication.
(4) R. E. Mesmer, C. F. Baes, Jr., and F. H. Sweeton, J. Phys. Chem., 74, 1937 (1970).
(5) (a) R. E. Mesmer and C. F. Baes, Jr., Inorg. Chem., 10, 2290 (1971). (b) Mesmer and Baes have assigned boehmite the formula α-AlOOH which in fact corresponds to diaspore (ASTM 5-0355).
(6) D. D. Macdonald and P. Butler, Corros. Sci., 13, 259 (1973).
(7) A. S. Quist and W. L. Marshall, J. Phys. Chem., 69, 2984 (1965).
(8) R. A. Robinson and R. H. Stokes, "Electrolyte Solutions," Butterworths, London, 1959.
(9) "Handbook of Chemistry and Physics," 50th ed, The Chemical Rubber Publishing Co., Cleveland, Ohio, 1969.
(10) G. C. Akerlof and H. I. Oshry, J. Amer. Chem. Soc., 72, 2846 (1950).

Thermodynamic Properties of a Hard-Sphere Solute in Aqueous Solution at Various Temperatures in Relation with Hydrophobic Hydration

M. Lucas

Département de Génie Radioactif, Commissariat à l'Energie Atomique, 92260 Fontenay-aux-Roses, France

(Received April 2, 1973)

The limiting variation with the solute molality m of some partial molal thermodynamic properties of a nonpolar molecular solute has been calculated by means of the scaled-particle theory. The variation of calculated $\partial V_2/\partial m$ with temperature appears to be closely related to the unusual variation of the pressure derivative of the compressibility of pure water. The calculated heat of dilution L_2 is also related to the temperature derivative of the water compressibility. Although the fit between calculated and experimental $\partial V_2/\partial m$ and L_2 is only qualitative, it suggests that the variations of these quantities with the temperature are not directly related to the solute influence on the water structure.

Introduction

Considerable importance has been ascribed to the fact that the partial molal volume V_2 of a hydrophobic solute decreases with increasing molality and that the relative partial molal heat content L_2 of such a solute is positive.

On this basis conclusions have been drawn regarding the ability of the solute to increase the hydrogen bond strength between water molecules.[1] However, the relative partial molal heat content L_2 of a solute such as tert-butyl alcohol increases markedly when the solution temperature

is raised,[2-5] suggesting that it might be negative at temperatures lower than $-10°$, although nmr measurements suggest that this alcohol is a stronger water structure promoter at low temperature than at high temperatures.[5] A straightforward extension of the scaled-particle theory[6-8] to aqueous solutions of nonpolar molecular solutes makes it possible to calculate some thermodynamic properties of the solute and their variation with the solute molality. These calculations suggest interpretations of these properties which are different from the current interpretation in terms of water structure promotion.

This paper presents the scaled-particle calculation, the comparison between calculated properties and experimental ones for the *tert*-butyl alcohol–water system, and an interpretation of some solute thermodynamic properties.

Theory

According to eq 10 of ref 6, the partial molal value V_2 of a molecular solute interacting with water through dispersion forces is

$$V_2 = \left(\frac{\partial G_i}{\partial p}\right)_T + \left(\frac{\partial G_c}{\partial p}\right)_T + \beta RT$$

where T is the absolute temperature, β is the solution isothermal compressibility, G_c is the molar free energy for cavity formation, and G_i is the molar free energy of interaction.

G_i is given by the second term in the right of eq 9 of ref 9. (The third term in the equation which includes the contribution of the solute polarizability is neglected since it is small compared to the second.) Then

$$G_i = -N \frac{32\pi}{9} \sum_{j=1}^{2} \rho_j \epsilon_{2j} \sigma_{2j}^2$$

where ρ_j is the particle j number density, ϵ_{2j} is the depth of the potential minimum in the Lennard-Jones (6–12) potential, and $\sigma_{2j} = d_2 + d_j/2$ where d_2 is the solute hard-sphere diameter and d_j is the diameter of the particle j.

G_c is given by the equation

$$\frac{G_c}{RT} = -\ln(1-y) + \frac{\pi PN}{RT} d^3 +$$
$$\frac{d^2}{(1-y)^3}\left(3Y - 6yY + \frac{9}{2} X^2 - \frac{9}{2} X^2 y + 3y^2 Y\right) +$$
$$\frac{d}{(1-y)^3}(3X - 6yX + 3y^2 X)$$

which is the hard-sphere part of eq 2-7 in ref 8 (the sign before $\ln(1-y)$ is misprinted in ref 8).

In this equation P is the pressure and N is Avogadro's number. In addition we have

$$y = \pi N(55a^3 + md^3)(6V^0_{H_2O})^{-1}(55.5 + mv)^{-1}$$
$$X = \pi N(55a^2 + md^2)(6V^0_{H_2O})^{-1}(55.5 + mv)^{-1}$$
$$Y = \pi N(55a + md)(6V^0_{H_2O})^{-1}(55.5 + mv)^{-1}$$

with $v = V_2/V^0_{H_2O}$ where V_2 and $V^0_{H_2O}$ are respectively the solute apparent molal volume and the pure water molal volume, d and a are respectively the solute and water hard-sphere diameter, and m is the solute molality in the solution. From the equation

$$\frac{G_c}{RT} = -\ln(1-y) + \frac{\pi N pd^3}{6RT} + \frac{3d^2 y}{1-y} + \frac{9X^2 d^2}{2(1-y)^2} + \frac{3dX}{1-y}$$

we have

$$\frac{\partial G_c}{\partial p} = \frac{\pi N d^3}{6} + RT\beta\left\{\frac{y}{1-y} + \frac{3d^2 y}{1-y} + \frac{9X^2 d^2}{(1-y)^2} + \frac{3dX}{1-y} + \right.$$
$$\left. \frac{3d^2 Y y}{(1-y)^2} + \frac{3dXy}{(1-y)^2} + \frac{9X^2 d^2 y}{(1-y)^3}\right\}$$

since $\partial y/\partial p$ is equal to βy, $\partial X/\partial p = \beta X$, and $\partial y/\partial p = \beta y$. Then

$$\frac{\partial G_c}{\partial P} + RT\beta = RT\beta(1-y)^{-3}\{(1 + 3d^2 Y + 3dX)(1-y)^2 +$$
$$(9X^2 d^2 + 3d^2 Y y + 3dXy)(1-y) + 9X^2 d^2 y\} + \frac{\pi N d^3}{6} =$$
$$RT\beta(1-y)^{-3}\{9d^2 X^2 + 3(1-y)(dX + d^2 Y) + (1-y)^2\} +$$
$$\frac{\pi N d^3}{6} \quad (1)$$

$$G_i = \frac{N 32\pi}{9V^0_{H_2O}}\left\{\frac{55.5N}{55.5 + mv}\epsilon_{12}\frac{(a+d)^3}{8} + \frac{mN}{55.5 + mv}\epsilon_{22}d^3\right\}$$

since

$$\frac{\partial}{\partial p}\left(\frac{55.5N}{V^0_{H_2O}(55.5 + mv)}\right) = \frac{\beta 55.5}{V^0_{H_2O}(55.5 + mv)}$$

Then

$$\frac{\partial G_i}{\partial p} = -\frac{32\pi N}{9V^0_{H_2O}}\beta RT\left\{\frac{55.5}{55.5 + mv}\frac{\epsilon_{12}}{kT}\frac{(a+d)^3}{8} + \frac{m}{55.5 + mv}\frac{\epsilon_{22}d^3}{kT}\right\} \quad (2)$$

then $V_2 = (1) + (2)$.

When m is vanishingly small, since then $X = y/a$ and $Y = y/a^2$, V^0_2 is given by the equation

$$V^0_2 = RT\beta_0(1-y)^{-3}[(1-y)^2 + c^2(3y + 6y^2) +$$
$$c(3y - 3y^2)] + r\frac{Na^3 c^3}{6} - RT\beta_0\frac{32\pi N}{9V^0_{H_2O}}\frac{\epsilon_{12}}{kT}\frac{(a+d)^3}{8} \quad (3)$$

where $d/a = c$. The last expression is also equal to $-RT\beta_0$ $2.67\, y\, (\epsilon_{12}/kT)\,(1 + c)^3$, since then $y = \pi Na^3/6V^0_{H_2O}$. Equation 3 may be derived from the equations of ref 6 except that in ref 6 dispersion terms are omitted.

From eq 1 and 2 it may be derived that

$$\frac{1}{V^0_2 - \pi Na^3 c^3/6}\frac{\partial V_2}{\partial m(m \to 0)} = \frac{1}{\beta_0}\frac{\partial \beta}{m(m \to 0)} +$$
$$\frac{1}{55.5}\frac{3y}{1-y}(c^3 - v) + \frac{1}{55.5 f(y)}\{(c - v)(3yc^2 - 3y^2 c^2) +$$
$$(c^2 - v)(18y^2 c^2 + 3yc - 3y^2 c) - (c^3 - v)y(2 - 2y + 3cy +$$
$$3c^2 y) + (1-y)^2 y 2.67[3y(c^3 - v)(\epsilon_{12}/kT)(1 + c)^3 +$$
$$(1-y)v(\epsilon_{12}/kT)(1+c)^3 - (1-y)(\epsilon_{22}/kT)8c^3]\} \quad (4)$$

where $f(y) = (1-y)^2 + c^2(3y + 6y^2) + c(3y - 3y^2) - (1-y)^3 2.67y(1 + c)^3(\epsilon_{12}/kT)$.[10]

In addition, we have

$$\beta = \left(\frac{1}{55.5V^0_{H_2O} + mV_2}\frac{\partial(55.5V^0_{H_2O} + mV_2)}{\partial p}\right)_T$$

Since if $f = ghi$ we have

$$\frac{1}{f}\frac{\partial f}{\partial x} = \frac{1}{g}\frac{\partial g}{\partial x} + \frac{1}{h}\frac{\partial h}{\partial x} + \cdots$$

we obtain

$$\frac{1}{\beta_0} \frac{\partial \beta}{\partial m}(m \to 0) = \frac{V^0_2}{55.5V^0_{H_2O}} \frac{(\partial V_2/\partial p)}{\partial(55.5V^0_{H_2O})/\partial p} =$$

$$-\frac{V^0_2}{55.5V^0_{H_2O}} + \frac{\beta^0_2 V^0_2}{55.5\beta V^0_{H_2O}} = \frac{1}{55.5}\frac{V^0_2}{V^0_{H_2O}}\left(\frac{\beta^0_2}{\beta_0}-1\right) \quad (5)$$

where

$$\beta^0_2 = -\frac{1}{V^0_2}\frac{\partial V^0_2}{\partial p}T$$

by the same procedure the equation

$$\beta^0_2 = \frac{(V^0_2 - \pi Na^3 c^3/6)\beta_0}{V^0_2} \times$$

$$\left[\frac{1}{(\beta_0)^2}\frac{\partial\beta_0}{\partial p} - \frac{3y}{1-y} - \frac{y}{f(y)}\frac{\partial f(y)}{\partial y}\right] \quad (6)$$

is derived from eq 3.

Equations 3, 4, 5, and 6 make it possible to compute $\partial V_2/\partial m$ ($m \to 0$) for a nonpolar solute (with or without dispersion forces) in water.

When no dispersion forces are present L_2 may be calculated as follows. The variation of the solution expansion coefficient is given by

$$\frac{1}{\alpha_0}\frac{\partial\alpha}{\partial m}(m \to 0) = \frac{1}{55.5}\left[\frac{\alpha^0_2}{\alpha^0}-1\right] \quad (7)$$

with

$$\alpha^0_2 = \frac{1}{V^0_2}\frac{\partial V^0_2}{\partial T} = \frac{V^0_2 - \Pi Na^3 c^3/6}{V^0_2} \times$$

$$\left[\frac{1}{\beta_0}\frac{\partial\beta_0}{\partial T} + \frac{1}{T} - \frac{3\alpha_0 y}{1-y} - \frac{\partial f(y)y\alpha_0}{\partial y f(y)}\right] \quad (8)$$

where α_0 is the pure water expansion coefficient. From eq 14 of ref 7

$$U = (\alpha T/\beta)(V_2 - \Pi Na^3 c^3/6) \quad (9)$$

Relating the molal internal energy charge for the solute transfer from the gas phase to its aqueous solution of molality m and setting the heat of dilution L_2 equal to $U - U_0 = m \partial U/\partial m$ ($m \to 0$), we obtain

$$\frac{1}{U_0}\frac{L_2}{m}(m \to 0) = \frac{1}{\alpha_0}\frac{\partial\alpha}{\partial m} - \frac{1}{\beta_0}\frac{\partial\beta}{\partial m} +$$

$$\frac{1}{V^0_2 - \Pi Na^3 c^3/6}\frac{\partial V_2}{\partial m} \quad (10)$$

with

$$U_0 = (\alpha_0 T/\beta_0)(V^0_2 - \Pi Na^3 c^3/6) \quad (11)$$

This calculation is interesting in that it makes apparent the importance of the term $(1/\beta_0)(\partial\beta_0/\partial T) + 1/T$ which appears in eq 8.

When dispersion forces are present, H_i is given by

$$\frac{32RT\pi N}{9V^0_{H_2O}(55.5 + mv)}\left[55.5\frac{(d+a)^3}{8}(\epsilon_{12}/kT) + md^3\epsilon_{22}/kT\right]$$

H is calculated at different molalities assuming $V_2 = V^0_2$ and $V^0_{H_2O}$ constant at all molalities and that the limit of $H - H_0/m$ ($m \to 0$) is equal to L_2/m ($m \to 0$). The assumption that $V_2 = V^0_2$ at all molalities implies that the parameter b in the equation $H - H_0 = am + bm^2$ is not correct but does not change the value of the limit of $H - H_0/m$ ($m \to 0$).

For the numerical calculations the necessary parameters are the water and solute hard-sphere diameters, ϵ_{22}/k
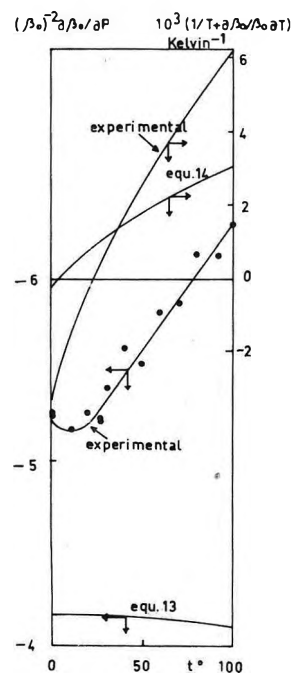

Figure 1. Plots of experimental and calculated $(\beta_0)^{-2}\partial\beta_0/\partial P$ and $1/T + \partial\beta_0/\beta_0 \partial T$ vs. temperature.

for the solute, ϵ_{11}/k for water, the pure water compressibility β_0, and the water expansion coefficient α^0 at various temperatures. The last two quantities are taken respectively from Tables IV and II from ref 11.

The experimental values of $(1/(\beta_0)^2)(\partial\beta/\partial P)(1/T)$ have been obtained from eq 33 and Table 10 of Kell's paper on the PVT properties of water.[12]

Figure 1 shows the plots of this quantity at various temperatures and of the quantity $[(1/\beta_0)(\partial\beta_0/\partial T) + (1/T)]_P$ compared to the values these quantities would have if the hard-sphere equation of state applied to water, in which case β_0 would be equal to[13]

$$\frac{V_{H_2O}}{RT}\frac{(1-y)^4}{(1+2y)^2} \quad (12)$$

which leads to

$$\frac{1}{(\beta_0)^2}\frac{\partial\beta^0}{\partial p} = -1 - 4y(1-y)^{-1} - 2y(1+2y)^{-1} \quad (13)$$

and

$$\frac{1}{T} + \frac{1}{\beta_0}\frac{\partial\beta_0}{\partial T} = \alpha_0[1 + 4y(1-y)^{-1} + 2y(1+2y)^{-1}] \quad (14)$$

Calculations are carried out with $a = 2.90$ Å.

Discussion

Calculations are carried out with a solute size equal to water (2.90 Å) and twice this size (5.80 Å) and with $\epsilon_{22}/k = 0$ (hard-sphere solute without dispersion forces) or ϵ_{22}/k of the same magnitude as for a nonpolar solute. For rare gases it is found experimentally that $\epsilon_{22}/k = 146(d - 2.58$ Å) K,[14] which gives $\epsilon_{22}/k = 46$ K for $d = 2.9$ Å and 465 K for $d = 5.8$ Å. For water ϵ_{11}/k is taken equal to 96 K. ϵ_{12}/k is equal to $(\epsilon_{11}\epsilon_{22})^{1/2}/k$.

1. Hard-Sphere Solutes ($\epsilon_{22}/k = 0$). Figure 2 shows plots of V^0_2, $\partial V_2/\partial m$, $\phi^0 K = -[\partial V^0_2/\partial P]_T$, and L_2/m for the two solute sizes considered, against the temperature. Consideration of the plots shows that $\partial V_2/\partial m$ and L_2 are negative at low temperature and positive at high tempera-
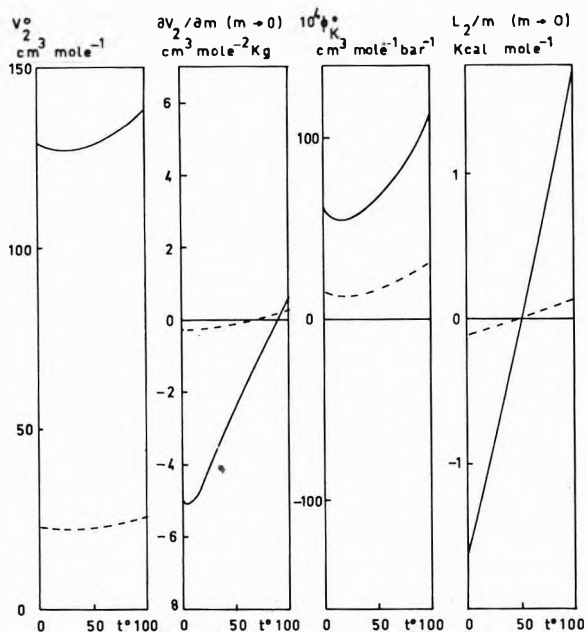
Figure 2. Plots of the solute partial molal thermodynamic quantities vs. the solution temperature: dotted lines, $d = 2.9$ Å, ϵ/k = 0 K; full lines, $d = 5.8$ Å, $\epsilon/k = 0$ K.

Figure 3. Plots of the solute partial molal thermodynamic quantities vs. the solution temperature: dotted lines, $d = 2.9$ Å, ϵ/k = 46 K; full lines, $d = 5.8$ Å, $\epsilon/k = 467$ K.

ture and that $\phi°K$ increases with the temperature. The shape of the curve for $\partial V_2/\partial m$ is especially interesting in that it shows a minimum. The shape of the curve for $(\beta_0)^{-2} \partial\beta_0/\partial P$ (Figure 1) is similar and calculations show that its variation with the temperature is the cause for the corresponding variation of $\partial V_2/\partial m$. In the same vein the important variation of L_2/m with the temperature and especially its negative value under ca. 40° is related to the similar variation of $1/T + \partial\beta_0/\beta_0 \partial T$ for pure water. The calculations show also that if this quantity is given by eq 14 (that is if water behaved as a hard-sphere fluid) then the variation of L_2/m with the temperature should be much smaller. It has been suggested that a hard-sphere solute enhances the H bonds between water molecules at temperatures lower than 4° and weakens these bonds at higher temperatures.[15]

The calculated values of $\partial V_2/\partial m$ and L_2/m for such a solute are apparently related to the peculiar variation of the derivative $\partial\beta_0/\partial P$ and $\partial\beta_0/\partial T$ for pure water rather than to the solute structural influence on water. In other words, the sign and magnitude of $\partial V_2/\partial m$ are probably not evidence for or against the water structure promotion by a solute (a table for the calculated thermodynamic quantities is given in the microfilm edition; see ref 10).

2. Nonpolar Molecular Solutes with Dispersion Forces $(\epsilon_{22}/k \neq 0)$. The introduction of dispersion forces with small values ($\epsilon_{22}/k = 46$ K) for a solute with the same diameter as water does not significantly change the properties (plotted in Figure 3). However, the properties of the solute with a diameter twice that of water are significantly modified by the existence of dispersion forces with $\epsilon_{22}/k = 465$ K. V^0_2 is significantly smaller and the minimum of V^0_2 is shifted to lower temperatures. $\partial V_2/\partial m$ is less negative.

The modifications of L_2/m are more difficult to rationalize. In the same figure, we have plotted experimental values of the corresponding quantities for *tert*-butyl alcohol as solute. It would have seemed more appropriate to have used a nonpolar solute. However, due to their poor solubility in water, data as $\partial V_2/\partial m$ or L_2/m are com-
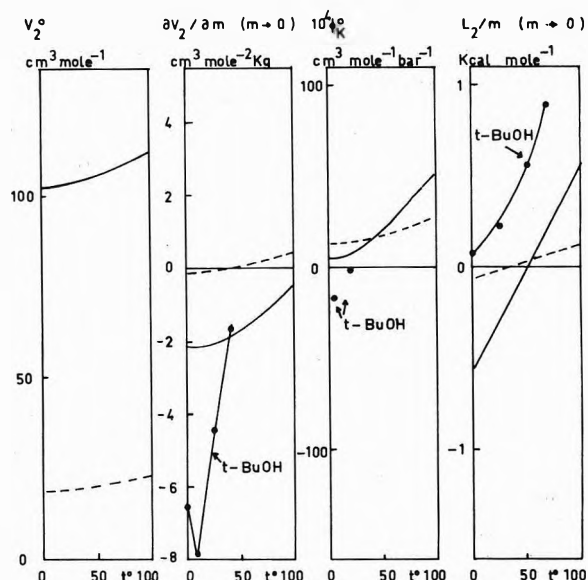
pletely absent from the literature. On the other hand, they are available for a solute as *tert*-butyl alcohol and have been ascribed to the nonpolar part of the molecule. The experimental $\partial V/\partial m$ has been computed from data of Franks and Smith.[16] From their very accurate measurements it may be deduced that $\partial V_2/\partial m$ is distinctly less negative at 0.5° than at 5°. Although the calculated and experimental values are different, the existence of a minimum in both cases is significant. It is difficult to explain this minimum if it is ascribed to the enhancement of H bonds by the solute since one should then have to hypothetize that it is a maximum at 5°. Nmr data show that the water structure promotion by the *tert*-butyl alcohol seems to increase monotonously when the temperature is decreased.[5] The calculated $\phi°K$ is very small at 0°. Experimental determinations of the adiabatic $\phi°K$ by Franks, *et al.*, show that it is generally negative at 5° for a variety of solutes and positive at 25°.[17] The isothermal $\phi°K$ is derived from the adiabatic one by addition of a term nearly equal to $2\beta_0(\partial V^0_2/\alpha_0\partial T)$.[18] Then the isothermal $\phi°K$ is certainly negative at 5° since $\partial V^0_2/\partial T$ is negative, and probably positive above 25°. The experimental variation with the temperature is certainly larger than the calculated one.

Finally, we have plotted in Figure 3 L_2/m for *tert*-butyl alcohol. The experimental limiting values of L_2/m have been calculated from data in ref 2, 3, and 4. The variations of experimental and calculated L_2/m with temperature are qualitatively similar except that the calculated one is more negative at all temperatures. In view of this fact it is difficult to accept the usual interpretation that a positive L_2 is caused by water structure promotion by the solute.[1]

The discrepancy between calculated and experimental quantities may be due to the polar character of t-BuOH not accounted for by scaled-particle theory and also some shortcomings of the scaled-particle approach. First the use of a constant-temperature independent hard-sphere radius may be questioned.[9] The equations giving the influence of dispersion forces also incorporate crude assumptions, for example a random distribution of molecules in the solution. Somewhat different equations have been used by

Tiepel and Gubbins.[9] The main difference is that the pressure term in their eq 11, which in Pierotti's and this paper yield the term $\Pi Na^3 c^3/6$ in the equation for V_2, yields a more complex term. The fit between calculated and experimental $\partial V_2/\partial m$ is much better but the fit for L_2/m is much worse when Tiepel and Gubbins equations are used, so that we cannot decide between the two sets of equations. However, the main conclusion of this paper is that scaled-particle theory makes it possible to ascribe the variation of the solute partial molal properties to the anomalous behavior of $\partial \beta^\circ/\partial P$ and $\partial \beta^\circ/\partial T$ for pure water rather than the solute structural effects.

Supplementary Material Available. The derivation of eq 4 will appear following these pages in the microfilm edition of this volume of the journal. Photocopies of the supplementary material from this paper only or microfiche (105 × 148 mm, 20× reduction, negatives) containing all of the supplementary material for the papers in this issue may be obtained from the Journals Department, American Chemical Society, 1155 16th St., N.W., Washington, D. C., 20036. Remit check or money order for $3.00 for photocopy or $2.00 for microfiche, referring to code number JPC-73-2479.

References and Notes

(1) J. E. Desnoyers, M. Arel, G. Perron, and C. Jolicoeur, *J. Phys. Chem.*, **73**, 3346 (1969).
(2) J. J. Kozak, W. S. Knight, and W. Kauzmann, *J. Chem. Phys.*, **48**, 675 (1968).
(3) W. S. Knight, doctoral dissertation, Princeton University, 1962.
(4) J. Kenttamaa, E. Tommila, and M. Martti, *Ann. Acad. Sci. Fennicae A II 93*, 1 (1959).
(5) M. M. Marciacq-Rousselot and M. Lucas, *J. Phys. Chem.*, **77**, 1056 (1973).
(6) R. A. Pierotti, *J. Phys. Chem.*, **67** 1840 (1963).
(7) R. A. Pierotti, *J. Phys. Chem.*, **69**, 281 (1965).
(8) J. L. Lebovitz and J. S. Rowlinson, *J. Chem. Phys.*, **41**, 133 (1964).
(9) E. W. Tiepel and K. E. Gubbins, *J. Phys. Chem.*, **76**, 3044 (1972).
(10) See paragraph at end of paper regarding supplementary material.
(11) F. Franks, Ed., "Water, a comprehensive Treatise," Plenum Press, New York, N. Y., 1972, Vol. 1, Chapter 10.
(12) G. S. Kell and E. Whalley, *Phil. Trans. Roy. Soc., Ser. A*, **258**, 565 (1965).
(13) F. H. Stillinger, *J. Chem. Phys.*, **35**, 1581 (1961).
(14) H. D. Nelson, Ph.D. Dissertation, Utrecht, 1967.
(15) M. Lucas *J. Phys. Chem.*, **76**, 4030 (1972).
(16) F. Franks and H. T. Smith, *Trans. Faraday Soc.*, **64**, 2962 (1968).
(17) F. Franks, J. R. Ravenhill, and D. S. Reid, *J. Sol. Chem.*, **1**, 1 (1972).
(18) J. E. Desnoyers and P. R. Philip, *Can. J. Chem.*, **50**, 1094 (1972).

The Free Solvated Electron in Hexamethylphosphoric Triamide[1]

G. Dodin and J. E. Dubois*

Laboratoire de Chimie Organique Physique de l'Université Paris VII, associé au C.N.R.S., Paris, France
(Received April 16, 1973)

Publication costs assisted by the Laboratoire de Chimie Organique Physique de l'Université Paris VII

The width of the esr narrow line from the solvated electron in hexamethylphosphoric triamide (HMPA)–sodium solutions arises from exchange narrowing and the activation energy for the hyperfine coupling modulation as well as the volume of the solvated electron increase with increasing solvent viscosity. When the viscosity is extrapolated to zero, the line width has a nonzero value resulting presumably from electron–nuclear spin dipolar coupling. The resonance line in the ideal nonviscous state might be attributed to a species we shall refer to as a "free" solvated electron which would consist of an electron trapped in a cavity formed by a layer of solvent molecules. The contributions to the experimental line width variation from both viscosity effects and technological artifacts arising from cavity shifts and 100-kHz modulation are easily differentiated provided certain experimental conditions are satisfied.

Introduction

Esr spectroscopy has been widely used to study the paramagnetic species formed in the solutions of alkali metals in organic solvents.[2] For solvents with low dielectric constants (ethers and amines), a hyperfine resonance signal arising from the interaction of the electron spin with the nuclear spin of the metal is observed; the spectrum is assigned to the monomer M.[2-4]

In solvents with higher dielectric constants such as liquid ammonia and hexamethylphosphoric triamide (HMPA) the resonance spectrum consists of a single line and is attributed to the solvated electron. In metal–ammonia solutions, the width of the resonance line is due to exchange narrowing;[5,6] the process of hyperfine coupling modulation is, however, controversial. According to the Kaplan and Kittel theory,[7] this modulation is due to the rotation of the solvent layer around the electron involving an interaction whose correlation time is the Debye dipolar relaxation time. On the other hand, Dewald and Lepoutre,[8] and more recently Lambert,[9] have suggested that the modulation of the hyperfine coupling could be achieved by the passage of the electron from one cavity to another *via* a tunneling mechanism resulting in a correlation time for the interaction corresponding to the lifetime of the electron in a given cavity. Whatever the modulation process, the exchange rate should follow the Arrhenius law; when log ΔH (where ΔH is the line width) is plotted against $1/T$ a straight line is indeed observed.[9]

The properties of alkali metal–HMPA solutions are quite similar to those of metal–ammonia solutions. However, esr studies appear somewhat ambiguous in the assignment of the observed single line spectrum. According to the various authors, the lines have widths as different as 35[10] and 200 mG[11] and are, nevertheless, attributed to the *same* species, the solvated electron. One may wonder if (a) several kinds of solvated electrons are present in HMPA or (b) the observed resonance signal results from the contribution of two relaxation mechanisms, one specific to a *unique* solvated electron and the other arising from the interaction of the solvated species with the surrounding medium.

Current theories of the structure of alkali metal–HMPA solutions make it possible to rule out the existence of several solvated electrons,[12] and we can therefore reasonably assume b as a working hypothesis. The present work has been developed along these lines.

Experimental Section

Recording of the Esr Spectra. The spectra were recorded with a Varian E-3 esr spectrometer. Temperatures were controlled by means of the Varian variable temperature accessory. Since calculation of relaxation times T_1 and T_2 is derived directly from line width measurements, one has to be sure that the observed width is the *actual* one and does not arise from some instrumental artifact.

As we have shown in a previous paper,[13] esr spectra should be recorded with samples of low filling factors. In the range of concentration of the Na–HMPA solutions we used, proper esr spectra are observed with 0.8-mm sample tubes; when 2-mm sample tubes are used, the filling factor is too high and the cavity frequency shifts. The automatic frequency control (AFC) locks the frequency of the klystron on that of the cavity and consequently gives to the high-frequency magnetic field a frequency beyond the resonance frequency of the spin system leading to the narrowing of the observed resonance line. This phenomenon is accounted for by the theory proposed by Dumais and Merle d'Aubigné[14] in the case of AFC narrowing of resonance lines from F centers.

If the AFC is disconnected in the experiment with the 2-mm sample tube, the recorded resonance line is identical with that recorded *with AFC* and 0.8 mm tubes.

Another technological perturbation of the observed line width may arise from the 100-kHz modulation detection which is not quite suitable for recording narrow resonance lines since the minimum detectable width is $\delta = 2\omega_m(\gamma)^{-1}$ where γ is the magnetogyric ratio of the electron, and $\omega_m = 2 I I \nu_m$; for $\nu_m = 100 \text{ kHz}$, $\delta = 70 \text{ mG}$.

Hyde and Brown[15] have shown, however, that line widths less than 70 mG can be measured with a 100-kHz modulation spectrometer if the phase of the lock-in detector is set away from its proper value; in this case, the resonance line is thereby distorted, and information from the line shape can no longer be obtained.

Measurement of H_1. H_1 is measured from the saturation data of DPPH and BDPA resonance signals for which the relaxation times T_1 and T_2 are known:[16] $T_1 = 8 \times 10^{-8}$ sec and $T_2 = 3.86 \times 10^{-8}$ sec for 1,1-diphenyl-2-hydrazyl (DPPH); $T_1 = 7 \times 10^{-8}$ sec and $T_2 = 6.75 \times 10^{-8}$ sec for α,γ-bisdiphenylene-β-phenylallyl (BDPA). The abscissa of the maximum of $d(H_1 \chi'')/d(\omega - \omega_0) = f(H_1)$ are respectively $H_{\text{max(DPPH)}} = 1.45$ G (the corresponding microwave power of 130 mW) and $H_{\text{max(BDPA)}} = 1.15$ G (microwave
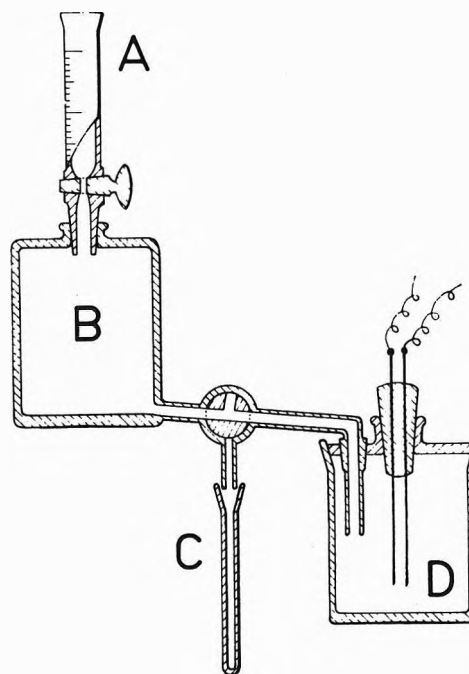

Figure 1. Apparatus for the preparation of Na–HMPA solutions: A, from the distillation unit; B, solution compartment; C, esr sample tube; D, conductivity bridge.
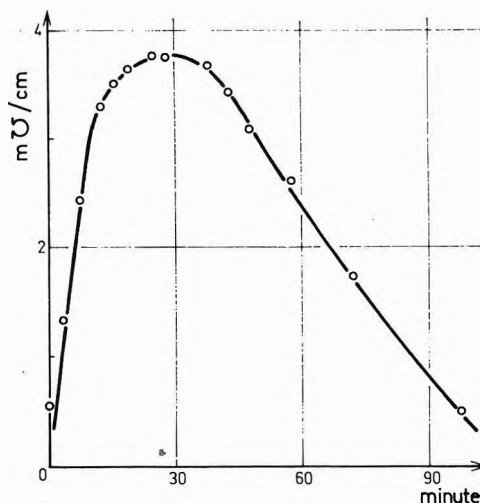

Figure 2. Electrical conductivity of Na–HMPA solutions at +8°. The initial $C_{\text{Na}}/C_{\text{HMPA}}$ ratio is 0.07; $t = 0$ refers to the time when the dissolution starts.

power of 84 mW); consequently, $H_1^2 = 16P$ if H_1 is expressed in gauss and P in watts.

Sample Preparation. Commercial HMPA (Prolabo) is distilled twice under reduced pressure; water concentration, as determined by the Karl Fischer method, is less than 300 mg/kg. The solvent is allowed to react with a known quantity of sodium (see Figure 1).

The metal does not dissolve immediately. Electrical conductivity (measured with a Wayne-Kerr bridge) reaches a maximum some minutes after the beginning of dissolution. The value of the maximum ($\sim 3.7 \times 10^{-3}$ ʊ/cm) is apparently not significantly affected by the variations of $C_{\text{Na}}/C_{\text{solvent}}$ ratio from 0.01 to 0.18 (where C_{Na} and C_{solvent} are the number of moles initially introduced in the apparatus), nor by temperature variation. A typical curve is presented on Figure 2.

The metal concentration *in the solutions* is estimated by the method described in ref 17. This method is, however, not accurate in evaluating the concentration of the *dissolved* metallic species since it is based on the titration of the *overall basicity* of the solution while the only basicity to be considered is that arising from the reaction

$$M + CH_3OH \longrightarrow MOCH_3 + \frac{1}{2}H_2$$
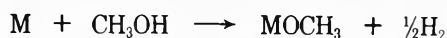
The viscosity of the solutions was measured with an Ostwald viscosimeter at the standard temperature of 20°.

Results

Line width measurements were effected at different sodium concentrations (with C_{Na}/C_{HMPA} ratios between 0.01 and 0.18, and effective metal concentrations, as measured by the above-mentioned method, between 0.3 and 0.6 M). Under these conditions we observed *no correlation* between line width variations and the metal concentrations, while line widths appeared to increase with increasing viscosities of the medium (see Tables I and II). The viscosity at 20° of the various samples is likely to be dependent on the state of decomposition of the solutions, the freshly prepared solutions being the least viscous. The independence of line width variations with the initial metal concentration is linked to the fact that the *effective* metal concentration is small, even for high C_{Na}/C_{HMPA} ratios. Similarly, Pollak[5] has shown, for Na-NH$_3$ solutions, that relaxation times are independent of C_{Na} for C_{Na}/C_{NH_3} ratios up to 10^{-2}.

Saturation Experiments. Resonance line saturation was studied for samples characterized by different viscosities, between -10 and 30°. When H_1 increases, the phase of the lock-in detector, initially set to 90°, shifts; the amplitude of the absorption line derivative decreases rapidly because of both saturation and phase shift effects. For a given power level, depending on sample, temperature, and initial phase setting, the recorded adsorption line is distorted (Figure 3).

To measure the true values of the derivative width and amplitude, the phase of the detector has to be adjusted for each H_1 value by means of the phase shifter so that the maximum amplitude for the adsorption derivative is reached.

No g shift is observed when H_1 increases.

We must mention that the minimum klystron power output corresponds to $H_1 = 56$ mG which is already greater than H_{max} (as defined previously). Since H_{max} cannot be determined, relaxation time measurements will be carried out by studying the line width variation as a function of H_1. The plot of ΔH *vs.* H_1 deriving from the Bloch equations shows for low H_1 values that the width of the line which begins to saturate is not significantly different from ΔH when H_1 approaches zero (while *the amplitude* of the derivative decreases sharply with $(H_1)^{-2}$ from $H_1 > H_{max}$).

The development of the Bloch equations leads to the classical result[18]

$$\left[\frac{\lim_{H_1 \to 0}\Delta H_{pp}}{\Delta H_{pp}}\right]^2 = \frac{1}{1 + \frac{1}{4}H_1^2\gamma^2 T_1 T_2}$$

where ΔH_{pp} is the peak to peak distance for the absorption derivative. T_2 is given by the relation
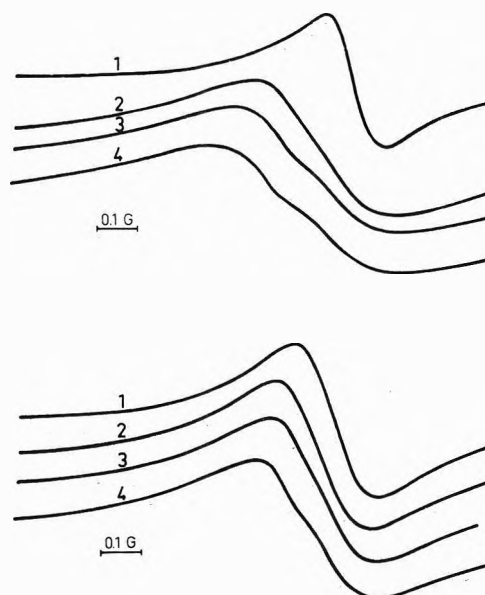
$$T_2 = 1.313 \times 10^{-7}/g\Delta H_{pp}$$

Figure 3. Saturated esr lines from Na-HMPA solutions: (upper spectra) $\varphi = 90°$, $T = 269°$K; the distortion of the line is observable at a power level of 8 mW (spectrum 2); (lower spectra) $\varphi = 90°$, $T = 293°$K; the distortion of the line is observable at a power level 2 of 6.3 mW (spectrum 3).

TABLE I: Experimental Values of the Relaxation Times T_1 and T_2 in Na-HMPA Solutions at 277°K

Sample	C_{Na}, M	ΔH_{pp}, mG[a]	T_2, sec	T_1, sec
1	0.38	61	1.075×10^{-6}	1.21×10^{-6}
2	0.58	56	1.17×10^{-6}	1.33×10^{-6}
3	0.52	47	1.395×10^{-6}	1.46×10^{-6}
4	0.45	39	1.65×10^{-6}	1.60×10^{-6}

[a] Modulation broadening is avoided by proper phase setting of the phase sensitive detector.

when $H_1 \to 0$ (see Table I).

Because of the instrument limitations mentioned previously, great significance should not be placed on the absolute value of line widths.

Line Width Variation with Temperature. The microwave power is taken at its lowest level which corresponds to $H_1 = 56$ mG. The phase of the phase sensitive detector was successively set to 110, 95, and 80° in different experiments. The lowest line width values for a given sample were observed with $\varphi = 110°$, and the largest with $\varphi = 80°$ (see Table II). The initial phase setting does not affect the slope from plot log $\Delta H = f(1/T)$.

Discussion

We shall assume first that the resonance lines are homogeneously saturated and that the behavior of the spin system is accounted for by the Bloch equations.

Phase Shifts. The distortion of the absorption line at various power levels depending on the initial phase setting is a consequence of a phase difference between the modulated signal and the modulation of the static magnetic field (100 kHz). This results from the modulation frequency ($\omega_m = 2\Pi\lambda_m = 2\Pi 10^5$) being equal to $(T_2)^{-1}$. Halbach[19] observed this phenomenon for spin systems obeying the Bloch equations. He derives a convenient method
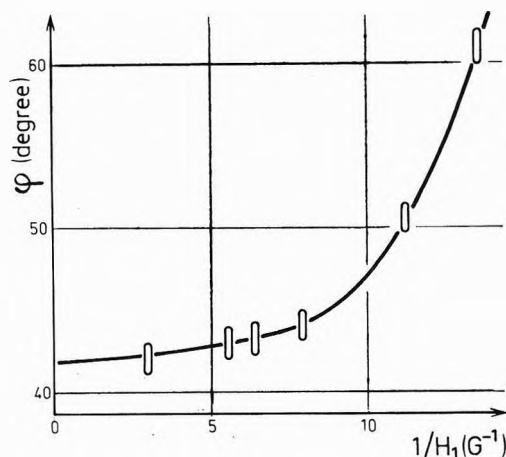
Figure 4. Esr of Na-HMPA solutions. Lock-in phase variations with $1/H_1$.

of evaluating relaxation time T_2 independently of the nonhomogeneity of the static magnetic field.

In the case of our experiments with Na-HMPA solutions, the equivalence of ω_m is obviously fortuitous since the frequency of the modulation is not adjustable on our spectrometer, but it has allowed us to evaluate T_2. According to Halbach's equations, the ordinate at the origin φ_0 of $\varphi = f(1/H_1)$ is related to ω_m and T_2

$$tg\varphi_0 = \omega_m T_2$$

A typical plot, the variation of φ vs. $1/H_1$, is shown in Figure 4. The calculated relaxation times T_2 are in good agreement with those from saturation data.

Activation Energy. As in Na-NH₃ solutions, we shall assume that the line width arises from exchange narrowing. The fact that activation energy, W_e, for the electron spin exchange, measured from the plot $\log \Delta H = W_e/kT$, depends on the solutions viscosity is an argument for a modulation mechanism which associates the correlation time for the interaction with the Debye dipolar relaxation time.[20]

Let us assume that the relaxation of the spin system is described by the following equations[21]

$$\frac{1}{T_2} = DC + A^2/3J(J + 1)\left[\frac{\tau}{1 + (\omega_N - \omega_e)^2\tau^2} + \tau\right]$$

$$1/T_1 = DC + 2A^2/3J(J + 1)\frac{\tau}{1 + (\omega_N - \omega_e)^2\tau^2}$$

where DC is a residual line width, ΔH_0, arising from the dipolar coupling (DC) of the nuclear and electronic spins.

J is the spin of the nucleus responsible for the relaxation; τ is the correlation time of the contact interaction; A is the hyperfine interaction between the nuclear spin J and the electron spin; ω_N and ω_e are the Larmor frequencies of the nucleus and the electron, respectively. When $(\omega_N - \omega_e)^2\tau^2 \ll 1$, then

$$1/T_1 = 1/T_2 = \Delta H_0 + 2A^2/3J(J + 1)\tau$$

If the correlation time τ is the Debye time

$$\tau = {}^4/_3\Pi r^3 \eta / kT$$

$1/T_2 = \Delta H_0 + {}^2/_3 A^2 J(J + 1)V\eta/kT$, where V is the volume of the solvated electron

$$\Delta H = \Delta H_0 + B\eta/kT \tag{1}$$

where $B = {}^2/_3 A^2 J(J + 1)V$ and ΔH_0 is the line width when η equals zero.

If we now consider the experimental results we see that line width variation with temperature is given by

$$\log \Delta H = \log (Ce^{W_e/kT})$$

where C is a constant corresponding to a residual line width when T goes on to infinity

$$\log \Delta H = \log \Delta H_0 + W_e/kT \tag{2}$$

From eq 1 and 2

$$\log \Delta H_0 + W_e/kT = \log (\Delta H_0 + B\eta/kT)$$

and

$$W_e/kT = \log (1 + B'\eta(T)/kT) \tag{3}$$

where $B' = B/\Delta H_0$. Assuming that viscosity variation with temperature may be accounted for by the Arrhenius law

$$\eta = \eta_0 e^{W_\eta/kT}$$

where W_η is the activation energy for viscosity and η_0 the viscosity at a reference temperature. Equation 3 becomes

$$W_e/kT = \log (1 + B'\eta_0 e^{W_\eta/kT}/kT) \tag{4}$$

From eq 4 the activation energy for the modulation of the hyperfine coupling, W_e, is expected to increase with the viscosity η_0 defined at a reference temperature, as experimentally observed, as well as with the activation energy for the viscosity, W_η. It is interesting to note that for sample 4 ($\eta = 4.1$ cSt at 20°) the activation energy W_e (1.4 kcal mol⁻¹) is equivalent to the activation energy W_η for pure HMPA ($\eta_{HMPA} = 3.7$ cSt at 20°) as reported by Gall and Moliton-Bouchetout.[22] However, for sample 1, the activation energy W_e (3.3 kcal mol⁻¹) can no longer be considered as having the same order of magnitude as the energy for the viscosity since such a high value of W_η whould lead to a viscosity at 20° much higher than 8.3 cSt observed experimentally. Consequently, we must assume the coefficient B' in eq 4 varies from one sample to the other (Table II).

If we admit that B', roughly, depends only on V (see eq 1 and 4), we will conclude that the volume of the solvated electron increases with increasing viscosity of the medium (see Table II). Physically, this means that the friction between the successive solvent layers around the electron increases leading to a more bulky species. Moreover, eq 4 shows that when the reference viscosity η_0 is extrapolated to zero, W_e approaches zero and the width of the esr line is ΔH_0 arising from dipolar coupling. In this ideal nonviscous state, ΔH_0 might be considered as the line width of a paramagnetic species having no interactions with the neighboring solvent molecules. This species will be referred to as a "free" solvated electron consisting of the

TABLE II: Activation Energies for Line Width Variation with Temperature in Na-HMPA Solutions

Sample[a]	W_e, kcal mol⁻¹	η (20°), cSt	B_i'/B_1' (20°)	r_i/r_1 (20°)[b]
1	3.3	8.3	14.7	2.45
2	2.87	6.6	8.1	2
3	2.33	5.4	4.1	1.6
4	1.4	4.1	1	1

[a] Samples and sample numbering are as in Table I. [b] r is the cavity radius.

electron trapped in a cavity formed probably by the first solvation layer and moving without, or at least with a minimal friction, in the medium.

This concept of a friction "free" solvated electron should be kept in mind in studies meant to determine physical properties *specific* to the solvated electron from the *overall properties* of a solvated electron interacting with the solvent systems. It is worth noting that the "free" HMPA-solvated electron might not be a mere construct, and the approach to its direct observation could be sought for. For example, we anticipate that the esr signal from a nearly *"free" HMPA-solvated electron* might be observed when HMPA-solvated electrons are introduced in solvents such as liquid hydrocarbons since the viscosity coefficients of the latter are low and their ability to replace HMPA molecules in the electron solvation layer is weak.[23]

References and Notes

(1) This article will be included in G. Dodin's doctoral thesis, University Paris VII.

(2) V. Nicely and J. L. Dye, *J. Chem. Phys.*, **53**, 119 (1970), and references cited therein.

(3) R. Catterall, J. Slater, and M. C. R. Symons, *J. Chem. Phys.*, **52**, 1003 (1970).

(4) R. Catterall, I. Hurley, and M. C. R. Symons, *J. Chem. Soc., Dalton Trans.*, 139 (1972).

(5) V. L. Pollak, *J. Chem. Phys.*, **34**, 864 (1961).

(6) D. E. O'Reilly, *J. Chem. Phys.*, **35**, 1856 (1961).

(7) J. Kaplan and C. Kittel, *J. Chem. Phys.*, **21**, 1429 (1953).

(8) F. J. Dewald and G. Lepoutre, *J. Amer. Chem. Soc.*, **78**, 2953 (1956).

(9) C. Lambert, "Metal-Ammonia Solutions," J. J. Lagowski and M. J. Sienko, Ed., Butterworths, London, 1970.

(10) R. Catterall, L. P. Stodulski, and M. C. R. Symons, *J. Chem. Soc. A*, 437 (1968).

(11) N. M. Alpatova, A. D. Grishina, and M. G. Formicheva, *Sov. Electrochem.*, **8**, 248 (1972); translation published Sept 1972 by Consultant Bureau.

(12) Mei Tak Lok, F. J. Tehan, and J. L. Dye, *J. Phys. Chem.*, **76**, 2975 (1972), and references cited therein.

(13) G. Dodin, C. Lambert, and J. V. Acrivos, to be presented at the Colloque Ampère, Kracovie, Poland, Sept 1973.

(14) J. C. Dumais and Y. Merle d'Aubigné, *Proc. Colloq. AMPERE (At. Mol. Etud. Radio Elec.), XUI, 1970*, 1(1971).

(15) J. S. Hyde and H. W. Brown, *J. Chem. Phys.*, **37**, 368 (1962).

(16) G. Alquié, Thesis, Orsay, 1967.

(17) S. I. Chan, J. A. Austir, and O. A. Paez, "Metal-Ammonia Solutions," J. J. Lagowski and M. J. Sienko, Ed., Butterworths, London, 1970.

(18) C. P. Poole, "Electron Spin Resonance," Interscience, New York, N. Y., 1967, p 695.

(19) K. Halbach, *Helv. Phys. Acta*, **27**, 259 (1954).

(20) A tunneling effect accounting for both hyperfine coupling modulation and electrical conductivity of the solutions as assumed for Na-NH₃ solutions[9] is unlikely to be valid in Na-HMPA solutions since the energy barrier for the electrical conductivities we have measured is expected to be much higher than the modulation barrier (which has the same order of magnitude as in Na-NH₃).

(21) A. Abragam, "The Principles of Nuclear Magnetism," Oxford University Press, London, 1961, p 308.

(22) J. Y. Gal and C. Moliton-Bouchetout, *Bull. Soc. Chim. Fr.*, **2**, 464 (1973).

(23) A. Mozumder, *J. Phys. Chem.*, **76**, 3824 (1972).

Relaxation Processes in Water. Spin-Lattice Relaxation of D₂O in Supercooled Water[1]

J. C. Hindman* and A. Svirmickas

Chemistry Division, Argonne National Laboratory, Argonne, Illinois 60439   (Received June 5, 1973)

Publication costs assisted by Argonne National Laboratory

Spin-lattice relaxation times, T_1, for D₂O have been measured in the supercooled region down to the homogeneous nucleation temperature using an emulsion of D₂O in *n*-heptane. Using a double exponential form of the relaxation equation, an activation energy of 14.9 ± 0.6 kcal mol⁻¹ and an entropy of 46.3 ± 2.6 cal deg⁻¹ mol⁻¹ have been derived for the low-temperature relaxation process. It is suggested that these large values for the entropy and energy may reflect a relaxation process involving cooperative motion of several water molecules.

It has become increasingly clear that the development and testing of models relating structure to relaxation in liquid water requires experimental data for transport processes over as wide a temperature range as possible. In particular, the marked non-Arrhenius behavior observed at low temperatures emphasizes the importance of measurements in the supercooled region. The development of an emulsion technique[2] for stabilizing small droplets (3.5 μ in diameter) without significant alteration in the liquid properties has made it possible to measure various physical properties in the supercooled region[2,3] down to the homogeneous nucleation temperature.[4] In the present communication we describe the results of a study of the spin-lattice relaxation time, T_1, for the deuteron in D₂O down

to −37°. An analysis of the results in terms of the two-process model is given.[5]

Experimental Section

The procedures for the T measurements have been described elsewhere.[5] The emulsions of D₂O in *n*-heptane were prepared according to Rasmussen's procedure.[2] Emulsions of 25 and 50 vol % D₂O were used. No significant difference in behavior was noted as indicated by the data given in Table I. Comparisons with a D₂O sample run at the same time (values plotted in Figure 1) also showed that no significant differences could be detected in the relaxation time behavior at temperature where measurements could be made on both kinds of samples.

TABLE I: Spin–Lattice Relaxation Time of D_2O in n-Heptane Emulsion

Temp, °K	T_1, sec	Temp, °K	T_1, sec
50 Vol % D_2O		50 Vol % D_2O	
287.6	0.346	257.3	0.0872
278.4	0.257		0.0876
275.8	0.218	251.7	0.0603
275.2	0.214		0.0595
270.7	0.178	242.4	0.0255
265.8	0.143		0.0243
260.9	0.108	237.9	0.0146
254.5	0.0726		0.0156
249.6	0.0496	237.2	0.0126[a]
244.6	0.0306		0.0119
240.4	0.0205	25 Vol % D_2O	
236.1	0.0138	257.3	0.0866
258.4	0.0959		0.0885
251.8	0.0604	251.7	0.0622
246.8	0.0385		0.0600
242.9	0.0247	242.4	0.0252
239.5	0.0150		0.0251
236.5	0.0127	237.9	0.0137
			0.0135
		237.2	0.0121[a]

[a] Indication of partial freezing.

Figure 1. Spin–lattice relaxation time of D_2O: O, D_2O in n-heptane; +, D_2O, present experimental data.

TABLE II: Fitting Parameters for Eq 1

	D_2O,[5] temp interval -18 to $178°$	$D_2O–D_2O$ in n-heptane, temp interval -37 to $144°$
a	1.7323×10^{-8}	1.2637×10^{-12}
b	5.152×10^3	7.479×10^3
c	7.010×10^{-3}	3.3670×10^{-3}
d	1.660×10^3	1.928×10^3
E_1[a]	10.24 ± 0.29	14.86 ± 0.64
E_2[a]	3.30 ± 0.06	3.83 ± 0.13

[a] Activation energies in kcal mol^{-1} (95% level).

Results

The experimental T_1 values are given in Table I. It was found that the freezing of the water in the emulsion did not appear to affect its properties. On warming and re-cooling, T_1 values in essential agreement were obtained. The only apparent difference was that, whereas in the initial cooling, T_1 values could be obtained slightly below the reported homonucleation temperature, in subsequent cooling, incipient freezing was noted at this temperature.

Values of $-\ln T_1$ for the D_2O and D_2O in n-heptane as a function of the reciprocal temperature are shown in Figure 1. Also shown in the figure is a least-squares computed curve for the double exponential equation

$$- \ln T_1 = [ae^{b/T} + ce^{d/T}] \qquad (1)$$

The fitting parameters for the equation are given in Table II. Close examination of Figure 1 as well as the larger standard deviation obtained in the present case indicates that the fit of this equation is not as good as previously obtained[5] in studies where the measurements were not made to as low a temperature (see Table II). As a consequence of the large number of observations the fit of the equation in the present case is forced with respect to the low-temperature points so that the deviations are most apparent in the high-temperature region. As a result the activation energy for the low-temperature process is more accurately defined than that for the high-temperature process. Actually, if we ignore the possibility of experimental uncertainties, the results suggest that we may need to consider more than two simple processes. Since the behavior of a variety of transport data in the high-temperature region is adequately represented by a simple Arrhenius equation, the complexity would necessarily be associated with the behavior in the low-temperature region. If, as suggested later in the text, the relaxation in the low-temperature region involves the cooperative motion of several water molecules. it would not appear im-
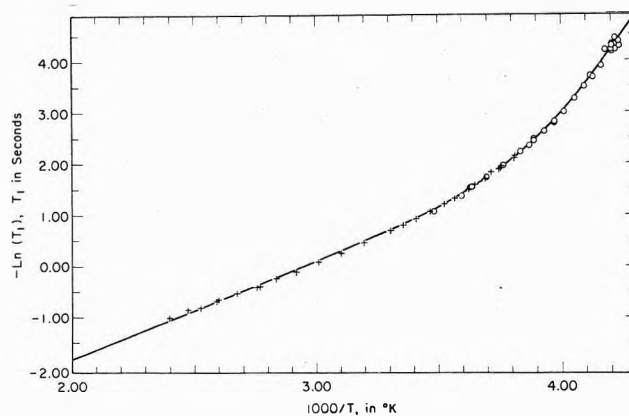
plausible to assume that the number of such molecules might exhibit a temperature variation with a consequent variation in the apparent activation parameters.

The magnitude of the activation energy, 14.9 ± 0.6 kcal mol^{-1}, associated with the low-temperature process is comparable with those reported for the $T_1(^1H)$,[6] $E = 14.1$ kcal mol^{-1}, diffusion,[7] $E = 14.5$ kcal mol^{-1}, and dielectric,[8] $E \simeq 14$ kcal mol^{-1}, relaxation processes in ice. The comparability of these activation energies supports the view that the hydrogen-bonded structure associated with the relaxing molecules is well defined in the liquid at the lower temperatures. It is therefore of interest to determine how closely the rotational relaxation in the liquid resembles that in the solid. That there appears to be a significant difference can be shown by using transition state rate theory to derive the activation entropies for the relaxation in the two cases. Assuming that the correlation times associated with the T_1 and dielectric relaxation are related in the solid as they appear to be in the liquid, we can use the equation[5]

$$k = 1/\tau = [ekT/h] \exp(\Delta S_c^*/R) \exp(-E/RT) \qquad (2)$$

where the frequency factor, A, for the Arrhenius equation is

$$A \equiv [ekT/h] \exp(\Delta S_c^*/R) \qquad (3)$$

For dielectric relaxation in ice, $\Delta S_c^* \simeq 8.8$ cal deg^{-1} mol^{-1}, while for the low-temperature, T_1 process in the liquid we calculate, $\Delta S_c^* = 46.3$ cal deg^{-1} mol^{-1}, an obviously significant difference.

The actual magnitudes of the energy and entropy terms are the significant factors with respect to the mechanism of relaxation. The energy value indicates that several hydrogen bonds are broken in the activation process. The

present data can be interpreted in terms of the proposed kinetic model which assumes that hydrogen bond breaking and rotation is a single process.[9] Fundamental questions are as follows. How many hydrogen bonds are broken? How many water molecules are involved? Does the relaxation correspond to the dissolution of a "cluster" of water molecules as suggested by Frank and Wen?[10] If we follow Kauzmann and consider that the dissolution of a cluster corresponds to a "vaporization" of molecules in a local region of the liquid, the ratio of ΔS_c^* to the molar entropy of vaporization should be approximately equal to the number of molecules involved in the activation.[11] This molar entropy of vaporization, $\Delta S'_{vap}$, is that for the vaporization of liquid water to water vapor occupying a volume equal to the "free volume" of the appropriate lattice configuration in the liquid, i.e.

$$\Delta S'_{vap} = \Delta S_{vap} - R \ln (V_{vapor}/V_{free}) \qquad (4)$$

Weissmann and Blum have used the cell theory of fluids to calculate the "free volume" for water at varying temperatures and intermolecular separations in an expanded ice lattice.[12] Their calculations would suggest approximately 10 eu as an upper limit for $\Delta S'_{vap}$, i.e., that more than four water molecules are involved. A similar calculation can be based on the ratio between the activation energy and the enthalpy for breaking a hydrogen bond. If we use the value of 2.5 kcal mol^{-1} for the breaking of the

bond in an O–D–O unit,[13] we would calculate that approximately three water molecules are involved. These results lend some support to the idea that the relaxation does involve cooperative motion of a group of water molecules although the uncertainties in the various parameters are too large at present to allow us to specify the number of molecules involved.

References and Notes

(1) Work performed under the auspices of the U. S. Atomic Energy Commission.
(2) D. H. Rasmussen and A. P. Mackenzie in "Water Structure at the Water-Polymer Interface," H. H. G. Jellinek, Ed., Plenum Press, New York, N. Y., 1972, p 126.
(3) C. A. Angell, J. Shuppert, and J. C. Tucker, submitted for publication in J. Phys. Chem.
(4) B. J. Mason, Advan. Phys., 7, 221 (1958).
(5) J. C. Hindman, A. J. Zielen, A. Svirmickas, and M. Wood, J. Chem. Phys., 54, 621 (1971).
(6) D. E. Barnall and I. J. Lowe, J. Chem. Phys., 48, 4614 (1968).
(7) H. Blicks, O. Dengel, and N. Riehl, Phys. Kondens. Mater., 4, 375 (1966); O. Dengel, E. Jacobs, and N. Riehl, ibid., 5, 58 (1966).
(8) R. H. Cole, J. Chem. Phys., 27, 33 (1957); R. Ruepp and M. Kass in "Physics of Ice," N. Riehl, B. Bullemer, and H. Engelhardt, Ed., Plenum Press, New York, N. Y., 1969, p 555.
(9) J. C. Hindman, submitted for publication in J. Chem. Phys.
(10) H. S. Frank and W. Y. Wen, Discuss. Faraday Soc., 24, 133 (1957).
(11) See D. Eisenberg and W. Kauzmann, "The Structure and Properties of Water," Oxford University Press, New York, N. Y., 1969, pp 212, 213.
(12) M. Weissmann and L. Blum, Trans. Faraday Soc., 64, 2605 (1968).
(13) G. E. Walrafen in "Water," F. Franks, Ed., Plenum Press, New York, N. Y., 1972, Chapter 5.

COMMUNICATIONS TO THE EDITOR

Electrochemical and Spectroscopic Studies of Cation Radicals. II. Anilinium-Type Radical Ion and Benzidine Dication Visible Spectra

Sir: As part of an on-going program concerning the study of aromatic organic cation radical behavior, we have been using chemical and electrochemical generation methods to obtain visible absorption spectra of para-substituted anilinium and N,N-dimethylanilinium radical ions. It is fundamental to this study that the spectra of the parent molecules, namely, the anilinium and N,N-dimethylanilinium cation radicals, be obtained and correctly assigned. We have been utilizing electrochemical data as indicators of radical stabilities in various media as a correlative tool for spectral radical generation studies and as a result of this work we have obtained the visible absorption spectra from the anodic oxidations of aniline, N,N-dimethylaniline (DMA), benzidine, and N,N,N',N'-tetramethylbenzidine (TMB) in various media. Presentation of these data is called for, we feel, in light of the spectral assignments concerning these species to be found in the chemical literature.

A good deal of attention has been directed toward the visible spectra of the aniline and DMA cation radicals; these spectra have been conspicuously reproducible over a wide range of media employing a number of generation techniques. Typical spectroscopic results from the literature are shown in Table I.[1-9]

The spectral curves obtained by anodic oxidations of the two anilines and two benzidines in both aqueous and nonaqueous media are shown in Figure 1. It is apparent that the aniline–benzidine and DMA–TMB pairs have identical visible spectra; in all cases the major peaks in the 400–500-nm region can be assigned to the dication forms (generated by loss of two electrons) of the benzidine molecules.[10-12] The aniline spectrum also contains a broad absorption in the 500–650-nm region which can be attributed to a second coupling product derived from aniline, 4-aminodiphenylamine.[12,13] More important, a comparison of the peaks in Figure 1 with the data of Table I indicates that the benzidine and TMB dications have absorption maxima at almost identical wavelengths to the reported aniline and DMA cation radicals,[14] respectively. Thus, the possibility exists that the spectral data reported for the aniline and DMA cation radicals actually correspond to the appropriate benzidine dications.

Careful scrutiny of the references contained in Table I provides convincing evidence against this proposal, particularly the studies done in glasses and those employing flash photolysis or pulse radiolysis techniques. These methods would, it seems, provide valid spectral data for all but the most unstable intermediate species. Since benzidines are formed from anilines by a second-order coupling reaction involving the cation radical, conditions

such as low amine concentration, low temperature, and slow diffusion (such as in a glass) should lend enhanced stability to the primary cation radicals; fast sampling methods would also be a positive factor. However, these conditions may be readily counterbalanced by aggregation of the parent molecules, both in solution and in glasses, thus facilitating the chemical decomposition processes. Each of the studies in Table I employed various of the positive factors mentioned above, but all reported basically the same data. In addition, the absorption maxima correlate with our spectral curves which were obtained under markedly "nonideal" conditions, namely, ambient temperatures, nonviscous solutions, and long sampling times.

From the foregoing discussion two facts emerge: (1) under oxidative conditions benzidines can be generated from anilines; (2) the benzidine dications have visible spectra with strong peaks in the 400–500-nm region (the benzidine cation radicals, which are in a disproportionation equilibrium with the parent and dication, have weaker absorption maxima in the area of 700–900 nm).

The following pieces of spectral and electrochemical information are also of significance.

(1) The oxidative generation of benzidines from aromatic amines by both chemical and electrolytic methods is a general reaction pathway.

(2) Electrochemical and spectroscopic studies have been employed to establish the fact that benzidine will form in appreciable amounts upon anodic oxidation of aniline only at low pH (1–4) and that even here the benzidine dication decomposes rapidly as the pH is raised, presumably by deprotonation and subsequent multiple couplings.[12] Thus, the likelihood of formation and dication stability of benzidine parallels the behavior attributed to the aniline cation radical.[3]

(3) The benzidine dication absorption is rapidly annihilated in the presence of parent aniline by either a fast chemical reaction or electron transfer process (the former appears more likely at this time).[12]

(4) Benzidine is more easily oxidized than aniline (and TMB more easily than DMA) and so any energy source that would cause oxidation of aniline would also be sufficient to oxidize any benzidine formed.

(5) In amine systems where the primary cation radical is sufficiently stable to be unambiguously assigned, the absorption maximum is at a considerably longer wavelength than the corresponding benzidine dication. Thus, triphenylamine cation radical has an absorption peak at 640–660 nm with a broad shoulder toward the blue,[4,15-17] while the tetraphenylbenzidine dication has a broad but well-defined band at 480 nm.[18,19] Similarly, diphenylamine cation radical absorbs at 680–690 nm (shoulder to the blue)[4,20] and the N,N'-diphenylbenzidine dication at 470–500.[20,21]

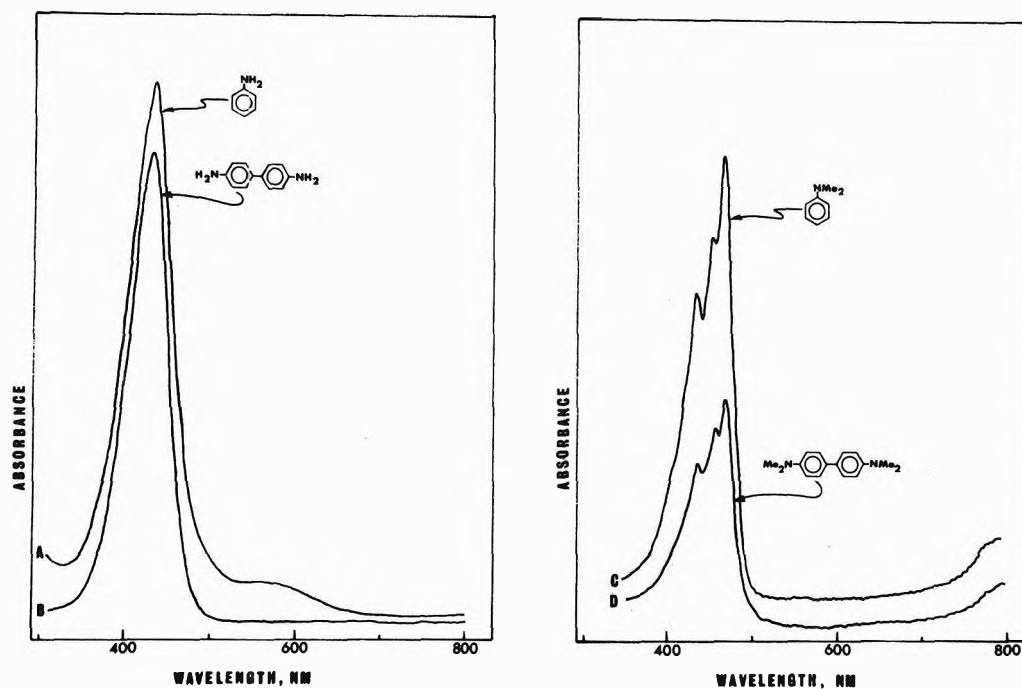(6) Extensive electrochemical studies indicate that the aniline and DMA cation radicals are extremely unstable

Figure 1. Absorption spectra (recorded on a Cary 14 spectrophotometer) for partially electrolyzed solutions under the following conditions: curves A and B, 10^{-4} M amine in 6 M H_2SO_4 at platinum; curves C and D, 10^{-3} M amine in MeCN–0.1 M tetraethylammonium perchlorate at platinum.

TABLE I: Spectroscopic Data for Anilinium and N,N-Dimethylanilinium Radicals

Experimental conditions	Aniline·+ [a]	DMA·+ [a]	Ref
Photooxidation (270 nm) in EPA glass[b]	386	459	1
Photolysis in EPA glass[b]	429 (shoulder at 405)		2
Flash photolysis in aqueous solution (pH 1–13), hexane, cyclohexare, and liquid paraffin	423 (shoulder at 400)	460	3
γ-Irradiation in CCl_4 at 77°K (glass)	420–430	475–480 (shoulder at 450)	4
Pulse radiolysis on neat aniline	385		5
Pulse radiolysis of 0.1 M aniline in cyclohexane	395		5
Pulse radiolysis of 0.1 M aniline in CCl_4	420		5
Pulse radiolysis of 0.01 M aniline in CCl_4	405		7
Pulse radiolysis of 10^{-4} M aniline in aqueous solution	420		6
Uv irradiation in MP,[c] EtOH at 77°K (glasses)		470,445	8
Laser photolysis of DMA–perylene in acetonitrile and pyridine		440–510 (peak positions unspecified)	9

[a] Wavelengths for visible absorption maxirra, in nanometers. [b] EPA is a polar matrix consisting of ether, isopentane, and alcohol. [c] MP is a nonpolar matrix comprised of methylcyclohexane and isopentane.

in solutions of polar solvents. We have attempted to measure the second-order coupling rate constants, particularly for DMA, but we can only state with any degree of certainty that the values are in excess of 10^8 mol^{-1} sec^{-1} and are more likely in the region of 10^{10}.

While it is possible that the aniline and DMA cation radicals and their corresponding benzidine dications have identical spectral characteristics, this is not to be anticipated. Nevertheless, the array of data in the literature characterizing these cation radicals is impressive and cannot be easily discounted. Still, we wish to suggest that the previously reported data for anilinium-type cation radicals be reconsidered in light of the foregoing discussion. With the view that these highly unstable cation radical species may as yet be undetected, we are continuing the search for unambiguous spectral and electrochemical evidence confirming their existence and properties.

References and Notes

(1) G. N. Lewis and J. Bigeleisen, *J. Amer. Chem. Soc.*, **65**, 2424 (1943).
(2) I. Norman and G. Porter, *Proc. Royal Soc., Ser. A*, **230**, 399 (1955).
(3) E. J. Land and G. Porter, *Trans. Faraday Soc.*, **59**, 2027 (1963).
(4) T. Shida and W. H. Hamill, *J. Chem. Phys.*, **44**, 2369 (1966).
(5) R. Cooper and J. K. Thomas, *J. Chem. Phys.*, **48**, 5103 (1968).
(6) A. Wigger, W. Grunbein, A. Henglein, and E. J. Land, *Z. Naturforsch. B*, **24**, 1262 (1969).
(7) H. D. Burrows, D. Greatorex, and T. J. Kemp, *J. Phys. Chem.*, **76**, 20 (1972).
(8) S. Arimitsu, K. Kimura, and H. Tsubomura, *Bull. Chem. Soc. Jap.*, **42**, 1858 (1969).
(9) Y. Taniguchi, Y. Nishina, and N. Mataga, *Bull. Chem. Soc. Jap.*, **45**, 764 (1972).
(10) A. Hakusui, Y. Matsunaga, and K. Umehara, *Bull. Chem. Soc. Jap.*, **43**, 709 (1970).
(11) B. Kratochvil and D. A. Zatko, *Anal. Chem.*, **40**, 422 (1968).
(12) J. Wheeler and R. F. Nelson, unpublished data.
(13) J. Bacon and R. N. Adams, *J. Amer. Chem. Soc.*, **90**, 6596 (1968).
(14) Throughout this paper, the term "cation radical" will refer to the paramagnetic radical ion formed by loss of a single electron from the parent aniline or DMA. In strong acid, the amines are, of

course, protonated, but it is likely that deprotonation would occur subsequent to electron transfer according to the scheme

$$\mathrm{ArNH_3}^+ \overset{1e}{\rightleftharpoons} \mathrm{Ar\dot{N}H_3}^+ \overset{H^+}{\rightleftharpoons} \mathrm{Ar\dot{N}H_2}^+$$

The species on the far right would be the anilinium "cation radical."

(15) D. W. Skelly and W. H. Hamill, *J. Chem. Phys.*, **43**, 3497 (1965).
(16) M. Kondo, M. R. Ronayne, J. P. Guarino, and W. H. Hamill, *J. Amer. Chem. Soc.*, **86**, 1297 (1964).
(17) G. N. Lewis and D. Lipkin, *J. Amer. Chem. Soc.*, **64**, 2801 (1942).
(18) E. T. Seo, R. F. Nelson, J. M. Fritsch, L. S. Marcoux, D. W. Leedy, and R. N. Adams, *J. Amer. Chem. Soc.*, **88**, 3498 (1966), and references therein.
(19) H. Hasegawa, *J. Phys. Chem.*, **66**, 834 (1962).
(20) G. N. Lewis and J. Bigeleisen, *J. Amer. Chem. Soc.*, **65**, 520 (1943).
(21) R. F. Nelson, Ph.D. Thesis, Kansas University, 1967.
(22) Present address, Department of Chemistry, University of Georgia, Athens, Ga. 30601.

Department of Chemistry   **James Wheeler**
University of Idaho   **Robert F. Nelson*** [22]
Moscow, Idaho 83843